UNIVERSITÀ DEGLI STUDI DI TORINO

DIPARTIMENTO DI NEUROSCIENZE "RITA LEVI MONTALCINI"

DOTTORATO DI RICERCA IN NEUROSCIENZE
CICLO XXIX

"Astrogliogenesis in the cerebellum results from progenitors with distinct fate potencies and proliferative behaviors"

TESI PRESENTATA DA: Dr.ssa Valentina Cerrato

TUTOR: Prof. Annalisa Buffo

COORDINATORE DEL DOTTORATO: Prof. Marco Sassoè

ANNI ACCADEMICI:

2014-2017

Table of contents

Chapter 1: General overview

1.1 The increasing complexity of (astro)glial heterogeneity

The history of the research on glial cells began in 1846, when the Professor of Pathology Rudolf Virchow described for the first time a “connective tissue” in the brain and spinal cord, acting as a cement in which the “proper nervous parts” seemed to be embedded. He termed it “neuroglia”, from the Ancient Greek word γλία, thus providing the concept of a gummy substance with the passive and uninteresting role of physical support to neurons and without any implication in brain functions. Consequently, glial cells were totally neglected for several decades after they were discovered. In the second part of the 19th century, during the golden age of cellular histology, specific staining methods were developed by several scientists such as Ramón y Cajal, Golgi, Weigert and Rìo-Hortega and many different forms of human glial cells were described and images published. Ramón y Cajal, the most renowned neuroanatomist of the 20th century, while studying and representing the cellular structure of the brain was very careful in his drawings not to mistake for neurons those strange-looking cells (i.e. glial cells) and published volumes of scientific papers on them. The evaluation of the existence of distinct morphologies within a population previously described to be very homogeneous led to the definition of the term “astrocyte”, first proposed in 1893 by Michael von Lenhossek, to refer to star-shaped neuroglial cells with numerous filaments radiating from their cell bodies. Slightly later, Kölliker and Andriezen further subdivided this category into “fibrous” and “protoplasmic” astrocytes, according to the shape and number of their processes and their localization in white or grey matter, respectively. (Fig. 1.1; reviewed in García-Marín et al., 2007; Kettenmann and Verkhratsky, 2008).

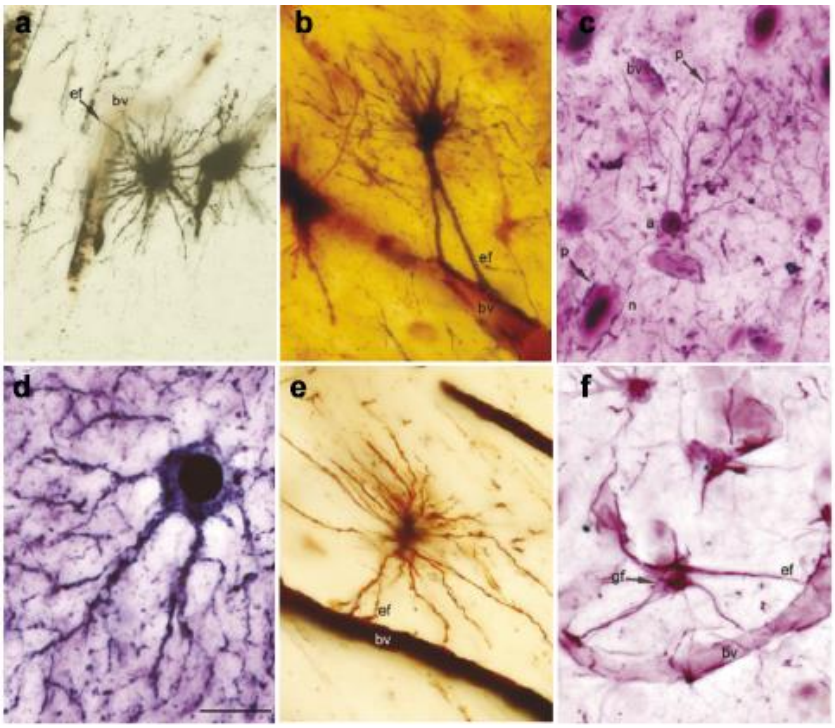

Figure 1.1. Protoplasmic and fibrous astrocytes from Cajal's original slides impregnated by distinct staining methods. (a-d) Protoplasmic astrocytes impregnated by the Golgi-Cox method (**a**), formol-uranium nitrate method (**b**), gold chloride sublimated method (**c**), and silver carbonated method (**d**). (**e-f**) Fibrous astrocytes impregnated by the Golgi-Kenyon method (**e**), and ammoniacal silver oxide method (**f**). a, astrocytes; bv, blood vessels; ef, endfeet; gf, gliofilaments; n, neurons; p, processes. Scale bar: 25 µm. (modified from García-Marín et al., 2007)

Despite the increasing evidence that the non-neuronal cells were quite diverse in their forms and underwent distinct changes in pathology, "neuroglia" has become a very generalized term covering cells with different origins, morphologies, physiological properties and functions. In detail, in the mammalian nervous system neuroglia are subdivided in peripheral nervous system (PNS) and central nervous system (CNS) cells. The first category comprises *Schwann cells*, *satellite glial cells* in peripheral ganglia, the *olfactory ensheathing cells* in the olfactory system and, finally, *enteric glia* residing in the homonymous nervous sysyem. On the other side, CNS glia are generally subdivided into *oligodendrocytes* (the myelinating cells in the CNS), *NG2-glia* (oligodendroglial precursors), and, finally, *astrocytes*.

In turn, astrocytes are themselves a highly heterogeneous population. The current knowledge, yet still incomplete, concerning their diversity across and within CNS regions, as well as their developmental mechanisms, will be therefore addressed in the next sections.

1.1.1 Heterogeneity of astrocytes and its implications in physiology and pathology

An increasing body of evidence supports the idea that astrocytes are morphologically, functionally and molecularly different. This heterogeneity is both "regional", distinguishing astrocyte populations belonging to functionally distinct neuronal networks of the CNS, and "local", among astrocytes within such networks. Of note, as organisms evolutionarily expand in complexity, all aspects of astroglial diversity evolve, starting from Nemadodes such as *C. Elegans*, with one of the most elementary nervous systems and very few and simple glial cells, and ending with higher vertebrates such as mammals, where both numbers and complexity of astrocytes are remarkably high (Verkhratsky, and Butt, 2013). In turn, among mammals themselves, astroglial diversity further increases in the brain of primates, especially humans. Here, the functional heterogeneity of astrocytes might be the result of the evolutionary remarkable increase in both their number and morphological complexity (Sherwood et al., 2006). These interspecies differences parallel the evolution in both size and functional capacity of the cerebral cortex in higher mammals, pointing to astrocytic complexity as a key component of computational potentiation through synaptic modulation and regulation of cortical circuitries (Oberheim et al. 2006; 2009). Hereafter, I will summarize, first, the advances made in the last decades in defining the multiform heterogeneity of astrocytes and, then, the current knowledge on how this faceted diversity is shaped during development. Nevertheless, the information concerning both these aspects is still incomplete. This creates an endless vicious circle, in which the still partial categorization of the astrocytic diversity makes, by definition, impossible to fully understand how this diversity is built. To exit from this cul-de-sac, I will propose, as a simple model to study the generation of astroglial diversity, the cerebellum, that owns a limited and well-characterized subset of astrocytes and is, therefore, very suitable to this purpose.

1.1.1.1 Morphological heterogeneity

The first cue that astrocytes might be a heterogeneous population came from the acknowledgment of two morphologically distinct astroglial types in the human white or grey matter, with characteristic *fibrous* and *protoplasmic* morphologies, respectively (Kölliker, 1896; Andriezen, 1896). In detail, the fibrous astrocytes populating the white matter yield the more classic "star like" appearance, with regular contours and cylindrical processes, whereas protoplasmic astrocytes in the grey matter have more irregular

"bushy" processes. Although this simple classification is still widely used, it is clearly insufficient and outdated. In fact, multiple morphologically distinct astrocytes were identified across distinct functional areas through the whole CNS, with peculiar densities and proliferation rates (Emsley and Macklis, 2006). Besides this interregional diversification, astrocyte populations within each functionally defined area also exhibit local phenotypic diversity. For instance, the coexistence of distinct types of cells expressing astrocyte-specific markers was reported within the rodent hippocampus, where two distinct kinds of astroglial cells were shown, both *in vitro* and *in vivo*, to display diverse morphologies: while a first type of cells possessed short, thin processes, a second group, resembling more protoplasmic astrocytes, had cell bodies with an irregular shape and very expanded nets (Matthias et al., 2003). Moreover, the cerebellar cortex hosts three peculiar astroglial phenotypes with distinct morphologies and layer allocations that allow their classification into *velate* and *protoplasmic astrocytes* of the Granule Layer (GL) and *Bergmann Glia (BG)*, aligned to the Purkinje cell layer (PCL; Fig. 1.2). While *velate* astrocytes possess "bushy" processes, the nearby *protoplasmic* cells, a very poorly represented type of GL astrocytes, have slender processes without any lamellar appendage. On the other side, *BG* have their somata aligned to the PCL and extend several ascending processes spanning radially the molecular layer (ML; Palay and Chan-Palay, 1974), thereby resembling radial glia cells (RG) present during CNS development. This latter phenotype, besides being distinct from the neighbouring astroglial cells in the cerebellar cortex, possess a strikingly different morphology than the typical protoplasmic appearance of grey matter astrocytes in most of the other brain regions (a specific section [1.3.2] will be dedicated to cerebellar astrocytes). In addition to BG, the cerebellar PCL hosts a second type, largely forgotten, of glia, called "feathered cell" of Fañanas. These cells were first identified (Fañanas, 1916) by a special staining procedure, the Cajal's gold sublimate technique (Cajal, 1926; Globus, 1927), and display a structure rather similar, but not identical, to that of BG, with smaller cell bodies less orderly located in the PCL and more branched processes, apparently disappearing in the upper third of the ML. Nevertheless, their identification by means of simple morphological criteria still remains quite hard, making Fañanas cells mostly left apart.

Similarly to *BG* of the cerebellum, *Müller cells* of the retina are another astroglial phenotype, whose morphology is reminiscent of RG and is easily distinguishable from the

other surrounding astrocytes of the retina: their soma reside at the centre of the inner nuclear layer, from which radially oriented processes emerge to span the thickness of the neuroretina and ramify in each retinal layer (Wang et al., 2017).

Besides the so far described intra-species heterogeneity, comparative studies between rodent and human astrocytes also highlighted big differences in terms of morphological variety. Indeed, the human neocortex hosts unique additional astroglial types absent in rodents, including the *interlaminar astrocytes*, that populate the superficial cortical layers and extend long processes to cortical layers 3 and 4, and *polarized astrocytes* located in layers 5-6, also projecting peculiar long processes. Moreover, human cortical astrocytes are both bigger, with a larger diameter and more numerous processes, and structurally more complex and diverse. Human white matter astrocytes are larger in diameter, too, although they resemble more their rodent counterpart (Oberheim et al. 2006; 2009).

Astrocytes responding to CNS injury or other neurological diseases such as trauma, ischemic damage, neuroinflammation, or neurodegeneration, also undergo macroscopic morphological changes, in a process known as “reactive astrogliosis”. In this context, hypertrophy of cell bodies and processes, together with the increase in the amount of interdigitations, are canonical morphological features of reactive astrocytes. Nevertheless, rather than being a uniform and stereotyped response, these morphological changes are highly variable among cells, and can be tuned according to the severity of the insult and to the proximity to the site of damage. Indeed, in healthy tissue and in mild to moderate astrogliosis, astrocytes occupy non-overlapping domains, whereas during severe astrogliosis elongated reactive astrocytes extensively intermingle. This happens particularly in the scar borders around the lesion: the more the hypertrophic reactive astrocytes lay far from the injury core, the more they appear “stellate” and have processes that overlap far less, until they become indistinguishable in phenotype from those in healthy tissue (Anderson, Ao and Sofroniew, 2014).

1.1.1.2 Molecular heterogeneity

Several advances in biochemistry and molecular biology over the last decades allowed the identification of distinct genetic markers that are now commonly used to define the whole astroglial lineage. Beside them, no markers are yet available to unequivocally discriminate

among the distinct astrocyte phenotypes populating the CNS, thus making very challenging the study of astroglial heterogeneity and its development. Nevertheless, many recent studies have better elucidated the astrocyte expression profile and how it can vary locally (Fig. 1.2) or across broad CNS regions (see table 1.1). The glial fibrillary acidic protein (GFAP) is one of the abovementioned pan-astrocytic markers, that, nevertheless does not show the same expression level in all astroglial cells. For instance, it was described to be expressed at distinct levels by cortical (low levels) and fibrous (high levels) astrocytes of the cerebral cortex and striatum (Bachoo et al., 2004; Lein et al., 2007). However, grey matter astrocytes were shown to express high levels of this intermediate filament protein in pathological conditions, suggesting a physiological suppression of the GFAP transcription in certain astrocyte populations (reviewed in Hewett, 2009). Other molecular differences between cortical and fibrous astrocytes have been described. For instance, the metastasis-associated protein-1, member of the S100 proteins family (therefore called *S100A4*), is expressed by fibrous but not in protoplasmic astrocytes (Aberg and Kozlova, 2000). Similarly, one of the four splice variants of the glutamate transporter type 2 (EAAT2/GLT1), is an exon 9-skipping form that has been shown to be localized primarily to white matter astrocytes (Macnab and Pow, 2007) whereas the astrocyte-specific gap junction protein connexin30 (Cx30) is found exclusively in grey matter cells (Nagy et al., 1999). Within the cerebellar territory, BG and velate astrocytes of the GL display distinct, but overlapping, molecular signatures. In detail, BG are enriched in AMPA receptors GluA1 and GluA4, and GLAST (Glutamate Aspartate Transporter), whereas velate astrocytes have low amounts of these transcripts and large amounts of the water channel aquaporin 4 (AQP4) (Saab at al., 2012; Papadopulos and Verkman, 2013; Farmer et al., 2016). Moreover, some components of the pathway of developmental morphogen Sonic hedgehog (Shh), comprising the transcription factor GLI1 and the receptors Patched1 and 2 (PTCH1/2) are also enriched in mature BG but not velate astrocytes (Farmer et al., 2016). Shh, secreted by Purkinje cells (PCs) also regulates the expression of the growth differentiation factor 10 (GDF10), also known as BMP3B, described to be selectively restricted to developing and mature BG (Mecklenburg et al., 2014). Of note, BG are among the very few kinds of astrocytes that constitutively express at adult stages the intermediate filament protein Vimentin, typical of immature and reactive astrocytes (Shaw et al., 1981). On the other hand, the expression of Kir4.1, a pivotal potassium channel subunit, was described to be higher in both BG and

GL astrocytes than in fibrous white matter astrocytes (Tang et al., 2009; Farmer et al., 2016). Similarly, a locally-specific expression of Kir4.1 was also observed in the spinal cord, highest in the ventral than in the dorsal horns (Olsen et al., 2007).

Importantly, the research group of Benjamin Deneen has very recently screened the population positive for ALDH1L1 (a broad marker of astrocytes in the adult CNS) according to its expression of CD51, CD63 and CD71. This allowed the identification of five distinct subsets of astrocytes across the olfactory bulb, cortex, brainstem, thalamus and cerebellum, each of them showing unique molecular signatures compared both to ALDH1L1-negative reference cells and to each other. Of note, through unsupervised cluster analysis, the authors also showed that each of these populations, regardless of region, usually clustered together, thus suggesting that each subset contains a conserved molecular identity across these distinct brain areas (Lin et al., 2017).

Besides this local heterogeneity, interregional molecular differences have also been described. Despite, as previously shown, protoplasmic astrocytes physiologically express low levels of GFAP, hippocampal astrocytes and BG of the cerebellum do the opposite (Wilhelmsson et al., 2006; Lein et al., 2007). Regional differences in the expression of the distinct isoforms of the glutamate transporters also exist: whereas EAAT2 levels are higher in the hippocampus than in the cerebellum, GLAST (EAAT1) shows the opposite pattern of expression (Lehre et al., 1995). More generally, a vast regional heterogeneity among astrocytes in the distinct regions of the CNS has been described also regarding the expression of glutamate receptors (AMPA and NMDA), transmitter receptors (GABAa, glycine, beta-adrenergic, purinergic and dopamine receptors), and ion channels (sodium and potassium; reviewed in Matyash and Kettenmann, 2009).

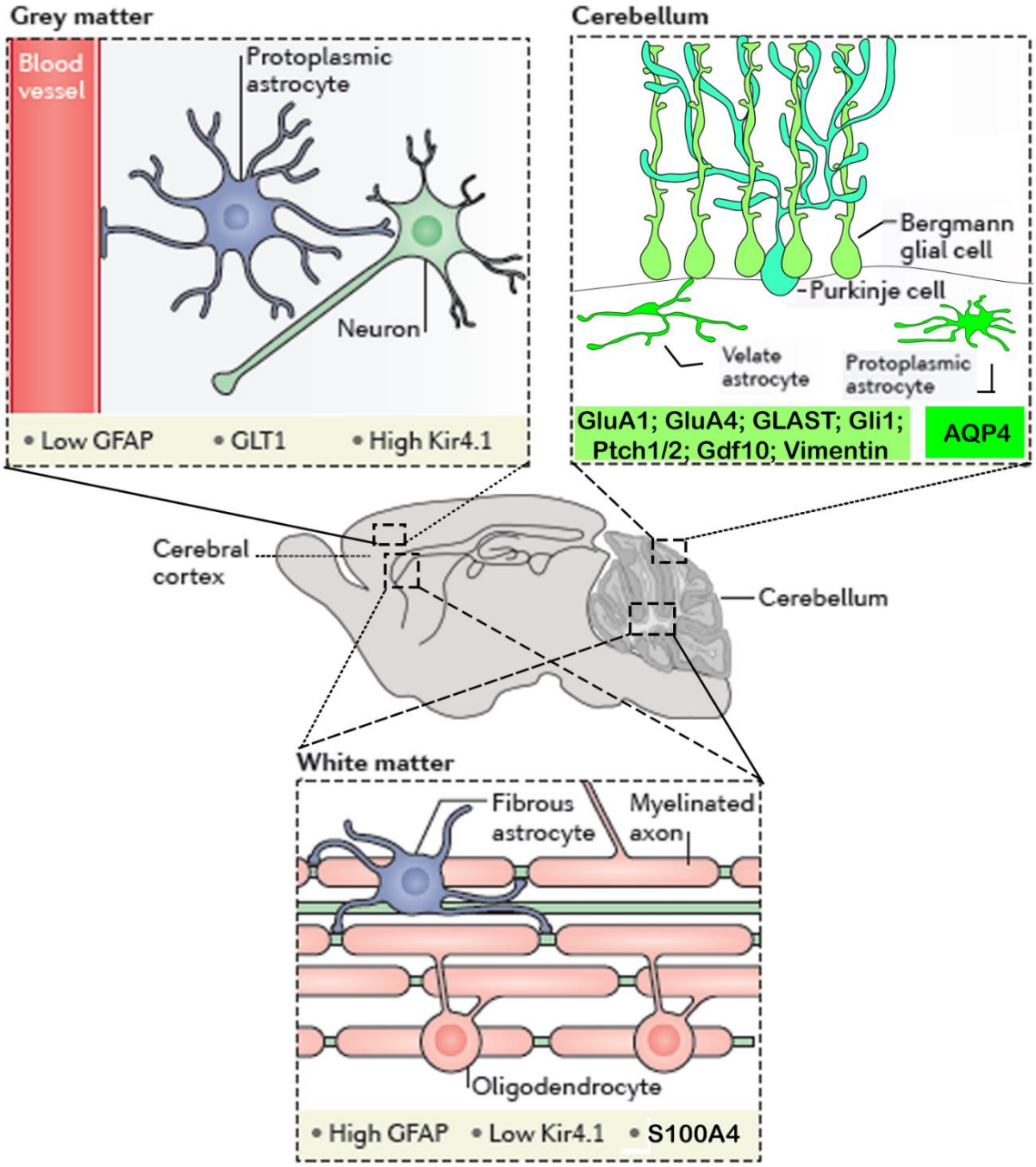

Figure 1.2. Local morphological and molecular heterogeneity of astrocytes. The schematics represent the morphological and molecular features of different types of astrocytes in the mouse brain. Protoplasmic astrocytes are located in the gray matter and have a radial morphology, contacting both neuronal synapses and blood vessels (upper left panel; see next section). On the contrary, fibrous astrocytes of the white matter have an elongated morphology and are in close contact with oligodendrocytes and myelinated axons tracts (bottom panel). In the cerebellum, three kinds of astrocytes can be found in cortical layers: Bergmann glia extend long processes in the molecular layer and enwrap Purkinje cells dendrites, whereas velate and protoplasmic astrocytes are located in the granular layer (upper right panel). In each panel, astrocytes markers differentially expressed by each kind of astrocytes are indicated (modified from Haim and Rowitch 2016).

1.1.1.3 Functional heterogeneity

Despite their original view as a mere physical support to neurons, astrocytes play a plethora of vital roles in both the developing and adult CNS (reviewed in Molofsky and Deneen, 2015). Indeed, RG, the primary astroglial progenitors, serve both as neural precursors and to provide the scaffolds for newborn neurons to migrate, before becoming gliogenic; then, during late embryonic and early postnatal development, immature astrocytes are thought to guide the still ongoing neuronal migrations and regulate both dendritic and axonal growth. Therefore, through the secretion of extracellular matrix proteins and/or signalling molecules, they promote and coordinate synapse formation, stabilization/elimination, neuronal survival and, later in the mature brain, synaptic plasticity. Moreover, together with pericytes and endothelial cells, astrocytes contribute to the formation of the blood brain barrier (BBB) with their endfeet and, thereafter, to its maintenance. In the adult brain, astrocytes represent a bridge between blood vessels and neurons, forming intricate endfeet structures on CNS microvessels on the one hand and associating with synaptic connections on the other. The anatomic relationship between endothelial cells, astrocytes, and neurons is termed “neurovascular unit”. In this context, astrocytes either are involved in blood flow regulation and in energy metabolism, taking up nutrients from the blood, metabolizing and providing them to neurons, or they regulate extracellular ion and neurotransmitter homeostasis. Furthermore, by secreting themselves transmitters and peptide hormones and expressing neurotransmitters receptors, they can directly modulate synaptic transmission.

Pioneer culture and transplantation experiments first identified functional differences among astrocytes from distinct brain regions: if mesencephalic but not striatal astrocytes were able to induce *in vitro* morphological changes in mesencephalic dopaminergic neurons (Denis-Donini et al. 1984), an opposite effect was observed in the growth and maintenance of adult serotoninergic axons, which were shown to extensively innervate the ventral mesencephalic tissue in presence of co-grafted cortical or striatal astrocytes and, to much lower extent, of homotopic mesencephalic astrocytes (Petit et al. 2001). Nevertheless, due to difficulties in manipulating astrocyte functions in a cell type and region-specific way, these observations still need to be fully confirmed *in vivo*. Moreover, several recent studies have shown that parenchymal astrocytes in non-neurogenic regions

of the adult brain can respond to injury by producing neurons or can be triggered to enter a neurogenic program by genetic reprogramming, thus suggesting that the neural stem cell (NSC) properties and activity might be retained or activated under certain circumstances in some mature astroglia (Magnusson et al., 2014; Nato et al., 2015; reviewed in Boda et al., 2017).

As described above, the heterogeneity of gene expression in astrocytes very often implies diverse roles, therefore providing an excellent entry point to investigate their functional heterogeneity. For instance, regional and temporal differences in the expression of surface or secreted proteins (SEMA3A, SLIT proteins, thrombospondins) were associated to changes in astrocyte-astrocyte or astrocyte-neuron interactions and resulted in distinct contributions to axonal orientation, synaptogenesis and neuronal survival (Nagy et al., 1999; Molofsky et al., 2014; Unni et al.,2012; Christopherson et al. 2005). Secondly, distinct expression levels of potassium and calcium channels result in differential calcium signalling and potassium uptake currents and, in turn, to a heterogeneous modulation of extracellular homeostasis and neuronal activity (reviewed in Matyash and Kettenmann, 2009). Regional differences in the regulation of extracellular homeostasis also result from distinct expression levels of glutamate transporters' isoforms (EAAT1 and EAAT2, see above). Moreover, the astroglial expression of neurotransmitter receptors (GABAergic, adrenergic, purinergic, serotonergic, muscarinic, and peptidergic receptors) exhibits regional heterogeneity and changes during development and in response to injury, thus affecting many aspects of astrocytes involvement in the modulation of synaptic transmission (reviewed in Porter and McCarthy, 1997; and in Matyash and Kettenmann, 2009). Distinct spatial and developmental patterns of neuropeptides expression were also described and translate into a big variety of trophic effects on neurons during development (i.e. the regulation of their number, axon and dendrite length, and neuronal phenotype; reviewed in Schwartz and Taniwaki, 1994). Eventually, differences in the expression of enzymes that break down dopamine, serotonine, and GABA also suggest differences in the role of astrocyte subsets in distinct brain regions in neurotransmitter metabolism (reviewed in Zhang and Barres, 2010) .

Of note, besides their wide range of functions in normal conditions, astrocytes take on additional roles in and as a consequence of disease. Indeed, reactive astrocytosis (see section 1.1.1.1) and its related functional changes are found in a big variety of brain

pathologies, such as traumatic, ischemic, neurodegenerative and neurodevelopmental disorders, as well as in epilepsy, and may contribute to both their onset and progression, but also to aiding in the regeneration process (reviewed in Molofsky et al., 2012; Sloan and Barres, 2014). In response to acute and invasive injuries (such as stab wound or brain ischemia), a subset of reactive astrocytes starts proliferating and, although they remain within their lineage *in vivo*, they were shown to acquire a stem cell potential in a more favourable environment *in vitro* (Buffo et al., 2008). Moreover, it was proposed that the proliferating reactive astrocytes found in close association to blood vessels might regulate both migration and proliferation of glial scar-forming pericytes (Bardehle et al., 2013). After proliferating, reactive astrocytes form a border between the lesion and the CNS tissue around it, in an attempt to demarcate the lesion and temporarily or permanently separate it from the surrounding tissue and from immune attacks (Voskuhl et al., 2009). This phenomenon was shown, on the one hand, to play a positive role in the acute repair process, limiting the extent of neurodegeneration and allowing the repair of the BBB (Faulkner et al., 2004), and, on the other hand, to be protective of the intact rest of the CNS, sequestering a potentially toxic lesion environment from it (Renault-Mihara et al., 2008). Additionally, although astrocytes scars have always been considered as physical barriers to axon regrowth in the CNS, this prevailing dogma has recently been refuted by the evidence that astrocyte scar formation aids rather than prevents axon regeneration (Anderson et al., 2016). On the other side, reactive astrogliosis is also very prominent in several chronic neurodegenerative diseases. In Alzheimer Disease, reactive astrocytes intimately associate with amyloid plaques: although this activation was often viewed as part of the neuroinflammatory neurotoxic response, reactive astrocytes were shown to be able to inhibit the formation and growth of amyloid plaques, as well as to degrade them (reviewed in Pekny and Pekna, 2013). In the context of injury and neurodegeneration, activated astrocytes can also affect the recruitment of blood-borne monocytes and migration, proliferation and activation of microglia, although the exact mechanisms are currently unknown. Eventually, reactive astrocytes are found through epileptic lesions and, in this context, can both promote and oppose seizure development through a variety of specific mechanisms, involving their effects on glutamate transport and release and their roles in buffering potassium and interstitial volume control (Wetherington, Serrano and Dingledine, 2008).

In addition, glia may be affected by disease-causing molecular defects and become dysfunctional (reviewed in Molofsky et al., 2012). For instance, Alexander's Disease is commonly considered to be a leukodystrophy clearly caused by astrocyte dysfunction, being due to a gain-of-function point mutation in an astrocyte-specific protein, GFAP. The exact mechanism of astrocyte dysfunction is unclear, but the presence of white matter injury indicates effects on oligodendrocytes and myelination. Dysfunctional astrocytes, as a consequence of the loss of the transcriptional repressor methyl-CpG-binding protein 2 (MeCP2), were also suggested to contribute to the neuronal developmental defects of Rett syndrome. Similarly, the loss of the FMRP protein in astrocytes has been suggested to contribute to the onset of the Fragile X mental retardation. Eventually, in Amyotrophic Lateral Sclerosis (ALS), glial cell dysfunction is causally implicated in mediating neuronal degeneration (Yamanaka et al., 2008), and ongoing reactive gliosis and inflammation are also thought to contribute to the disease progression (Maragakis and Rothstein, 2006).

1.1.2 Generation and specification of the astroglial heterogeneity in the CNS

As described above, with their broad morphological, molecular and functional heterogeneity, astrocytes play a central role in CNS physiology and pathophysiology. However, to fully understand the contribution of astrocytes to brain function and dysfunction, the gap between their development and physiology still needs to be completely bridged. Importantly, since functional defects in astrocytes could be due to abnormal developmental programs, a better understanding of their development is required to shed new light on the disorders in which they have shown to be implicated and, possibly, to point to new therapeutic strategies.

To date, our knowledge about astroglial development lags behind that of neurons and oligodendrocytes, as a result of the lack of (1) reliable markers to selectively characterize distinct astrocytes and their precursors at distinct stages *in vivo*, (2) methods to perform gene manipulation *in vivo* without affecting neural stem cells and neurogenesis and (3) *in vitro* systems capable of fully recapitulating the physiological properties of mature astrocytes observed *in vivo* (although more reliable protocols have been recently proposed; Ugbode et al., 2016; Hertz et al., 2017).

Three distinct sources for astrocytogenesis have been postulated in the CNS. The traditional view posits that radial glia, through asymmetric divisions, produce intermediate

progenitor cells (Miyata et al., 2004) which, in turn, in the embryonic subventricular zone (SVZ) expand in number before producing astrocytes (Noctor et al., 2004; 2008). On the other side, RG were also shown, after their last asymmetric division, to translocate and directly transform into astrocytes (Noctor et al., 2004). Eventually, astrocytes can be produced, during postnatal development, as a result of a massive *in situ* proliferative event of differentiated astrocytes, as described for the postnatal cortex (Ge et al., 2012).
In the following sections, the current knowledge on the mechanisms of astrogliogenesis in both the embryonic and postnatal brain will be discussed.

1.1.2.1 Temporal switch from neurogenesis to (astro)gliogenesis: who? When? How?

Like neurons, glial cells in the developing CNS derive from neuroepithelial cells that line the cerebral ventricle and the spinal canal. Indeed, at the beginning of neurogenesis, neuroepithelial progenitors differentiate into RG, which, in turn, act as primary progenitor cells and produce, according to a finely regulated time schedule, neurons, oligodendrocytes, astrocytes precursors and, eventually, transform into astrocytes themselves (Noctor et al., 2002; reviewed in Kriegstein and Alvarez-Buylla, 2009; reviewed in Mallamaci 2013).

The tightly regulated developmental interval during which RG along the VZ transit from neurogenesis to gliogenesis is commonly known as “gliogenic switch” and occurs, in mice, at around E12.5 in the developing spinal cord and between E16-E18 in the emerging cortex (Rowitch 2004; Ge et al., 2012). To allow this switch to happen, two distinct but related molecular processes must occur: the cessation of neurogenesis and the activation of gliogenesis. Neurogenesis must be inhibited to make these cells competent to express the gliogenic potential, possibly through a response to gliogenic cues. The pleiotropic Notch pathway was shown to inhibit neurogenesis and to be necessary for the generation of glial cells, through the induction of transcriptional repressors, such as the *Hes* genes, that in turn prevent the expression of proneural genes, such as the Neurogenins (reviewed in Louvi and Artavanis-Tsakonas, 2006; Gaiano et al., 2000). The binding of ligands such as Delta and Jagged to Notch receptors on the cell surface leads to the translocation in the nucleus of the Notch intercellular domain (NICD) which forms a transcriptional complex with the

coactivator Mastermind and the DNA-binding protein recombination signal binding protein for immunoglobulin kappa J region (RBPJ). Moroever, the Notch signalling pathway itself, together with the interleukin-6/Janus kinase/signal transducer and activator of transcription (IL-6/JAK/STAT), and the BMP2/4/small mothers against decapentaplegic (SMAD) pathways, are known as major inductive signals for astrocytic specification (Fig. 1.3; reviewed in Shimazaki and Okano, 2016). In detail, cytokines belonging to the IL-6 family, such as ciliary neurotrophic factor (CNTF), leukemia inhibitory factor (LIF), and cardiotrophin-1 (CT-1), activate the JAK family of non-receptor tyrosine kinases via binding to the receptor complex and induce the activation of STAT1 and STAT3 (Barnabe-Heider et al., 2005). In parallel, BMP2/4 bind to a tetrameric complex of type I and type II serine/threonine kinase receptors (BMPR1/2), thereby activating SMAD transcription factors. In turn, the BMP/SMAD and JAK/STAT pathways act synergistically via the co-operative action of SMAD1 and STAT3 through a complex formation with the transcriptional coactivator p300. All these signalling cascades result in the activation of astrocyte-specific genes, thereby inducing astrocytic specification. Nevertheless, before the acquisition of the gliogenic competence in the early neurogenic phase, the activation of BMP/SMAD and JAK/STAT pathways cannot induce differentiation of NSCs into astrocytes, rather, BMPs facilitate neuronal differentiation at this stage. Indeed, distinct promoter regions of glia-specific genes, including the *STAT3*-binging site, are epigenetically silent at first, due to high levels of DNA methylation and repressive histone marks, and the epigenetic modification of such genes is a prerequisite for the acquisition of the gliogenic competence (Molné et al., 2000; Mehler et al., 2000; Takizawa et al., 2001). Several transcription factors have been shown to be involved in this competence change in developing NSCs. At midgestation, the expression of a SRY (Sex determining Region Y)-box 9 (SOX9) increases and induces the expression of the transcription factor nuclear factor I (NFI) A, which is involved in the initiation of gliogenesis (Deneen et al., 2006; Kang et al., 2012). In turn, NFIA forms a complex with SOX9 to induce a subset of glial-specific genes, such as *Apcdd1* and *Mmd2*, and also mediates Notch signalling-induced demethylation of *GFAP* gene promoter in NSCs (Namihira et al., 2009). Eventually, *mir-153*, a CNS-specific evolutionally highly conserved miRNA, has been recently identified as modulator of the neurogenesis-to-gliogenesis switch by targeting NFIA and NFIB, which has also been shown to be required for astrogliogenesis. Indeed, overexpression of *miR-153* results in inhibition

of astrogliogenesis and maintenance of NPCs in an undifferentiated state in ESC-derived cultures and *in* vivo in the developing cortex. Conversely, inhibition of *miR-153* in early neurogenic progenitors induces precocious expression of NFIA/B and astrogliogenesis (Tzuyama et al., 2015). *MiR-17 and 106a/b (miR-17/106*) were also identified as critical regulators for neurogenesis-to-gliogenesis switch in neuroepithelial cells downstream of chicken ovalbumin upstream promoter-transcription factor I and II (COUP-TFI and COUP-TFII; Naka-Kaneda et al., 2014): *mir-17/106* decreases in a time-dependent manner in developing NPCs, leading to an increase of one of their targets, mitogen-activated protein kinase 14 (MAPK14), which, in turn, is essential for the acquisition of the gliogenic competence.

Importantly, the term "gliogenic switch" might be misinterpreted as the existence of progenitor cells that literally switch from being neurogenic to gliogenic. Nevertheless, all the aforementioned evidences of mechanistic parallels between neurons and glial cells do not necessarily imply this fate-switch occurrence, although some evidence has already been provided in both the cortex (Noctor et al., 2004) and the cerebellum (see section 1.3.4). Indeed, these distinct lineages could derive from independent neuron- or glia-committed populations of precursors, although their existence still needs to be demonstrated. Similarly, it is still a matter of debate whether bipotent progenitor exist that generate both astrocytes and oligodendrocytes. Indeed, pioneer studies on the rat optic nerve showed conflicting results: whereas *in vitro* experiments reported the existence of these progenitors (Temple and Raff, 1985), *in vivo* transplantation studies supported the opposite view (Espinosa de los Monteros et al., 1993; Groves et al., 1993). More recently, genetic fate mapping analyses of NG2-expressing cells, presumably the earliest glial committed cells arising from the germinal zones of the CNS (at around E14 in mice), have shown that these cells produce both oligodendrocytes and protoplasmic astrocytes of the ventral forebrain and spinal cord during embryonic but not postnatal development; moreover, contrary to the findings of the early culture studies, they have revealed that these same cells in white matter tracts, including the optic nerve, do not generate astrocytes (Zhu et al., 2008; Huang et al., 2014). Importantly, these fate mapping studies irreversibly labeled large numbers of cells, without allowing the distinction between a single multipotent progenitor giving rise to both cell types and a progenitor pool comprising distinct progenitor cells, each giving rise to only one subtype. Nevertheless, not even clonal

analyses have led to conclusive results. Indeed, by retrovirus-mediated clonal analysis in chicks, Rompani and Cepko revealed that retinal astrocytes and oligodendrocytes are produced by multipotent progenitors (Rompani and Cepko, 2010). On the other side, conditional genetic fate mapping of NG2 cells after a low level of Cre induction at E16.5 failed to reveal clusters containing both astrocytes and oligodendrocytes in the forebrain, suggesting that distinct subsets of embryonic NG2 cells, rather than bipotent precursors, are the source of these two cell subtypes (Zhu et al., 2011).

Likewise, whether distinct astrocyte subtypes derive from separate or common progenitors still has to be clarified.

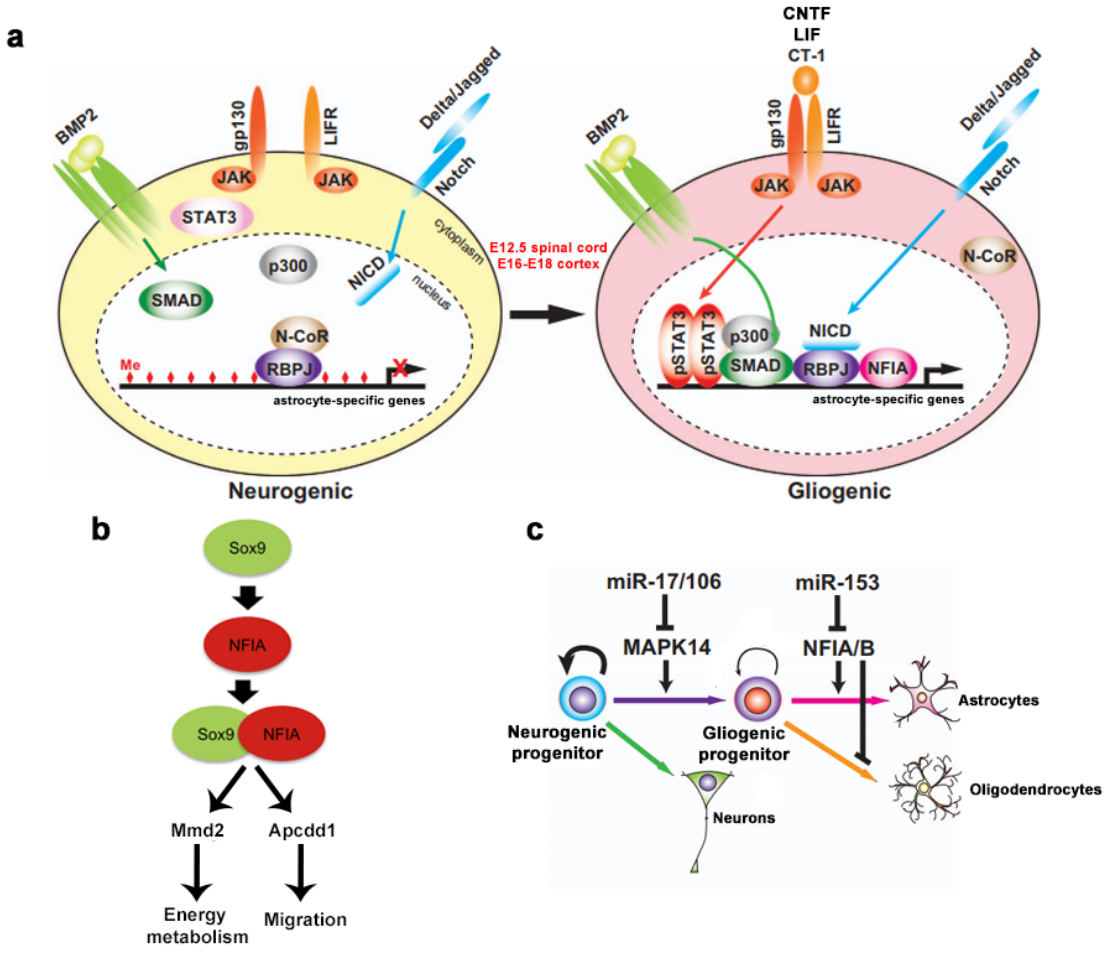

Figure 1.3. Regulation of astrocyte-specific genes transcription in NSCs in response to gliogenic signals. (a), In the early-neurogenic period, the promoters of astrocyte-specific genes in NSCs are highly methylated (diamonds in red) severely limiting access by transcriptional activators downstream of gliogenic signals. Moreover, a repressor complex containing N-CoR, a co-repressor, may associate with RBPJ, further contributing to this inhibition. After acquisition of gliogenic competence, NFIA induces demethylation of the

promoter, and the activation of JAK/STAT signaling via gp130/LIFR by increase of specific ligands (CTNF, LIF or CT-1) secreted from neurons leads to the formation of STAT3/SMAD/p300 complex on the promoter in co-operation with BMP signaling. The translocation of N-CoR to the cytoplasm may allow association of NICD to RBPJ, further resulting in de-repression and astrocytic specification. **(b)**, SOX9 induction of NFIA regulates the initiation of gliogenesis, in the first steps of neural stem cell commitment to the glial lineage. In turn, a SOX9/NFIA complex is formed which controls the induction of *Apcdd1* and *Mmd2*, astrocyte-specific genes which promote the migration of astrocyte precursors and energy metabolism, respectively. **(c)**, In the early neurogenic period, *miR-17/106* represses MAPK14 and inhibits the transition from neurogenic to gliogenic progenitors; *miR-153* represses NFIA/B expressions which in turn are essential for astroctytic specification. NFIA has also been shown to suppress oligodendrocyte differentiation (modified from Shimazaki and Okano 2016; Kang et al., 2012).

.

1.1.2.2 Embryonic patterning of radial glia and its influence on astroglial heterogeneity

Although RG appear as a very homogeneous population, they are regionally specialized to produce distinct neurons subtypes, and subsets of oligodendrocytes and astrocytes. Indeed, during early development, a finely regulated combination of morphogens (such as Shh, fibroblast growth factors - FGFs -, WNTs and bone morphogenetic proteins - BMPs -) controls the expression of homeodomain transcription factors, that further cross-repress each other, resulting in a precise patterning of the neural tube and cortical primordium along the dorso-ventral (D-V) axis. This forms tight boundaries from which different subtypes of neurons will emerge (reviewed by Muzio and Mallamaci, 2003; Mallamaci and Stoykova, 2006; Ulloa and Briscoe, 2007; Campbell, 2003) and which will be conserved also during gliogenesis, thereby influencing the generation of astrocytes subtypes (reviewed in Freeman and Rowitch, 201380 and Molofsky et al., 2012).

This was first demonstrated in the embryonic spinal cord, where timely regulated gradients of Shh ventrally and BMPs dorsally trigger the formation of the boundaries of the p0, p1, p2 and p3 domains, which will generate IN subtypes, and of the pMN domain, source of motor neurons (Jessell et al., 2000; Fig. 1.4 a,b). At around E12.5 in mice, RG in the ventricular zone of the spinal cord transit from neurogenic to gliogenic. Functional analyses of genes coding for the distinct domain-specific transcription factors allowed to investigate the spatial pattern of both oligodendrocytes and astrocytes generation. For instance, OLIG1 and OLIG2, two basic-helix-loop-helix (bHLH) proteins expressed in the pMN domain, were

shown to promote first a motor neuron and later a glial-cell fate, acting as transcriptional repressors of other transcription factors that might themselves be antagonists of motor neuron or oligodendrocyte development. As a result, *Olig1/2* double mutant and *Olig2* single mutant mice lack both motor neurons and oligodendrocyte precursor cells (OPCs) and develop a ventrally-expanded p2 domain, with more INs and astrocytes of the V2 class (reviewed in Rowitch and Kriegstein, 2010). This ventral expansion of the dorsal p2 domain is due to the further repression by OLIG1/2 of another bHLH protein, the *stem cell leukemia (SCL)* transcription factor, normally restricted to the p2 domain where it promotes the generation of astrocytes and, in turn, suppresses OLIG2 and oligodendrocytes production. Therefore, the cross-repressive interaction between the bHLH transcription factors SCL and OLIG2 is required to maintain astrocytes and oligodendrocytes production in the proper domains (Muroyama et al., 2005). Moreover, the combinatorial expression of PAX6 and NKX6.1 also specifies three molecularly distinct subtypes of ventral white matter astrocytes, which in turn can be identified by the combinatorial expression of the guidance molecules Reelin and SLIT1: (1) Reelin-positive VA1 astrocytes, the most dorsal, derive from progenitors within the p1 domain expressing PAX6 in the absence of NKX6.1; (2) VA2 astrocytes, both Reelin and SLIT1-positive, derive from the co-expression of PAX6 and NKX6.1 within p2 and are located in an intermediate white-matter domain; (3) VA3 astrocytes, expressing solely SLIT1 and deriving from NKX6.1-expressing progenitors in p3, are the most ventral (Hochstim et al., 2008).

On the whole, these evidences indicate that both astrogliogenesis and oligodendrogenesis in the ventral neural tube result from a finely regulated expression of homeodomain transcription factors that, cross-repressing each others, define the boundaries of restricted domains from which different subtypes of astrocytes and oligodendrocytes will emerge.

Similarly to the spinal cord, distinct gradients of expression of transcription factors along the rostro-caudal (R-C) and D-V axes result in the partitioning of the neuroepithelium into progenitor domains that lead to patterned origins for most types of neurons (Fig. 1.4 c,d). In detail, the developing forebrain can be divided into four organizing centers: a dorsal hem, source of BMPs and WNTs; a ventral center, source of Shh; and two rostral regions which are the sources of FGF8 or transforming growth factor-α (TGF-α) and FGF7, respectively. This subdivision results in the regionalized expression, within the germinal territories, of Neurogenin (NGN) 1, NGN2 and GLI3 dorsally and of ASCL1, Distal-Less

Homeobox (DLX) 1 and DLX2 ventrally. As a result, excitatory pyramidal cells are produced from the dorsal telencephalon, whereas distinct classes of INs are derived from specific progenitor domains within the ventral telencephalon (Hoch et al., 2009). After the gliogenic switch, astrocytes and oligodendrocytes are produced from the very same domains. During embryonic development, the dorsal region, including the cortex, is the source solely of astrocytes, whereas the ventral regions, including the lateral and medial ganglionic eminences (LGE and MGE, respectively) and the pre-optic area, are the sources of astrocytes and of sequential waves of OPCs, that will only afterwards reach the cortex. Indeed, a first wave of oligodendrocytes derives at around E12.5 from NKX2.1-expressing precursor cells located in the ventral telencephalon (MGE) and arrives in the cortex at around E16 in the mouse. Here, will later on migrate also the secondary waves of oligodendrocytes, produced at around E15 from GSH2-expressing precursor cells in the LGE and/or MGE. Only at birth, another wave of cortical oligodendrocytes arises, this time from EMX1-expressing precursor cells from the dorsal cortex itself. Interestingly, most of the ventral early-generated oligodendrocytes disappear after birth, so that the majority oligodendrocytes present in the adult cortex appear to be derived from more dorsal progenitors (reviewed in Kriegstein and Alvarez-Buylla, 2009).

On the whole, the onset of gliogenesis in both the forebrain and spinal cord appears to be a both spatially and timely regulated process, in which dedicated RG in each domain of the above described germinal regions make their switch in their due time to give rise to specific subsets of cells. Nevertheless, under the astrocytes perspective, whether subsets of astrocytes deriving from diverse and segregated domains also show distinct molecular and functional properties still needs to be fully elucidated, as well as the degree of heterogeneity of those cells sharing the same spatial origin.

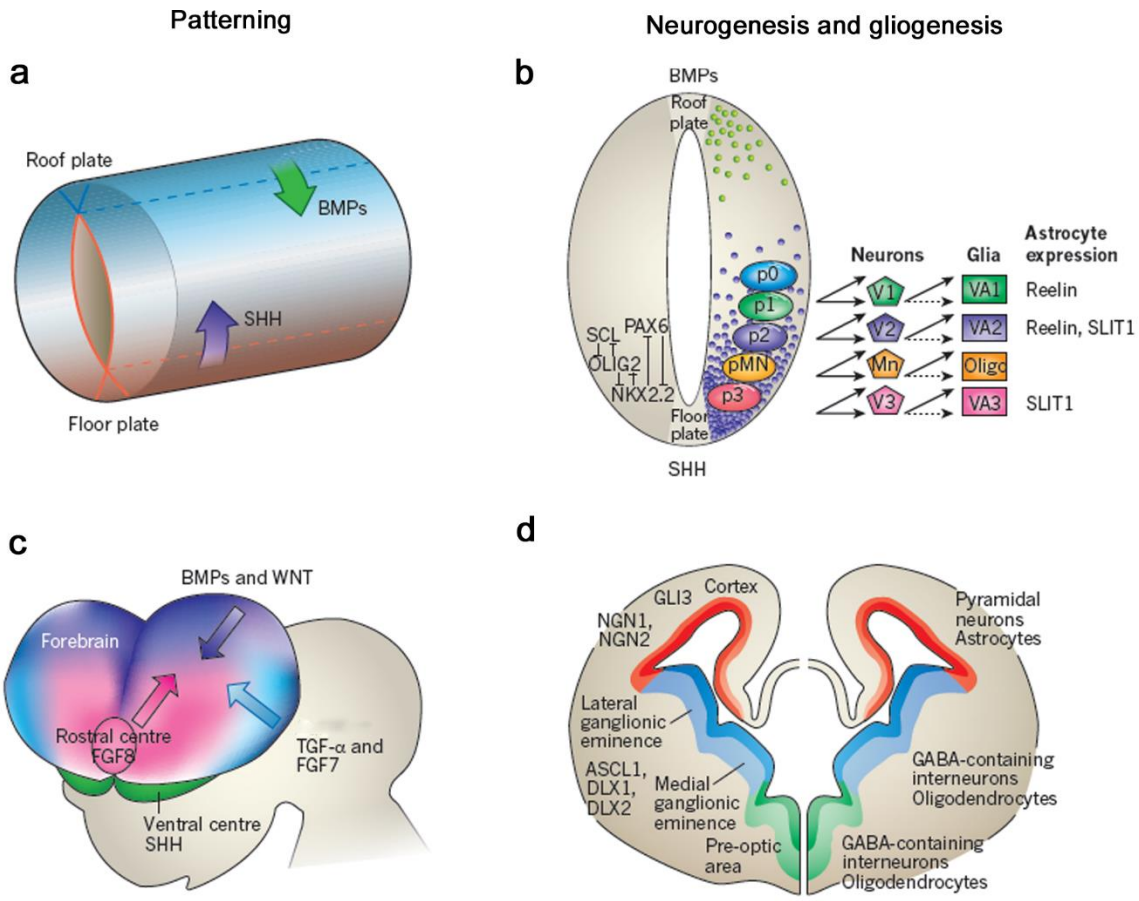

Figure 1.4. Patterning of the neural tube and forebrain. (**a**) The primitive neuroepithelium of the neural tube is patterned by organizing signals, emanating from the ventral floor plate (such as SHH, purple) and roof plate (BMPs, green). (**b**) Cross-sectional view of the neural tube. Progenitors of motor neurons and interneurons are formed within distinct regionally restricted domains of the ventral neural tube: the p0, p1, p2 and p3 domains for interneuron subtypes, and the pMN domain for motor neurons. Shh (whose gradient is shown in purple circles) regulates the expression of NKX2.2, OLIG2, PAX6 and SCL ventrally. After the gliogenic switch, embryonic OPCs are derived mainly from the pMN domain. Three astrocyte subtypes have been identified: VA1 astrocytes (which express PAX6 and reelin, derived from p1) are the most dorsal; VA3 astrocytes (which express NKX6.1 and SLIT1, derived from p3) are the most ventral; and VA2 astrocytes (which express PAX6, NKX6.1, reelin and SLIT1, derived from p2) are located in an intermediate white-matter domain. (**c**) Organizing centres of the forebrain. These include a dorsal source of BMPs and WNTs (purple); a ventral centre (green), source of SHH; and two rostral regions, which are sources of FGF8 (pink), and transforming growth factor-α (TGF-α) and FGF7 (blue), respectively. (**d**) Coronal view of the embryonic (~E14.5) forebrain shows its division into dorsal and ventral regions that are specialized for producing different neuron and glial-cell types. The dorsal region includes the cortex (red), source of pyramidal neurons and astrocytes. The ventral region includes the lateral and medial ganglionic eminences (blue) and the pre-optic area (green), sources of GABAergic interneurons and oligodendrocytes. Transcription factors that are associated with dorsal (NGN1, NGN2, GLI3) and ventral (ASCL1, DLX1, DLX2) patterning and cell fate specification are indicated (modified from Rowitch and Kriegstein, 2010).

Once specified, astrocytes are supposed to migrate from their domains of origin and colonize their final destinations across all areas of the CNS, before starting the process of terminal differentiation. Distinct modes of migration can be postulated: according to a multimodal fashion, following both tangential and radial trajectories, astrocytes from distinct origins might intermix through the tissue; alternatively, they might migrate in restricted segmental fashion that would spatially resemble their domains of origin. Moreover, astrocytes dispersion within the expanding tissue might also result from a secondary *in situ* amplification of intermediate progenitors. Sophisticated fate-mapping techniques, exploiting various regionally expressed Cre recombinase lines or clonal labelling through viral vectors, allowed to perform lineage tracing of RG and their astrocyte progenies in distinct domains and to conclude that astrocytes in all domains of both the spinal cord and forebrain maintain a strictly segmental distribution through a unique event of migration along RG trajectories (Tsai et al., 2012). The same authors also showed that, even after injury or ablation of astrocytes in specific domains, viable astrocytes of adjacent domains do not show any secondary tangential migration.

Thus, in contrast to highly migratory oligodendrocytes and to many neurons, astrocytes can be defined as the least migratory neuroepithelial derivative in the CNS: their final location can faithfully predict their domain of origin. This raises the possibility that astrocytes may become diversified within distinct domains of the CNS to exert diverse region-specific functions, therefore further increasing the degree of complexity of astroglial heterogeneity.

The molecular and cellular processes that regulate astrocyte precursors segregation *in vivo* are still poorly defined: the aforementioned spatial heterogeneity could be specified by cell-intrinsic mechanisms, derived from the interaction between pattering mechanisms and pro-glial transcription factors, and/or by cell-extrinsic mechanisms, such as neuron-derived signals that could regulate astrocytes development according to their specific developmental needs. Although no definitive data are yet available to solve this issue, Molofsky and colleagues (Molofsky et al., 2014) have suggested that astrocytes positional identity might be at least in part cell intrinsically defined. Indeed, besides showing that the secreted molecule *Semaphorin 3a* (SEMA3A) is selectively expressed in ventral but not dorsal astrocytes of the postnatal spinal cord and is necessary for the survival of α- but not of the adjacent γ-motor neurons *in vivo*, the authors performed *in vitro* co-culture

experiments to address whether this protein acted directly on motor neurons without other extrinsic intermediates, and observed that the SEMA3A-dependent regional properties of astrocytes (such as the inhibition of neurite outgrowth and complexity) were retained independently from local environmental cues. These results suggest that astrocytes allocation in specific domains is regulated by intrinsic, regionally-encoded gene expression profiles and, in turn, translates into a region-specific regulation of neuronal survival, connectivity and functional activity. Nevertheless, these observations do not exclude the existence, in parallel, of cell-extrinsic stimuli deriving from the cross-talk with neuronal neighbours, which therefore need to be further investigated.

1.1.2.3 Biphasic amplification of astroglial progenitors

A unique feature of the development of the astrocyte lineage in both the spinal cord and the forebrain is a wave of proliferation of intermediate progenitor cells occurring after their migration to populate the nascent parenchyma. Indeed, the total number of astrocytes in the mouse brain goes through a 6 to 8-fold increase during the first three weeks of postnatal development (Bandeira et al., 2009).

The presence of proliferating glial cells within the mouse cortex was first reported half a century ago, in studies involving [^{3}H]thymidine incorporation in the DNA during postnatal development (Smart et al., 1961). These data suggested that the big number of astrocytes found in the adult brain was not only due to NSCs proliferation, but also to the capability of astroglial progenitors to divide outside the VZ. Nevertheless, to what extent this local proliferation contributed to postnatal astrocyte production was still unknown, due to difficulties in distinguishing cells generated locally from those derived from elsewhere. Indeed, two studies have recently corroborated those old results in both the forebrain and spinal cord, by pulsing experiments with the thymidine analogue BrdU (Bromodeoxyuridine) at different developmental time points, thus unequivocally demonstrating that astrocytes precursors retain a proliferative capability even after leaving the VZ (Ge at al., 2012; Tien et al., 2012). In detail, a comprehensive study in the cortex fate mapped astrocyte progenitors through Brdu-pulse labelling, retroviral labelling and live imaging, demonstrating that local, symmetric, divisions generate about half of the mature cortical astrocytes (Ge et al., 2012). An analogous study in the spinal cord found that the

proliferation of ALDH1L1-expressing astrocyte progenitors peaks at two distinct time points, first at E14.5, when RG are still lining the ventricle, then at E16.5, in the local parenchyma, where additional rounds of cell division occur until postnatal day (P) 4 (Tien et al., 2012). This timing for astrocytes proliferation in the spinal cord is earlier than in the forebrain, where local amplification mostly occurs postnatally, thus mirroring the caudal to rostral pattern of maturation of the CNS.

Therefore, these data demonstrate that astrocytes development differs a lot from neuronal development, in which neuroblasts are already post-mitotic after birth. Moreover, they suggest that astrocyte proliferation is a bimodal event, starting with a wave of asymmetric divisions from RG before migration, which, in addition to self-renew RG, generate astrocyte-restricted progenitors (called both "intermediate astrocyte precursors" and "pioneer precursors"), intended to migrate to their final positions and, once there, to symmetrically amplify generating more astrocytes. No molecular markers, however, are still available to distinguish cells in these distinct developmental stages.

Seeking for the molecular mechanisms regulating this bimodal way of proliferation, Li and colleagues found that the Raf/MEK/ERK signaling pathway in the cerebral cortex is critical for glial specification and for both waves of proliferation (Li et al., 2012). Indeed, conditional deletion of MEK1 and MEK2 during the gliogenic phase dramatically reduced the numbers of mature glia postnatally, and modestly increased the numbers of later born neurons. Multiple pathways were shown to be involved, including the transcription factor ETV5/ERM, which has been implicated in glial differentiation in the drosophila eye (Franzdóttir et al., 2009). Consistent with this, conditional loss of function of the upstream BRAF during the gliogenic period decreased astrocyte proliferation in the developing spinal cord, and activation via the V600E oncogenic mutation promoted it (Tien et al., 2012). Moreover, in the developing cerebral cortex, both the Egf- receptor (EGFR) and the secrete ligand FGF9 were described to promote the proliferation of astrocyte-committed progenitors (Viti et al., 2003; Lum et al., 2009), whereas the transcription factor SIP1 antagonizes it through FGF9 repression (Seuntjens et al., 2009). Furthermore, the transcription factor EMX2, known to control several processes during cortical development (Mallamaci et al., 2000; Muzio et al., 2002; 2005) and whose strong expression in the early neurogenic pallium drops concomitantly with the decline of neurogenesis (Mallamaci et al., 1998), was also shown to inhibit gliogenesis *in vitro* (Brancaccio et al., 2010), acting as key

modulator of the proliferation rates of cortical astrocyte-committed progenitors, as later demonstrated both *in vitro* and *in vivo* (Falcone et al., 2015). Indeed, EMX2 expression in cortical stem cells inhibits astrogliogenesis during the neurogenic phase, by cell-autonomously downregulating both EGFR and FGF9 and therefore leading to a decreased proliferation of astrocyte-committed progenitors (Falcone et al., 2015).

Nevertheless, it is not clear whether the mechanisms identified so far act to regulate symmetric versus asymmetric divisions. Moreover, the second, local, wave of amplification could be also regulated by extrinsic environmental factors, which might "instruct" resident progenitors to proliferate in response to specific needs.

1.1.2.4 The staging of astrocyte differentiation: the missing markers

In the past years, several markers were employed in astrocyte developmental studies that might be used to broadly define the molecular signature of astrocyte precursors at the distinct steps of maturation. Nevertheless, none of them is stage-specific and, rather, they are broadly expressed over multiple steps of astrocytes' development, from either neurogenic to gliogenic RG and/or through the distinct stages of astrocyte maturation until its completion (See table 1).

For instance, the transcription factor NFIA, which was found to be both necessary and sufficient for embryonic gliogenesis (Deneen et al., 2006), is initially expressed in all gliogenic RG that occupy the VZ, and, as development progresses, its expression is maintained during intermediate precursors' migration and until astrocytes become mature. A similar pattern of expression is that of GLAST, covering all the astroglial lineage starting from RG when they are still neurogenic. In addition, these markers are not fully astrocyte-specific: they were shown to be expressed also in oligodendrocyte precursors populations until late embryonic stages, and NFIA can also label mature motor neurons (Kang et al., 2012). Moreover, SOX9 was also shown to regulate early gliogenesis through its regulation of NFIA induction and its association with NFIA itself during subsequent developmental stages (Kang et al., 2012). Again, however, the expression of this transcription factor is maintained through adulthood, as indicated by a very recent paper, in which FACS-purified adult astrocytes have been subjected to RNA sequencing and *Sox9* has been identified as a novel nuclear marker specific, in the adult, for mature astrocytes in the major areas of the CNS (Sun et al., 2017). Therefore, although its importance as a

pan-astrocyte selective marker, this transcription factor does not demarcate the transition from developing to mature astrocytes. On the other side, Nestin and Vimentin were shown to be expressed by RG but not mature astrocytes (or at least by few, such as Vimentin-expressing BG in the adult cerebellum; Gilyarov, 2008; Shaw et al., 1981). Nevertheless, both these proteins are expressed already at the stage of neurogenic RG, therefore not allowing to distinguish between the neuronal and glial lineages.

Other markers traditionally used to label and study astrocyte intermediate proliferating precursors are the Brain Lipid Binding Protein (BLBP) and the Fibroblast Growth Factor Receptor 3 (FGFR3), which, however, are also expressed during the neurogenic stages, making them less astrocyte-specific (Anthony et al., 2004; Pringle et al., 2003; Owada et al., 1996). On the other side, the folate metabolic enzyme ALDH1L1 was shown to be expressed by astrocyte intermediate precursors (Anthony et al., 2007) but, at the same time, was identified as a broad adult astrocyte-specific marker, not expressed in other CNS cell types, and reporter mice as well as Cre lines exploiting its promoter confirmed its utility in the context of specific mature astrocyte labelling (Cahoy et al., 2008). Eventually, the intermediate filament protein GFAP, broadly exploited to study the astrocyte lineage, is first expressed by primates' RG before they become gliogenic, and it is then maintained in astrocytes through adulthood (Levitt et al., 1980). On the other side, however, RG of both chick and rodents lack GFAP, whose expression only starts much later in development and gradually increases to reach the adult pattern of mature astrocytes (Bignami et al., 1974; Pixley et al., 1984). Therefore, GFAP expression appears to be species-specific and, as that of all the aforementioned markers, hardly exploitable to follow the transition from neurogenic to gliogenic RG as well as of astrocyte progenitors through their distinct developmental steps.

Importantly, in the last years, gene-expression profiling on astrocyte precursor populations in the spinal cord have eventually shed more light on the distinct patterns of gene expression associated with diverse stages of astroglial development. Indeed, in a first study published in 2013, Molofsky and colleagues (Molofsky et al., 2013) performed a microarray analysis of highly purified flow-sorted populations of E13.5, E14.5 or E17.5/E18.5 ALDH1L1-positive spinal cord cells. Performing gene coexpression analyses of the obtained datasets, they identified three temporally distinct patterns ("modules") of gene expression, highly enriched for genes associated with astrocyte development and temporally correlated with

early, middle, and late embryogenesis. Moreover, the screening for functional classes of genes suggested different functional roles for glia at different developmental stages, such as axon guidance, active biosynthesis and modulation of neuronal signalling and synaptic plasticity in early, middle and late modules, respectively. Eventually, the authors identified NFE2L1 as a novel gliogenic transcription factor, promoting astrocyte and oligodendrocyte maturation as part of a Sox9 regulatory program. Similarly, Chaboub and colleagues (Chaboub et al., 2016) have very recently performed an analogous gene expression profiling of astrocyte populations from E12.5 to P7 in the spinal cord, exploiting an intersectional approach that combined the GLAST-*dsRed* reporter mouse line with the antibody CD15, widely used for neural precursor cell isolation but also expressed by astrocytes. In this way, they have revealed four distinct stage-specific gene induction patterns that could be broadly categorized, based on their GO properties, into two functional stages of lineage development: proliferation/migratory and metabolic/physiological. Importantly, this biphasic wave of functional gene expression in the developing mouse spinal cord is consistent with recent *in vitro* studies performed on human astrocytes, suggesting that they also contain two stages of lineage development (Zhang et al., 2016). Moreover, Chaboub and colleagues also have identified ASEF, TOM1L1, MGFE8, and GPR37L1 as new markers of the intermediate stages of astrocyte development and through functional studies on one of these genes, *ASEF*, revealed that mice lacking it exhibited impaired astrocyte differentiation during development.

Of note, both these datasets represent a very powerful and ready-to-use resource for the further discovery of genes involved in distinct stages of gliogenesis. Nevertheless, similar information should be obtained also for CNS regions other than the spinal cord, in order to eventually and unequivocally identify universal stage-specific markers along the astroglial lineage that, alone or in combinations, might be thereafter exploited to target astrocyte progenitors at the diverse developmental stages and precisely define their contribution to all aspects of mature astrocytes' heterogeneity.

1.1.2.5 Morphological maturation of astrocytes and acquisition of mature markers expression

Mature astrocytes, regardless of their anatomical location in the grey or white matter, typically occupy large and non-overlapping domains, composed of numerous branches and fine processes. These fine processes, termed “peripheral astrocyte processes” (PAPs), are usually distant from the soma and occupy about 80% of the astrocytes surface area, hosting various membrane proteins such as ion channels, ligand receptors, and transporters and extensively contacting synapses. Therefore, they are considered primary sites for active astrocyte and neuron signaling (Reichenbach et al., 2009). Interestingly, although most astrocytes are known to be produced during the first postnatal week in mice, the complete maturation of these fine processes only occurs in the following 3-4 weeks, in parallel with the induction in the maturing astrocytes of several important astroglial genes, such as *GLT1*, connexins *(Connexin 43* and *30*) and potassium channels (like *Kir4.1*), which indeed represent some of the most characteristic and important functions of astrocytes in the CNS. Thus, astrocytes undergo dramatic morphological and molecular changes during their developmental maturation (Yang, Higashimori and Morel, 2013). Nevertheless, the mechanisms underlying these changes remain largely unknown. Extrinsic signals like CT-1 (Barnabé-Heider et al., 2005) secreted by early-differentiated neurons are likely to be implicated in early astrocyte fate specification. This hypothesis is supported by the evidence that GLT1 and Connexins 43/30, normally expressed at low levels (GLT1) or absent (Connexins) in cultured astrocytes, are highly induced in a dose-dependent manner when astrocytes are co-cultured with neurons (Yang et al., 2009; Koulakoff et al., 2008). Moreover, cultured astrocytes show, in general, a gene profile much more similar to that of immature rather than mature astrocytes *in vivo* (Cahoy et al., 2008), further suggesting that neuronal signaling may play important roles in their maturation. Indeed, gene expression studies in acutely isolated astrocytes of the brain revealed that developing astrocytes express several neurotransmitter receptors (Lovatt et al., 2007; Cahoy et al., 2008), allowing them to receive neuronal signals. In addition, although there is still not direct evidence that neuronal activity can modulate the PAPs formation during astrocyte maturation, direct application of glutamate was shown to induce rapid filopodia motility in cultured astrocytes (Lavialle et al., 2011). Therefore, it is likely that both secreted neuronal signals, such as activity-dependent neurotransmitters and small proteins like CT-1, and

contact-dependent signaling, such as the Notch-JAG1 interaction described to be necessary for BG maturation (Eiraku et al., 2005; this topic will be more deeply addressed in section 1.3.5), can play important roles in astrocyte developmental maturation. Molecular mechanisms for astrocyte maturation, especially downstream pathways that mediate potential neuronal signaling, are essentially unknown. As various pathways/mechanisms involved in early astrocyte specification have already been characterized (see above), it would be interesting to test whether any of these pathways also regulate developmental maturation of astrocytes at a later stage.

As discussed above, the molecular maturation of astrocytes implies the induction of several important astroglial genes. Nevertheless, molecules for the definitive identification of mature astrocytes are still scarce and imperfect (see table 1.1). Indeed, several markers are known at this purpose, including GFAP, S100β, Aldolase C, GLAST, GLT1, and aquaporin 4, Vimentin, Glutamate synthetase, Kir4.1 and Connexins 30/43 but neither they are uniformly expressed in all astrocytes (as GFAP, see section 1.1.1.2) nor they fully label both the cell body and all processes (as aquaporin 4, which is localized to astrocytes endfeet). In the last years, however, some improvements were made in this field. Indeed, as reported in the previous section, the folate metabolic enzyme ALDH1L1 (which is although also expressed in some oligodendrocytes; Yang et al., 2011) and the nuclear marker SOX9 have been recently identified as broad adult astrocyte-specific markers; on the other hand, distinct molecules were shown to be differentially expressed by distinct mature astrocytes subtypes across and within diverse brain regions (see section 1.1.1.2). Nevertheless, despite these progresses in this context, a comprehensive identification of other reliable, astrocyte-specific, mature pan-astrocyte and subtype-specific markers is still needed.

MARKER	STAGE(S)	CAVEAT(S)
NFIA	Gliogenic switch, intermediate precursors, mature astrocytes	Also expressed in oligodendrocyte precursors and mature motor neurons
GLAST	Embryonic RG, gliogenic switch, intermediate precursors, mature astrocytes (high in BG and low in velate astrocytes of the cerebellum)	Also expressed in some oligodendrocyte precursors
SOX9	Gliogenic switch, intermediate precursors, mature astrocytes	Also expressed during neurogenic stages in RG and oligodendrocyte precursors

Nestin	Embryonic RG	Also expressed during neurogenic stages in RG; also expressed in BG and astrocyte precursors in developing postnatal cerebellum
Vimentin	Embryonic RG and few mature astrocytes (BG in the cerebellum)	Also expressed during neurogenic stages in RG
BLBP	Intermediate precursors and some mature astrocytes	Also expressed during neurogenic stages in RG
FGFR3	Intermediate precursors and some mature astrocytes	Also expressed during neurogenic stages in RG and in some oligodendrocyte precursors
ALDH1L1	Intermediate precursors and broadly in mature astrocytes	Expressed early in RG that may be still neuron-committed; also labels some oligodendrocytes
GFAP	From embryonic RG to adult astrocytes in primates; mature astrocytes in chick and rodents	Expressed in BG before they become gliogenic (in primates)
Aldolase C	Intermediate precursors or mature astrocytes	Also expressed in Purkinje cells
CD44	Intermediate precursors and mature astrocytes	
GDF10/BMP3B	Embryonic gliogenic RG of the cerebellum, developing and mature BG	
Glutamine synthase	Late precursors and mature astrocytes	
S100B	Mature astrocytes	Also labels some oligodendrocyte progenitors
S100A4	Mature (fibrous) astrocytes	
GLT1	Mature astrocytes (the splice variant exon 9-skipping form primarily in fibrous astrocytes)	
Connexin 30	Mature grey matter astrocytes	
Aquaporin 4	Mature astrocytes (high expression in velate astrocytes of the cerebellum)	Only localizes to astrocytes endfeet
Kir4.1	Mature astrocytes (high expression in cortical astrocytes of the cerebellum, low in WM astrocytes)	

Table 1.1. Markers of astrocytes and their progenitors. This table summarizes some of the markers currently known to label distinct stages of astrocyte maturation and mature astrocytes. When information is available, subtype-specific expression of these markers is highlighted as well as the caveats in exploiting such molecules to study the mechanisms of astrocytes development (modified from Molofsky et al., 2012; Chaboub and Deneen, 2013; for detailed references on each marker see text).

As discussed in the previous sections, astrocytes in the mammalian CNS display a huge inter- and intra-regional morphological, molecular and functional heterogeneity. Nevertheless, this diversity is very far from being fully unveiled and, currently, is still under deep investigation. Similarly, the mechanisms through which this diversity is shaped during development are still undetermined. Several distinct studies have been addressing, in the last years, this topic and will be therefore reported in the next section.

1.2 Approaches to tackle the ontogenesis of astrocyte heterogeneity: focus on lineage studies

The investigation of the vast astroglial heterogeneity and of how it takes shape during development has become an ever-growing field of research in the last years. Indeed, as described above, astrocytes' diversity is critical for brain physiology and dysfunctions. Therefore, a precise understanding of astrocyte development is crucial to fully define their heterogeneity and could help understanding and treating a variety of developmental disorders, including, for example, neuropsychiatric diseases. To this aim, lineage cell tracings, in parallel with the above discussed molecular analyses, represent a very powerful way to define the origin, fate and behaviour of selected cells in specific tissues or organisms.

Several tools were developed in the past to investigate the ontogenesis of neuronal lineages, and were applied to similarly track the onset of astroglial diversity. Nevertheless, some limitations in the so far developed tools and approaches make the achievement of a conclusive knowledge on this topic very challenging. These issues will be therefore discussed in the next sections.

1.2.1 Lineage tracing and clonal analyses applied to astrogliogenesis: potentials and limitations

Lineage tracings include a broad range of approaches, including clonal analyses that allow to analyse the fate of single progenitors and track their whole progeny. Some of these lineage tracing approaches, successfully employed to track the ontogenesis of the well-defined neuronal diversity, have been applied in the last years to similarly investigate the astroglial lineage, yet with some not negligible limitations and leading to inconclusive results. This is mainly due to the still incomplete, although rapidly growing, knowledge about the diversity of astrocytes, which makes, by definition, very hard to fully understand how this diversity is built.

Viral labelling approaches.

In order to randomly target pioneer cells and retrospectively infer their fate, defective retroviral infections can be used to stably introduce a single reporter gene (such as *LacZ*, *alkaline phosphatase*, *GFP*s and other fluorescent proteins, or *Luciferase*) into embryonic progenitors (Turner and Cepko, 1987; Turner et al., 1990). To this aim, small amounts of virus in each injection allow to trace single and spaced progenitor cells, whose descendants can then be followed based on their positional identity: following infection, a single DNA copy of the defective recombinant retrovirus is integrated into the host genome as a provirus, without allowing secondary infections and leading to strictly cell-autonomous labelling, and is stably transmitted to all descendants. This tool was largely used to trace both neuronal (Noctor et al., 2001) and glial lineages in the cortex (Zerlin et al., 2004). Nevertheless, Zerlin and colleagues (Zerlin et al., 2004) did not manage to selectively label astrocyte-committed progenitors, since some of their clones contained both astrocytes and oligodendrocytes. Similarly, Costa and colleagues (Costa et al., 2009) performed *in utero* transductions at distinct neurogenic phases with low titers of replication-defective retroviral vectors encoding different fluorescent proteins (GFP and RFP). This technique was indeed very useful to understand when the glial fate restriction occurs and to demonstrate the existence of bipotent (neuron-glial) progenitors in the early developing cortex. Nevertheless, as intrinsically defined by the aim of that study, retroviral infection was again not selective for astrocyte precursors and appears therefore hardly applicable to target them at distinct developmental stages. Several attempts were made in the past to

direct viral vectors towards astrocytes and their progenitors, but they did not lead to definitive results, with incomplete targeting and with a residual transduction of non-astrocytic cells. Among them, a LCMV-pseudotyped lentiviral vector displaying a particular tropism for astroglial cells was developed (Stein et al., 2005; Buffo et al., 2008), which is although able to infect also multipotent NSC with an astroglial phenotype at early developmental stages (Parmigiani et al., 2015). Therefore, additional studies are still needed to fully characterize the tropism of these vectors and, exploiting the growing knowledge about the molecular diversity of astrocytes and their precursors, to develop more specific viral tools. In this regard, the tropism of viral vectors could be changed according to the interaction of the viral surface proteins with cell-specific receptors, limiting transgene expression with specific promoters or blocking transgene expression in unwanted cells. Some other restrictions in the exploitation of this tool are broadly related to its technical limitations. First, recombinant murine retroviruses such as the murine leukemia virus (MLV) can integrate in the host genome only when the target cell undergoes mitosis and, therefore, do not infect post-mitotic or resting cells, resulting in non-uniform targeting of the progenitor pool. Second, the intra-uterine injection of the virus in mice can damage the embryo and lead to inflammatory responses. Third, the expression level of the reporter gene depends on the site of integration of the provirus in the host genome and this expression can also be silenced by a variety of epigenetic repression mechanisms. Last, since independent virions can infect nearby dividing cells, this method does not always allow the identification of sibling relationships and is not applicable to those areas where a great deal of migration occurs along distinct paths and the progenies of distinct clones intermingle. The “CHAPOL” retroviral vector library overcomes this last issue, being based on a library of viruses in which each member encodes a histochemical reporter gene (such as *lacZ*) and carries a unique oligonucleotide tag, which can be eventually recognized by PCR after single cell isolation (Golden et al., 1995; Fuentealba et al., 2015). This approach leads to the unambiguous identification of clones, yet, it maintains all the aforementioned technical limitations associated to retroviral injections, together with the practical difficulties of isolating single cells from the tissue.

Genetic fate mapping approaches.

The development of transgenic mice and cell-specific and/or Tamoxifen(Tx)-inducible variants of Cre recombinases provided a new approach to label progenitor cells and

perform prospective lineage analyses without a need for invasive manipulation of the embryos (reviewed in Legué and Joyner, 2015). In this approach, the marking of the selected progenitor cells involves a permanent change in their DNA that is transmitted to the whole progeny. To do so, a Cre mouse line, in which the expression of the Cre recombinase (often in its Tx-inducible variant "CreERT2") is driven by a cell-specific promoter opportunely chosen to label the progenitor pool of interest, must be crossed with a reporter mouse line such as R26R-*lacZ* (Soriano, 1999) or R26R-YFP (Srinivas et al., 2001), so as to allow the constitutive expression of the GFP or lacZ proteins through the Cre-LoxP system and trace the progeny over time. However, the reliability of this tool is limited when a constitutively active form of Cre is used: the specificity of cell-labelling is strictly dependent upon the regulatory sequence chosen to drive the recombinase expression and can be hampered by the physiological changes of promoter activity during development. The use of an inducible variant of Cre recombinase overcomes this issue, leading to a genetically and timely-controlled recombination event, which occurs only over an approximately 24-h time period after Tx administration. At this purpose, low doses of Tx can be applied to determine cell lineages (Magavi et al., 2012; Gao et al., 2014), however, recombination is less efficient than that driven by constitutive Cre, thus leading to a mosaic marking of the progenitor pool. Genetic fate mapping experiments were indeed used to target RG in the distinct progenitor domains in both forebrain and spinal cord and allowed to investigate how astrocytes disseminate from their sites of origin within the VZ (see section 1.1.2.2.). Nevertheless, they were not specific for the astroglial lineage, since the exploited promoters are active in RG before the gliogenic switch, and they did not shed light on clonal relationships among cells. Indeed, with this method, the whole population of pioneer progenitors is equally labelled, not allowing to perform a proper clonal analysis at the single cell level. Moreover, these genetic approaches are still hardly applicable to the investigation of the ontogenesis of astroglial heterogeneity, since they imply a previous knowledge about precursors-specific markers that, for the astroglial lineage, is still not available (see section 1.1.2.4). In the next future, profiling of astrocyte progenitors at distinct developmental phases may lead to the identification of stage-specific genes useful to generate new mouse lines for genetic fate mapping and tools for conditional knockout and, therefore, to understand the relative contribution of specific subsets of progenitor cells in the ontogenesis of astroglial diversity.

Genomic integration of fluorescent reporters.

In order to differentially label single progenitor cells and uncover clonal relationships *in vivo*, the expression of several reporters was exploited by more recent approaches. Among them, the mosaic analysis with double markers system (MADM; Zong et al., 2005) relies on two reciprocally chimeric marker genes, each containing the N terminus of one marker and the C terminus of the other marker interrupted by a loxP-containing intron, that have been knocked into the same locus on homologous chromosomes: Cre-mediated interchromosomal recombination regenerates the functional marker genes on a pair of chromatids, whose X or Z segregation (i.e. the recombinant chromatids segregate to different cells or congregate to the same cell, respectively) can thereafter generate distinct combinations of labelled cells. Nevertheless, this technique cannot be considered fully appropriate to analyse clonal relationship, provided that isolated and stochastic recombination events occur to label too few clonally related cells. On the other side, other techniques similarly based on genetic multicoloured cell labelling, allow to perform larger and more reliable clonal analyses. In detail, the Brainbow (Livet et al., 2007) transgenes exploit the Cre/lox recombination to create a stochastic choice of expression between three-to-four fluorescent proteins (XFPs) both *in vitro* and *in vivo* in transgenic mice, where their tandem integration yields up to ten combinatorial XFPs expression, thereby providing a way to distinguish adjacent neurons and visualize other cellular interactions. This tool was further exploited to create a stochastic multicolour reporter mouse line named "Confetti" (Snippert et al., 2010), by inserting the Brainbow-2.1 construct, encoding four fluorescent proteins driven by the strong CAG promoter, into the Rosa26 locus. Upon Cre recombination, a loxP-flanked Neomycin (Neo) cassette is removed and the multicolour construct recombines to result in four possible fluorescent outcomes. The murine Brainbow-2.1 construct was also exploited to generate three Drosophila melanogaster variants, called Flybow (Hadjieconomou et al., 2011), in order to study neural network architecture and formation in this organism. Eventually, the three lentiviral gene ontology (LeGO) vectors (Weber et al. 2011) coding for red, green or blue (RGB) fluorescent proteins, when simultaneously transduced in selected cells, similarly result in the generation of numerous random combinations of colours and allow the analysis of clonal cell fates both *in vitro* and *in vivo*. Nevertheless, these techniques rely on the combinatorial expression of up to four fluorescent reporters and may, therefore, lead to misinterpretations in clonal

relationships (the so called “splitting” and “lumping” errors, i.e. when siblings are interpreted as members of different clones or when the descendants of distinct progenitors are considered clonally related, respectively). Recently, the non-viral PiggyBac transposon-mediated genomic integration of up to twelve plasmids coding for six fluorescent reporters (i.e. EGFP, mTSapphire, mCerulean, yellow fluorescent protein - YFP - and monomeric Kusabira Orange - mKO -, each one expressible either in the cytoplasm or in the nucleus) has proved to be a very useful tool to perform lineage tracings at the single cell level. This approach, named Star Track, was originally developed to follow single astroglial progenitors and their derivatives under physiological and pathological conditions, using the hGFAP promoter (García-Marqués and López-Mascaraque, 2012; Martín-López et al., 2014; García-Marqués and López-Mascaraque, 2016). Along this line, the first clonal analysis performed exploiting this technique addressed the fate of E14 astroglial progenitors of the forebrain (García-Marqués and López-Mascaraque, 2012) and suggested that cortical and white matter astrocytes located within the same regions of the mature brain derive from distinct, fate-restricted, precursors. Nevertheless, further clonal studies at different and, putatively, more precocious developmental stages are still required to verify whether less committed progenitors exist. The high versatility of this tool was thereafter exploited to trace all neural cell types derived from single embryonic and postnatal progenitors, by replacing the astroglial-specific promoter with a ubiquitous one (Ubiquitin C promoter, UbC) and taking advantage of the Cre-lox strategy to avoid the expression of non-integrated copies of the plasmids (Figueres-Oñate et al., 2016). Therefore, this powerful tool in a way integrates the traditional genetic fate mapping approaches based on transgenic mouse line, now allowing to retrospectively follow different lineages at the single cell level by simply changing the regulatory sequence that drives the reporters’ expression. Moreover, with the high number of fluorescent combinations, it surpasses a lot the other fluorescent reporters-based approaches: since each of the six reporter proteins can be expressed either in the cytoplasm or in the nucleus, the number of the total theoretical combinations is 4096. Further, the plasmids can be integrated in a variable number of copies in the genome of each progenitor cell, resulting in distinct fluorophore intensity levels and exponentially increasing the amount of possible combinations. Nevertheless, in the study of the ontogenesis of astroglial diversity in the CNS, this tool still holds some important limitations. Indeed, although hGFAP regulatory sequences have been extensively used, this

marker is not uniformly expressed in all astrocytes. Recently, new pan-astrocytic markers such as the folate metabolic enzyme ALDH1L1 and SOX9 (see section 1.1.2.4) have been uncovered by gene-expression profiling of purified astrocytes and could therefore be exploited to obtain more reliable results. Moreover, the identification of the distinct astrocyte subtypes within each clone, merely relies on morphological parameters, which, as previously discussed, are not enough to define the broad astroglial diversity. This limit will likely be overcome as soon as, hopefully, subtype-specific astrocyte markers are identified and the morphological and molecular heterogeneity of astrocytes is unveiled.

To partially solve these issues, the molecular heterogeneity of astrocytes in the brain is currently being deeply investigated through genome-wide expression analyses: FACS or MACS purified astrocytes from the distinct layers of the cerebral cortex (Gotoh, 2017 ; Bairaktar and Rowitch, 2017) as well as from the diencephalon or cerebral cortex (Götz, 2017) are being subjected to RNAseq expression profiling in order to look for genes enriched in a region-specific manner and to identify novel candidate markers. To validate these putative markers and analyse their spatiotemporal expression patterns, a novel automated single molecule RNA fluorescent in-situ hybridization (smFISH) technique has also been developed and, combined to confocal imaging, allows to quantify RNA puncta at the single astrocyte level throughout brain sections (Bairaktar and Rowitch, 2017). These developing techniques represent a very powerful tool that awaits its application in the investigation of the molecular heterogeneity of astrocytes across and within many other brain regions, leading to the discovery of new reliable subtype-specific genes which will in turn help in dissecting more deeply the final clone composition.

1.2.2 Beyond lineage studies: the potential contribution of mathematical modelling

In the field of developmental neuroscience, the understanding of the cellular basis of brain building is a crucial point. Along this line, fundamental questions are what kind(s) of progenitor cells act as sources of distinct cell lineages, and how they proliferate, migrate, and differentiate to create a brain of the appropriate composition and size. The complexity of these processes relies on multiple cell behaviours, three spatial dimensions and time-dependent changes, that cannot be fully captured through the snapshots provided by conventional lineage tracing and clonal analyses as those presented above. Live imaging

and sophisticated tagging approaches offer significant advancements by enabling explicit in vivo/ex vivo assessment of progenitor division pattern and potential.

Yet, to integrate complexity and reach a systemic level of understanding, empirical data can be implemented with mathematical models where the behavior of progenitor cells can be computationally simulated and compared to the empirically-collected data in order to consolidate data-derived interpretations and make generalized predictions.

For instance, a fundamental question in the field of developmental biology is how the unfolding of neural lineages during histogenesis is regulated. In a simplified view, individual progenitors can generate parallel predetermined lineages or undergo stochastic choices (Cayouette et al., 2003). In the first model, variation may be due to the existence of multiple types of progenitors, and thus multiple fixed lineages that differ between them but are each deterministic (Cayouette et al., 2003; Livesey and Cepko, 2001). Alternatively, precursors can have stochastic behaviors. In this instance, a given progenitor does not have a predefined pattern of mitosis or progeny fate specification. Its lineage is the result of random choices of cell fates made at each cell division by the progeny.

Both models have been found to explain the process of neurogenesis at different sites in the brain. For instance, high resolution quantitative clonal analysis of mouse cortical lineage progression revealed a remarkably deterministic and coordinated developmental program of progenitor behavior defined by a sequential quantal production of neurons followed by predictable progression to gliogenesis (Gao et al., 2014). However, accurate in vivo lineage tracing data and bar-code-based analyses of zebrafish retinal cells were shown to fit with a simple stochastic mathematical model, according to which the retinal neurons are derived from a set of equipotent progenitor cells that are subjected to stochastic factors controlling lineage progression (He et al., 2012; see also former *in vitro* results from rat retinal progenitors, Gomes et al., 2011). Despite apparent randomness, however, in stochastic examples, the fate of an individual cell can still display some bias (i.e., it is statistically predictable) suggestive of deterministic components. For instance, in the above cited study on zebrafish retina, specific combinations of fates appear with higher frequencies than predicted by pure unbiased stochastic choices (He et al., 2012; Chen, Li Desplan 2012). Thus, discussion on how progenitors progress to produce the variety of neurons is still open and the development of an integral model combining both stochastic and deterministic inputs is envisaged for the future, at least in specific brain territories.

Notably, data on astrogliogenesis so far have not been challenged with mathematical modelling nor integrated in models with the same accuracy and detail compared to results on generation of neurons. However, mathematical modelling could be extremely valuable in the glial field not only for a full understanding of brain histogenesis, but also to provide clues on how astroglial heterogeneity emerges by the properties of gliogenic progenitors, that is, according to determistic or stochastic behaviors.

1.3 The cerebellum: an excellent model to study the generation of astroglial diversity

As discussed above, the identification of astroglial subtypes in the mature brain is severely limited by the scarce understanding of their heterogeneity. This is true especially in rodents, where, so far, only up to three and five astroglial subtypes five astroglial subtypes have been recognized according to their morphology and molecular signature, respectively, even in extensively studied territories such as the cerebral cortex (see sections 1.1.1.1 and 1.1.1.2). Such a poor comprehension of astroglial diversity strongly restrains the investigations on the ontogenesis of this heterogeneity, as potential different astrocyte subsets can be hardly distinguished in most CNS areas at the moment.

The cerebellum offers a valuable opportunity to overcome some of the current limitations in this field. Indeed, it is characterized by a moderate number of well-characterized astroglial subtypes, easily and unequivocally distinguishable according to their morphology and allocation within its well-known and simple laminar architecture. Moreover, its development has been extensively investigated and largely explained.

The mature cerebellum in mammals is composed of two symmetric lateral hemispheres, phylogenetically younger and therefore referred as the *neocerebellum*, and of a medial region called “vermis”, evolutionarily older and named *paleocerebellum* (Fig. 1.5a). Macroscopically, the cerebellum can be further divided into cortex, white matter (WM), and cerebellar nuclei (CN): the cortex occupies the entire surface and has evolutionarily increased its extension from fishes, to birds, to mammals through the appearance and gradual increase of fissures and folia, which from a midsagittal section have the appearance of a “tree”. In the cerebellar vermis, all mammals have a similar basic pattern of ten lobules

separated by fissures and further subdivided in sublobules by secondary indentations, whose number and complexity increase with evolution (Fig. 1.5b). Microscopically, each folium is composed of three discrete cell layers that surround the WM and the CN: (i) a granule layer (GL) containing granule cells (GCs), Golgi cells, unipolar brush cells (UBC) and granular layer astrocytes (GLA); (ii) a monolayer of Purkinje cell (PC) and Bergmann glial (BG) cell bodies, beneath which are located the Lugaro cells; (iii) a cell sparse molecular layer containing GC axons (parallel fibers), PC dendrites, BG fibers, and basket and stellate cells (Fig. 1.5c).

Here below, before more deeply addressing astroglial diversity in the cerebellum, I will provide a brief overview on cerebellar development, which is the frame where my PhD project is placed.

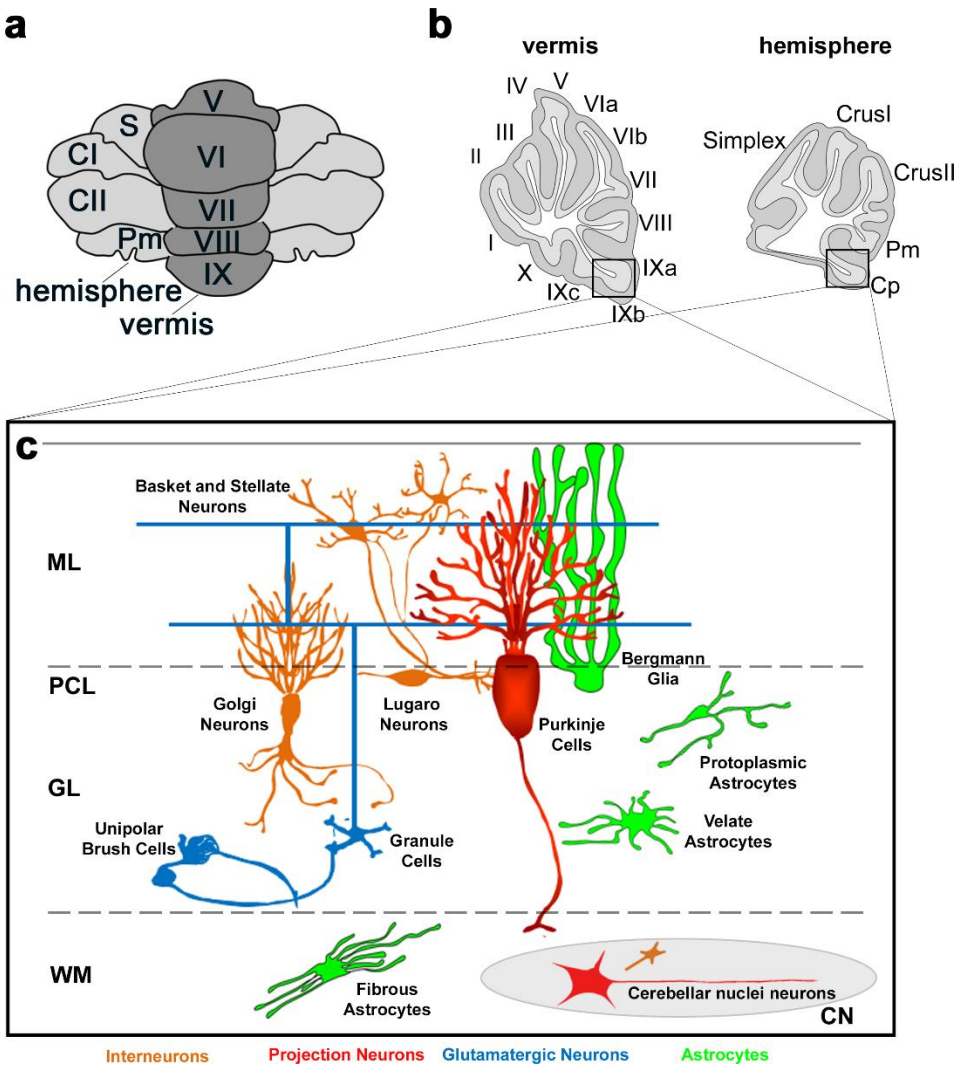

Figure 1.5. Macroscopic and microscopic cerebellar structure. (**a**) Representation of the dorsal view of the mouse cerebellum. The mature cerebellum is composed of two lateral and symmetrical hemispheres and a medial part, called vermis. (**b**) Representation of sagittal sections of the mouse cerebellar vermis and

hemispheres. Both the vermis and the hemispheres are subdivided into lobules by primary and secondary fissures whose pattern is highly conserved among mammals. Each lobule is composed of three cell layers that surround the white matter (WM) and the cerebellar nuclei (CN), where fibrous astrocytes and CN neurons are found, respectively. From inside to outside: the granular layer (GL) hosts glutamatergic Unipolar Brush Cells (UBC) and granule cells, as well as velate and protoplasmic astrocytes; along the Purkinje cell layer (PCL), the somata of Purkinje cells and Bergmann glia are found, and, just beneath it, are located the inhibitory Lugaro neurons; the molecular layer (ML) contains GC axons (parallel fibers), PC dendrites, BG fibers, and inhibitory basket and stellate interneurons.

1.3.1 Cerebellar development

The word “cerebellum” literally means “little brain”. Nevertheless, this definition does not properly mirror reality. Indeed, this structure represents in amniotes one of the most architecturally elaborate regions of the CNS, and in humans it contains over half of the total mature neurons in the brain. Moreover, its complexity is appreciable also at the functional level: besides contributing to sensory-motor processing, the cerebellum has been also associated with higher cognitive functions, such as learning, memory, emotional processing and speech (Adamaszek et al., 2017). Nevertheless, this macroscopic complexity at both structural and functional levels hides a peculiar histological simplicity: various, well characterized, cell types are organized in a well-defined cytoarchitecture, which is shaped during development through a complex multistep process, finely regulated by both cell-autonomous programs and inductive environmental cues.

1.3.1.1 Origin and definition of the cerebellar anlage

The various regions of the CNS derive from a cytologically homogeneous sheet of epithelial cells, the neural plate, which arises during gastrulation from the dorsal ectoderm. The invagination of the neural plate leads to the formation of the neural tube, which begins as a single layer but then goes through a series of drastic transformations that eventually create three distinct regions of growth. More in detail, the most anterior portion of the neural tube starts transforming even before the posterior portion is complete and swells into three primary vesicles: from anterior to posterior, the prosencephalon (anlage of the forebrain), the mesencephalon (anlage of the midbrain) and the rhomboencephalon (anlage of the hindbrain, comprising the metencephalon rostrally and the myelencephalon caudally; Gilbert, 2000).

Starting from the end of the nineteenth century, several efforts were made to define the physical margins of the neural territory from which the cerebellum is specified. Originally, the cerebellar anlage was thought to entirely derive from the metencephalon (His, 1890). Later, it was concluded that this region was not the sole origin of the whole cerebellum. Rather, early elegant studies that aimed at defining the boundaries of the brain neuromeres using quail-chick grafting highlighted that it arises from the caudal portion of the mesencephalic vesicle and the rostral portion of the metencephalic vesicle (Martinez and Alvarado-Mallart, 1989; Hallonet et al., 1990; Hallonet and Alvarado-Mallart, 1997; reviewed in Sotelo, 2004; Alvarado-Mallart, 2005). Nevertheless, this idea was later overturned by mapping the molecular boundary between the midbrain and hindbrain, showing that all cerebellar cells emerge in this region at around embryonic day (E) 8.5 in mice (Millet et al., 1996). Here, the so called "isthmus" plays a key role in shaping the cerebellar territory. Namely, transplantation experiments of the isthmic tissue into the diencephalon or myelencephalon were shown to change the fate of the surrounding cells, inducing the formation of ectopic midbrain or cerebellar structures, respectively (reviewed in Sotelo 2004 and Alvarado-Mallart 2005). These observations confirmed the role of the isthmus as an "organizer" for the patterning of both the midbrain and the cerebellum, presumably through the production of inductive signals, and led to its name of "isthmic organizer" (IsO; Fig. 1.6).

The IsO does not correspond to any finite anatomical region and is delimited by molecular, rather than morphological, boundaries. Specifically, it is located at the margins of the expression domains of the two homeobox transcription factors OTX2 and GBX2, expressed in the forebrain/midbrain and hindbrain, respectively, starting at E7.5 in mice. Several genetic experiments demonstrated that these two factors define the positioning of the IsO through a mutual repression, where GBX2 suppresses the expression of OTX2 in the metencephalon, thus allowing the formation of the cerebellum (Simeone et al., 1993; Millet et al., 1999; Broccoli et al., 1999; Wurst and Bally-Cuif 2001). Some other genes, as *Fgf8*, *En1-2*, *Pax2* and *Wnt1*, were shown to have their expression domains centered in the IsO. They are essential for a correct development of the cerebellum, as revealed by loss of function studies that resulted in the deletion of most of the mesencephalic and/or metencephalic regions (Thomas and Capecchi, 1990; McMahon and Bradley, 1990; Wurst et al., 1994; Favor et al., 1996; Meyers et al., 1998). Among these, FGF8 is the major

signalling molecule in the midbrain-hindbrain boundary, as evidenced by experiments in chick embryos and quail-chick chimeras (Hidalgo-Sanchez et al., 1999), from electroporations of the two isoforms *Fgf8a* and *Fgf8b* in chick embryos (Sato et al., 2001) and, particularly, from the proof that beads containing FGF8 protein induced midbrain and cerebellar tissues when ectopically transplanted (Crossley et al., 1996; Martinez et al., 1999). The latter inductive effect mirrors what observed in the chimeric embryos (Martinez et al., 1991; Marin and Puelles, 1994) thus indicating that FGF8 alone can mimic the activity of the whole IsO. The requirement of FGF8 for cerebellar development was further confirmed by loss-of-function studies, through conditional deletion either of the gene itself or of its spliceform *Fgf8b* at the midbrain-hindbrain boundary (Chi et al., 2003; Guo et al., 2010). The expression of FGF8 in the IsO is tightly regulated by several distinct transcription factors (reviewed in Joyner et al., 2000; Wurst and Bally-Cuif, 2001). In the midbrain, the Lim homeobox gene 1b (*Lmx1b*), induced by OTX2 and repressed by GBX2, prevents the expression of FGF8 in the same territory and triggers the secretion of WNT1. In turn, WNT1 promotes the up-regulation and secretion of FGF8 by the neighbouring GBX2-positive cells in the hindbrain (Adams at al., 2000; Matsunaga et al., 2002, reviewed by Carletti and Rossi, 2008). This complex mechanism results in FGF8 secretion to be restricted to those cells located at the boundary between the *Otx2* and *Gbx2* expression domains. Moreover, in a positive feedback, FGF8 itself induces the expression of LMX1b and, consequently, that of WNT1, which in turn maintains the expression of EN1, positively regulating FGF8 expression (reviewed by Wang and Zoghbi, 2013). Nevertheless, the expression of FGF8 is transient. Indeed, a decreasing gradient of its concentration is fundamental for both cell survival and the development of the distinct cerebellar regions (Xu, Liu and Ornitz, 2000; Suzuki-Hirano et al., 2010). Thus, the timely and spatially regulated expression of specific molecular signals at the midbrain/hindbrain junction builds the morphogenetic activity of the IsO and is crucial for the specification of the cerebellar territory.

Knowledge about the dorso-ventral patterning in this region is instead much more incomplete. In this regard, BMPs and Shh, which regulate neural development in the spinal cord (see section 1.1.2.2), were also shown to be involved in the specification of the dorso-ventral regionalization of the midbrain/hindbrain region and in cerebellar development. Indeed, BMP-mediated inductive signals from cells within and adjacent to the roof plate at the midbrain/hindbrain boundary have been shown to directly regulate the expression of

markers of dorsal neural character, such as *Msx* genes, cell proliferation and local cell death in both the hindbrain and forebrain (Arkell et al., 1997; Furuta et al., 1997). Moreover, BMP signaling is sufficient to promote neural crest cell fate in hindbrain and midbrain neural plate tissues, as highlighted by studies in the chick embryo (Muhr et al., 1997), and, later, promotes the generation of granule cell progenitors from rhombic lip, germinative neuroepithelium of the cerebellum located dorsally in the neural tube (Alder et al., 1999). In parallel, Shh, initially produced by the floor plate, a ventral midline signalling center which extends along the neuraxis, is required for normal development and dorso-ventral patterning of the mid/hindbrain boundary. Indeed, the perturbation of normal Shh signals through retrovirus-mediated ectopic expression during the early somite stage of chick embryogenesis resulted in a severe malformation of the mid/hindbrain junction region, likely related to Shh proliferative and ventralizing activities (Zhang et al., 2000). Further, the importance of Shh signaling in the correct development of the anterior hindbrain was demonstrated through conditional mutagenesis of distinct members of the pathway (i.e. Gli2 and Gli3; Blaess et al., 2006)

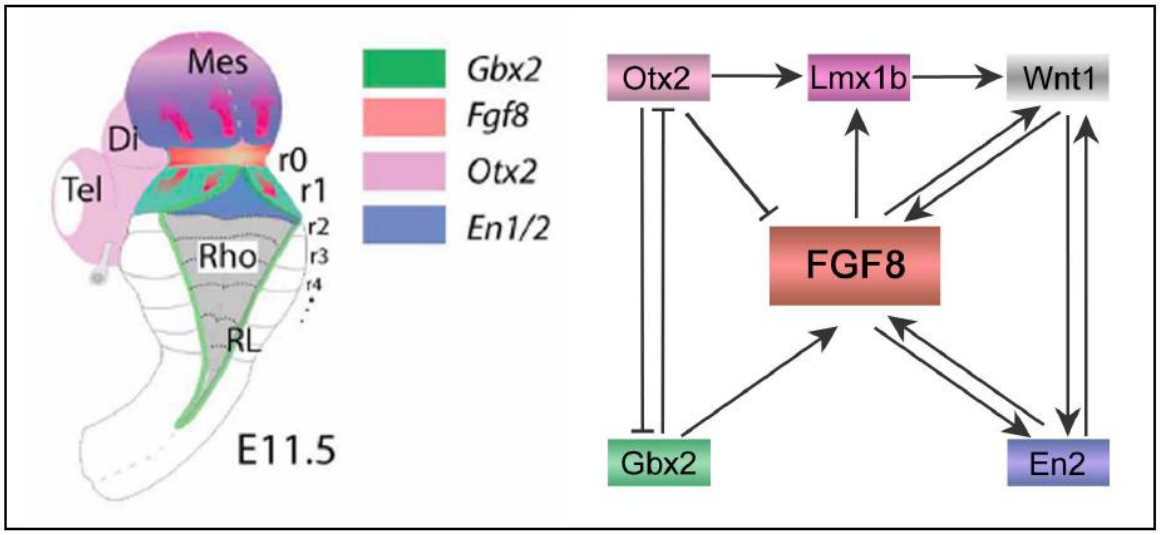

Figure 1.6. Patterning of the midbrain/hindbrain region. The isthmic organizer (IsO) controls the proper formation of the mid/hindbrain region. The activity of the IsO is exerted through a reciprocal interaction or repression of several transcription factors expressed in defined territories. A central role in this process is mediated by FGF8 (modified from Wang and Zoghbi, 2001; Martinez et al., 2013).

1.3.1.2 Specification of cerebellar progenitors from the primary germinative niches

After the initial establishment of the cerebellar territory, between E9 and E11 in mice the primordium consists of two dorso-laterally symmetric bulges located on both sides of the rhomboencephalic midline, which at around E15 in mice (Louvi et al., 2003) eventually fuse in the primary cerebellar plate (Carletti and Rossi, 2008).

In contrast to other CNS regions, where the sole primitive ventricular neuroepithelium gives rise to all neuronal and astroglial phenotypes, the embryonic cerebellum consists of two germinative niches, the ventricular zone (VZ) and the rhombic lip (RL). From these two niches, the distinct subtypes of cerebellar neurons and astrocytes are generated, as clarified by genetic and viral lineage tracing studies (see Leto, Arancillo, Becker et al. 2015 for review). Two bHLH proteins, namely ATOH1 (also known as MATH1) and the pancreatic transcription factor 1a (PTF1A), are mutually exclusive and confer the spatial identities of the cerebellar progenitors located in the RL and VZ, respectively. Their deletion was shown to result in the complete loss the neuronal phenotypes specified from the corresponding germinative niche (Ben-Arie et al., 1997; Wang et al., 2005; Hoshino et al., 2005; Pascual et al., 2007). Moreover, ectopic expression of ATOH1 in the VZ and of PTF1A in the RL highlighted the strong and mutually exclusive specification potential of these two transcription factors (Yamada et al., 2014). This strict regionalization by bHLH transcription factors is very reminiscent of that in the telencephalon (Wilson & Rubenstein, 2000).

The Rhombic Lip (RL)

The RL is the source of cerebellar glutamatergic neurons and is governed by the expression of ATOH1 (MATH1; Ben-Arie et al., 1997), which occurs in the midbrain/hindbrain boundary as early as E9.5 and persists selectively in the RL and in many of its derivatives. Selective ablation of *Atoh1* results in the complete loss of the granule cells (GC) population without affecting PCs, thus highlighting the precise compartmentalization of these two lineages in the embryonic cerebellum (Ben-Arie et al., 1997). For several years, only granule cells were thought to derive from this niche. Nevertheless, it was later demonstrated that RL derivatives also comprise other cerebellar glutamatergic cells, i.e. excitatory neurons in the CN and unipolar brush cells (UBC), generated prior than granule cells (Machold and Fishell 2005; Wang et al., 2005; Englund et al., 2006; Fink et al., 2006). Namely, glutamatergic

neurons are produced from RL progenitors according to a well-defined time schedule: CN neurons are the first to move from the RL at around E10-E12.5 in mice, followed by progenitors of UBCs (E12.5-E18.5) and, shortly later, by GC precursors (E13– perinatal; Fig. 1.7b). Notably, this very same temporal schedule is followed even when glutamatergic neurons are ectopically produced from the VZ, after ectopic expression of ATOH1 (Yamada et al., 2014), thus suggesting that glutamatergic progenitors in the RL may be multipotent and change their temporal identity as development proceeds. More in detail, the first wave of RL progenitors follows a subpallial migratory pathway and eventually become CN excitatory neurons (Machold and Fishell 2005; Wang et al., 2005; Fink et al., 2006). A second pool of TBR2-positive (+) cells is supposed to leave the RL and colonize the embryonic prospective white matter (PWM) before homing in the GL (Sekerkova et al., 2004; Englund et al., 2006), although a proper fate mapping analysis is still needed to confirm . Shortly later, GC progenitors migrate tangentially from the RL along the cerebellar surface forming the EGL, that will persist for the whole postnatal development. Here, GC precursors intensely self-amplify and maintain MATH1 positivity until they become postmitotic, when they eventually migrate inwards to form the mature GL.

The Ventricular Zone

The second germinative neuroepithelium of the embryonic cerebellum is the VZ, whose name derives from its location facing the IVth ventricle. This niche is the source of most types of cerebellar GABAergic neurons as well as of astrocytes and it is characterized by the expression of a bHLH transcription factor already known to participate in pancreatic development, PTF1A. PTF1A is expressed by VZ progenitors: its abrogation was shown to result in the inhibition of the production of GABAergic neurons in the cerebellar primordium and, eventually, in the peculiar loss of the entire cerebellar cortex (*cerebelless mice*, Hoshino et al., 2005). Moreover, in *Ptf1a*-null mice the VZ was shown to unusually produce GC, rising the fascinating hypothesis that cerebellar progenitors in the VZ possess an intrinsic glutamatergic developmental program (Pascual et al., 2007). Nevertheless, relatively few mutant cells were later shown to undergo this transformation, rather, the *cerebelless* phenotype was demonstrated to be due to an early and ultimate fate switch from cerebellar to ventral brainstem extraxerebellar cell fates occurring in *Ptf1a* mutant

mice (Millen et al., 2014). On the other hand, PTF1A ectopic expression in precursors in the dorsal telencephalon, which are physiologically the source of solely glutamatergic neurons, results in the ectopic production of GABAergic neurons with their typical morphological and migratory features (Hoshino et al., 2005). Thus, PTF1A appears to be both necessary and sufficient for the GABAergic neuron specification in the cerebellar territory.

In contrast to the RL, that uniformly produces all types of cerebellar glutamatergic neurons, the PTF1A-expressing VZ can be divided into distinct domains recognized as responsible for the generation of different classes of GABAergic neurons (reviewed by Dastjerdi et al., 2012; Hori and Hoshino 2012; Fig. 1.7a). At the early neurogenic stage (around E12 in mice), this primary niche can be divided dorsally and ventrally into two domains, which express E-cadherin strongly or weakly, respectively (Minaki et al., 2008; Mizuhara et al., 2010). These two domains host GABAergic progenitors that were further distinguished by the expression of two non-overlapping transcription factors, GSX1 (rostrally) and OLIG2 (caudally). Lineage tracing revealed that, while the GSX1 territory hosts PAX2+ IN progenitors, the OLIG2-expressing domain gives rise exclusively to PCs (Seto et al., 2014). This is consistent with the observation that, in the tissue overlying the *Gsx1* and *Olig2* domains, two non-overlapping populations of postmitotic immature neurons can be distinguished and differentially express PAX2 and CORL2, that label inhibitory INs and PCs, respectively (Minaki et al., 2008; Seto et al., 2014). Interestingly, the gradual ventral expansion of the *Gsx1* domain as development proceeds inhibits OLIG2 activity and consequently leads to the production of INs at the expense of PCs that are no longer produced after E13. The PTF1A-positive cerebellar VZ was further reported to express other proneural genes, encoding the bHLH transcription factors Neurogenin (NGN) 1, NGN2 and ASCL1 (Zordan et al., 2008). ASCL1 broadly overlaps the PTF1A-exressing domain from early embryonic stages and it was shown to participate in the specification of all GABAergic neurons (Grimaldi et. al., 2009; Sudarov et al., 2011). On the other side, NGN1 and 2 appear to differently regulate the generation of GABAergic neurons. Namely, NGN1-expressing progenitors produce all inhibitory INs but those in the CNs, together with a subset of PCs (Vue et al., 2007; Lundell et al., 2009; Kim et al., 2011), whereas NGN2 is responsible for the cell cycle exit of PC progenitors and their maturation (Florio et al. 2012). Thus, the cerebellar VZ appears to be a mosaic of distinct progenitor subtypes, defined by the expression of spatially regulated combinations of transcription factors.

Like RL-derived glutamatergic neurons, GABAergic cells are generated from VZ progenitors according to a well-defined time schedule, as clearly elucidated by birthdating studies (Miale and Sidman 1961; Pierce 1975; Altman and Bayer 1997; Morales and Hatten 2006; Fig. 1.7b). The first cells to be born are GABAergic nucleo-olivary projection neurons in the CN, shortly after followed by PCs (between E10.5 and E13.5 in mice). Progenitor cells immediately migrate into the cerebellar plate, which is then populated by postmitotic precursors of the CN neurons located below the cerebellar surface and, underneath, by postmitotic PCs organized in a multi-layered structure. Between E14 and E17, CN neurons and PCs migrate to opposite directions, reaching their final positions in the deep cerebellar parenchyma and beneath the nascent EGL, respectively. Of note, distinct cohorts of PCs born on distinct days were shown to settle in distinct medio-lateral (M-L) and antero-posterior (A-P) positions. Indeed, if early birthdating analyses in rat had already gave a hint of a gradient of production of PCs from lateral (hemispheres) to medial (vermis; Altman and Bayer 1997), more recent fate mapping analyses exploiting the *Ascl1* promoter in mice have confirmed the predicted and distinct M-L organization of the PCs targeted on different days (Sudarov et al., 2011): the PCs of the hemispheres are generated earlier compared to those of the vermis. Along the A-P axis of the medial vermis, instead, the earliest born PCs were shown to occupy the central lobes, followed by those settled in the posterior and, at last, anterior lobes (Altman and Bayer, 1997; Sudarov et al., 2011).
On the other side, GABAergic IN phenotypes are generated during late embryonic and postnatal development from common precursors. Namely, inhibitory INs were shown to derive from a common pool of progenitors that appear in the VZ at around E13. While CN interneurons are directly generated from VZ progenitors, all the others originate from ventricular precursors that migrate from the VZ to the overlying parenchyma. Here, they continue to proliferate until late embryonic and postnatal development (Zhang and Goldman, 1996), producing different interneuron categories according to a peculiar inside-out sequence from GL to the molecular layer (ML; Altman and Bayer, 1997; Schilling, 2000; Leto et al., 2006; Leto et al., 2009).
Besides the so far discussed neurogenic potential of VZ progenitors, it is now well accepted that also astroglial cells derive from this germinative niche (Altman and Bayer, 1997; Yamada and Watanabe, 2002; Mori et al., 2006; Sudarov et al., 2011). A dedicated section will be focussed on this topic (see section 1.3.4).

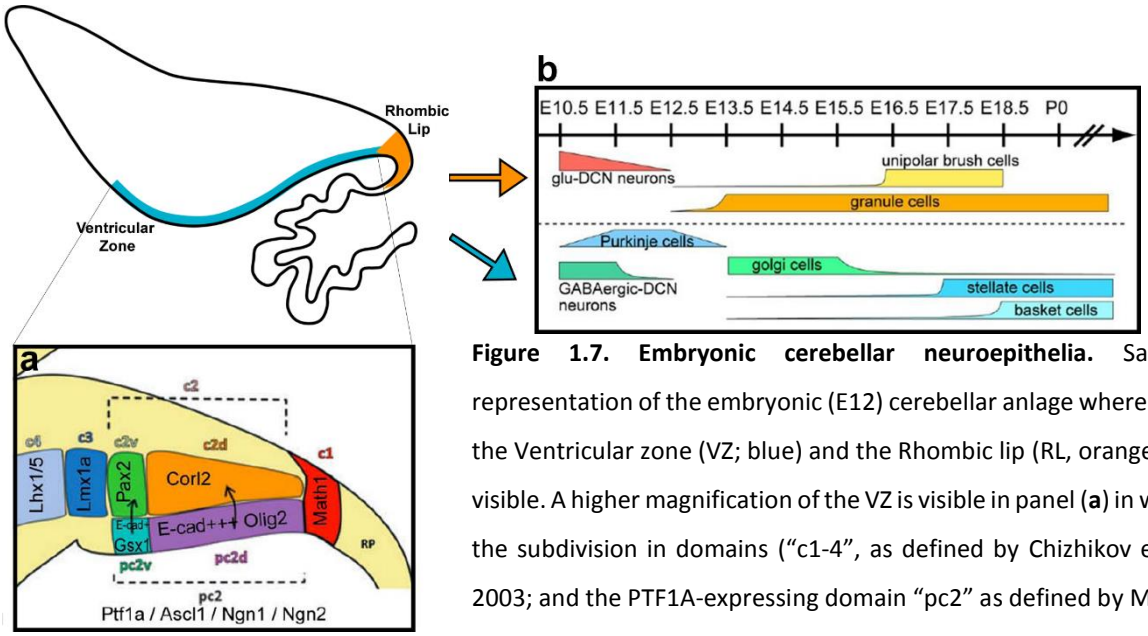

Figure 1.7. Embryonic cerebellar neuroepithelia. Sagittal representation of the embryonic (E12) cerebellar anlage where both the Ventricular zone (VZ; blue) and the Rhombic lip (RL, orange) are visible. A higher magnification of the VZ is visible in panel (**a**) in which the subdivision in domains ("c1-4", as defined by Chizhikov et al., 2003; and the PTF1A-expressing domain "pc2" as defined by Minaki et al., 2008) and subdomains can be appreciated. (**b**) shows the temporal schedule of delamination and migration from the RL (upper part) and VZ (lower part). (Adapted from Hori and Hoshino et al., 2012).

1.3.1.3 Secondary germinative niches and their derivatives

One of the peculiarities of the cerebellum is that, whereas at the end of the embryonic development the proliferative activity of the RL and VZ gradually ceases and these primary niches disappear, cycling progenitors form new germinative sites in the nascent cerebellum, where their proliferation and/or specification continues until postnatal stages (Fig. 1.8). Thus, an intense expansion of cerebellar precursors occurs in these secondary niches during the first two postnatal weeks of development, resulting in a massive growth of the cerebellar tissue (De Luca et al., 2009; Leguè et al., 2015). Single BrdU pulses clearly defined three discrete sites of intense cell proliferation in the postnatal cerebellum: the external granular layer (EGL), the prospective white matter (PWM) and a thin cellular rim at the interface between the nascent GL and ML, where the PC somata are located, the PCL (Yuasa et al.,1996; Parmigiani et al., 2015).

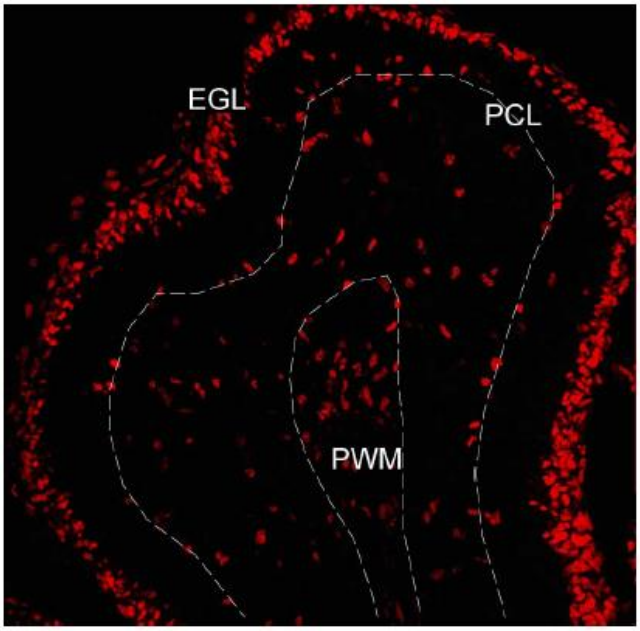

Figure 1.8. Proliferative sites in the postnatal cerebellum. Sagittal section of the cerebellar lobule IV/V at postnatal day (P) 4 in which proliferating cells were labelled by 5-bromo-2'-deoxyuridine (BrdU, red) 6 hours before sacrifice. EGL, external granular layer; PCL, Purkinje cell layer; PWM, prospective white matter.

The External Granular Layer (EGL)

Between E13.5 and E16 in mice, precursors derived from the RL, already specified towards the GC lineage and therefore called granule precursor cells (GCPs), migrate tangentially over the dorsal surface of the cerebellar primordium to form the EGL. In this germinative layer, which covers the surface of the cerebellum until P16 and then gradually disappears, GCPs undergo a prolonged clonal expansion through many symmetric divisions. This generates a population of granule neurons that outnumbers the total neuronal population of the cerebral cortex. In detail, the EGL can be divided into an outer and inner half (termed oEGL and iEGL), where GCPs actively proliferate or stop dividing, respectively. Importantly, the proliferation activity of GCPs in the EGL needs to be tightly regulated for the cerebellar foliation process to properly occur. Indeed, the cerebellum has a peculiar morphology consisting of folia separated by fissures, on which the A-P organization of the distinct sensory-motor circuits is built. The origins of this complex morphology were ascribed to the GCPs proliferation and inward thickening corresponding to the prospective fissures, acting as a driving force to form the so called “anchoring centers” (Sudarov and Joyner, 2007).

Several mitogenic pathways were acknowledged as possible regulators of GCP proliferation in the oEGL. ATOH1 and N-myc, required for GCs specification from the RL, were described to be also essential for the expansion of the pool of progenitor cells in the EGL at early

postnatal stages (Ben-Arie et al., 1997; Knoepfler et al., 2002). Beside them, Shh secreted by PCs is a major driver of GCPs expansion. Evidences of PCs involvement in the maintenance of GCPs pool came from several experimental observations, in which their loss was in turn accompanied by degeneration and death of nearby GCPs (reviewed in Sotelo, 2004). Distinct functional tests performed *in vitro* and *in vivo* eventually demonstrated that PCs exert their pro-proliferative role through the secretion of Shh (Dahmane and Ruiz-i-Altaba, 1999; Wallace, 1999; Wechsler-Reya and Scott, 1999). Moreover, Shh signalling correlates spatially and temporally with fissure formation and its levels were shown to regulate the complexity of cerebellar foliation, as demonstrated in mutant models in which the Shh pathway had been perturbed (Corrales et al., 2006). In the iEGL, cells stop responding to Shh and, therefore, stop proliferating and begin the final steps of maturation, as confirmed by the decreased expression of the Shh target gene *Gli1* (Corrales et al., 2004). Another pathway involved in the expansion phase of GCPs is that of Notch2, activated through homotypic cell-to-cell contacts. Indeed, the Notch2 ligand Jagged1 (JAG1), expressed by GCPs themselves, binds to Notch2 on the surrounding cells therefore stimulating their proliferation and inhibiting their differentiation (Solecki et al., 2001).

The final A-P position of granule neurons in the EGL appears to be temporally linked to the time of delamination from the RL, with GCPs that migrate first (E13.5) being located more anteriorly than those that exit at later time points (Machold and Fishell, 2005). Clonal analyses performed with the MADM method allowed to follow the development of single GC clones, showing that GCPs within each family stop dividing and differentiate *en masse* within a narrow time window of about two days (Espinosa and Luo, 2008). Newly born GCs, then, initially migrate tangentially along the M-L axis in the iEGL (Komuro et al., 2001) and subsequently move radially along the fibers of Bergmann Glia, forming the GL underneath the PCL (Chédotal, 2010; Komuro and Rakic, 1995, 1998). This switch from tangential to radial migration was described to be regulated by Semaphorin 6a (SEMA6a; Kerjan et al., 2005). Of note, mature GCs send their parallel fibers to contact PC dendrites in the overlying tissue, and thereby form the molecular layer (ML), according to an inside-out temporal pattern. Contrariwise, the cell bodies of sister GCs are randomly positioned in the IGL (Espinosa and Luo, 2008; Zong et al., 2005).

The Prospective White Matter (PWM)

As opposed to the EGL, which hosts intermediate progenitor cells homogeneously committed towards a GC phenotype, the cerebellar PWM, active from late embryonic to postnatal life, appears as a mosaic of distinct cellular populations at different maturation stages. These cells include progenitors of inhibitory interneurons, astroglial cells and oligodendrocytes with their newly-born descendants at different maturation stages (Zhang and Goldman, 1996; Leto et al., 2006; Grimaldi et al., 2009; Silbereis et al., 2009; Fleming et al., 2013), as well as a minority of multipotent progenitor cells with NSC-like properties (Klein et al., 2005; Lee et al., 2005) and bipotent progenitors generating both interneurons and astrocytes (Parmigiani et al., 2015).

As described above (see section 1.3.1.2) all cortical interneurons derive from common precursors with a high degree of plasticity that emigrate from the VZ and continue proliferating, during late embryonic and postnatal development, in the nascent WM (PWM). Here, age-dependent environmental cues appear to have a strong instructive activity on the progenitors' fate towards a specific laminar fate (Leto et al., 2009). These local instructive cues were shown to act specifically on sensitive local cells, since extracerebellar cells heterotopically grafted into the postnatal PWM fail to mature into cerebellar phenotypes and differentiate by unfolding cell-autonomous programs typical of their native sites (Milosevic et al., 2008; Rolando et al.,2010). Unfortunately, how the instructive function of the PWM is molecularly built still remains to be elucidated. Nevertheless, one can argue that the inductive signals are likely to derive, in the rapidly evolving cerebellar tissue, from developing populations close to the PWM, namely CN neurons during embryonic development and PCs at later developmental stages (reviewed in Leto et al., 2008). Importantly, Shh produced by PCs was described to regulate the proliferation of GABAergic interneuron progenitors within and near the cerebellar VZ (Fleming et al., 2013; De Luca et al., 2014); nevertheless, it is still not clear whether this same morphogen or other molecules derived from PCs can also influence aspects related to their maturation, such as migration or the acquisition of specific phenotypes.

Besides the aforementioned precursors fate-restricted towards the interneuronal lineage, the postnatal PWM was also described to host another pool of progenitor cells, CD44-positive and capable of exclusively differentiate into astrocytes (Cai et al., 2012), as well as less-committed precursors, displaying NSCs-like markers and astroglial features, with both

neurogenic and gliogenic potentials (Silbereis et al., 2009; Fleming et al., 2013; Parmigiani et al., 2015). Specific sessions will be later devoted to address these topics (see sections 1.3.3 and 1.3.4).

The Purkinje Cell Layer (PCL)

The common view numbers among the secondary germinative niches of the postnatal cerebellum the sole EGL and PWM described above. Nevertheless, the postnatal PCL hosts proliferative cells (referred as PCL precursors) considered to be progenitors of Bergmann Glia, as well as postmitotic cells of this astroglial type, and can therefore be mentioned among the secondary germinative sites of the cerebellum (Yuasa et al., 1996; Yamada and Watanabe, 2002; Sudarov et al., 2011; Buffo and Rossi, 2013). PCL precursors are considered to develop from cerebellar RG by migration of their soma and retraction of their apical processes, and display a high mitotic activity during the whole first postnatal week (Ramon y Cajal, 1911; Yuasa et al., 1996; Altman and Bayer, 1997). As GCPs in the EGL and interneuron progenitors in the VZ, also PCL precursors express molecules of the Shh pathway (Dahmane and Ruiz-i-Atalba, 1999; Corrales et al., 2004), nevertheless, this morphogen was described to regulate their maturation and differentiation rather than their proliferation (Dahmane and Ruiz-i-Atalba, 1999).

Notably, as PWM progenitors, PCL precursors display similar traits of immature astroglia and NSC markers such as SOX1 and SOX2 (Alcock and Sottile, 2009), a signature which is maintained through cerebellar maturation into adulthood (Sottile et al., 2006). Moreover, as recently highlighted through a transcriptomic comparison, striking similarities exist between the molecular signatures of both developing BG (i.e. PCL progenitors) and the embryonic outer RG (oRG, also referred as “basal RG – bRG –“) located in the subventricular zone of the developing cerebral cortex and responsible for the generation of the majority of cortical neurons, thus pointing to a common mechanism of bRG and BG generation (Heng et al., 2017). In addition, with a single basal process, these two kinds of cells are also very similar under the morphological point of view (Hansen et al., 2010). Although these morphological and molecular similarities with NSCs might suggest that PCL precursors in the postnatal PCL retain a neurogenic potential, recent evidence has excluded a contribution of the PCL to physiological cerebellar neurogenesis during postnatal

development (Parmigiani et al., 2015). However, as indicated by recent experiments, these cells may undergo an adaptive reprogramming following a major postnatal depletion of GCPs and, after migrating into the EGL, may produce GCs (Wojcinski et al.,2017). On the other side, SOX1/2 expression detected in both developing and mature BG, together with the neurosphere-forming ability of BG progenitors *in vitro* raises the question whether these cells may represent a novel and abundant stem cell population in the adult cerebellum. However, the first and so far unique evidence of this possibility came only very recently, when a rare and undifferentiated SOX2-expressing cell population has been identified in the adult PCL, intermingled with BG (Ahlfeld et al., 2017). These SOX2-positive precursors can physiologically generate NeuN-positive cells, whose number increases when mice are exposed to physical exercise and which can integrate into the cellular network. Nevertheless, further investigation is needed to understand the phenotype of these cells whether a lineage relationship exists between the neurogenic SOX2-positive precursors and SOX2-expressing BG, in view of a full understanding of this newly discovered process.

Both the components of the PCL, PCs and BGs, play also a crucial role in the phase of cerebellar foliation, starting after the inward thickening of the EGL (see "The External Granule Layer (EGL)" in the current section). Indeed, a folding of the PCL, still in the form of a multilayer, was shown to occur where the GCPs accumulate, predicting the future position of the fissures: both PCs dendrites and BG fibers near the anchoring centers converge towards the base of each fissure, thereby allowing the correct unfolding of the foliation pattern. The maturation of a given fissure, then, proceeds in synchrony with the development of PCs and PCL progenitors throughout that same fissure and with their gradual transition from a multilayer into a monolayer (Sudarov and Joyner, 2007; Hoser et al., 2007; Ma et al., 2012; Li et al., 2014).

1.3.2 The phenotypic heterogeneity of cerebellar astrocytes

As previously mentioned, the cerebellum is characterized by a remarkable anatomical and functional complexity, which is mirrored not only by the variety of its neuronal phenotypes, but also by a notable heterogeneity of astroglial cells. In this context, each highly peculiar morphological feature is associated to specific functional properties, unique among the

astroglial cells of the entire CNS. Despite this, in the last decades the interest on the development, lineage, heterogeneity and functions of cerebellar astrocytes has lagged behind studies on cerebellar neurons and circuits. As a result, while the mechanisms of neuronal diversification have been widely investigated and partially clarified, astrogliogenesis remains poorly explored.

Back in 1911, the Nobel Prize Santiago Ramón y Cajal first described the glial cells of the cerebellum and classified them into three main categories (Fig. 1.9). Indeed, according to their morphology and layering in the cerebellar tissue, he could distinguish (i) glial cells in the WM characterized by processes oriented along the direction of axons, (ii) astrocytes of the GL with star-shaped bushy processes, and (iii) "the neuroepithelial cells with Bergmann fibres", with cell bodies aligned to the PCL, several radial processes spanning radially through the ML, and terminal endfeet contacting the pial surface. Afterwards, high voltage electron microscopy studies, allowing to approach the Golgi preparations at a much higher resolution, basically confirmed this first classification and revealed the presence of a rarer type of GL astrocytes, called "protoplasmic", with thin processes devoid of lamellae (Palay and Chan-Palay, 1972; Fig. 1.9). Moreover, these studies allowed the discovery of veil-like appendages emanating from the processes of the other type of GL astrocytes (therefore called "velate" astrocytes), and described their relationship in the local neuropil with groups of GCs and glomeruli, the synaptic structures composed of mossy fibres rosettes, Golgi neuron boutons and GC dendrites. Similarly, BG processes were shown to ensheath the entire dendritic tree and soma of PCs, thereby suggesting an involvement of both kinds of cortical astrocytes in the compartmentation of the local circuitries. On the other hand, the closer inspection of WM astrocytes led to their classification as "fibrous" astrocytes. A special staining procedure, the Cajal's gold sublimate technique (Cajal, 1926; Globus, 1927), also allowed, early in 1916, to identify a second astroglial phenotype located in the PCL intermingled with BG, called "feathered cell" of Fañanas (Fañanas, 1916). Nevertheless, provided their morphological similarity to BG, their identification still remains quite hard, making these cells largely forgotten. On the other side, the mature cerebellar ML, instead, seems to be devoid of cells with a typical star-shaped astroglial morphology.

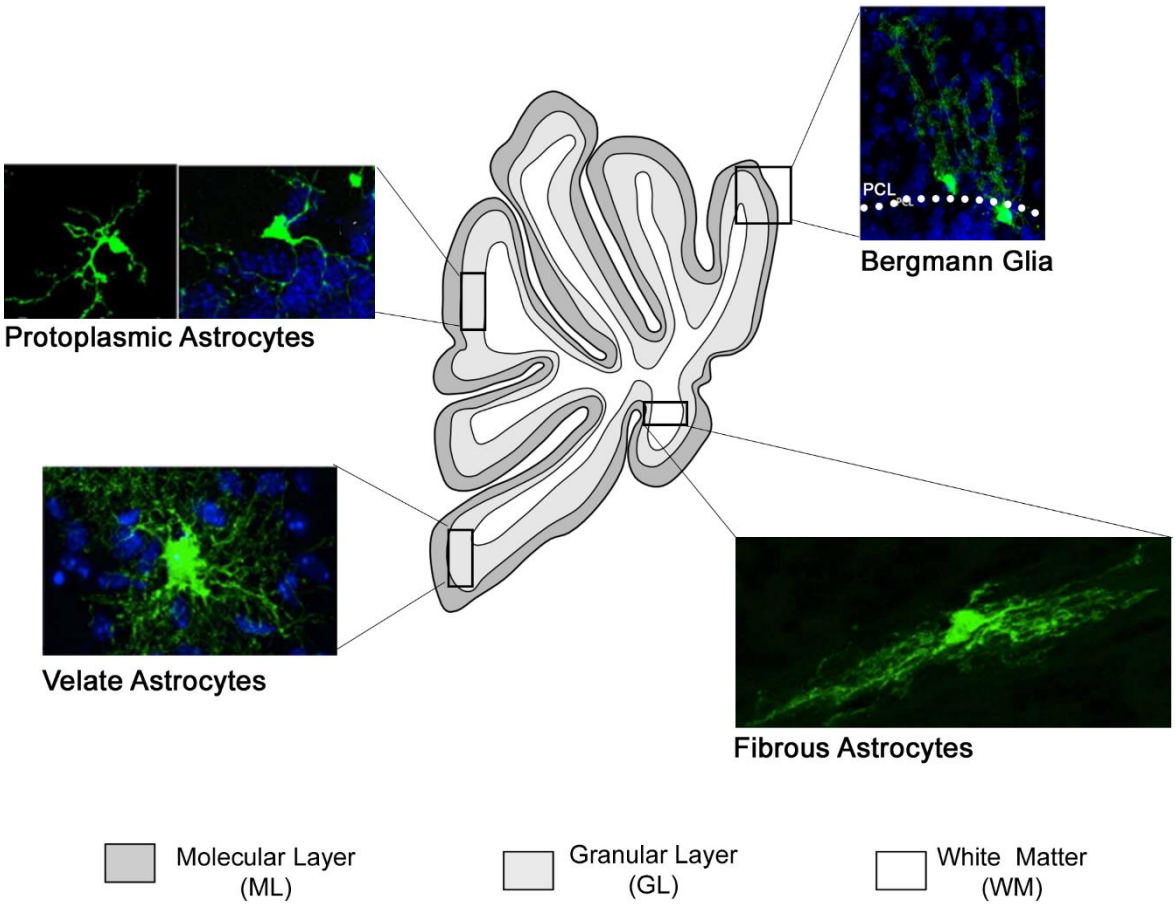

Distribution for markers for cerebellar astrocytes in adult mice

	hGFAP	mGFAP	S100b	BLBP	Glast	Sox9	Sox2
PCL(BG)	++	++	++	++	++	++	++
GL	+	++	++	+	++	++	++
WM	+	++	+	+	++	++	++
DCN	+	+	++	+	++	++	++

++ frequent, + less frequent

Figure 1.9. Distinct astroglial subtypes of the cerebellum The mature cerebellum includes various astroglial phenotypes displaying a typical morphology depending on the layer occupied. Bergmann glia cells (BG) possess a cell body in the Purkinje cell layer (PCL) and radial processes extending to the pial surface. In the granular layer (GL) there are two different types of astrocytes: velate astrocytes with fine and elaborated processes and more rare protoplasmic astrocytes. Finally, fibrous astrocytes with long processes oriented in the direction of axons are typical of the white matter (WM). These subtypes can be distinguished only by means of morphological criteria, since neurochemical marchers are shared by all the different types with minor variations (see table).

1.3.3 Origin of cerebellar astrocytes

The first report on the origin of cerebellar astrocytes came from Santiago Ramón y Cajal himself, who in 1911 investigated the cerebellar development of different species and concluded that all cerebellar glia derive from the VZ, as later demonstrated by fate mapping analyses (Hoshino et al., 2005; Mori et al., 2006; Sudarov et al., 2011). Moreover, he argued that BG progenitors result from the retraction of the apical processes of radial cells lining the VZ of the cerebellar anlage, subsequently radially delaminating towards the nascent parenchyma by attaching their endfeet to the pial surface (Ramón y Cajal, 1911). Anatomical investigations on neurochemically identified glia later provided evidence consistent with this interpretation, indicating that cerebellar BG, at least in part, are generated through this process (Yuasa et al., 1996; Yamada and Watanabe, 2002). In further support of this notion, it has been recently demonstrated that aberrant FGF/ERK signaling in RG lining the ventricle does not allow their transformation into BG and results into a disorganized cerebellar layering and in the absence of folia (Li et al., 2014). Of note, the growth and differentiation factor 10 (GDF10), glial marker specific for both developing and mature BGs, has been recently shown to be expressed in the posterior VZ of the hemispheres and through the whole VZ of the midline vermis (Mecklenburg et al., 2014). Therefore, although it is still not known whether gliogenic progenitors lining the cerebellar VZ are compartmentalised in distinct domains, this evidence suggests that, at least in the lateral cerebellum, BG may selectively derive from precursors located in the posterior VZ.

As first shown by Altman and Bayer (1997) by the analysis of ^{3}H-thymidine-labelled material, the delamination of BG precursors and their translocation towards the nascent parenchyma occurs soon after the completion of PCs genesis and their emigration from the VZ, at around E14 in mice (Yuasa et al., 1996; Yamada and Watanabe, 2002). PC and BG precursors show a very contiguous spatial distribution during their migration in the developing cerebellar tissue: migrating BG progenitors are situated just beneath the front line of migrating PCs and finally disperse below the pial surface, where, after birth, they further compact around the monolayer of PCs. This close relationship between PCs and BGs suggests that they maintain a tight interaction, possibly implicated in their further maturation. BG precursors intermingle with PCs in the PCL and form an thick layer of proliferative cells that continue dividing for the whole first postnatal week. Concomitant with the massive glial migration towards the cerebellar parenchyma, the VZ is reduced in

thickness and cell number and becomes a simple epithelium (i.e. the ependymal layer). This also results from a second wave of delamination, described as occurring during late embryonic development. These other astroglial-like progenitors were described to reach the PWM, where they proliferate to produce parenchymal astrocytes as well as GABAergic interneurons (Altman and Bayer, 1997; Yamada and Watanabe, 2002; Parmigiani et al., 2015). Whether PWM astroglial progenitors can also produce some BG or whether BG progenitors in the PCL (hereafter referred as PCL progenitors or PCLp) can in turn contribute other astrocyte subtypes still remain to be established. Similarly, the dynamics and timing of the amplification of astroglial progenitors are largely unknown.

A small contribution of the RL to cerebellar astrogliogenesis has also been proposed (Sievers et al., 1994), but so far remains controversial (Swarz and Del Cerro, 1977; Hallonet et al., 1990; Hallonet and Le Douarin, 1993; Gao and Hatten, 1994; Alder et al., 1996; Zhang and Goldman, 1996; Okano-Uchida et al., 2004; Machold et al., 2007; Hoshino, 2012).

In conclusion, three main sources of astrocytes can be postulated in the developing cerebellum: the embryonic VZ is the primary source of astrocytes which, however, according to the current knowledge, before final specification, delaminate from the VZ to the PCL first and, later, to the PWM and go through an intermediate phase of amplification. Nevertheless, the contribution of each of these three germinative sites to cerebellar astroglial diversity still needs to be elucidated. Similarly, a fundamental question that awaits to be answered is whether or not the distinct astrocyte types belong to separate lineages and originate from equivalent or fate-restricted progenitors. In this respect, the well characterized and clearly distinguishable astroglial phenotypes offer a clear experimental advantage compared to more complex and phenotypically undefined systems such as the cerebral cortex. Last, as demonstrated to occur in the cerebral cortex (Noctor et al., 2004), the extent through which a direct transformation of embryonic RG into specific cerebellar astroglial phenotypes without any subsequent proliferation event contributes to cerebellar astrogliogenesis still awaits clarification.

1.3.4 Lineage relationship between cerebellar neurons and astrocytes

As previously discussed, cerebellar neurons and astrocytes are generated by the same germinative niches and according to a precise temporal sequence, raising the hypothesis that they might be clonally related. Indeed, several fate mapping analyses, in which embryonic progenitors were targeted and followed based on the expression of specific markers, suggested a common origin between the two lineages. In detail, when classical RG markers were used, such as BLBP, GLAST and TNC, the labeled progenies comprised cerebellar GABAergic neurons as well as BG and parenchymal astrocytes (Yuasa et al., 1996; Anthony et al., 2004; Mori et al., 2006; Anthony and Heintz, 2008). Moreover, *in vivo* targeting of ventricular RG through injections of LCMV-pseudotyped lentiviral vectors displaying a particular tropism towards astroglial cells demonstrated that RG are able to generate astrocytes and interneurons during late (E15) embryonic development (Parmigiani et al., 2015). On the other side, when fate mapping was performed exploiting the regulatory regions of transcription factors known to be necessary for the specification towards the neuronal lineage, some astrocytes could be detected among the offspring cells as well. Indeed, both PTF1A- and NGN2-expressing progenitors, located in distinct domains of the embryonic VZ, were shown to be able to generate a small number of astrocytes (Hoshino et al., 2005; Florio et al., 2012). Moreover, both BG and parenchymal astrocytes appeared to be produced by ASCL1-positive progenitors, whose expression occurs in the VZ between E10.5 and E13.5, overlapping that of PTF1A and Neurogenins (Sudarov et al., 2011). Nevertheless, the low frequency of astroglial cells observed in these studies questioned the actual origin of most cerebellar astrocytes from these cell populations.

Common ancestors for cerebellar neurons and glia are also suggested by distinct functional studies performed at embryonic stages. Indeed, manipulation of Notch/BMP signaling resulted in an altered balance between the numbers of neurons and astrocytes, with macroscopic cerebellar defects. Selective Notch ablation in the cerebellar territory resulted in a reduction of both neurons and astrocytes and to hypomorphic cerebella, due to a too rapid exhaustion of the progenitor pool (Lutolf et al., 2002). On the contrary, a constitutive activation of the same signaling promoted the generation of astrocytes at the expense of neurons (Machold et al., 2007). On the other side, in the absence of the BMP-repressor Bmi1, the number of astrocytes increased concomitantly to the decrease in the amount of

interneurons (Jacobs et al., 1999; Zhang et al., 2011). Moreover, both *Ascl*1 null (Grimaldi et al., 2009) and conditional knockout mice lacking this transcription factor specifically in the cerebellar VZ (Sudarov et al., 2011) showed lower numbers of PAX2+ interneurons and increased SOX9+ astrocytes in the cerebellum, compared to wild type animals. Conversely, when ASCL1 expression was increased in the cerebellar VZ, interneurons increased at the expense of GLAST- and S100β- expressing astrocytes (Grimaldi et al., 2009).

Several evidences based on both *in vitro* and *in vivo* studies have also pointed to the existence of bipotent neuroglial precursors in the postnatal cerebellum and PWM (Silbereis et al., 2009; Lee et al., 2005; Klein et al., 2005; Fleming et al., 2013). However, the most conclusive evidence was recently provided by Parmigiani and colleagues (Parmigiani et al., 2015). In this study, by *in vitro*, *ex vivo* and *in vivo* clonal analyses at the single progenitor level, the authors showed that GABAergic interneurons and astrocytes share a common ancestor in the PWM. Examining whether such progenitors also exist at earlier developmental ages and, if so, what neuron and astroglia subpopulations they might generate will be of particular interest in the future.

1.3.5 Differentiation of cerebellar astrocytes

In early co-culture studies, cerebellar neurons were shown to profoundly influence the morphology, antigenic profile and proliferative rates of cerebellar astroglia. Indeed, when added to cultured astrocytes, neurons could reduce astrocytes' proliferation, induce their morphological change from flattened to multipolar or BG-like shapes, and downregulate specific antigens (Hatten, 1985; Nagata et al., 1986). While the processes of maturation of WM and GL astrocytes still remain mostly undetermined, the available evidence on cerebellar astrocytes differentiation almost exclusively concerns BG. The reasons for a major interest in addressing BG maturation compared to the other cerebellar phenotypes can be arguably found in their highly specialized and peculiar phenotype and in their demonstrated crucial functions in supporting cerebellar development at both the cellular and structural level. Therefore, hereafter, I will focus specifically on this phenotype, presenting the available evidences about the acquisition of their typical morphology and layering, and subsequently addressing their molecular maturation.

Maturation and maintenance of BG morphology.

After withdrawal of their apical process, RG displace their cell body toward the cerebellar cortex, where they undergo several morphological changes to produce BG and, together with developing PCs, form a multi-layered structure, which later gradually transforms into a monolayer. Differently from RG that possess a single basal branch, to acquire their mature phenotype BG must extend multiple ascending processes (usually three to six per cell) that cross the ML. In the rat, these multiple branches emerge during postnatal development, increasing in number until the end of the first postnatal week and then decreasing, in parallel with the expansion and reduction of the EGL (Shiga et al., 1983), suggesting that granule cells contribute to regulate BG process formation (see later). At early maturation stages, BG fibres are rather smooth with small enlargements and excrescences that progressively grow to bushy expansions covering most of the radial process (Shiga et al., 1983) and establishing tight interactions with Purkinje cell synapses. For the induction of the proper morphological phenotype, BG progenitors need to interact with three components of the cerebellar environment: the subpial basement membrane, PCs and GCs. The basement membrane lies on the surface of the cerebellar cortex and it is deposited by meningeal elements during early development; for correct BG polarization, process outgrowth and positioning in the PCL, BG endfeet need to be tightly anchored to it. If this anchorage is defective, BG fibers fail to properly form and orient and BG cell bodies translocate to the ML, resulting in a severe disruption of cerebellar foliation and layering (Sievers et al., 1994; Li et al., 2014). Several receptors and intracellular transduction pathways were implicated in this anchorage. They include β1-integrins (Graus-Porta et al., 2001; Frick et al., 2012) and other molecules associated to their intracellular domains, such as the integrin-linked kinase ILK (Belvindrah et al., 2006), the ABL family of tyrosine kinases (Qiu et al., 2010), as well as RIC-8A (a guanine nucleotide exchange factor in the G-coupled receptor pathway; Ma et al., 2012). These molecules provide link with rho-type GTPases, such as CDC42 (Belvindrah et al., 2006), to regulate F-actin assembly at the tips of outgrowing BG processes. A-dystroglycan and dystroglycan-glycosiltransferase, members of the dystrophin-dystroglycan complex and both expressed by BG, were also recognized as regulators of the correct BG maturation and adhesion to the basal membrane (Moore et al., 2002; Qu and Smith, 2005; Satz et al., 2008). Therefore, both β1-integrin and α-dystroglycan receptors and their associated pathways are necessary for this critical

ontogenetic step, mediating a bidirectional interaction with components of the extracellular matrix.

With their tight interaction with developing BG, PCs have been described to impact specifically on BG morphological maturation through Shh (Dahmane and Ruiz-i-Altaba, 1999) as well as through other distinct pathways including Notch pathway, neuregulins and FGF signalling. During the second and third postnatal week of development, BG fibers undergo cytoarchitectonic changes including both increasing number of radial processes and formation of lamellae (Yamada and Watanabe, 2002). All these transformation events are intimately associated with PC dendrites growing (Yamada et al., 2000). Namely, PCs express on their surface the DNER (Delta/Notch-like EGF-related) receptor, that, through the interaction with Notch expressed in BGs, controls the formation of radial fibers and BG layering (Eiraku et al., 2005). Experimental DNER deletion retards the formation of radial fibers and results in abnormal arrangement of BG, which, nonetheless, is recovered after the third week of life. This suggests that DNER action is transient and that additional Notch ligands may be present in the surrounding environment to compensate for DNER functions. Along this line, it is to note that the canonical Notch ligand JAG1 is broadly expressed in the postnatal cerebellum by both GCs and BG itself (Stump et al., 2002) and its deletion from all VZ cerebellar progenitors results in the loss of BG contact with the pial surface, in clear defects in fibers development and in the reduction of BG numbers (Weller et al., 2006). Similarly, conditional deletion of Notch1/2 or the downstream target RBPJ in hGFAP-positive precursors resulted in clear defects in BG monolayer formation, accompanied by impaired differentiation of BG fibers (Komine et al., 2007). Moreover, Delta-like1 in BG was described to be the major Notch ligand responsible for the correct growth of BG fibers, layering and expansion (Hiraoka et al., 2013).

Further influence on BG development is exerted by the underlying GCs, that represent an additional source of JAG1 (Stump et al., 2002). GCPs migrate along BG fibers through the interaction between neuregulin-1 (NRG) and its receptor ERBB4 (Rio et al., 1997): during their migration, they provide additional differentiation-promoting signals through the NRG pathway itself and the secretion of FGF9. Indeed, the application of a soluble form of NRG induced a radial phenotype in astrocytes *in vitro*, and this effect was blocked by the overexpression of a dominant negative form of ERBB4 in glial cells, that also inhibited the migration of GCs. Interestingly, Notch has been proposed to act synergistically with NRG by

upregulating ERBB and thus enhancing the response to NRG signals (Schmid et al., 2003). Moreover, the growth factor FGF9, secreted by GCs and acting on FGFR1/2 in BG, was also observed to control fiber formation and markers expression (Lin et al., 2009). Indeed, *in vitro* and *in vivo* ablation of FGF9 signaling resulted in star-shaped multipolar astrocytes, suggesting that this factor participates in the fate choice between radial BG and stellate astrocytes. Moreover, *in vivo* ablation of FGF1 and FGF2 in hGFAP-expressing progenitors led to a reduction in the number of BGs (Müller Smith et al., 2012).

In addition to the extrinsic influence of the surrounding neurons on astrocyte differentiation, some cell-intrinsic determinants are known to be involved in the morphological maturation of cerebellar astrocytes. Among these, the SOX proteins of group C are known to be strongly expressed in the developing nervous system and have been associated with maturation of both neurons and glia. So far, studies in the cerebellum have focussed on the family member SOX4, whose overexpression in hGFAP-expressing precursors led to a failure in RG migration into the position normally taken by BG and in the absence of radial fibers projecting towards the pial surface (Hoser et al., 2007). These defects in BG maturation were accompanied by cerebellar malformations and ataxia. Conversely, multipolar astrocyte morphologies did not appear to be affected. Thus, the correct maturation of the BG monolayer requires SOX4 down-regulation, suggesting that this transcription factor interferes with the molecular cascades implicated in BG differentiation. Importantly, SOX2, another member of the same family associated with NSC self-renewal and differentiation (Pevny and Nicolis, 2010; Gómez-López et al., 2011), is known to be expressed in the PCL by both developing and mature BG and has very recently been associated to a so far unknown neurogenic niche in the adult cerebellum (see section 1.2.1.3). Nevertheless, its function in BG maturation still needs to be explored. On the other side, SOX9, member of the SOX proteins of group E recently described as astrocyte-specific nuclear marker in most regions of the adult brain included the cerebellum (Sun et al., 2017), was shown to be dispensable for the development of cerebellar astrocytes (Hashimoto et al., 2016).

Among other cell intrinsic component affecting BG formation, *PTEN* deletion in hGFAP-positive cells also induced the disappearance of glia with the typical BG morphology without affecting other parenchymal astrocytes, thus revealing that active PTEN signalling is intrinsically required for correct BG differentiation and maintenance of a polarized

phenotype (Yue et al., 2005). Moreover, a misalignment of BG and abortive formation of radial fibers that often do not contact the pial surface was observed in absence of the ubiquitin ligase Huwe1 (D'Arca et al., 2010). The deletion of Ptpn11, coding for the tyrosine phosphatase Shp2, was also shown to block BG formation from RG and to affect cerebellar foliation, pointing to the critical role of ERK signaling in BG induction (Li et al., 2014). Finally, after deletion of the tumor suppressor gene adenomatous polyposis coli (*APC*) in GFAP-expressing cells, BG differentiation proceeds normally during the first postnatal week, but at later stages BG cell bodies translocate to the ML, then losing contacts to the pial surface and acquiring a stellate morphology (Wang et al., 2011). This indicates that the radial phenotype not only has to be actively promoted but also continuously maintained.

Maturation of molecular profiles

Distinct cerebellar astrocyte phenotypes were shown to display distinct, although overlapping, molecular signatures (see section 1.1.1.2). Nevertheless, the mechanisms of molecular and functional maturation of cerebellar astrocytes have been very little addressed and are mostly unknown. A recent study came out in 2016 *in vivo* unveiled the role for Purkinje cells-derived Shh in regulating the molecular and functional profile of cerebellar cortical astrocytes (Farmer et al., 2016). Indeed, by blocking Shh signaling in BGs and by constitutively activating it in granular velate astrocytes, which are physiologically exposed to lower amounts of Shh than BGs, the authors showed that the two subtypes are interchangeable under both the molecular and functional point of view in both the postnatal and adult cerebellum. In detail, Shh signalling was shown to sustain in BG GluA1, GluA4, GLAST and Kir4.1 expression, prevent AQP4 expression, and maintain AMPA receptor–mediated currents. When this signaling is constitutively activated in velate astrocytes, these cells could acquire the same molecular and functional signature of BG. Nevertheless, these molecular and functional changes were not mirrored by morphological modifications, suggesting that, besides neuron-derived cues, either other environmental stimuli or intrinsic differentiation programs are needed to fully create astrocyte complexity in the mature cerebellum.

On the whole, the available data indicate that BG maturation requires tight and timely-regulated stimuli coming from the surrounding environment as well as intrinsically defined mechanisms. An impairment of these regulatory mechanisms often results in a failure in

acquiring or maintaining a radial morphology and in the acquisition of a stellate multipolar shape, which may therefore represent a default program of differentiation for cerebellar astroglial precursors. On the other side, the mechanisms of specification of the other stellate astroglial phenotypes are completely unexplored and still need to be investigated.

1.3.6 Functional specialization of cerebellar astrocytes

As in other CNS regions, cerebellar astrocytes influence the development and the later maintenance and functioning of the neuronal circuitry. As previously discussed, the more extensively studied astrocytes in the cerebellum are BGs (reviewed in Buffo and Rossi, 2013), whose functions have been partially described in both development and adult life and will be therefore addressed hereafter.

Developmental functions

During cerebellar development, cerebellar radial glia and their daughter BG provide physical trails to guide the migration of distinct cell types and regulate the directional elongation of axons and dendrites. As previously described (see section 1.2.3), developing PCs and BGs form complex interactions through which they reciprocally orchestrate their maturation. In the embryo, PCs migrate from the VZ by physically attaching to the processes of RG, in a highly regulated process suggested to be mediated, at least in part, by several adhesion molecules (Yuasa et al., 1991; Hatten, 1999; Redies et al., 2011). Parallel to the conclusion of this migration, RG appear to translocate in order to originate BG progenitors (i.e. PCL progenitors), whose terminal maturation is then finely regulated by young PCs themselves, as formerly discussed (see section 1.3.5). Subsequently, PCL progenitors play important roles in both cerebellar foliation (see section 1.2.1.3) and layering, two parallel processes crucial for cerebellar corticogenesis. For the proper formation of the cerebellar layers, PCL progenitors also act as a scaffold for both granule cells and inhibitory interneurons along opposite routes, allowing them to settle in their final positions within the GL and ML, respectively. Briefly, the interaction of migrating GCs with BG consists of two distinct phases: granule cells first induce guidance properties in BG (Hatten, 1985; Rio et al., 1997) and, then, specific recognition and adhesion mechanisms regulate cell navigation along glial axes, from the EGL towards the forming GL (Hatten, 1999; Solecki, 2012). On the other side, BG have been proposed to be involved in the

guidance of basket and stellate cells from the PWM outwards: a direct contact between migrating interneurons and BG fibers has been observed both *in vivo* (Guijarro et al., 2006; Simat et al., 2007) and in cerebellar explants *in vitro* (Guijarro et al., 2006). Nevertheless, it is still uncertain whether interneurons use BG scaffolds as unique guidance in an exclusive route or different phases of migration are regulated by different cell types (such as granule cells with their axons and parallel fibers).

Functions in synaptogenesis

BG also actively participates to the maturation of PC synapses. Indeed, the last phases of BG differentiation, when they acquire mature traits and properties, is concomitant with the outgrowth of PC dendrites and their synapses development. Following a proximo-distal direction from the deepest to the outermost regions of the ML, BG fibers extend numerous processes that gradually enwrap PCs dendrites and their growing synapse and have been suggested to provide both physical and trophic support for the elongation of the PC tree (Yamada et al., 2000; Ango et al., 2008). Estimates on the number of PC synapses that BG microdomains encompass ranges from ~2000–6000 (Reichenbach et al., 1995). Notably, calcium currents through AMPA receptors were shown to be required for the maintenance of BG processes enwrapped around PC dendritic spines (Iino et al., 2001), as confirmed by the evidence that conditional deletion of calcium-permeabe AMPA receptors GluR1 and GluR4 resulted in the retraction of these processes (Saab et al., 2012). Such glial sheaths appear indispensable for the correct formation of PC synapses with both climbing and parallel fibers: the retraction of these glial membranes, where GLAST is located, resulted in severe impairments in the clearance of synaptically released glutamate, with consequent defects in synaptic signaling and plasticity and related behavioral dysfunctions (Shibuki et al., 1996; Watase et al., 1998; Tao et al., 2011). Moreover, the morphological changes in these fine glial processes wrapping Purkinje cell synapses were also shown to cause an abnormal multiple innervation of PCs by climbing fibers (Iino et al., 2001). Physiologically, a similar multiple innervation also occurs during development, but it is known to completely eliminated by postnatal day 15 (Mariani and Changeux, 1981). Therefore, a normal BG maturation appears indispensable to control the final number of synapses as well as their stabilization (Iino et al., 2001; Lippman Bell et al., 2010; Saab et al., 2012). On the other hand, BG also guide stellate INs axons on PCs dendrites and regulate the formation of their synapses preferentially at the intersection between BG fibers and PC

dendrites: this scaffolding is mediated by a member of the L1 family immunoglobulin protein Close Homologue of L1 (CHL1), which is localized to apical BG fibers and stellate cells during the development of stellate axon arbors. In CHL1-null mice, stellate axons fail to properly grow and the numbers of GABAergic synapses on PCs are reduced, with signs of synaptic degeneration, a phenotype which is essentially reproduced when CHL1 is selectively ablated in BG (Ango et al., 2008).

Functions in circuit activity

Afterwards, within the adult cerebellar circuit, BG actively participate in shaping the electrical activity. Indeed, BG processes almost completely enwrap the synapses formed between PCs, parallel fibers, climbing fibers and ML interneurons, forming the so called "microdomains" (Hoogland and Kuhn, 2010), and can tightly control local extracellular increases of neurotransmitters. Moreover, glutamate release in the extracellular space following the stimulation of parallel (Clark and Barbour, 1997) as well as climbing fibers (Bergles et al., 1997) induces calcium transients in individual BG microdomains, which are mediated by calcium permeable AMPA receptors and reflect the activity of the BG glutamate transporter GLAST (Grosche et al., 1999). Thus, BG are intensively implicated in the removal of glutamate from extracellular space to prevent spillover of the neurotransmitter at Purkinje cell synapses. Furthermore, by means of calcium signaling, BG can rapidly regulate potassium ions in the extracellular environment, thereby tightly controlling membrane potential of adjacent PCs (Wang et al., 2012). These calcium and potassium waves have been suggested to play a metabolic and neuroprotective role, provided their increase with age and hypoxia (Mathiesen et al., 2013).

On the other side, very little is known about the specific functions of astrocytes in the GL and WM. It is conceivable that, in all cortical layers, the different types of astrocytes carry out typical ''astrocytic'' tasks in the regulation of tissue homeostasis (Kimelberg, 2010). Nevertheless, their physical relationship with synapses is strongly different among layers: processes of velate astrocytes in the GL do not strictly ensheath ML synapses as BG do with PCs, rather, they enclose small groups of GCs and completely enwrap the glomeruli but never penetrate within the complexes, so as to isolate synaptic complexes and partition subsets of mossy fibers conveying different types of information (Chan-Palay and Palay, 1972; Palay and Chan-Palay, 1974; Hoogland and Kuhn, 2010). Despite a direct evidence of

this function is still missing, the difference above described between velate astrocytes and BGs suggests that the former do not exert the fine synaptic regulation described for BGs in the molecular layer. However, similarly to BGs, spreading calcium waves have been recorded from GL astrocytes. These events encompassed spontaneous subcellular transient that could diffuse to involve nearby elements and were influenced by purinergic signalling (Hoogland et al., 2009; Hoogland and Kuhn, 2010). Nevertheless, whether velate astrocytes have other unique properties is still unclear and needs elucidations.

1.4 Outline of this thesis work

Despite the common view of astrocytes as a fairly homogeneous population, an ever-increasing body of evidence supports their morphological, molecular and functional heterogeneity both across and within distinct regions of the developing and adult CNS. This heterogeneity, far from being fully unveiled, is currently under intense scrutiny and, intriguingly, very little is known on how it emerges during development. On the contrary, the ontogenesis of the well-characterized neuronal diversity has been deeply investigated in the past decades, revealing that distinct neuronal phenotypes within several brain regions, such as the retina, cerebral cortex, spinal cord and cerebellum, are specified from common progenitors according to tightly regulated spatiotemporal patterning processes, and, down to the level of single progenitors' lineages, clarifying many of the molecular mechanisms underlying specific competence states.

From an ontogenic standpoint, astrocyte heterogeneity has been proposed, at least in the cerebral cortex (García-Marqués and López-Mascaraque, 2012), to be related to the clonal identity of cells, unveiling a new level of astrocyte diversity likely associated with specific regional functions. In this view, astrocytes generated from the same progenitor are likely to share the same molecular and functional features that distinguish them from other clones. Nevertheless, it is still unknown whether and to what extent these evidences apply to other brain areas, where astrocyte lineage tracing analyses at the single progenitor level are still needed. Moreover, the results collected so far may be biased by the poor resolution of the astrocyte phenotypic and molecular heterogeneity in the studied area, mainly due to a lack of markers to distinguish different cell phenotypes with similar morphologies. Furthermore, whether and how the developmental potential of astroglial progenitors, in terms of both progenies composition and size, is regulated over time remains to be defined.

During my PhD studies, I spent most of my efforts in addressing these open issues by using the cerebellum as a model of investigation. Indeed, the cerebellum is an excellent system to study astrocyte ontogenesis. The simple laminar architecture of this region makes the cerebellar major astroglial subtypes easily recognizable by layer allocation and morphology. Despite that, the available knowledge on the ontogenesis of cerebellar astrocytes is still limited. It essentially concerns the origin of astrocytes from RG lining the ventricle and the notion that intermediate progenitor cells with astroglial features

delaminate from the VZ to secondary gliogenic niches, where they intensively proliferate for the whole first postnatal week. Nevertheless, the fate competence of both embryonic and postnatal cerebellar astrocyte progenitors and whether it changes over time still need to be unveiled. Therefore, by means of distinct *in vivo* approaches that allowed to perform an unprecedented quantitative analysis of astrogliogenesis, I investigated the origin of astrocyte diversity in the cerebellum, following retrospectively the progenies of both single embryonic and postnatal progenitors and addressing their developmental potential and mechanisms over time.

The main issues addressed in my PhD thesis can be summarized as follows:

How the diverse astrocyte phenotypes emerge through the unfolding of individual embryonic lineages. By means of *in vivo* clonal analyses exploiting the novel Star Track technique, I retrospectively followed individual lineages in order to understand whether and to what extent the diverse astroglial phenotypes are clonally related. This issue was addressed by paying a particular attention on the influence of time on both progenitors' fate potency and their offspring's features and checking for possible recurrent modularities in clone composition.

To address these issues, I performed the first Star Track experiments in Madrid, in the laboratory of Prof. Laura López-Mascaraque where the technique was developed, during a training stay supported by a NENS Exchange Grant. To perform cluster analyses on clones, instead, I took advantage of the kind help of Claudio de'Sperati, Università Vita-Salute San Raffaele.

What is the contribution of postnatal progenitors localized in secondary germinal niches to cerebellar astrogliogenesis. Starting from the evidence that the majority of gliogenesis in the cortex occurs after birth from locally dividing astrocyte precursors (Ge et al., 2012), I asked whether a similar *in situ* production of astrocytes did take place in the cerebellar cortex as well, where proliferating progenitors with astroglial features are allocated in the PCL, one of the three secondary germinative niches of the postnatal cerebellum (see section 1.3.1.3). The fate potency of such proliferating progenitors was investigated through retrospective *in vivo* clonal analysis.

- *How layer specific dynamics affect postnatal astrogliogenesis*. To investigate whether astrocytes settled in distinct layers proliferate according to different mechanisms, I performed thymidine analogues-based proliferation analyses focusing on postnatal development, when the maximal expansion of precursors in the cerebellar parenchyma occurs together with the concomitant maximal growth of the cerebellum (Legué et al., 2015). Moreover, starting from embryonic stages and spanning the whole first postnatal week, I similarly addressed whether the distinct astrocyte subtypes differentiate according to layer-specific dynamics.

- *What are the rules governing cell fate decision of cerebellar astrocyte progenitors*. The main goal was to understand whether the distinct kinds of clones observed in the *in vivo* clonal analysis are generated by a single multipotent progenitor that stochastically makes its fate choice or by fate restricted precursors predestined to produce only specific astrocyte types. In a first attempt to solve this issue, we took advantage of a simple mathematical model, based on the assumption that all astrocyte progenitors belong to a homogeneous multipotent population, and compared the outcome of the Star Track clonal analysis to *in silico* simulated lineages. To address this issue, I took advantage of the expertise in mathematical modelling of Marion Betizeau, University of Zurich.

- *Identification of intrinsic regulators of defined astroglial phenotypes' development*. In search for transcription factors cell autonomously involved in the development and/or maturation of cerebellar astrocytes, I performed *in vivo* loss of function studies of *Sox2*, previously described to be required for the development and maintenance of NSC/RG in both developing and adult CNS (Pevny and Nicolis, 2010; Gómez-López et al., 2011) and known to be expressed in the PCL by both immature and mature BG (Sottile et al., 2006; Alcock and Sottile, 2009).

Chapter 2: Materials and Methods

2.1 Experimental animals

Experimental procedures were performed on the following mouse lines: C57BL/6, hGFAP-green fluorescent protein (GFP, Zhuo et al., 1997), GLAST^{CreERT2} (Mori et al., 2006) crossed with R26R$^{Confetti/+}$ (R26R^{Confetti}; Snippert et al., 2010) or Sox2$^{fl/fl}$ (Favaro et al., 2009) mice, and Wnt1-Cre (Danielian 1998) crossed with Sox2$^{fl/fl}$. For analyses performed on Wnt1-Cre;Sox2$^{fl/fl}$ animals, we used as controls mice carrying the Sox2flox conditional mutation either in homozygosis (Sox2$^{fl/fl}$) or in heterozygosis (Sox2$^{fl/+}$), as well as Wnt1-Cre;Sox2$^{fl/+}$ animals, which were mostly phenotypically undistinguishable from Sox2$^{fl/fl}$ and Sox2$^{fl/+}$ animals despite the lack of a *Sox2* allele (see Supplementary Table 1). Mice of either sexes were included. The day of vaginal plug detection was defined as embryonic day zero (E0) and the day of birth was considered as postnatal day zero (P0). Mice were maintained on a 12 hr day／night cycle with adequate food and water. All procedures were in accordance with the European Communities Council Directive (2010/63/EU and 86/609/EEC), the National Institutes of Health guidelines, and the Italian Law for Care and Use of Experimental Animals (DL26/14). They were approved by the Italian Ministry of Health and the Bioethical Committee of the University of Turin. The study was conducted according to the Arrive guidelines.

2.2 *In utero* electroporations (IUE)

E12 or E14 pregnant mice were deeply anesthetized by inhalation of isofluorane administered in conjunction with a mixture of 30:70 O2/N2O throughout the surgery duration and placed on a warming blanket. The skin and the muscular abdominal wall were cut and the uterine horns were exposed. Embryos were constantly maintained moist with physiological saline and were trans-illuminated with a cold light to hit the proper injection site. Using a picopump connected to a glass microcapillary tube, 2µl of the hGFAP-Star Track plasmid mixture (2–5 µg/µL of DNA in 0.1% fast green; García-Marqués and López-Mascaraque, 2012) were injected into the IVth ventricle of each embryo in order to reach the cerebellar VZ and stably mark VZ primary progenitors (Kita et al., 2013). After injecting all embryos, the heads were placed between the forceps-shaped electrodes of a BTX electroporator (Holliston, MA, USA) and one train of 5 square pulses was applied (30V or 35V for E12 and E14 electroporations, respectively; 50 ms followed by 950 ms intervals). Afterwards, the uterine horns were positioned back into the abdominal cavity, and both

muscle and skin were sutured. Pregnant mice recovered under a warm lamp and then were returned to their home cage. After surgery, the analgesic Rimadyl (5µg/g) was subcutaneously administered to reduce postsurgical pain. Injected embryos were allowed to develop normally and were analyzed at postnatal day (P)0 or P30.

2.3 Local and systemic administration of Tamoxifen

To allow Cre recombination exclusively in radial precursors of the PCL, we topically administered Tamoxifen (Tx) citrate crystals (Sigma-Aldrich) on the pial surface of the vermis of GLAST^{CreERT2};R26R^{Confetti} mice at P6, to selectively target glial endfeet as previously described (Parmigiani et al., 2015). To this aim, mice were anesthetized by hypothermia.

To activate the Cre recombinase in GLAST^{CreERT2};Sox2$^{fl/fl}$ mice, Tx (20 mg/ml solution dissolved in corn oil) was administered via subcutaneous injection for pups (20 µg/g body weight) or via oral gavage for adults (5 mg/40 g body weight). Mice were given a single Tx injection at P2 or at 6 months of life. As for experiments performed in Wnt1-Cre;Sox2$^{fl/fl}$ animals, Sox2$^{fl/fl}$, Sox2$^{fl/+}$ and GLAST^{CreERT2};Sox2$^{fl/+}$ mice were used as controls (see Supplementary Table 1).

2.4 Thymidine Analogues

Bromodeoxyuridine (BrdU, Sigma-Aldrich) and 5-ethynyl-2'-deoxyuridine (EdU, Invitrogen) were dissolved at 10 mg/ml in sterile saline and administered via subcutaneous injections for pups or via intraperitoneal injections for adults. The same dose of 100 µg/kg body weight was used for both analogues. EdU was injected 6 hours before sacrifice, to increase the chance of labelling dividing astrocytes. For BrdU labeling, samples were incubated in 2N HCl for 20 minutes at 37°C, washed with borate buffer (pH 8.5) for 10 min, and processed for anti-BrdU antibody staining. EdU was detected using a commercial kit (Click.iT®, Life Technologies) after the immunohistochemical reactions.

2.5 Histological and Immunohistochemical procedures

Under anesthesia (hypothermia for pups up to P6 and intraperitoneal injection of a mixture of ketamine -100 mg/kg; Ketavet, Bayern, Leverkusen, Germany- and xylazine -5 mg/kg; Rompun, Bayer, Milan, Italy- for older mice) animals were transcardially perfused with an

appropriate volume of 4% paraformaldehyde (PFA) in 0.12 M phosphate buffer (PB), pH 7.2–7.4. Brains were removed, stored overnight (o/n) in the same fixative at 4 °C, washed in Phosphate Buffered Saline (PBS) and finally cryoprotected in 30% sucrose in 0.12M PB. The cerebella were then embedded and frozen over dry ice in OCT (TissueTEK), sectioned in the parasagittal plane at 30 µm using a cryostat and collected in PBS (P30 juvenile and adult cerebella) or placed directly onto glass slides (E13-P7 cerebella). For immunolabelling, sections were incubated o/n at room temperature with the appropriate primary antibodies dissolved in PBS with 1.5% donkey or goat serum (Jackson ImmunoResearch) and 0.25% Triton X-100 (Sigma-Aldrich): anti-S100β (1:1000, mouse, monoclonal; Sigma), anti-GFP (1:700, rabbit, polyclonal; Invitrogen), anti-GFP (1:700, chicken, polyclonal; Aves Labs), anti-RFP (1:1500, rabbit, polyclonal, Rockland) anti-BrdU (1:500, rat, monoclonal; Abcam), anti-glial fibrillary acidic protein (GFAP, 1:1500, rabbit, polyclonal; Dako), anti-brain lipid binding protein (BLBP, 1:500; rabbit, polyclonal; Abcam); anti-phospho(p)-vimentin (1:500; mouse, monoclonal, MBL International); anti SOX2 (1:500, rabbit, polyclonal; Merck Millipore); anti Calbindin (1:1500, rabbit, monoclonal; Swant). Sections were then exposed for 2h at room temperature to secondary species-specific antibodies conjugated with Alexa Fluor 488, Alexa Fluor 555 or Alexa Fluor 647 (1:500; Invitrogen), or Cy3 (1:500; Jackson ImmunoResearch). Cell nuclei were visualized using 4',6-diamidino-2-phenylindole (DAPI; Fluka). After processing, sections were mounted on microscope slides with Tris-glycerol supplemented with 10% Mowiol (Calbiochem).

For Star Track clonal analysis, P0 and P30 cerebella were parasagittally cut in 50 µm-thick serial sections. For $R26R^{Confetti}$ stainings, 60 µm-thick serial sections were obtained with a vibrating microtome (Leica). When the thickness of the sections was >30 µm, they were incubated for 48h at 4°C in primary antibody solution containing 1.5% donkey serum and 2% Triton-X100. Secondary antibody incubation was performed o/n in PBS with 1.5% donkey serum and 0.5% Triton-X100.

2.6 Data analysis and image processing

Histological specimens were examined using an E-800 Nikon microscope connected to a color CCD camera or a Leica TCS SP5 confocal microscope. For Star Track clonal analysis, confocal images were acquired under fixed excitation and absorption conditions for each fluorophore as previously described (García-Marqués and López-Mascaraque, 2012). In

some instances, we applied the colocalization analysis provided by the LAS AF software (Leica) to display in white/purple marker co-expression at the pixel level. Adobe Photoshop 6.0 (Adobe Systems) was used to adjust image contrast and assemble the final images. On the basis of confocal images, clone distribution was mapped by either Neurolucida 7.0 (MBF Bioscience) or Reconstruct softwares (Fiala, 2005; version 1.1) that defined spatial coordinates for each cell, subsequently employed to calculate cell distances with a Python script. Quantitative evaluations (cell counts, proliferation, birthdating and cleavage plane orientation analyses) were performed on confocal images by NIH ImageJ software (http://rsb.info.nih.gov/ij/). Three to six animals were analyzed for each time point or experimental condition. Measurements were derived from at least three sections per animal.

2.7 Definition of clones and clonal analyses

To evaluate the expression of hGFAP-Star Track constructs (García-Marqués and López-Mascaraque, 2012) the whole cerebellar territory was analyzed. Every cell was examined for the presence of each fluorophore and cells with the same combination of fluorescent proteins were defined as part of the same clone. Labelled astrocytes were categorized according to their morphology and layering and the cellular identity of P30 clones exclusively labelled with nuclear markers was confirmed a posteriori by anti-GFAP immunostaining (Fig. 2.1). For P0 analyses in the still developing cerebellar territory, we distinguished as layers the PWM and the Cortex, based on differences in cellular density as detected by autofluorescence and validated by DRAQ5 staining (not shown). At this age, astroglial cells with cytoplasmic staining were recognized by their morphology (see results) while those presenting only nuclear labelling were excluded from analysis due to impossibility to define their phenotype by morphological criteria.

The number of cells in each clone was analyzed and will be thereafter referred as “clone size”. Medio-lateral (M-L) clone dispersion was estimated based on the number of sections that included each clone. Clones included in one single section were categorized according to the section thickness (50 μm). Antero-posterior (A-P) clone dispersion was estimated qualitatively as clone distribution through the cerebellar lobules.

In order to highlight those cases that may reflect the specific behavior of direct transformation from RG progenitors, the minimal requirement to be part of a clone was

set to 1 cell. Overall, we found 568 hGFAP-Star Track-labeled clones, comprising a total of 255 fluorescent combinations. Among them, 89% appeared with a frequency of less than 8 x 10^{-3} and only two marks were present at the highest frequency (2 x 10^{-2}). On the whole, frequencies were within the range analyzed in García-Marqués and López-Mascaraque (2012) and therefore all combinations were included. For the complete list of Star Track clones, see Supplementary Table 2.

For clonal analysis in R26R^{Confetti} mice, the entire lobules IV-V and IX were analyzed. This reporter strain enables the distinction of progenies derived from different single progenitors thanks to the stochastic and exclusive expression of one out of four fluorescent proteins. In order to visualize different fluorophore combinations, sections were stained with anti-GFP antibody that recognizes GFP, YFP and CFP and with anti-RFP antibody for RFP. Clone types marked with GFP were then discriminated according to the localization of the green staining: nuclear (corresponding to GFP, even if we did not observe any clone expressing the nuclear GFP), cytoplasmic (corresponding to YFP) or membrane-associated (corresponding to CFP), as previously described (Calzolari et al., 2015). Beside expression of the same colour, identification of cells belonging to the same clone was based on location in the same lobule and lobular wall (considering the WM as dividing each lobule in two walls), as derived from StarTrack analyses. For the complete list of Confetti clones, see Supplementary Table 3.

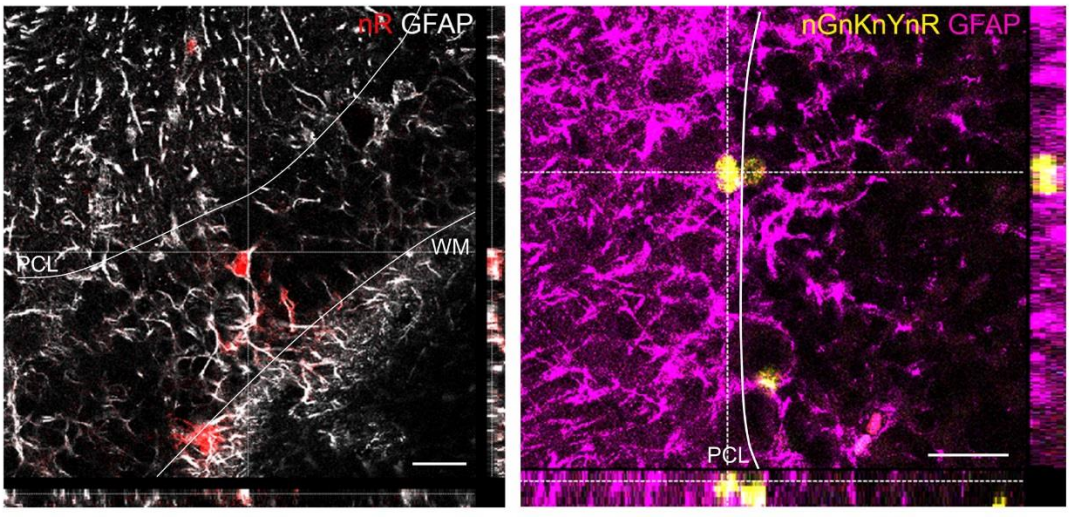

Figure 2.1. GFAP immunostaining confirms the astrocytic identity of cells labeled with nuclear markers. Reslices of single step images of labeled cells after anti-GFAP staining (white/purple) unequivocally clarify the

astrocytic identity of cells labeled solely with nuclear markers. n, nuclear; R, red (mCherry); G, GFP; K, mKO; Y, YFP; WM, white matter; PCL, Purkinje cell layer. Scale bars: 30 µm.

2.8 Analysis of clusters

To assess whether cells were uniformly distributed within the cerebellar tissue or rather formed clusters, we focused on E12-P30 heterogeneous clones (i.e. clones composed of distinct astrocyte phenotypes) that were especially numerous and large in size, and performed a nearest neighbor distance (NND) analysis followed by a cluster analysis, the former to verify the presence of cell aggregates (clusters) and the latter to estimate the number and size of clusters as well as their composition in terms of cell category types. A significant departure of the actual cumulative distribution of NND from a random distribution was considered as sign of clustering (Gao et al 2014). To this end, for each clone type we generated a uniformly distributed random sample of spatial coordinates, using the same number of observations and the corresponding cerebellar volume, and the cumulative distribution of the resulting NDDs was computed. For both empirical and randomly generated data, we fitted an asymmetric sigmoidal function (Richard's model) using the least square method.

Cluster analysis was performed with the k-means method, using accounted variance to estimate the optimal cluster number (100 replicates, max 5 clusters, threshold set to 95% of accounted variance). In order to maximize the chance of finding clusters and to limit the overestimation of cluster numbers , only clones with a minimum of 6 cells and clusters with a minimum of 3 cells were considered. Although cluster analysis is considered to be more an exploratory than a confirmatory approach (Estivill-Castro 2002), results were confirmed by visual inspection, which suggested that clustering errors (e.g., cases in which cells are spatially but not anatomically close to each other, or cases where isolated cells are forced into a cluster) remained low. The mean intra-cluster inter-cell distance for triple clones without WMA was then used as an additional criterion to classify cortical clones at P6 (see section 2.7).

2.9 Determination of cleavage plan orientation

Anti-p-vimentin staining was used to identify BG progenitors in the PCL undergoing mitosis (Kamei et al., 1998). The cleavage plane orientation was measured by calculating the angle

between the equatorial plate of Dapi-stained nuclei and the PCL trajectory. Angle values of 0°- 30° were defined as horizontal, 30°- 60° as oblique, and 60°- 90° as vertical. Only cells in anaphase or telophase were analyzed, in at least three different animals per time point (50-86 cells analyzed in total per time point).

2.10 The stochastic simulation algorithm

Approach.

To investigate the rules that govern the cell fate decision of cerebellar RG, we checked the validity of a model that assumed all astrocyte progenitors as belonging to a homogeneous multipotent population. This was done by generating clones in silico with discrete-time stochastic simulations, using a variant of the Stochastic Simulation algorithm, also known as the Gillespie algorithm (Gillespie, 1976; Sandman, 2008). The E12-P30 clones were used as a reference because of the quantitative nature of the data (n = 284 clones) and the diversity of the clone subtypes (the rare CNA-containing clones were not taken into account). The empirical outcomes (i.e. clone size, proportions of astrocytes, ratio of astrocyte types per clone, proportions of clone types and subtypes) were compared to the in silico simulation of 3000 clones (i.e. 10 batches of 300 clones, each one having a number of clones similar to E12-P30 empirical clones).

Description of the simulation algorithm.

Step 0:

- Initialization of the transition probabilities;
- Initialization of the type of the root cell (70% multipotent progenitors - MP -, 30% postmitotic astrocytes, proportions taken from those of multicellular vs unicellular clones at P30; within the 30%, the discrete proportions of BG, GLA and WMA unicellular clones were used to determine the fate of already postmitotic astrocytes at the beginning of the simulated lineages);

Step 1:

- Each MP undergoes a division event. Each daughter cell has a certain probability of remaining a MP (pMP; i.e. probability of cell cycle re-entry) or becoming a post mitotic astrocyte (pAstro; i.e. probability of cell cycle exit). Daughter cell fates were determined

stochastically, according to the division proliferation/differentiation probabilities;
- If no MP in the clone jump to Step 2;

Step 2:

- Each post mitotic astrocyte has a certain probability to become a GLA (pGLA), BG (pBG) or WMA (pWMA) and undergoes differentiation stochastically according to the differentiation transition probabilities;

Iterate Step1 and Step2 until all cells differentiate.

Justification for a one-compartment and discrete-time model

Due to a lack of data regarding migratory fluxes of cerebellar astrocyte progenitors through the developing cerebellum, a space-independent model was built, and the pMP was kept constant regardless of the localization of each MP in the distinct emerging cerebellar layers. A range of pMPs were tried in the simulations (0.4 to 0.5 with a step of 0.005; 5 replicates of 3000 clones were generated in each case) and the best pMP was defined as the one minimizing the sum of square of the residuals on the clone size distributions (pMP = 0.465). Simulations of fate decisions in stem cells are usually implemented in a time continuous fashion using Monte Carlo simulations and the Gillespie algorithm (Clayton et al., 2007). Such approaches require an analytical description of the cell cycle length. Due to the lack of robust data on the cell cycle length of astrocyte progenitors through the extended period of cerebellar development, a discrete time model was preferred. Each step of the simulation corresponds to a generation in the lineage. Equivalence between discrete and continuous stochastic simulations has been demonstrated by Sandmann (2008). The probabilities that a daughter cell became a postmitotic astrocyte of a specific kind were generation-dependently set on the basis of our birthdating analyses (see section 3.1.10) and of previous reports (Leto et al., 2011). To determine the correspondence between the number of generation and P0, we made use of the E12-P0 clones. To this aim, the size of the simulated clones at distinct generations was compared with our experimental E12-P0 clone size. This allowed us to find out at which generation the simulated clone size distribution matched the P0-observed clone size distribution (6th generation with pMP = 0.465). Using this reference, we were able to convert the developmental time into number of generations and make use of the birthdating results.

2.11 Statistical analyses

Following Legué and colleagues (Legué et al., 2015), to account for correlation within-mice and sample size variability, we used Generalized Estimating Equations (GEE) with exchangeable correlation structure for both count data (Poisson distribution with log link function) and continuous variables (normal distribution with identity link function). Pairwise comparisons were analyzed with sequential Bonferroni's tests. When necessary, a logarithmic transformation was applied prior to statistical evaluation to reduce skewness and compensate extreme values, as well as to properly analyze cell type ratios (mean ratios were computed as geometrical means, i.e., arithmetic means of individual logarithmic ratios converted back to original metrics through exponential transformation). Chi square and Fisher exact tests were used for frequency analyses, depending on sample size. Pearson's r was used for correlation analyses. In the simulation model, the proportions of clone type and subtypes in simulated vs empirical lineages were compared using a Chi-square test; simulated and observed clone sizes using a Wilcoxon test. 95% confidence intervals of the means were computed through bootstrap with the method of bias corrected and accelerated percentile method (N=1000). Alpha level was set to 0.05. In clonal analyses, when not otherwise specified, data are expressed as means of values of each clone ± SEM. For other kinds of analyses, when not otherwise specified, data are expressed as mean ± SEM. Analyses were performed using Matlab (Mathworks inc), GraphPad Prism (GraphPad Software) and SPSS (IBM).

For global evaluations, analyses were applied on all clone types formed from E12, E14 or postnatal progenitors. As specified in the Results, more detailed analyses on clone types and subtypes were only applied on major populations (E12-P30, E14-P30, Homogeneous clones: WMA, GLA, BG; Heterogeneous clones: BG+GLA+WMA, BG+GLA; E12-P0, E14-P0 Homogeneous clones: PWM, Cortex; Heterogeneous clones). Only P values < 0.05 are reported in the Figures. Details on applied tests and results are summarized in Supplementary Table 4.

Chapter 3: Results

3.1 Ontogenesis of astroglial diversity in the cerebellum

The first aim of this work was to investigate the emergence of astroglial heterogeneity in the cerebellum, disclosing lineage relationships within this population and addressing the dynamics and timing of the amplification of astroglial progenitors.

3.1.1 Embryonic waves of astrogliogenesis populate distinct cerebellar regions

In order to study the origin of the distinct astroglial phenotypes in the cerebellum, as a first step we employed the Star Track system (García-Marqués and López-Mascaraque, 2013; see section 1.2.1), which allows to target single progenitors and trace their fate. This technique is based on multiple plasmids that, after stochastic integration into the genome given by the Piggy Bac transposase, drive the expression of up to 12 different fluorescent proteins (6 nuclear and 6 cytoplasmic) in the tagged cells and their progenies (Fig. 3.1a). This allows the classification of cells labelled by the same color combination as part of the same clone. Here, RG in the cerebellar VZ (Fig. 3.1b) and their astroglial descendants were marked by Star Track plasmids carrying the hGFAP promoter after electroporation in the IVth ventricle of mouse embryos at embryonic age (E)12, a fully neurogenic phase, or E14, formerly reported as the beginning of gliogenesis (Yuasa et al., 1996; Sudarov et al., 2011; Kita et al., 2013; Li et al., 2014; see section 1.3.3). Of note, the apparent delamination of some E12-tagged progenitors was already appreciable at E13 (Fig. 3.1c), thereby suggesting that gliogenesis in the cerebellar anlage starts earlier than E14. With both E12 and E14 electroporations, only one half of the cerebellar anlage was targeted, arguably due to the electrodes' orientation (Fig. 3.1e). Yet, cells were rather diffusely spread along the M-L and A-P axes in partly overlapping territories (Fig. 3.1e,f).

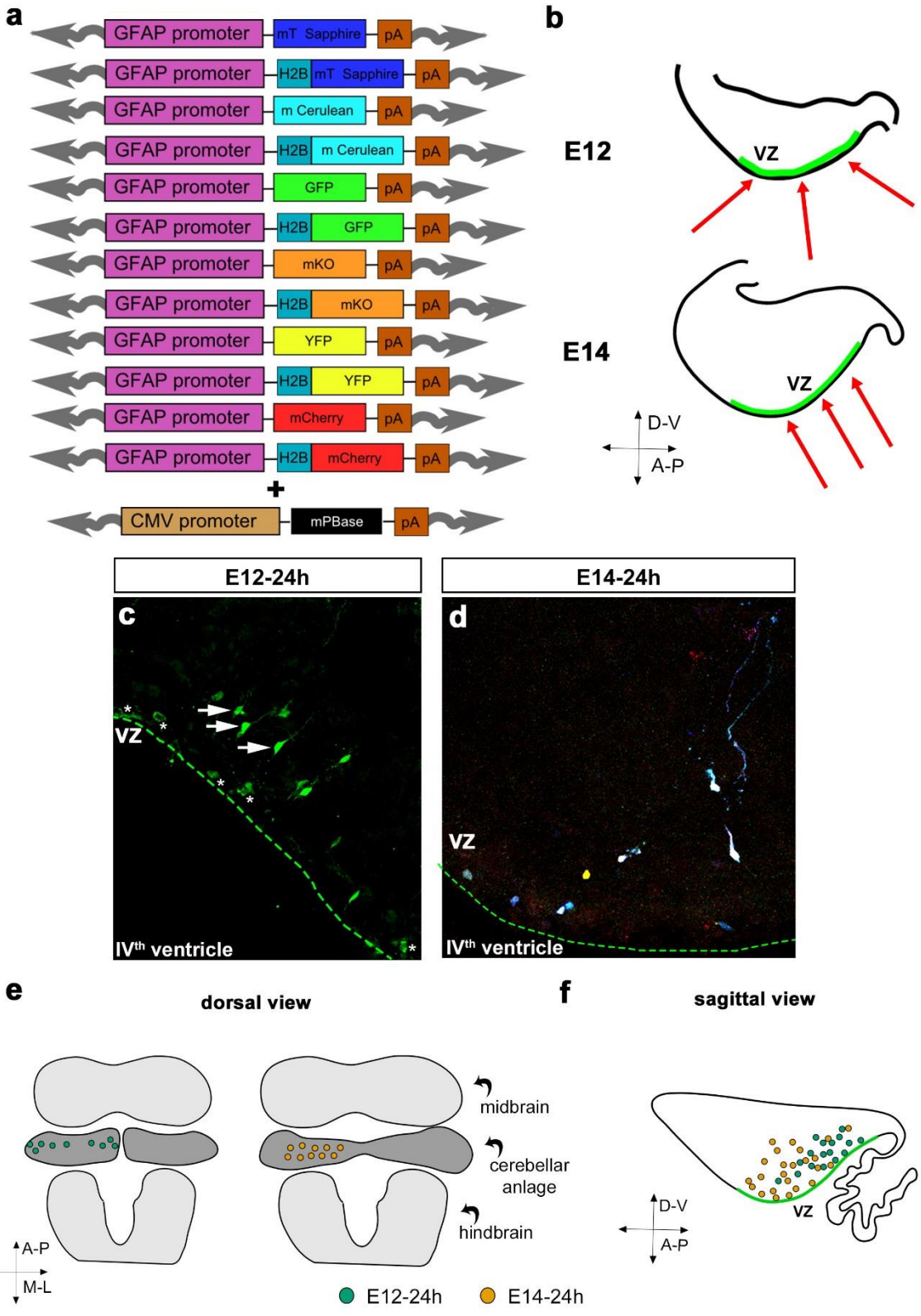

Figure 3.1. Electroporation of E12 and E14 cerebellar ventricular zone. (**a**) Schematic representation of the hGFAP Star Track plasmids mixture. (**b**) IUE at E12 and E14 are performed to target the cerebellar ventricular zone (VZ). (**c-d**) Analyses of embryos performed 24h after both E12 (**c;** Star Track cytoplasmic eGFP plasmid) and E14 (**d;** whole Star Track mixture) IUE confirm targeting of the VZ. Arrows point to progenitors tagged at E12 that appear to be delaminating at E13. Asterisks point to progenitors still located in the VZ. (**e-f**)

Representative distributions of E12- (green) or E14-targeted (orange) ventricular RG along the M-L (**e**) or A-P (**f**) axes derived from three embryos. Only one half of the whole cerebellar anlage is hit at both time points and cells are spread mediolaterally and along the A-P axis in partly overlapping territories. The VZ is homogeneously targeted along the A-P axis. Each dot represents a pool of cells found in proximate positions; based on the cerebellar symmetry around the midline, all cells were projected on the same half cerebellar primordium. IUE, in utero electroporation; M-L, medio-lateral; A-P, antero-posterior; D-V, dorso-ventral. Scale bars: 30 μm.

To investigate the composition of mature clones and examine their features, analyses were first of all performed at the end of cerebellar maturation (postnatal day -P-30). At this stage, astrocytes were categorized according to their morphology and layering: for both tested ages, tagged astrocytes included all typical cerebellar phenotypes comprising fibrous astrocytes of the white matter (WMA), velate astrocytes of the granule layer (GLA) and BG (Fig. 3.2a-c). Rarely, astrocytes were also observed in cerebellar nuclei (CNA). Thus, gliogenic RG populate the cerebellar VZ from early embryonic ages. Notably, clones targeted at E12 or E14 displayed complementary medio-lateral (M-L) localizations: the vast majority (80%) of E12-P30 clones settled in the cerebellar hemispheres (Fig. 3.2d), whereas E14-P30 clones were exclusively (100%) confined to the vermis. This latero-medial shift in clone settlement is reminiscent of the sequence of birth of PCs, that starts with neurons located in the hemispheres and paravermis (Altman and Bayer, 1997; Sudarov et al., 2011; see section 1.3.1.2).

Clones also had a specific distribution along the antero-posterior (A-P) axis (Fig. 3.2e-g). The E12-P30 clones were widely distributed throughout all folia of the hemispheres with no defined pattern in the paravermis/vermis (Fig. 3.2e,f). However, E14-P30 clones were more segregated, populating the vermis in both its anterior (lobules I-V) and posterior-nodular lobules (VIII-X), but being absent from the central lobules (VI and VII, Fig. 3.2e,g). This pattern, together with evidence that RG lining the ventricle can be still detected at E15 (Yuasa et al., 1996; see Fig. 3.1c), suggest that, after E14, a further VZ-derived astrogliogenic wave might populate these central structures, which are the last to be formed (Legué et al., 2016).

In summary, gliogenic RG are present in the cerebellar VZ already at E12 and are capable of producing all the variety of cerebellar astrocytes, according to a program that appears to follow cerebellar morphogenesis and the spatiotemporal pattern of Purkinje cell genesis,

but with a delay.

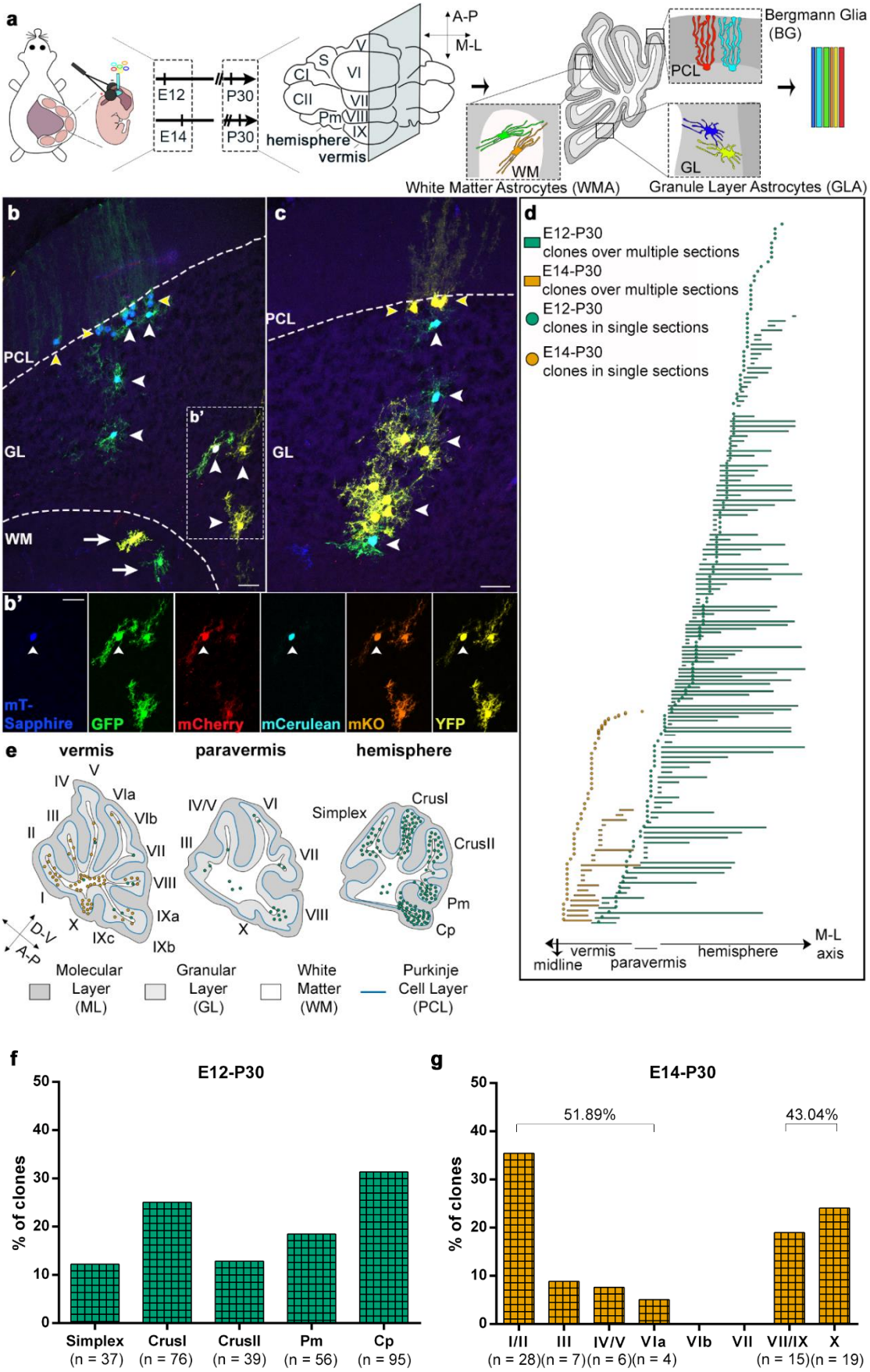

Figure 3.2. Design of the Star Track analysis and clonal allocation in the adult cerebellum. (**a**) Schematic representation of the experimental design. The hGFAP-Star Track mixture was electroporated at E12 or E14 and clonal analysis was performed at P30. (**b-c**) Electroporated astrocytes were found in all cerebellar layers in P30 mice and comprise WMA (white arrows), GLA (white arrowheads) and BG (yellow arrowheads). In **b'**, two sister GLA share the same combination of fluorescent proteins, whereas the third GLA (white arrowhead) displays a different color combination, indicating its origin from a different progenitor. (**d**) Schematic representation of the relative M-L extension of each clone. E12-P30 clones preferentially settle in the cerebellar hemispheres and span through several sections, with the only exception of those in the vermis/paravermis. E14-P30 families display a limited dispersion and are exclusively located in the vermis. Based on the cerebellar symmetry around the midline, all clones are projected on one half cerebellum. The paravermis is defined as that region where lobule IX fades and lobule X is still present. (**e-g**) Distribution along the A-P axis. When clones are found to settle in >1 lobule, they are counted in each corresponding folium. (**e**) Diagrams are representative of clone distribution along the A-P axis. E12-P30 clones are homogeneously distributed in all lobules of the hemispheres, while E14-P30 ones preferentially occupy the ventral vermis, including both anterior and posterior folia. Each dot corresponds to 1-2 clones. (**f-g**) The distribution along the A-P axis is plotted as percentages of E12-P30 (**f**) or E14-P30 (**g**) clones in the lobules of the hemisphere or vermis, respectively. E12-generated clones are broadly distributed in all lobules of the hemspheres, whereas families deriving from E14 progenitors preferentially allocate in the most anterior and posterior lobules of the vermis. S, Simplex; CI and CII, CrusI and CrusII; Pm, Paramedian; Cp, copula pyramidis; M-L, medio-lateral; A-P, antero-posterior. Scale bars: 30 µm. n= number of clones. Green=E12-P30 clones; orange=E14-P30 clones.

3.1.2 Gliogenic ventricular progenitors undergo a developmental restriction in their differentiation potential

The analysis of clone composition revealed two main clone types: "homogeneous" clones (HomCs), formed by astrocytes with the same morphology and layering (Fig. 3.3a-c), and "heterogeneous" clones (HetCs), including distinct phenotypes distributed across different layers (Fig. 3.3d-e). Both types were generated at the two examined time points, although with different frequencies (P=0.009). E12 progenitors gave rise to similar proportions of HomCs and HetCs, whereas E14 progenitors predominantly produced HomCs, suggesting a reduction in the differentiation potential of the progenitors (Fig. 3.3f-g).

HomCs for each cerebellar astroglial phenotype were found at both time points examined, with WMA and GLA clones being the most represented (Fig. 3.3f-g). However, compared to E12-P30 clones, the E14-P30 WMA HomCs doubled in their frequency (Fig. 3.3f-g; P< 0.001)

while the BG fraction decreased by half (P=0.021). Among E12-P30 HetCs, 17.6% comprised three astroglial phenotypes (BG+GLA+WMA, “triple clones”; Fig. 3.3d,f), whereas this proportion halved in E14-P30 clones (Fig. 3.3g, 7.8%; P= 0.023). On the other hand, HetCs including both GLA and BG (BG+GLA, “double clones”; Fig. 3.3e) were similarly represented in both sets of experiments (P= 0,748; Fig. 3.3f-g). CNA HomCs and other kinds of HetCs including almost any combinations of astrocytic phenotypes were found at both time points but in very limited numbers and without significant changes (Fig. 3.3f-g). Therefore, they were not taken into account for detailed quantitative analyses of clone features.

Interestingly, analysis of the contribution of HomCs or HetCs to the total number of BG or GLA showed that, although HomCs were more numerous in the whole clone population, 90% of all cortical astrocytes were part of HetCs at both time points (Fig. 3.3h-i). This suggests that HetCs contain more cells per clone than HomCs in this territory. Regarding WMA, they were predominantly included in HetCs after E12 electroporations, and in HomCs at the later time point.

Thus, the variety of cerebellar astrocytes is generated by RG with distinct fates that coexist at both E12 and E14. A RG subset generates HomCs, while other RG display a multipotent behavior and produce HetCs comprising either only cortical astroglia (double clones) or including also WMA cells (triple clones). The latter type of clones becomes significantly reduced during development, in line with a restriction in progenitor differentiation potential. Notably, this reduction parallels the increase in the fraction of WMA HomCs, suggesting a progressive lineage segregation of WM fates from those of other astrocyte phenotypes.

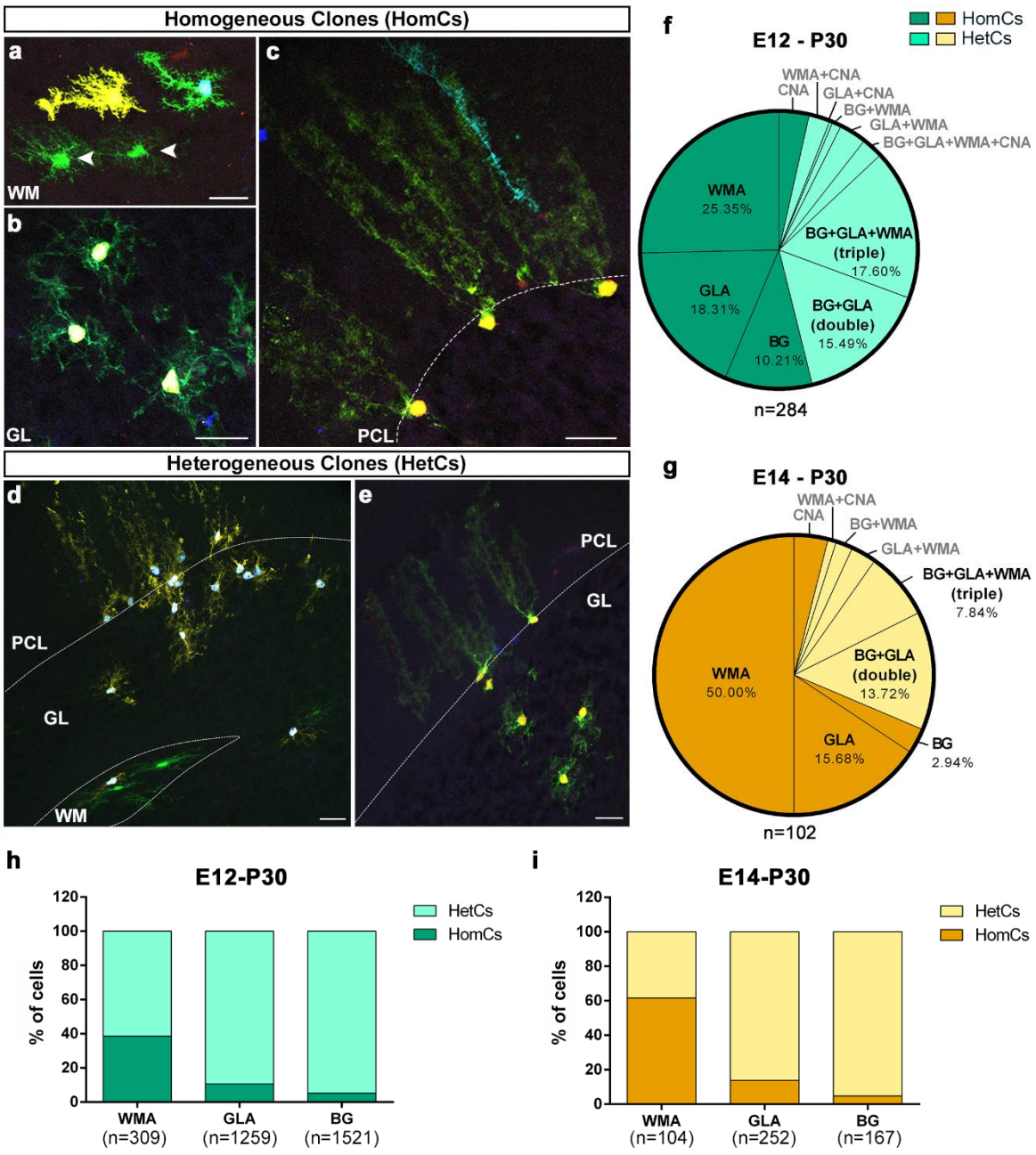

Figure 3.3. Composition of clones derived from E12 or E14 progenitors. (**a-c**) HomCs composed of WMA (**a**; arrowheads indicate sister cells), GLA (**b**) or BG (**c**) are generated by both early and late-tagged progenitors. (**d,e**) The two major types of HetCs include triple clones made of BG+GLA+WMA (**d**) and double clones made of BG+GLA (**e**). (**f,g**) HomCs (dark shade) and HetCs (light shade) are produced in different frequencies by E12 (**f**) and E14 progenitors (**g**; P=0.009) . Among HetCs, BG+GLA+WMA clones are more numerous among E12 compared to E14 clones (P=0.023), while BG+GLA clones do not vary (P=0,748). Pies illustrate pooled data from 3 (E12-P30 clones) or 4 (E12-P30 clones) animals. (**f**) Minor fractions: CNA=3.52%, WMA+CNA=2.47%, GLA+CNA=0.35%, BG+WMA=1.06%, WMA+GLA=3.17%, WMA+BG+GLA+CNA=2.47%. (**g**) Minor fractions: CNA=3.92%, WMA+CNA=0.98%, BG+WMA=1.96%, WMA+GLA=2.94%. **h** and **i** show the contribution of HomCs and HetCs to the total number of each astroglial phenotype after E12 or E14 electroporations, respectively. About 90% of both E12 (**h**) and E14 (**i**) derived BG and GLA are part of HetCs. On the other hand,

WMA are mostly included in HetCs and HomCs when they derive from E12 (**h**) and E14 (**i**) progenitors, respectively. WMA, white matter astrocytes; GLA, granule layer astrocytes; BG, Bergmann glia; CNA, cerebellar nuclei astrocytes. Scale bars: 30 μm; P values are calculated from Fisher's exact test; n=number of clones. Green=E12-P30 clones; orange=E14-P30 clones.

3.1.3 Astrocyte clone size is affected by spatiotemporal factors and declines with the degree of clone homogeneity

Analysis of the number of cells in each clone (clone size) revealed that it was markedly lower in E14-P30 clones compared to E12-P30 families (Fig. 3.4a; E12-P30, 14.58 ± 1.46 cells/clone; E14-P30, 6.05 ± 1.35 cells/clone, P=0.002). Moreover, HomCs typically consisted of only one or two cells (Fig. 3.4a-d), with E14-P30 clones being smaller than E12-P30 clones (Fig. 3.4a; P<0.001). They were remarkably distinct from HetCs (P<0.001), which overall ranged from 3 to 134 cells in size and also displayed a clear trend to become smaller with time, although this variation did not reach statistical significance (Fig. 3.4a; E12-P30, 30.2 ± 3.03; E14-P30, 19.41 ± 4.69, P=0.081). Further analysis of HomC subtypes highlighted that WMA clones were smaller compared to the other phenotypes (Supplementary Table 4; Fig 4c,d). In addition, single cell families constituted about half of all E12-P30 and E14-P30 HomCs (Fig. 3.4e,f) and dominated in both WM and GL (Fig. 3.4e-h). Conversely, in most cases BG HomCs included more than 1 cell (Fig. 3.5g,h), indicating a higher amplification for this latter phenotype.

HetCs triple clones were the largest, with an average size of 37.90 ± 4.57 cells/clone for E12-P30 cells that tended to decline in E14-P30 clones (27.00 ± 9.91; Fig. 3.4b; P=0.317). E12 triple clones were also significantly bigger than double BG+GLA clones (P<0.001), that instead showed a comparable size of about 15-16 cells on average, regardless of their developmental origin (Fig. 3.4b).

In summary, HomCs amplify very little compared to their heterogeneous counterpart, thus showing that clone size positively correlates with the degree of clone heterogeneity. Moreover, progressing from early hemispheric to late vermian astrogliogenesis, lineages undergo restriction in their amplification potential.

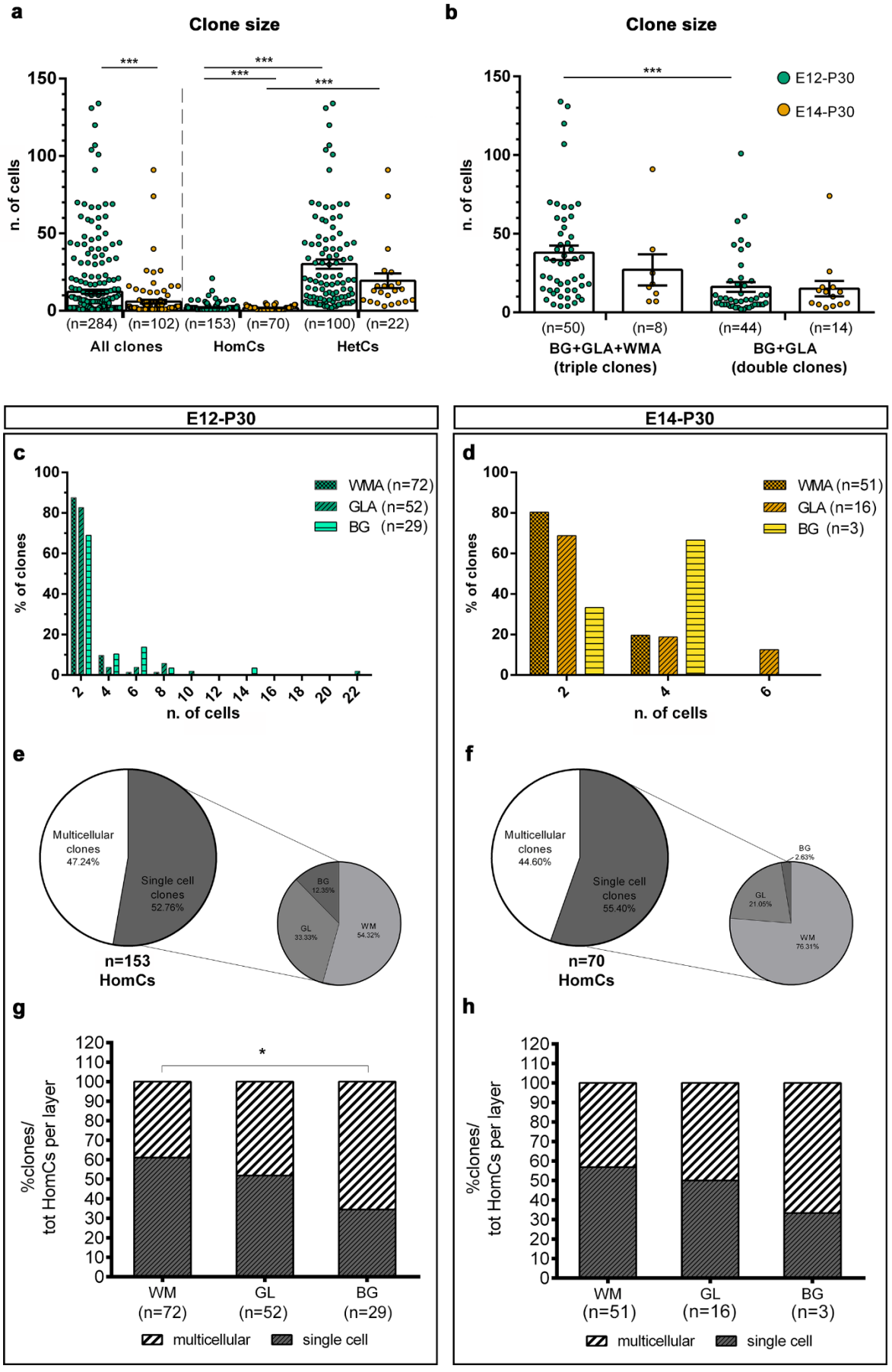
a
Clone size
n. of cells
150
100
50
0
***
***
***
***
(n=284)
(n=102)
(n=153)
(n=70)
(n=100)
(n=22)
All clones
HomCs
HetCs
b
Clone size
n. of cells
150
100
50
0
***
E12-P30
E14-P30
(n=50)
(n=8)
(n=44)
(n=14)
BG+GLA+WMA
(triple clones)
BG+GLA
(double clones)
E12-P30
E14-P30
c
% of clones
100
80
60
40
20
0
WMA (n=72)
GLA (n=52)
BG (n=29)
2
4
6
8
10
12
14
16
18
20
22
n. of cells
d
% of clones
100
80
60
40
20
0
WMA (n=51)
GLA (n=16)
BG (n=3)
2
4
6
n. of cells
e
Multicellular clones 47.24%
Single cell clones 52.76%
BG 12.35%
GL 33.33%
WM 54.32%
n=153
HomCs
f
Multicellular clones 44.60%
Single cell clones 55.40%
BG 2.63%
GL 21.05%
WM 76.31%
n=70
HomCs
g
%clones/
tot HomCs per layer
120
110
100
90
80
70
60
50
40
30
20
10
0
*
WM
(n=72)
GL
(n=52)
BG
(n=29)
multicellular
single cell
h
%clones/
tot HomCs per layer
120
110
100
90
80
70
60
50
40
30
20
10
0
WM
(n=51)
GL
(n=16)
BG
(n=3)
multicellular
single cell

Figure 3.4. Quantitative analyses of clone size. (**a-b**) Scatter plots of clone size. (**a**), E12-P30 clones (green) are overall bigger than E14-P30 clones (orange; P=0.002). This same trend is maintained when comparing HomCs and HetCs, although statistical significance is not always reached. E12-P30 HomCs appear to decrease in size from E12 to E14 (P<0.001). Similarly, HetCs tend to be bigger at E12 than at E14 (P=0.081). (**b**) Triple BG+GLA+WMA clones are the biggest clone type and tend to be smaller when later generated (P=0.317). Double BG+GLA clones are smaller than triple clones (P<0.001) and display the same average size in the two data sets (***, P<0.001; P values are calculated from GEE analysis). (**c,d**) The frequency distribution of the size of E12-P30 (**c**) and E14-P30 (**d**) HomCs shows that the vast majority of them are formed by ≤ 2 cells. Namely, in both data sets, WMA HomCs are the smallest. (**e-h**) A relevant amount of E12-P30 (**e**) and E14-P30 (**f**) HomCs composed of only one cell and are found in all cerebellar layers. (**g**) and (**h**) show the proportion of single cell clones in each layer after E12 and E14 electroporations, respectively. More than half of the homogeneous clones in both WM and GL are found as single cells, whereas individual clones among BG families are less frequent (Fisher's exact test shows a statistically significant difference between WM and BG at E12; *, P=0.0265). n=number of clones.

3.1.4 HetC composition reveals a consistent stoichiometry of astroglial phenotypes

An intriguing feature of HetCs is the possible presence of a recurrent architecture in the composition of the astroglial families. This, in turn, may reflect a well-defined developmental program controlling the clone structure. Thus, we investigated the contribution of each astroglial phenotype to HetCs.

Upon examining the total number of WMA, GLA or BG across the entire HetC population, we found that in E12-P30 triple clones WMA were significantly fewer than GLA and BG (P<0.001). However, these latter components appeared in very similar numbers in both triple and double clones (Fig. 3.5a), indicating a broad and parallel amplification of cortical astrocytes and a limited expansion of WM cells.

We next inquired whether this global picture resulted from a clone-level phenomenon. The WMA:GLA:BG ratio computed in a clone-wise manner was 1 : 4.069 ± 0.148 : 4.220 ± 1.150, thus confirming a similar contribution of the cortical phenotypes (P=0.769) and their consistent predominance over WMA at the clone-level (Fig. 3.5a).

This pattern was confirmed also in triple E14-P30 clones, though less marked than in E12-P30 cells (1 WMA : 2.469 ± 1.342 GLA : 2.077 ± 1.501 BG; similar contribution of cortical components, P=0.073, Fig. 3.5b), in line with the trend for a decreased size of later-

generated clones.

Interestingly, although not apparent from the mean values of individual cortical components (Fig. 3.5b), in both E12-P30 and E14-P30 double clones there was a prevalence of BG over GLA (GLA:BG, E12-P30, 1 : 1.519 ± 1.140 vs. E14-P30, 1 : 1.554 ± 1.232, P>0.999). Indeed, the BG:GLA ratio was significantly higher in double clones than in triple ones (P<0.001) at both E12 and E14.

Altogether, these data reveal a remarkably consistent architecture in HetCs, and support distinct amplification dynamics for cortical and WM components within triple clones, and for sister BG and GLA across double and triple clones.

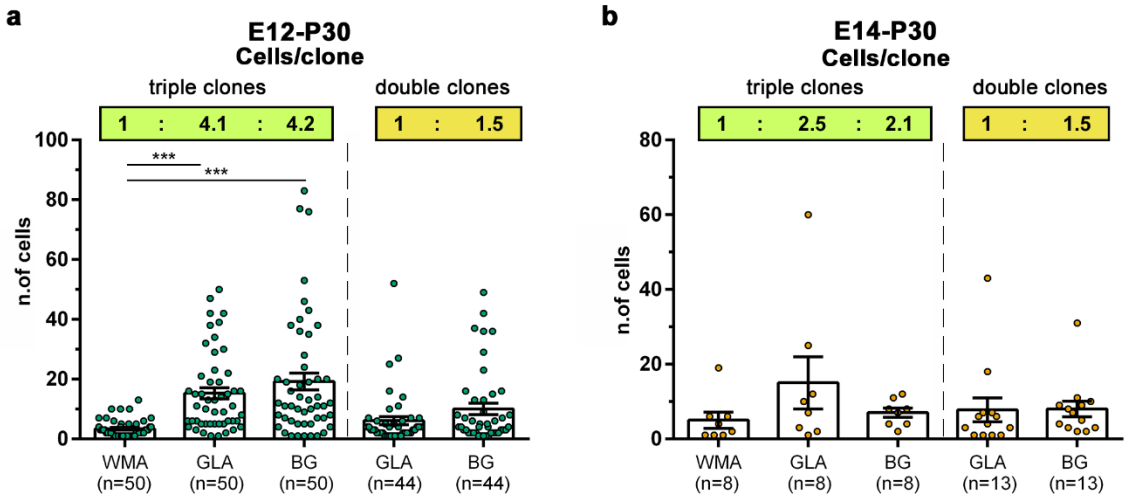

Figure 3.5. Stoichiometry of clone composition. (**a, b**) Scatter plots show the number of distinct astroglia phenotypes in triple and double clones after E12 (**a**) or E14 (**b**) electroporations. In E12-P30 triple clones, WMA are less numerous than cortical astrocytes (P<0.001). The numbers of GLA and BG are very similar at both time points (E12, P=0.769; E14, P=0.073). The insets report the clone-wise stoichiometry as geometric means of ratios, which is not always evident in the global scatter plots, and which confirms the joint expansion of GLA and BG in triple clones, whereas in double clones BG prevail over GLA. ***, P<0.001; P values are calculated from GEE analysis; n=number of clones.

3.1.5 Clone dispersion follows clone size and is constrained by lobule morphogenesis

To shed further light on how astroglia contribute to cerebellar morphogenesis, we analysed clone dispersion. Estimation of the longest width of each clone along the M-L axis (Fig. 3.6a-b) showed that M-L dispersion profoundly decreased over time both in the whole

population (Fig. 3.6a, P<0.001), and within clone types (HomCs, P=0.031; HetCs, P<0.001). HetCs were much more dispersed than HomCs (E12-P30, P<0.001; E14-P30, P=0.016) and triple clones displayed a larger extension compared to double ones (Fig. 3.6b; E12-P30 P<0.001; E14-P30 P=0.01), with the E12-P30 subset being the most dispersed (P<0.001). Thus, M-L clone dispersion increases according to the degree of heterogeneity and decreases as development progresses, thereby closely resembling the pattern of changes in the clone size. Indeed, correlation analysis of size and dispersion (Fig. 3.6c-d) confirmed that spatial distribution was significantly influenced by clone size (corr. coefficients E12-P30=0.74; E14-P30=0.69; P<0.001), pointing to cell numerosity as a primary factor determining the spatial dispersion of the clones.

Analysis of clone arrangement along the A-P axis that, due to the folded structure of the cerebellum, corresponds to allocation in distinct lobules, showed that most of clones localized in single lobules independent of their time of origin (Fig. 3.6e), with the only exception of E12-P30 triple clones that predominantly dispersed in two and rarely in three or four contiguous folia. Thus, overall clones display a limited A-P dispersion. Moreover, cortical components of HetC clones were mostly found within the same lobular wall (i.e. the same side of the lobule divided by the WM; 67% and 86% of cases, as calculated for E12-P30 triple and double clones, respectively), indicating a remarkable degree of segregation at the lobule level.

Taken together, while clones expand along the M-L axis according to their size without apparent constraints, they display a limited capability to disperse along the A-P axis and are predominantly confined within single lobules. Hence, astroglial clones may rarely traverse the border of fissures between lobules, suggesting that the bulk of astroglial amplification occurs after fissure establishment.

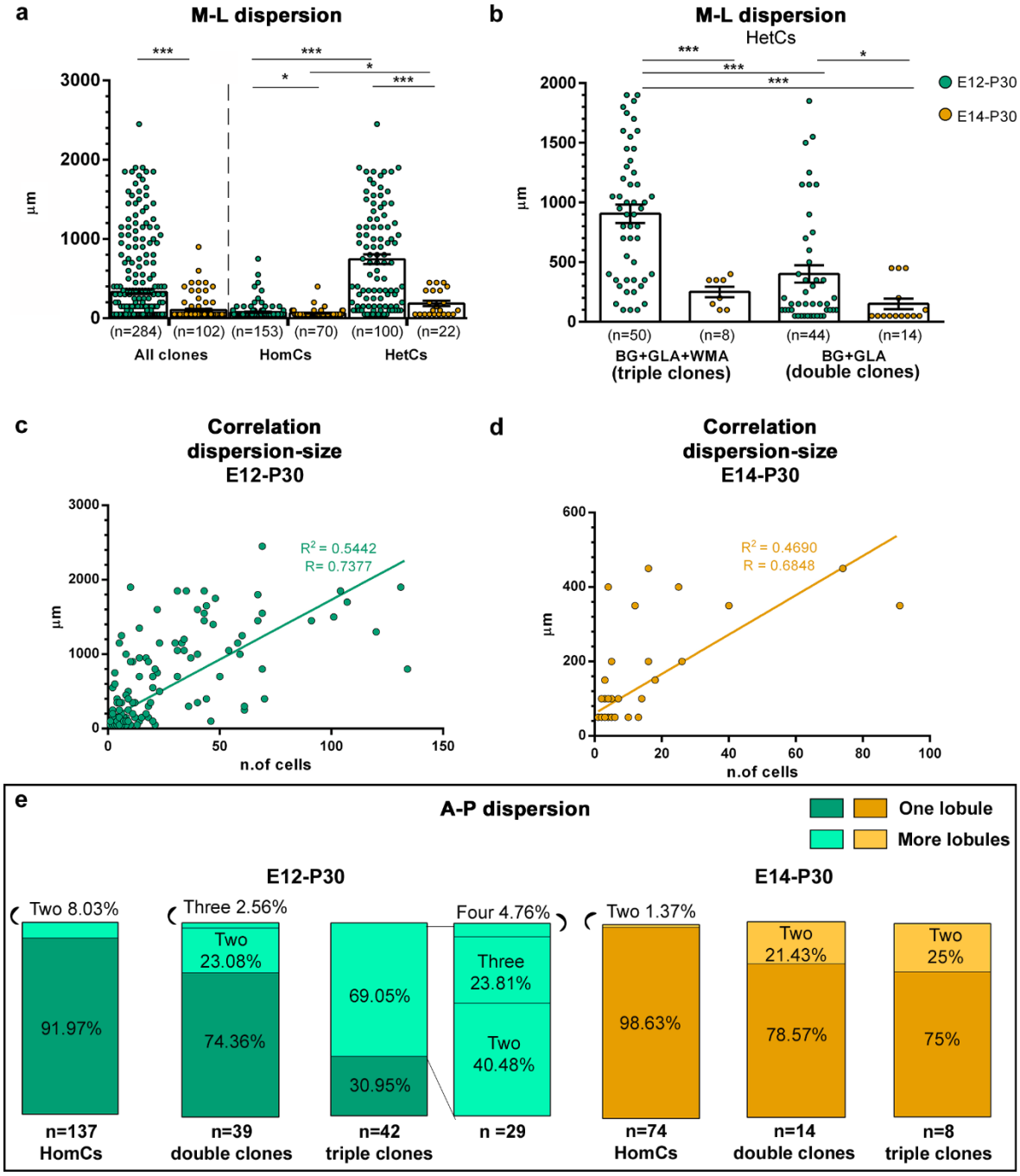

Figure 3.6. Quantitative analysis of clone dispersion along the M-L and A-P axes. (**a-b**) Dispersion along the M-L axis of clones tagged at E12 (green) or E14 (orange). (**a**) Scatter plots show that dispersion greatly decreases over time (P<0.001). HomCs are mostly found in a single cerebellar section, whereas HetCs are much more dispersed (E12-P30, P<0.001; E14-P30, P=0.016). (**b**) Among HetCs, triple clones are more expanded than double clones in both populations (E12-P30 P<0.001; E14-P30 P=0.01). Namely, E12 triple families are the most dispersed (P<0.001). (**c-d**) Correlation analysis shows a positive correlation between clonal size and M-L dispersion in both E12-P30 (**c**, n=254 clones) and E14-P30 (**d**, n=92 clones) populations (corr. coefficients E12-P30=0.74; E14-P30=0.69; P<0.001). (**e**) Distribution of clones along the A-P axis of E12-P30 and E14-P30 clones. HomCs and double clones tagged at E12 mostly settle in a single lobule, whereas triple clones are often found in more than one lobule. E14-P30 clones are overall found in one lobule. ***,

P<0.001; *, P<0.05; P values are calculated from GEE analysis; n=number of clones.

3.1.6 HetC are formed by modular architecture

In order to appraise possible regularities in local amplification of clonally related progenies of ventricular precursors, we analyzed clones in terms of potential building blocks, or modules. Indeed, qualitative inspection of 3D localization of distinct HetCs suggested that their broad dispersion was not due to a scattered distribution of sister cells. Rather, clones seemed to contain spaced-out cell clusters. To identify spatial relationships within HetCs, we performed an analysis of the nearest neighbour distance (NND) in E12 HetCs. This analysis revealed a significant degree of clustering in both double and triple clones, as shown by their different distributions as compared to random distributions (always p<0.001, Fig 3.7a). Interestingly, the cortical component (BG + GLA) of triple clones appeared undistinguishable from that of double ones, suggesting similar modalities of cortical colonization, and reflecting the separate allocation for WMA.

The presence of clustering was confirmed by means of a cluster analysis on the spatial layout of cortical cells (Fig 3.7b-d). This analysis revealed that i) the mean number of clusters per clone was quite low in both double and triple clones (2 and 3, respectively); ii) the mean number of cells per clone was fairly similar across clone types (10 and 13, respectively for double and triple clones); iii) clusters' spatial extension, as indexed by the mean intra-cluster inter-cell distance, was smaller in double than in triple clones, being respectively 210 um (95% confidence interval = 167-280 um) and 365 um (95% confidence interval = 313-412 um).

To get insight on how clusters contribute to form the corresponding clones, we analyzed their composition. In double clones, the vast majority of clusters (85%, Fig. 3.7d) comprised both BG and GLA, with a predominance of BG over GLA (Fig. 3.7e). The mean BG:GLA ratio was 1.8 (95% confidence interval, 1.4 – 2.2), with a rather sharp distribution (kurtosis=3.1) peaking at 2.2. This pattern indicates that double clones are formed by a cluster typology characterized by a clear predominance of BG over GLA – most commonly an approximately two-fold ratio, suggesting that double clones are built upon unitary stereotyped modules.

In triple clones, clusters were also formed mostly by both BG and GLA cell types (81%, Fig.

3.7d), but the BG:GLA ratio was 1.1, in line with the clone-wise stoichiometry of triple clones. However, clusters in triple clones showed a dual pattern of BG:GLA ratio, according to whether or not they contained WMA (Fig. 3.7f,g). Indeed, in the former case BG and GLA were almost uniformly represented inside clusters, with a mean ratio of 0.9 (95% confidence interval, 0.7 – 1.2) and low kurtosis (1.9). By contrast, in the latter case the BG:GLA ratio distribution was more similar to that observed in double clones, that is, BG predominated (mean ratio=1.3, kurtosis=3.2). Hence, when WMA are produced, the modular clonal architecture is not any longer evident, either because it is masked by WMA or because it is disrupted.

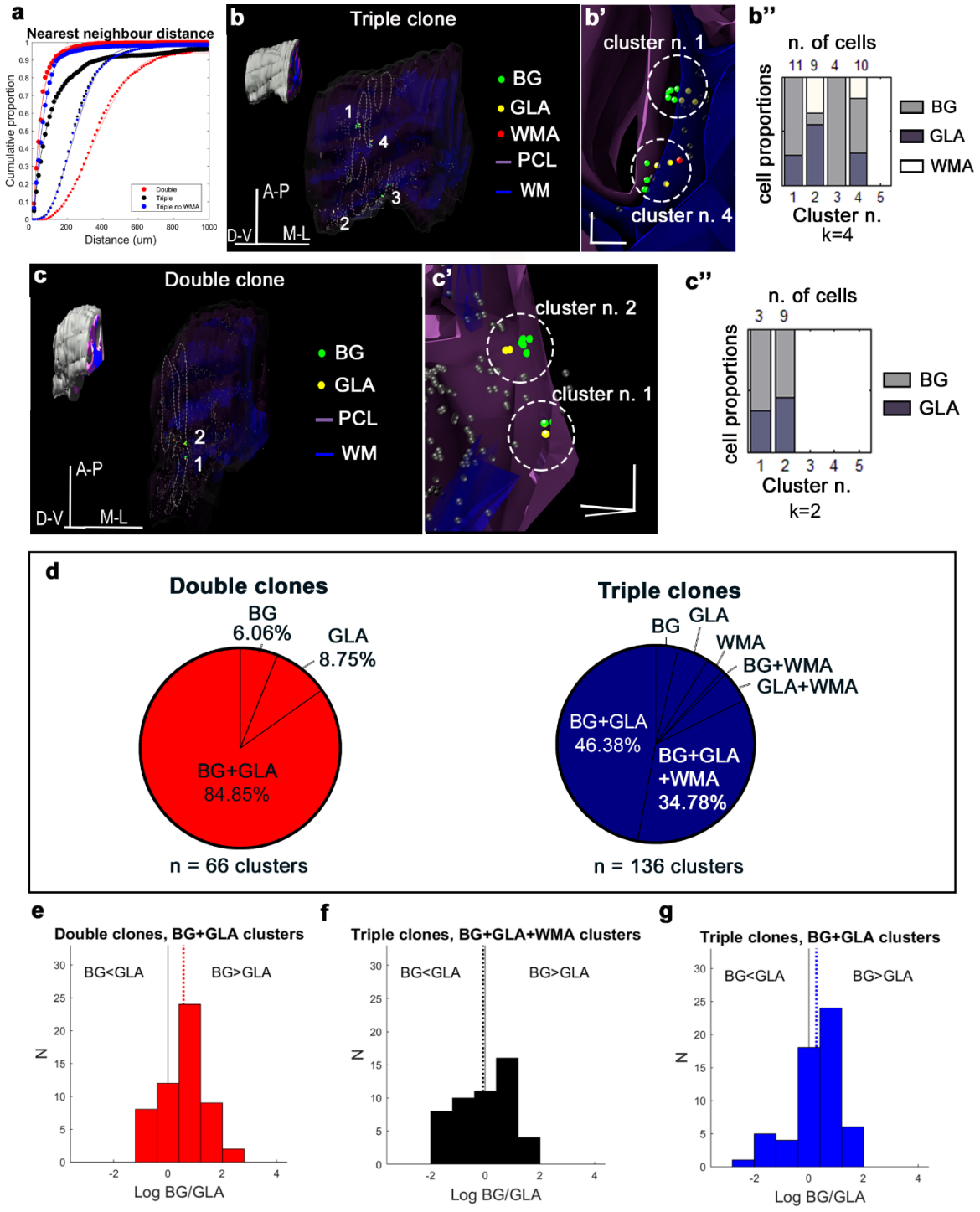

Figure 3.7. Modularity of Heterogeneous clones. (**a**) Cumulative proportions of intra-cluster, cell-to-cell nearest neighbour distance. Both double (red) and triple (blue and black) clones show a high degree of clustering when their distributions are compared to random distributions (light blue and light red, p<0.001). Symbols represent empirical proportions. Dotted lines are the fitted curves. (**b,c**) Cluster analysis confirms the presence of clustering in both double and triple clones. 3D reconstructions of a representative triple (**b**) and double (**c**) E12 clone highlight the presence of distinct space-out clusters composed of BG (green spheres) and GLA (yellow spheres). (**b**) also contains WM cells (red spheres). (**b', c'**) Higher magnifications of two representative clusters (dashed circles) out of the four recognized by cluster analysis of the triple clone in (**b**)

and of the two clusters forming the clone in (**c**). Grey spheres represent cells of other clones. Blue structure, white matter tract; purple surface, PCL. Plots in (**b''**) and (**c''**) show the number (k) and composition (in terms of cell type and n. of cells per cluster) of the clusters identified in the representative triple (**b**) and double (**c**) clones, respectively. Each cluster is arbitrarily associated to a cluster number (cluster n.). (**d**), Analysis of clusters composition reveals that most (>80%) of clusters in both double (red) and triple (blue) clones comprise both BG and GLA. (**e-g**), BG:GL ratio distributions in clusters comprising both BG and GLA. In double clones (**e**, number of clusters = 55) the mean ratio is 1.8, revealing a predominance of BG over GLA. Clusters in triple clones containing WMA (**f**, number of clusters = 49) show similar amounts of BG and GLA, with a ratio of 0.9, whereas clusters in triple clones devoid of WMA (**g**, number of clusters = 58) have BG predominating over GLA (ratio 1.3). No of bins = 10. Vertical solid lines indicate 1:1 ratio, vertical dashed lines indicate the actual mean ratio. BG, Bergmann glia; GLA, granule cell astrocytes; WM, white matter; PCL, Purkinje cell layer; M-L, medio-lateral; A-P, antero-posterior; D-V, dorso-ventral.

3.1.7 Different fates and specific features of clones emerge postnatally

To get insight into the dynamics of clone amplification and allocation, we analyzed clones at birth (P0, Fig. 3.8a), during active astrogliogenesis, and asked if the clonal pattern and features detected at P30 were already established at this time point. Similar to mature ages, E12 targeted astrocytes were for the most part settled in lateral P0 cerebella, whereas, E14-P0 clones were preferentially located medially (Fig. 3.8b), showing that the M-L allocation of astrocytes was defined already at birth.

Most clones settled in the PWM (Fig. 3.8c) and comprised cells with similar morphologies (HomCs, Fig. 3.8c) including both elements with the typical fibrous shape of WMA, and cells with a long process extending from the cell body towards the pial surface (Fig. 3.8a'). These latter cells resembled RG detached from the VZ formerly proposed as a source of BG (Ramón y Cajal, 1911). A minor proportion of radial cells instead still formed clones contacting the VZ. About 30-40% of clones (Fig. 3.8c) were also found in the nascent cortex, where cells already displayed morphologies distinctive of polarized bona fide BG precursors with a radial basal process in the PCL (PCLp) or stellate GLA progenitors (GLAp, Fig. 3.8a''). HetC families were rare and included a very small fraction composed of PCLp and GLAp, or cortical and PWM cells (Fig. 3.8c).

At difference with P30 data, the average size of both E12-P0 and E14-P0 clones was small and remarkably similar in absolute terms (Fig. 3.8d; E12-P0 3.7±0.41; E14-P0 3.22±0.21).

However, consistent with P30 results, HetCs already contained more cells compared to HomCs (Fig. 3.8d and Supplementary Table 4; E12-P30, P<0.001; E14-P30, P<0.001). This feature was reflected in the trend of HetCs to be more broadly distributed medio-laterally compared to HomCs (Fig. 3.8e). Nevertheless, E12-P0 and E14-P0 M-L dispersions did not yet differ globally at this time point (Fig. 3.8e; P=0.502). Along the A-P axis, P0 clone distributions essentially resembled that observed at P30 (Fig. 3.8b) with E12-derived clones distributed homogeneously and E14-derived cells predominantly allocated to anterior regions with some E14-P0 clones in posterior lobules, where E14-P30 clones also settled.

Altogether, these results show that at birth, while the positional choice of clones along the cerebellar axes appears for the most defined, layer allocation, size and degree of dispersion are not yet achieved, thereby indicating that the specific features of E12- and E14-derived clones are essentially acquired after birth.

In support of this view, the comparison of P0 and P30 data, showed that with time HetCs proportionally increased in the whole clone population for both E12- and E14-derived cells (Fig. 3.8f; E12-P0, P<0.001; E14-P0, P=0,0003). Interestingly, this correlated with a reduction of PWM HomCs by half (Fig. 3.8f, P<0.001) at E12, and with a decline of cortical HomC at E14 (Fig. 3.8f, P=0,0324), suggesting that the hemisphere PWM and the vermian nascent cortex still hosted multipotent progenitors capable of producing HetCs. Intriguingly, a closer inspection of cortical HomC phenotypes showed a significant reduction in the fraction of PCLp HomC at both time points examined (Fig. 3.8f, P<0.001). Therefore, PCLp at birth in both hemispheres and vermis may behave as a source for various astroglial phenotypes.

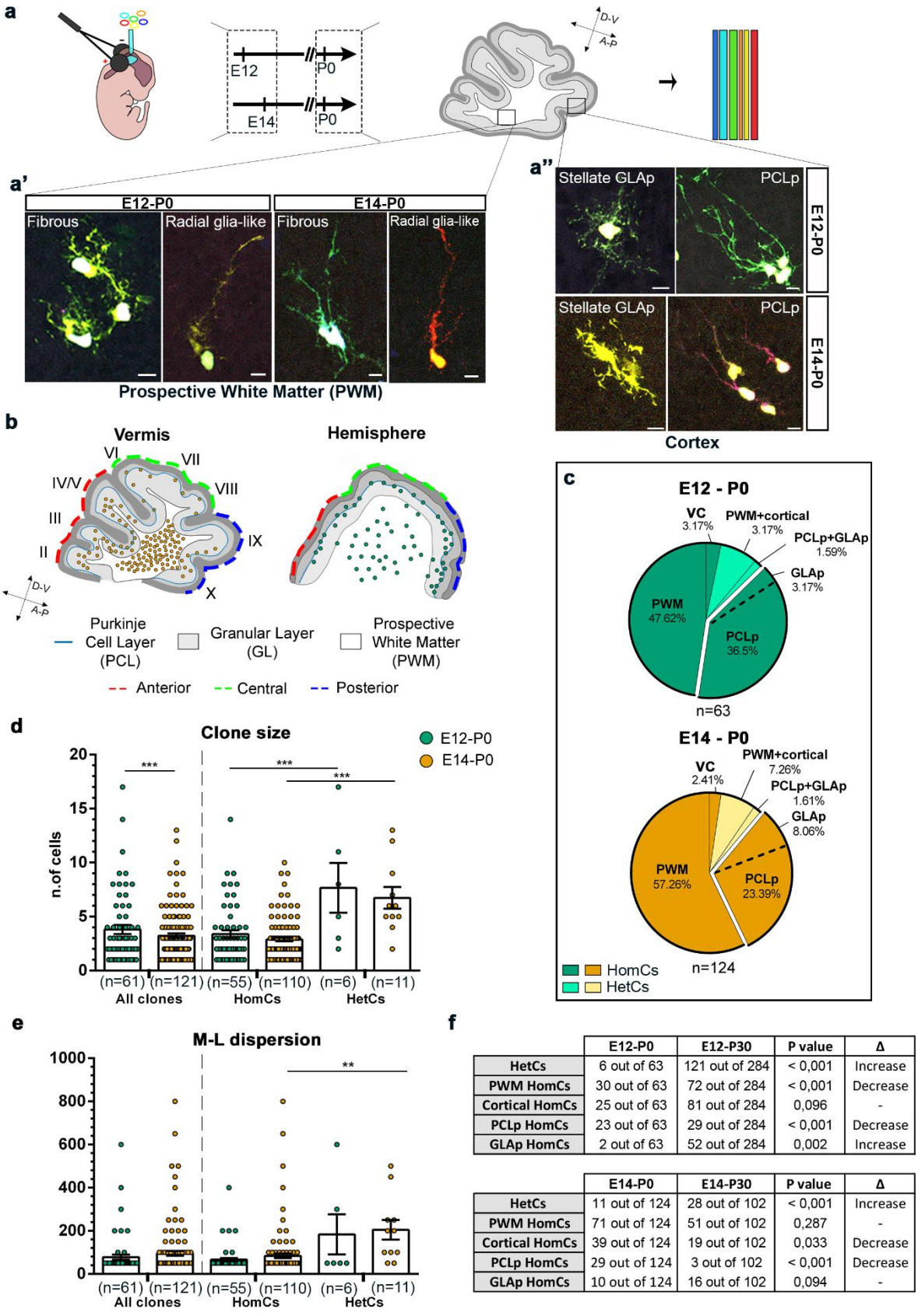

f

	E12-P0	E12-P30	P value	Δ
HetCs	6 out of 63	121 out of 284	< 0,001	Increase
PWM HomCs	30 out of 63	72 out of 284	< 0,001	Decrease
Cortical HomCs	25 out of 63	81 out of 284	0,096	-
PCLp HomCs	23 out of 63	29 out of 284	< 0,001	Decrease
GLAp HomCs	2 out of 63	52 out of 284	0,002	Increase

	E14-P0	E14-P30	P value	Δ
HetCs	11 out of 124	28 out of 102	< 0,001	Increase
PWM HomCs	71 out of 124	51 out of 102	0,287	-
Cortical HomCs	39 out of 124	19 out of 102	0,033	Decrease
PCLp HomCs	29 out of 124	3 out of 102	< 0,001	Decrease
GLAp HomCs	10 out of 124	16 out of 102	0,094	-

Figure 3.8. Short-term analyses of clones. (**a**) Schematic representation of the experimental design. In utero electroporation of the hGFAP-Star Track mixture was performed at E12 or E14 and clonal analysis at P0. Representative examples of tagged cells at P0 comprising fibrous cells in the PWM (**a'**), stellate GLA and PCL

precursors of BG (GLAp and PCLp) in the developing cortex (**a''**), and radial-glia like cells in the PWM (**a'**). (**b**) Schematic representation of clonal distribution along the A-P and M-L axes. Early Clones tagged at E12 (green) are settled in the lateral cerebellum and are homogeneously distributed in all the developing lobules. Clones tagged at E14 (orange) are found in the vermis and preferentially allocate in the anterior lobules. (**c**) Clonal distribution within cerebellar layers. After both E12 and E14 electroporations, HomCs are mostly found in the PWM at P0. A relevant proportion is also found in cortical layers ("exploded" section), mostly as clones composed of PCLp. HetCs are still rare and include clones with cells in the two developing cortical layers or in both PWM and cortex. Pies illustrate pooled data from 3 animals per time point. (**d**) Scatter plots show the size of E12 (green) and E14 (orange) clones at P0. Early and late tagged clones show a very similar size. At both time points, HomCs are smaller than HetCs (E12-P30, $P<0.001$; E14-P30, $P<0.001$). (**e**) Scatter plots show the M-L dispersion of E12 and E14 major clones at P0. E12 and E14 clones do not differ in their M-L dispersion. HetCs at both time points tend to be more broadly distributed than HomCs (***, $P<0.001$; **, $P<0.01$; P values are calculated from GEE analysis). Table in (**f**) summarizes the numbers of clones in each layer at P0 and P30 and the P values resulting from their comparisons by Fisher's exact test. Scale bars: 10 µm; n=number of clones. PWM, prospective white matter; GL, granular layer; PCL, Purkinje cell layer; GLAp, granular layer astrocyte precursors; PCLp, Purkinje cell layer precursors; VC, ventricular cells.

3.1.8 PCL-progenitors are the source of distinct astroglial phenotypes after birth

Because data suggested that PCLp may give rise to HetCs, we set out to gain insight into their progeny. To this aim, we employed Confetti reporter mice ($R26R^{Confetti}$, Snippert et al., 2010; Calzolari et al., 2015) that enable the distinction of progenies derived from different single progenitors by means of the stochastic and exclusive expression of one out of four fluorescent proteins. We crossed $R26R^{Confetti}$ with *GLAST*^{CreERT2} mice and performed a superficial administration of Tamoxifen (Tx) (Parmigiani et al., 2015. Fig. 3.9a) postnatally (P6) to induce recombination in PCLp contacting the pial surface. Whole population analysis in the cerebellar vermis at P30 showed that PCLp progenies were composed of both BG and GLA (Fig. 3.7b-d). To understand whether a single PCLp was indeed the source of distinct astroglial types, we investigated the clone composition: clones were either composed of only BG or comprised both BG and GLA expressing the same fluorophore (Fig. 3.9b,c). GLA HomCs in the deep GL (Fig. 3.9d) were rarely observed and may have been derived by occasional diffusion of Tx to parenchymal precursors or by the direct transformation of PCLp into GLA. Double clones and BG HomCs represented similar fractions of the overall clone population, indicating an equal probability for a PCLp to self-renew or to produce a GLA (Fig.9e).

Interestingly, HetC double clones were significantly bigger than BG or GLA HomCs (Fig. 3.9g), consistent with the higher amplification of HetCs shown in embryonic analyses. Notably, the GLA:BG ratio (Fig. 3.9h) revealed a predominance of BG and, in line with the sampling of both double and triple embryonic families, displayed a value (1.2) intermediate to that of triple and double E12 clones.

According to the behavior of radial progenitors (RG/outer RG) in the developing telencephalon (Shitamukai et al., 2011; LaMonica et al., 2013), the choice of PCLp to produce distinct progenies (i.e. BG or GLA) might be due to a different cleavage plane during cell division, determining the inheritance of the radial process. However, pVimentin-labeled proliferative PCLp displayed predominant horizontal cleavage planes ($P<0.001$) with frequencies stable at all time points examined (main effect of time, $P=0.107$; Fig. 3.9i-l). Thus, factors other than the division mode influence the cell fate of the PCLp progeny. In summary, postnatally PCLp can generate GLA and contribute BG+GLA clones.

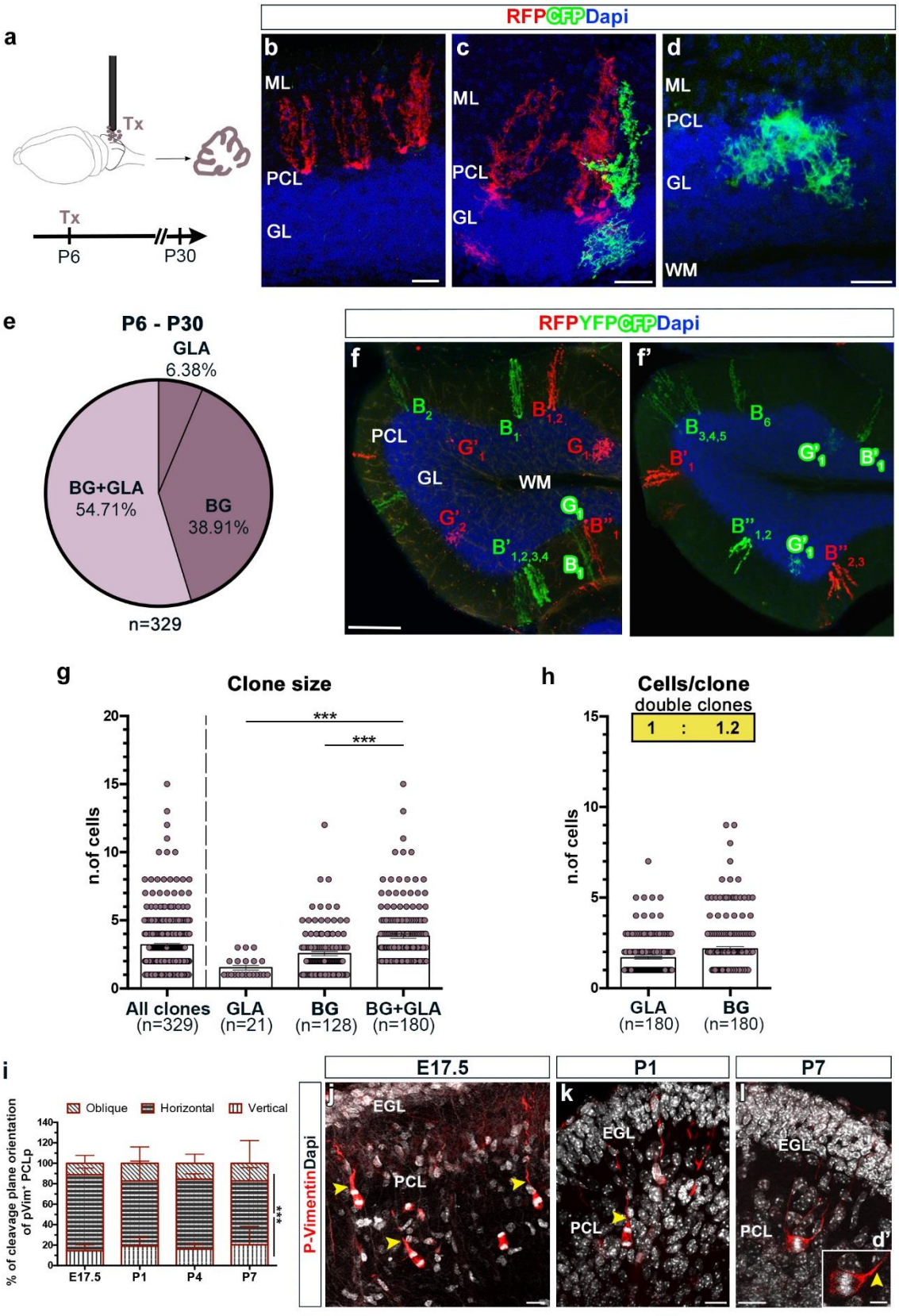

Figure 3.9. PCL-precursors generate BG and part of GLA postnatally. (**a**) Experimental design of superficial administration of tamoxifen (Tx) to induce Confetti-recombination in radial Glast^{+}-precursors in the PCL (PCLp). (**b**-**d**) Analysis after serial sections reconstruction at P30 reveals the existence of sister astrocytes (i.e. expressing the same color) arranged in different types of clones: BG clones (**b**), clones composed of BG+GLA

(**c**) and rare GLA clones (**d**). (**e**) Quantification of the relative proportion of each clone type derived from P6-tagged PCLp. A significant percentage of double BG+GLA clones is found (Chi-square test P<0.001). The pie illustrates pooled data from 3 animals. Example of P6-derived clones (**f**-**f'**) distributed in one or two adjacent sections. (B=BG, G=GLA; superscripts indicate distinct clones, subscripts indicate sister cells). (**g**) Scattered plots of clone size. BG+GLA clones are always bigger in size compared to clones composed of only BG or GLA (***, P<0.001; P values are calculated from GEE analysis). (**h**) Scatter plots show the number of distinct astrocytes phenotypes in double clones. The insets report a geometric mean of ratios, which highlights the prevalence of BG over GLA. (**i**) Frequency distribution of the cleavage plane orientations in p-Vimentin$^+$ PCLp at different time points. PCLp preferentially divide with a horizontal cleavage plane throughout cerebellar development (***, P<0.001 calculated from GEE-poisson regression analysis). No statistically significant differences are found in the distribution of cleavage plane orientation among the time points analyzed: Chi-square test P = 0.7236. Mean values were calculated from 3 animals per time point. (**j**) During late embryonic phase, radial progenitors delaminate from the VZ and start to colonize the developing PCL and keep dividing through horizontal divisions. (**k-l'**) After birth, proliferating PCL-progenitors maintain a horizontal cleavage plane parallel to the PCL, independently of the position of the radial process (highlighted by yellow arrowheads). (**l'**) Magnification of a single confocal plane of the p-Vimentin$^+$ cell in **l** shows the cleavage plane orientation of the nucleus during telophase. EGL, external granular layer; GL, granular layer; PCL, Purkinje cell layer. WM, white matter; Scale bars: 30 µm (**b**-**d**), 100 µm (**f**-**f'**); 20 µm (**j**-**l**), 10 µm (**l'**).

3.1.9 Astroglial precursors amplify according to layer-specific dynamics after birth

The different sizes of cortical and WMA HomCs and the distinct contribution of astrocyte phenotypes to HetCs (few WMA and more numerous cortical elements) suggested distinct layer-specific proliferative activities. This hypothesis was addressed at postnatal stages, when the maximal expansion of precursors in the cerebellar parenchyma occurs (see above) with the concomitant maximal growth of the cerebellum (Legué et al., 2015, De Luca et al., 2009).

Active proliferation of astroglial progenitors was examined by performing a single thymidine analogue (EdU) injection at P1, P4 or P7 (Fig. 3.10a-d") in hGFAP-GFP mice (Zhuo et al., 1997). EdU-positive (+) hGFAP$^+$ precursors exhibited different proliferative behaviours in distinct territories. PCLp divided extensively, showing a peak of proliferation at P1, which gradually decreased afterward. Cycling hGFAP$^+$ cells in the PWM and GL followed the same trend, although with an overall lower proliferation rate (Fig. 3.10a-d"). Both layer-specific amplification rates and proliferation decline were further confirmed by analyses of cell cycle re-entry (Fig. 3.10e-h'''), indicating that all astroglial precursors

undergo an early proliferation burst until P4. Notably, PCLp were the most actively amplifying cells even at later time points, in line with the marked numerosity of BG in both HomCs and double clones at P30.

Taken together, astroglial progenitors in the cerebellum do not proliferate homogeneously in either time or space during the first postnatal week. Rather, they undergo an early proliferative burst during the first days of life and expand according to layer-specific dynamics, suggesting a prominent regulatory role of local factors.

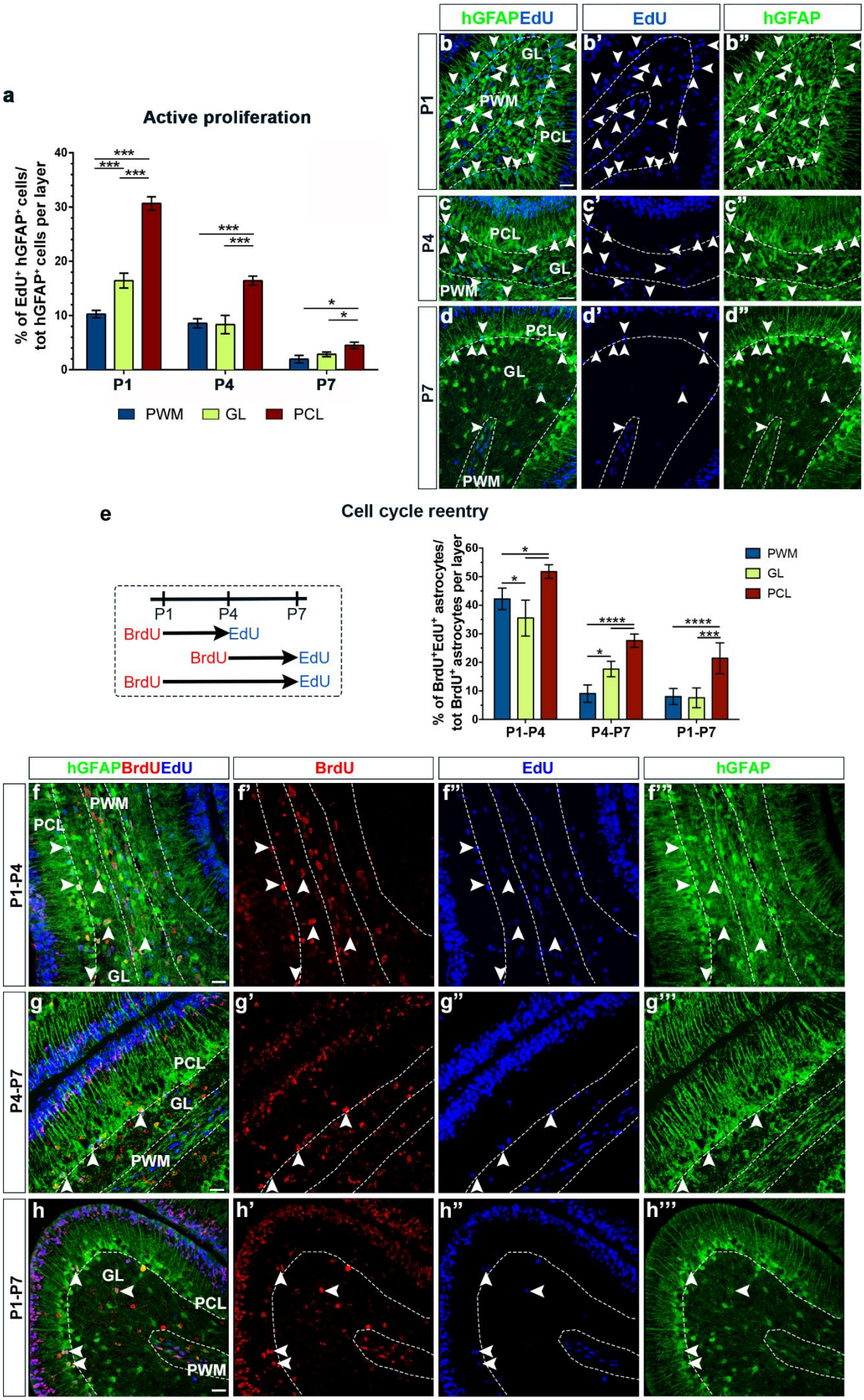
a
Active proliferation
% of EdU+ hGFAP+ cells/ tot hGFAP+ cells per layer
P1
P4
P7
PWM
GL
PCL
hGFAPEdU
EdU
hGFAP
b
b'
b''
c
c'
c''
d
d'
d''
e
Cell cycle reentry
BrdU
EdU
% of BrdU+EdU+ astrocytes/ tot BrdU+ astrocytes per layer
P1-P4
P4-P7
P1-P7
hGFAPBrdUEdU
BrdU
f
f'
f''
f'''
g
g'
g''
g'''
h
h'
h''
h'''

Figure 3.10. Proliferation analyses of cerebellar postnatal progenitors. (**a**-**d**) Analysis of active proliferation of astrocytes in different layers during early postnatal development. (**a**) Percentage of EdU-incorporating astrocyte precursors among total hGFAP$^+$ cells subdivided per layers. EdU was administered 6 hours before sacrifice at P1, P4 and P7 to detect actively proliferating cells. At all analysed time points the active proliferation varies among layers. Mean values were calculated from 3 animals per time point. In **b**-**d"** arrowheads point to double labelled proliferating precursors, highlight the overall reduction in the proliferation activity (P<0.001) and point to a higher number of proliferating cells in the PCL compared to the other layers.

(**e**) Schematic representation of the experimental design of the cell cycle re-entry analysis: a first thymidine analogue (BrdU) was injected at P1 or P4 in hGFAP::GFP mice, while the second one (EdU) at P4 or P7, 6 hours before sacrifice. Then triple-labelled cells were analyzed and plotted in the graph as percentage among total BrdU$^+$/hGFAP$^+$ cells per layer. At each time point PCL-precursors re-enter more frequently the cell cycle compared to astrocytes in other layers. In the PWM after P4 there is a significant drop in the proportion of astrocytes performing another division. The same trend is also present, though less evident, in the GLA. Mean values were calculated from 3 animals per time point. (**f**-**h'''**) Images represent sagittal sections at the different time points analyzed after double thymidine analog labelling: (**f**-**f'''**) P1-P4, (**g**-**g'''**) P4-P7 and (**h**-**h'''**) P1-P7. Merged and single channels for BrdU (red), EdU (blue) and GFP (hGFAP, green) stainings are presented. Arrowheads point to some triple labelled cells. *, P<0.05; ***, P<0.001: all P values calculated from GEE-poisson regression analysis.

3.1.10 Astroglial phenotypes differentiate according to a layer-dependent temporal pattern

To complement the proliferation studies, we performed a birthdating analysis in hGFAP-GFP mice. Retention of high BrdU levels (BrdU^{high}) in astrocytes at P30 after a single pulse of BrdU at E15, P1, P7 or P15 identified cells that had left the cell cycle to undergo differentiation approximately at the time of BrdU injection. When dividing astrocyte precursors were tagged at E15, BrdU^{high}hGFAP+ cells were very rarely found (Fig. 3.11a,d), highlighting that proliferative progenitors at E15 rarely differentiate without further amplification. Interestingly, the sole mature WM hosted few BrdU^{high} astrocytes (Fig. 3.11d, g), showing some first astrocytic differentiation already at E15. Conversely, the highest percentages of BrdU^{high} cells were observed in the first postnatal week, with minimal labelling at the later time point (Fig. 3.11a, e-f). Additionally, mature WMA were born predominantly at P1 (Fig. 3.11a-b") while the bulk of BG differentiated at the end of the first postnatal week (Fig. 3.11a, c-c"). GLA instead appeared to be generated with a constant rate throughout the first 7 days of life (Fig. 3.11a-c").

To gain additional information on the balance between amplification and differentiation, in the same samples we examined cells with low BrdU levels ($BrdU^{low}$) indicative of analogue dilution after repetitive divisions (empty arrowheads in Fig. 3.11b-f). After BrdU administration at E15, all astrocyte phenotypes displayed $BrdU^{low}$ staining, indicating that they were produced through multiple divisions of the tagged proliferating progenitors (Fig. 3.11d, g-i). When progenitors were marked at P1, amplification ($BrdU^{low}$) clearly prevailed over cell cycle exit ($BrdU^{high}$) (Fig. 3.11g-i and empty arrowheads in Fig. 3.11b-b"). At later stages, astrocyte amplification continued only in the cortical layers, although most cells in all territories had already stopped proliferating. These data confirm both an intense amplification of astroglial progenitors early postnatally and distinct generation dynamics for astrocytes in the WM and cortical layers.

Thus, shortly after birth, WMA exit the cell cycle, showing a limited expansion phase. Conversely, GLAp continue to divide for a longer time. In addition, PCLp differentiate after an extended expansion during which they appear overall more proliferative compared to GLAp and PWM precursors.

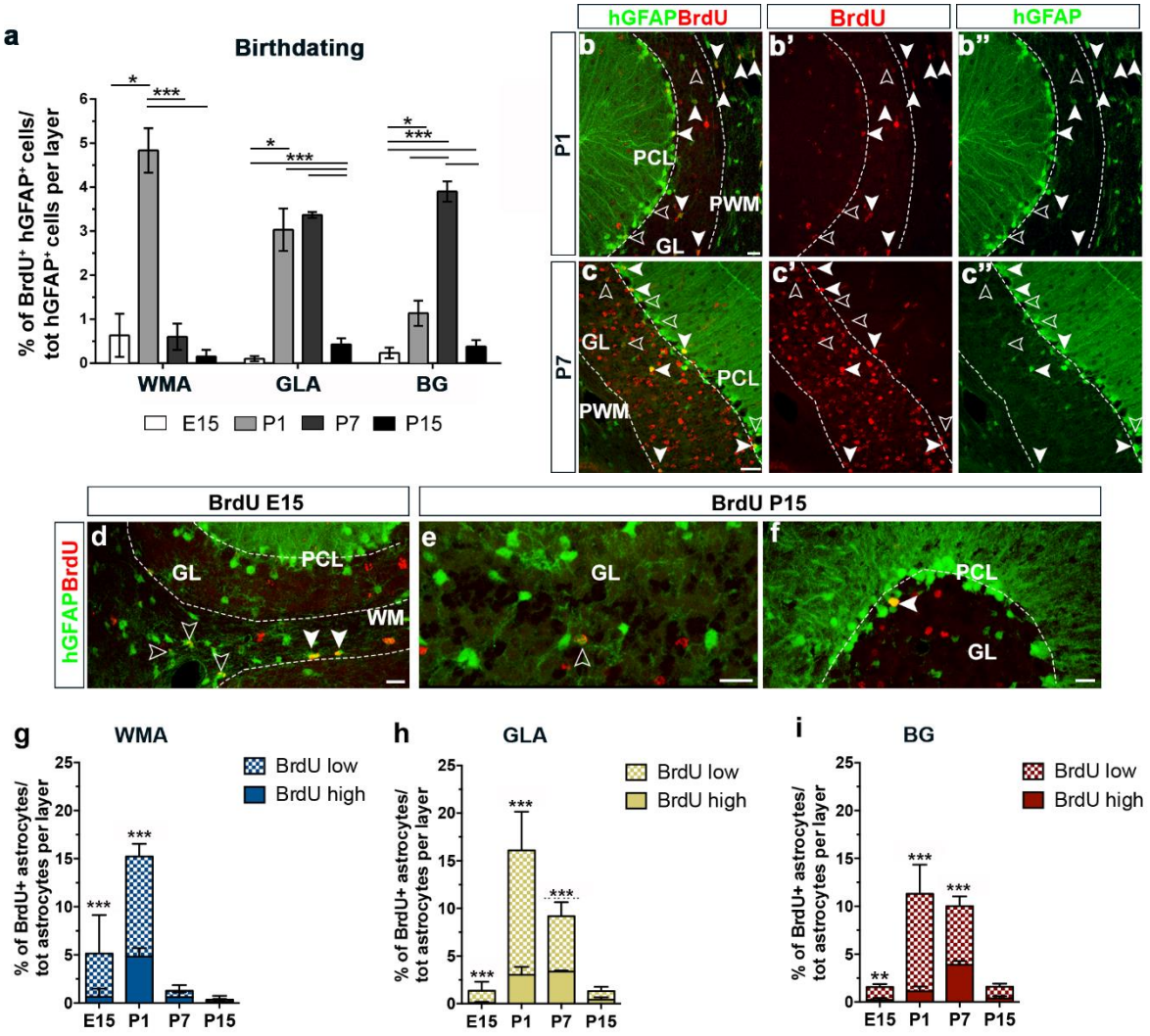

Figure 3.11. Birthdating analysis of cerebellar astrocytes. (**a**-**c”**) Birthdating of astrocytes retaining a strong BrdU signal (BrdU^{high}) after the completion of the maturation process (P30). The histogram (**a**) shows that numerous WMA exit the cell cycle already at P1 while GLA and BG differentiate later. (**b**-**b”**, **c**-**c”**) Full and empty arrowheads point to astrocytes retaining a strong (BrdU^{high}) or a diluted (BrdU^{low}) BrdU signal, respectively. (**d**-**f**) Representative images of P30 cerebella of mice injected with BrdU at the beginning (E15, **d**) and the end (P15, **e, f**) of astroglial development. Full and empty arrowheads point to cells with BrdU^{high} or BrdU^{low} positivity, respectively. (**g**-**i**) Comparison between BrdU^{high} and BrdU^{low} WMA (**g**), GLA (**h**) and BG (**i**) astrocytes at the different birthdating time points analysed. *, P<0.05; **, P<0.01; ***, P<0.001, calculated from GEE analysis. Mean values were calculated from 3 animals per time point. PWM, prospective white matter; GL, granular layer; PCL, Purkinje cell layer; WM, white matter. Scale bars: 30 µm.

3.1.11 Distinct fate-restricted progenitors are likely to coexist in the E12 cerebellar VZ

Our Star Track *in vivo* clonal analysis highlighted that the cerebellar VZ hosts gliogenic RG capable of producing distinct types of clones and whose differentiation potentials decrease over time. Nevertheless, this evidence did not imply that the distinct fates (i.e. clones subtypes) observed came from multiple, distinct, types of predestined RG rather than to a homogeneous population of multipotent progenitors (MPs) that stochastically had made their fate choice. As a first attempt to explain the rules governing the cell fate decision of cerebellar astrocyte progenitors, we tested the validity of the simplest model assuming the existence of a single multipotent progenitor pool. To this aim, lineages were simulated *in silico* according to defined rules of proliferation and differentiation into astrocyte subtypes (for details see section 2.10; Fig. 3.12a-c) and their outcome was compared to our empirical E12-P30 Star Track clones. In these simulations, MPs were assumed to maintain the same properties in space (i.e. probability to generate daughter cells which will remain MPs and proliferation rate; Fig. 3.12b), whereas the probabilities of production of the distinct astrocyte subtypes were defined according to our birthdating analyses (see section 3.1.10) and previous reports (Leto et al., 2011), and were strictly dependent on in which generation they appeared (Fig. 3.12c).

The stochastic model defined above produced clones whose size was in good agreement with the observed clones (Fig. 3.12d). However, it failed to capture the proportions of clone subtypes, with too many BG+GLA+WMA, BG+WMA and GLA+WMA clones at the expense of all HomCs (i.e. BG, GLA, and WMA HomCs) and BG+GLA clones (Fig. 3.12e). On the other side, the overall proportions of astrocyte subtypes matched well the observations, with only slightly too many WMA (Fig. 3.12f). Nevertheless, in the simulated triple BG+GLA+WMA clones there were too many WMA compared to BG and GLA, leading to a lower mean ratio of BG and GLA over WMA compared to that of the observed triple clones (Fig. 3.12g).

Interestingly, the comparison between the simulated lineages at generation 6 (which was defined as approximately corresponding to P0; see section 2.10) and our empirical E12-P0 clones revealed that, already at this early stage, the amount of simulated HetCs was much higher than expected (Fig. 3.12h). Indeed, the proportions of clone subtypes were not

correctly captured by the model, with too many mixed PWM+cortical clones at the expense of the other subtypes, comprising both cortical HetCs (PCLp + GLAp) and cortical or PWM HomCs (Fig. 3.12i).

Overall, these results suggest that the single multipotent progenitor hypothesis can be ruled out and, rather, point towards several fate-restricted progenitor types coexisting at E12 in the cerebellar VZ.

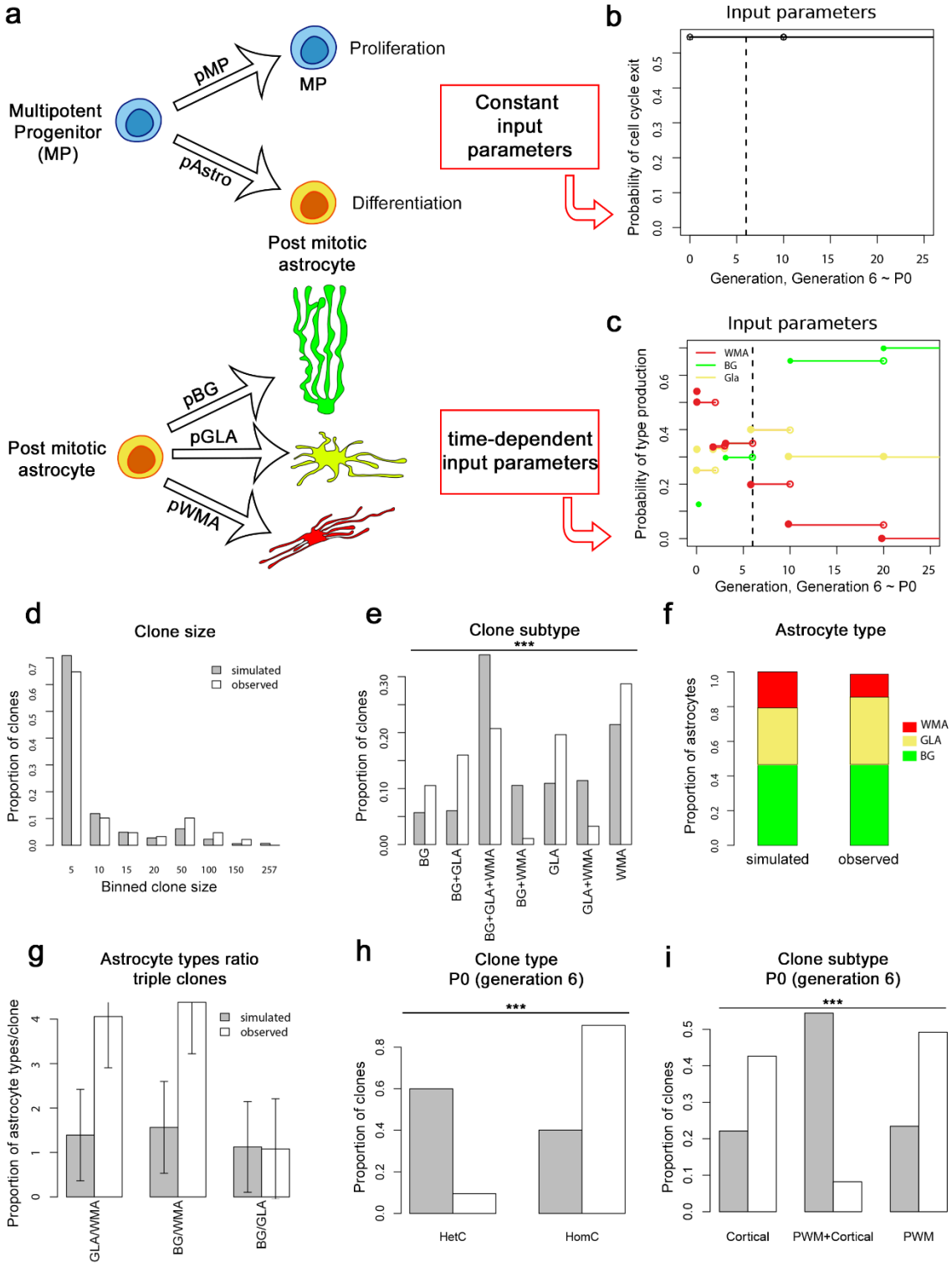

Figure 3.12. Rules and outcomes of the simulation model. (a-c) A schematic representation in (**a**) shows the distinct probabilities, kept constant as shown in (**b**), for each daughter cell at each division of either remaining a multipotent progenitor (pMP = 0.645) or differentiating into a post mitotic astrocyte (pAstro). In this last case, the probabilities of generating the distinct astrocyte subtypes (pBG vs pGLA vs pWMA) are generation-dependently set according to the birthdating experiments, as shown in (**c**). Bar graphs in (**d-g**) show the outcomes of the simulated lineages, whose clone size (**d**) and proportions of astrocyte subtypes (**f**) appear

quite similar to those of the observed clones. On the other side, the proportions of clone subtypes are not well recapitulated (**e**; P < 2.2e-16), neither the relative, too high, amount of WMA compared to BG and GLA in triple clones (**g**). (**h-i**) Simulated and E12-observed lineages were compared at P0 (corresponding to generation 6). Too many HetCs (**h,** P = 2.402e-15) are found in simulated lineages compared to empirical clones, due to the generation of too many PWM+cortical clones at the expenses of the other subtypes (**i;** P = 6.114e-12). Cortical clones comprise PCLp HomCs, GLAp HomCs ad PCLp+GLAp HetCs; PWM+Cortical clones comprise PWM+PCLp, PWM+GLAp and PWM+PCLp+GLAp HetCs. Astro, postmitotic astrocyte; BG, Bergmann glia; GLA, granular layer astrocyte; WMA, white matter astrocyte.

3.2 Role of *Sox2* in BG development and maintenance

Our in vivo clonal analyses revealed that astrogliogenesis in the cerebellum occurs from embryonic RG through distinct lineages according to a precise spatio-temporal pattern. They also allowed to uncover the previously unknow role of BG progenitors in the PCL (i.e. PCL progenitors) as bipotent gliogenic precursors, capable of generating both BG and GLA but not WMA. Provided this newly discovered role of PCL progenitors, as a further step we aimed at getting a deeper insight into their developmental mechanisms. To this end, we focused on the transcription factor SOX2, member of the SOXC family previously demonstrated to be required for the development and maintenance of NSC/RG in both the embryo and in postnatal neurogenic regions such as the hippocampal dentate gyrus (DG; Pevny and Nicolis, 2010; Gómez-López et al., 2011), and known to be expressed in the PCL by both developing and mature BG (Sottile et al., 2006; Alcock and Sottile, 2009). Based on the molecular and morphological similarities shared by developing RG and BG (see section 1.3.1.3), SOX2 represented a promising candidate as an intrinsic regulator of BG development and maintenance.

3.2.1 Wnt1-Cre-mediated *Sox2* deletion in the whole cerebellum leads to alterations of Bergmann glia monolayer formation

As a first step, we looked at SOX2 expression in the cerebellum, by double immunofluorescence for SOX2 and other cell-type-specific antibodies. Early postnatally (i.e. P7), SOX2 was clearly expressed in the PCL by BLBP-positive (+) BG but not in adjacent

Calbindin+ PCs (Fig. 3.13a-d’’’), in agreement with previous reports (Shiwaku et al., 2010). SOX2 was also expressed by parenchymal astrocytes of the GL and PWM (Fig. 3.13a-c). The same pattern of expression was maintained in adult cerebella at 8 months of age (Fig. 3.13g-h’’)

After confirmation of SOX2 expression in both developing and mature BG, we then addressed the consequences on BG development of SOX2 early embryonic loss in the whole developing cerebellar territory. To this end, we made use of Wnt1-Cre, active in the developing midbrain-hindbrain region (from which the cerebellum will arise, see section 1.3.1.1) from E 9.5 (Danielian, 1998) and crossed the Wnt1-Cre transgenic mouse line to that carrying a $Sox2^{flox}$ conditional mutation (Favaro et al., 2009). As expected, SOX2 expression was not detected in mutant Wnt1-Cre;$Sox2^{flox}$ cerebella neither at P7 not at 8 months of age (Fig. 3.13e,f,i,j).

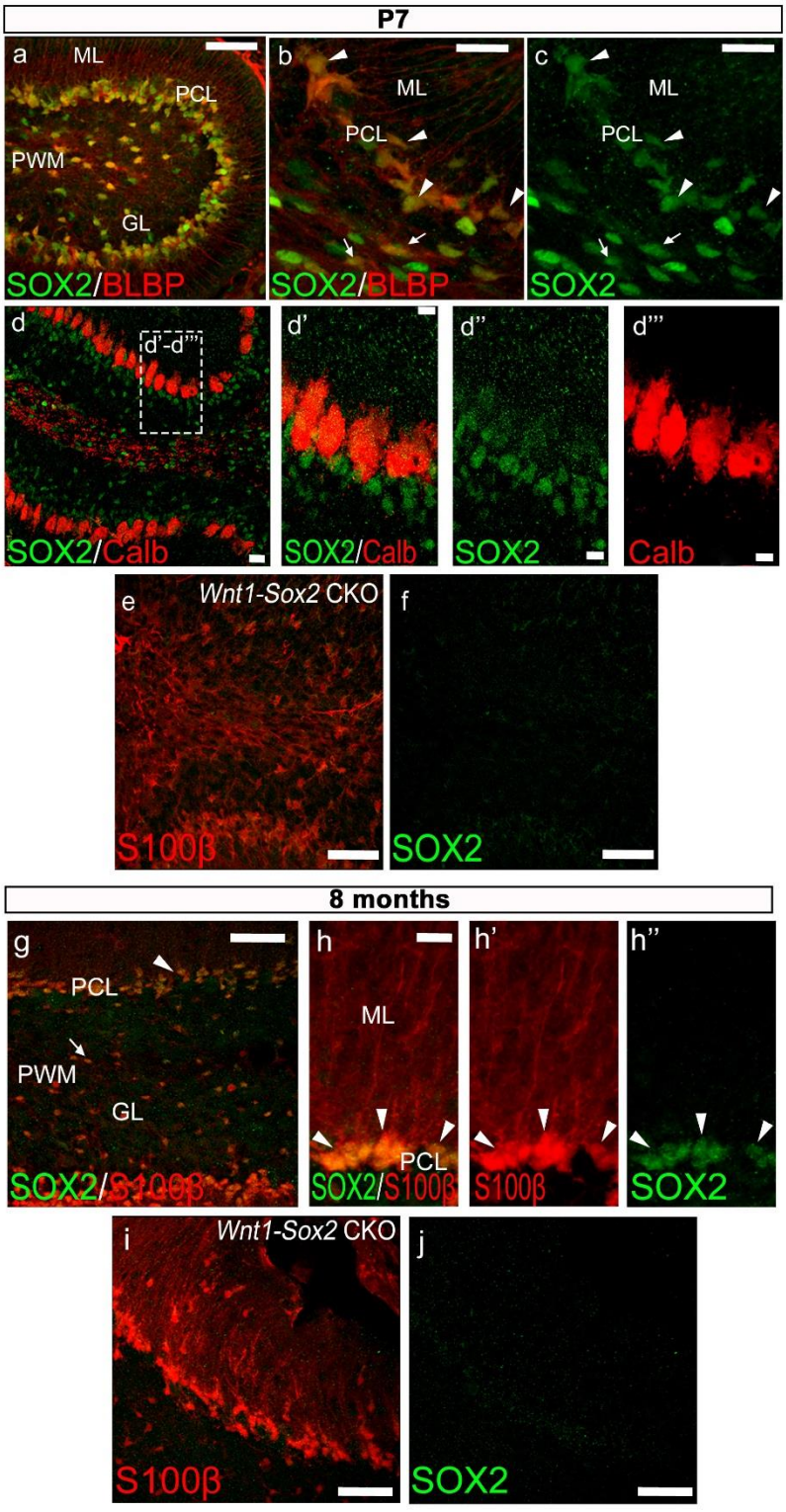

Figure 3.13. SOX2 expression in postnatal and adult cerebellum. (**a-d'''**). SOX2 (green) is expressed in the postnatal P7 cerebellum and SOX2+ cells colocalize with BLBP+ (red in **a,b**) BG in the PCL (arrowheads in **b-c**) and with parenchymal astrocytes of the GL and PCL (arrows in **b-c**). (**d-d'''**) Conversely, SOX2+ cells do not colocalize with Calbindin+ PCs (red in **d,d',d'''**), indicating that it is not a marker for this neuronal phenotype. P7 mutant Wnt1-Cre;Sox2^{flfl} cerebella do not express SOX2 (**e,f**). (**g-h''**), An expression pattern similar to P7 is maintained in S100β-positive cells in the adult cerebellum at 8 months. Mutant Wnt1-Cre;Sox2^{flfl} cerebella

do not express SOX2 neither at 8 months (**i, j**), showing a total deletion of the gene also at this stage. ML, molecular layer; PCL, Purkinje cell layer, GL, granular layer, PWM, prospective white matter. Scale bars: a, e-j, 50 µm; B-D, 20 µm; d'-d''', 10 µm.

Then, we looked for possible alterations, in mutants, of developing and mature BG, by performing immunofluorescence with antibodies against BLBP and S100β to recognize developing BG at P7, or S100β and GFAP to recognize fully differentiated BG at P19 and 8 months. At P7, mutant (Wnt1-Sox2 CKO) and control cerebella did not reveal evident differences in BLBP+ glial cell number (i.e. square density in each layer), morphology, or localization (Fig. 3.14, compare d-f, mutant, with a-c, control). At P19, in controls, S100β/GFAP+ BG were orderly aligned with their cell bodies along the PCL, and their radial projections extended across the ML, as characteristic of BG (Fig. 3.14g-g''); in mutants, however, numerous cell bodies positive for S100β and GFAP, suggestive of mislocalized BG cells, were observed in the ML (Fig. 3.14h-h''), representing about 23% of total cells (Fig. 3.14n). GFAP immunofluorescence (staining the cytoplasm more intensely than S100β) showed that ectopic cells had a non-radial, abnormal morphology (Fig. 3.14h''). Ectopic cells were still abundant at 8 months (Fig. 3.14l,m, compare to controls in i-k; Fig. 3.14o); GFAP+ cells (particularly the ectopic ones, but also the ones aligned along the PCL), showed a characteristic aberrant, multipolar morphology, with dense arborizations (Fig. 3.14m, see magnified insert).

By comparison, no significant differences in non-ectopic BG cell numbers were found in the mutant PCL compared to control animals at P19 (Fig. 3.14p); similarly, also the number of parenchymal astrocytes of the GL and WM remained overall stable among genotypes (GL, Wnt1-Sox2 CKO = 945.4±43.5 vs CTRL = 801.3±53 cells/mm^2; WM, Wnt1-Sox2 CKO = 1606±349.5 vs CTRL = 1487±474.7 cells/mm^2). Moreover, at 8 months, neither the density nor the morphology of both Calbindin+ PCs and Parvalbumin+ interneurons appeared changed between mutants and controls (PCs, Wnt1-Sox2 CKO = 1390±137 vs CTRL = 1425±77 cells/mm^2; Interneurons, Wnt1-Sox2 CKO = 718.1±128 vs CTRL = 772.7±59 cells/mm^2).

In conclusion, both the localization and morphology of BG are progressively altered during postnatal life in *Sox2* mutant mice, without apparently affecting neuronal and parenchymal astrocytes development.

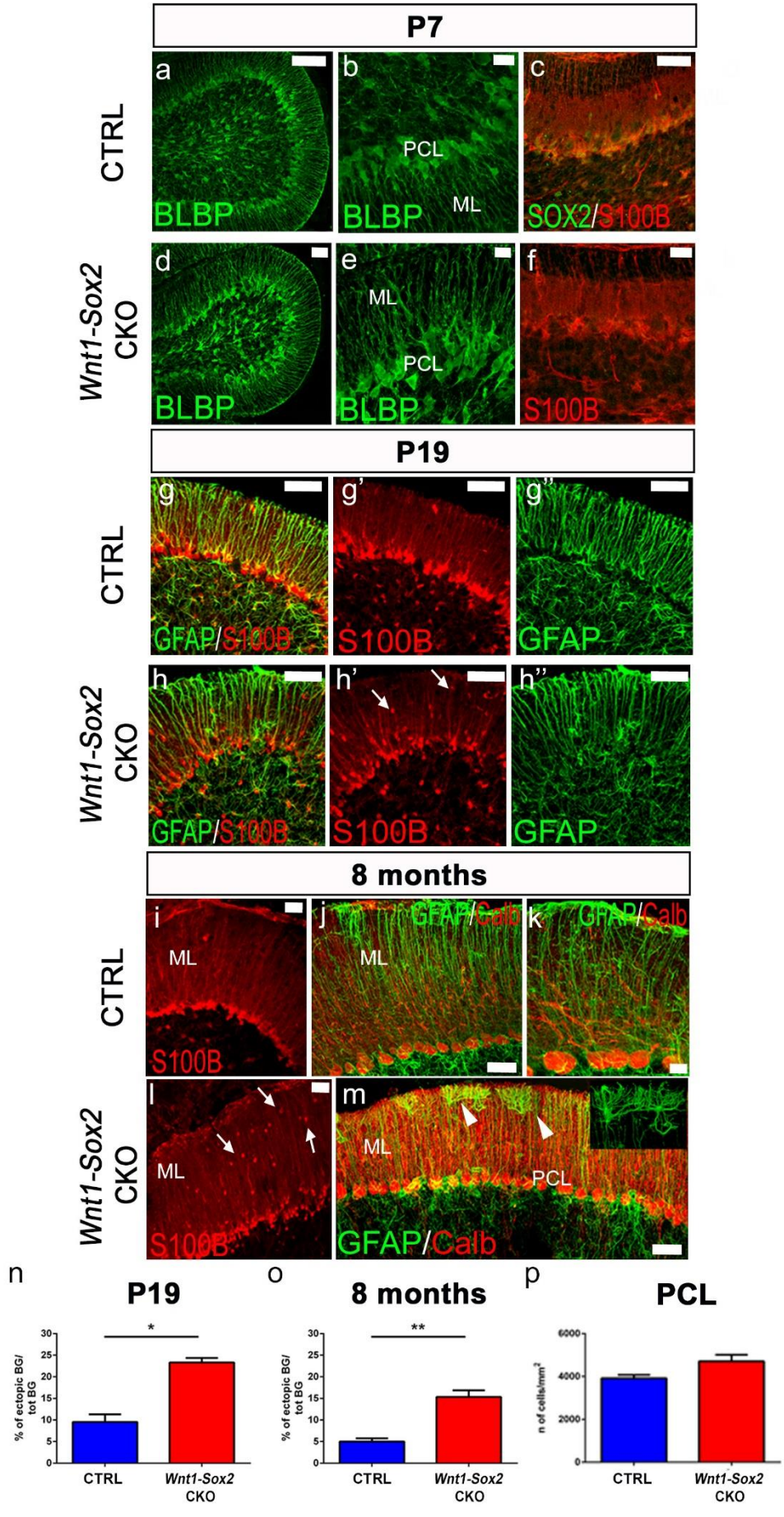
P7
CTRL
a
BLBP
b
PCL
ML
BLBP
c
SOX2/S100B
Wnt1-Sox2 CKO
d
BLBP
e
ML
PCL
BLBP
f
S100B
P19
CTRL
g
GFAP/S100B
g'
S100B
g''
GFAP
Wnt1-Sox2 CKO
h
GFAP/S100B
h'
S100B
h''
GFAP
8 months
CTRL
i
ML
S100B
j
GFAP/Calb
ML
k
GFAP/Calb
Wnt1-Sox2 CKO
l
ML
S100B
m
ML
PCL
GFAP/Calb
n
P19
% of ectopic BG/ tot BG
CTRL
Wnt1-Sox2 CKO
o
8 months
% of ectopic BG/ tot BG
CTRL
Wnt1-Sox2 CKO
p
PCL
n of cells/mm²
CTRL
Wnt1-Sox2 CKO

Figure 3.14. Wnt1-Cre;Sox2$^{fl/fl}$ mutants show postnatal BG alteration. (**a-m**) Glial cells were labelled with specific markers as BLBP, S100β and GFAP in control (CTRL, **a-c, g-g'', i-k**) mice and in mutant Wnt1-Cre;Sox2^{flfl} cerebella (Wnt1-Sox2 CKO, **d-f, h-h'', l-m**) at different ages. At P7 (**a-f**) no significant differences are detected in BG monolayer formation, as BG cells are similarly labelled with BLBP and S100β in the arising PCL of both genotypes. At P19 (**g-h''**) ectopic S100β+ cells appear in the mutant ML (**h-h''**; arrows in **h'**) and these cells remain in the adult cerebella at 8 months (arrows in **l**). GFAP staining confirms the presence of mislocalized BG in the mutant ML, characterized by aberrant multipolar morphology (arrowheads in **m**, inset). (**n-p**) Quantification of S100β+ cells in P19 and 8 months mutant and control cerebella (P19: Wnt1-Sox2 CKO, n = 2, CTRL, n = 3; 8 months: Wnt1-Sox2 CKO, n = 3, CTRL, n = 3) confirms the significant presence of ectopic BG cells in the mutant ML (**n, o**; student T test, P19, $P < 0.05$; 8 months, $P < 0.005$), whereas not significant differences are detected in the density of BG correctly aligned to the PCL (**p**). n= number of animals. ML, molecular layer; PCL, Purkinje cell layer, GL, granular layer, WM, white matter. Scale bars: a, c, f, g-h'', j-k, m, 50 µm; b 20 µm; d, i, l 30 µm; e, 10um.

3.2.2 *Sox2* postnatal deletion in radial glia leads to ectopic, abnormal and disorganized Bergmann glia

The defects in BG observed in Wnt1-Cre;Sox2$^{fl/fl}$ mutants, in which *Sox2* was ablated in the whole cerebellar primordium and in all cerebellar progenies, appear to arise only postnatally. This observation raised the question whether *Sox2* could be cell-intrinsically required, during postnatal development, for BG to correctly develop and maintain their characteristics. To answer this question, we deleted *Sox2* in BG postnatally, by means of a Tamoxifen-inducible Cre recombinase encoded by a GLAST^{CreERT2} transgene (Mori et al. 2016). GLAST^{CreERT2};Sox2$^{fl/fl}$ mice were administered with Tx at P2. Cerebella were then analyzed at 1 month (P30) or 8 months of age (Fig. 3.15). Cre induction led to efficient ablation of *Sox2* from S100β+ BG along the PCL, reaching about 60% (Fig. 3.15a-f, compare a-c, control, with d-i, mutant; Fig. 3.15j). In controls (CTRL) at P30 (Fig. 3.15a-c), the S100β+ BG (red) were largely SOX2+ (green), formed an ordered array of cells with their cell bodies aligned in the PCL, and were only very rarely (5%; Fig. 3.15k) ectopically located in the overlying ML; by contrast, in mutant mice of the same age (GLAST-Sox2 CKO; Fig. 3.15d-i), approximately 16% of S100β+ BG showed wide disorganization, with their cell bodies localized throughout the ML (Fig. 3.15 compare panel e, mutant, with panel b, control; Fig. 3.15k). Of note, SOX2 immunofluorescence confirmed the absence of SOX2 from most (~80%) ectopic BG in the ML (Fig. 3.15j, arrows in Fig. 3.15g,h). S100β/GFAP

immunofluorescence at 8 months confirmed the persistence, in mutants, of widely disorganized and mislocalized BG, representing about 15% of the whole BG population (Fig. 3.15n), similarly to what observed in Wnt1-Cre;Sox2$^{fl/fl}$ mutants of the same age (Student T test, P=0.9389). Moreover, as revealed by GFAP immunostaining, these ectopic BG showed a higher GFAP expression and an abnormal morphology (panel m, GLAST-Sox2 CKO, compared to panel l, CTRL), together with a disruption of their normal, radial organization and the acquisition of a multipolar-like shape with short processes (Fig. 3.15, compare m, GLAST-Sox2 CKO, to l, CTRL).

Therefore, these findings confirm that the peculiar phenotype of mislocalized BG observed postnatally in Wnt1-Cre;Sox2$^{fl/fl}$ animals was due to a cell autonomous effect of *Sox2* deletion in BG themselves, and therefore point to *Sox2* intrinsic requirement, during postnatal life, for the correct maintenance of the BG monolayer, as well as for the preservation of their characteristic radial morphology.

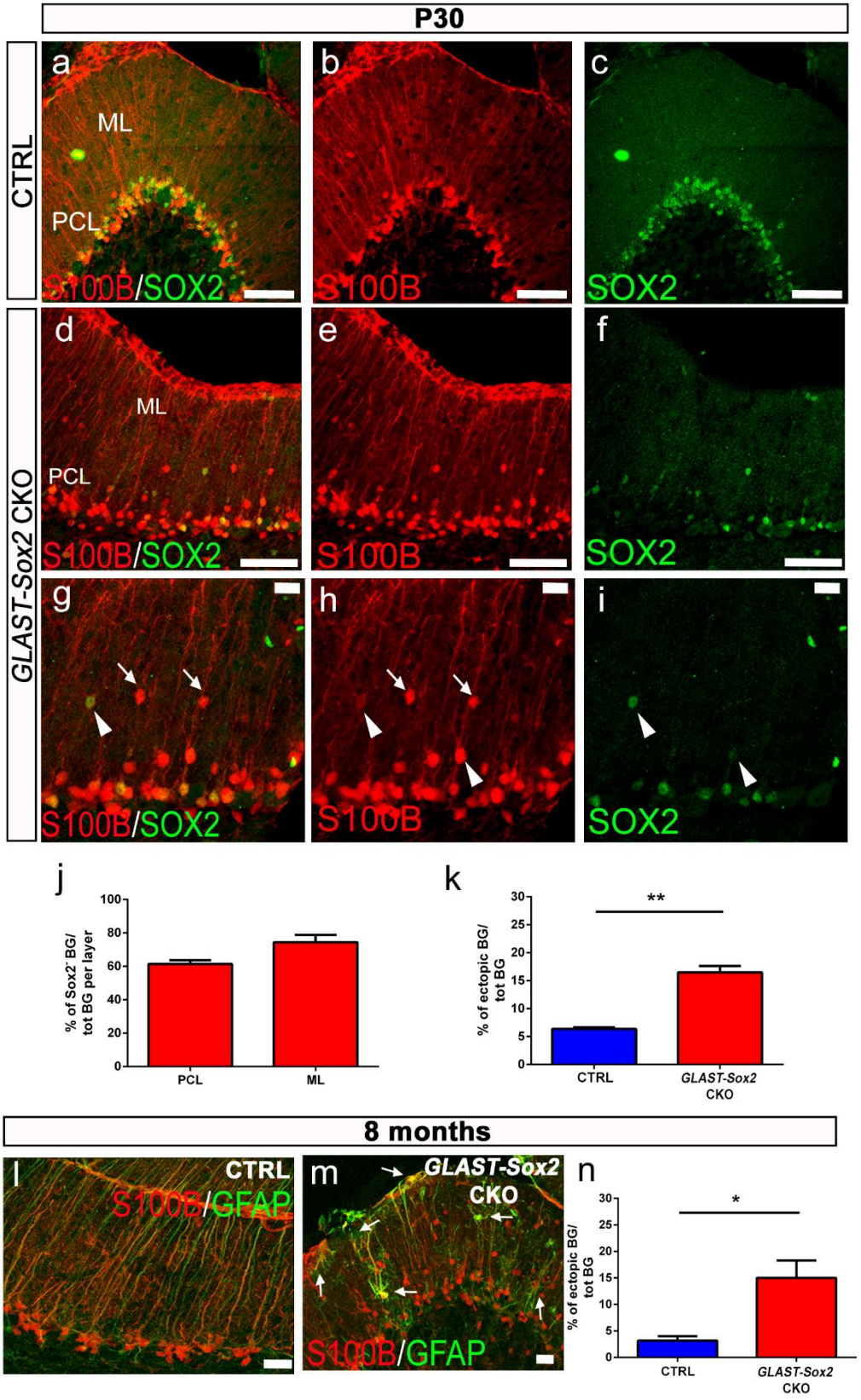

Figure 3.15. GLAST^{CreERT2};Sox2^{flfl} mutants confirm postnatal BG alterations. (a-i) Compared to controls (CTRL; **a-c**), where S100β- and SOX2-expressing BG are neatly ordered along the PCL, GLAST^{CreERT2};Sox2^{flfl} cerebella induced with Tx at P2 (GLAST-Sox2 CKO; **d-i**) showed, at P30, high numbers of mislocalized S100β+ BG cells in

the ML that had mostly lost SOX2 expression (arrows in **g, h**; arrowheads in **g-i** point to ectopic BG still expressing SOX2). Bar graphs in (**j**) highlight the high percentages of S100β+ cells, in both PCL and ML of P30 GLAST^{CreERT2};Sox2^{flfl} cerebella (n=3 animals), not expressing SOX2, showing the efficient ablation of the gene. (**k**) The fraction of ectopic S100β+ cells on the total S100β+ population was significantly higher in mutant cerebella with respect to control littermates (Student T test, P<0.005; GLAST-Sox2 CKO, n = 3, CTRL, n = 3). (**i, m)** A similar pattern of ectopic BG was maintained at 8 months of life (arrows in **m** indicate mislocalized BG detected with S100B and GFAP and showing an aberrant, multipolar, morphology). (**n**) Similarly to what observed at P30, the fraction of ectopic BG over the total population found at 8 months in mutant mice was significantly higher than in controls (Student T test, P< 0.05; GLAST-Sox2 CKO, n = 4, CTRL, n = 4). n = number of animals. ML, molecular layer; PCL, Purkinje cell layer. Scale bars: a-i, 50 µm; l,m, 20 µm.

3.2.3 *Sox2* is not required for the maintenance of BG monolayer and morphology in the mature cerebellum

Our data show that *Sox2* is cell autonomously required, during postnatal development, for the correct arrangement of BG in a monolayer along the PCL and for the maintenance of their peculiar radial morphology. These findings further raised the question whether *Sox2* was necessary to maintain these features at adult stages as well, when the maturation of BG is fully completed. To answer this question, we exploited the same GLAST^{CreERT2}Sox2$^{fl/fl}$ mouse line used in the previous experiments, this time administering Tx at 6 months, when cerebellar development is accomplished. Cerebella were then analyzed at 8 months of age. As for postnatal *Sox2* deletion, SOX2 immunostaining revealed an efficient ablation of the gene from S100β-expressing BG in 6 months-induced mutant mice (Fig. 3.16, compare c, control, to f, mutant). Interestingly, independently from SOX2 expression, in both controls (Sox2$^{fl/fl}$ or Sox2$^{fl/+}$) and mutants nearly all S100β+ BG displayed their peculiar radial morphology and were correctly organized in a monolayer lining the PCL. Only a very small fraction (~5%) of BG were located in the overlying ML, similarly to controls (Student T test, P=0.5562).

Overall, these data reveal that *Sox2*, necessary for the correct development and maintenance of BG during their postnatal development, is not needed for BG to preserve their features at adult stages, when their maturation is fully accomplished.

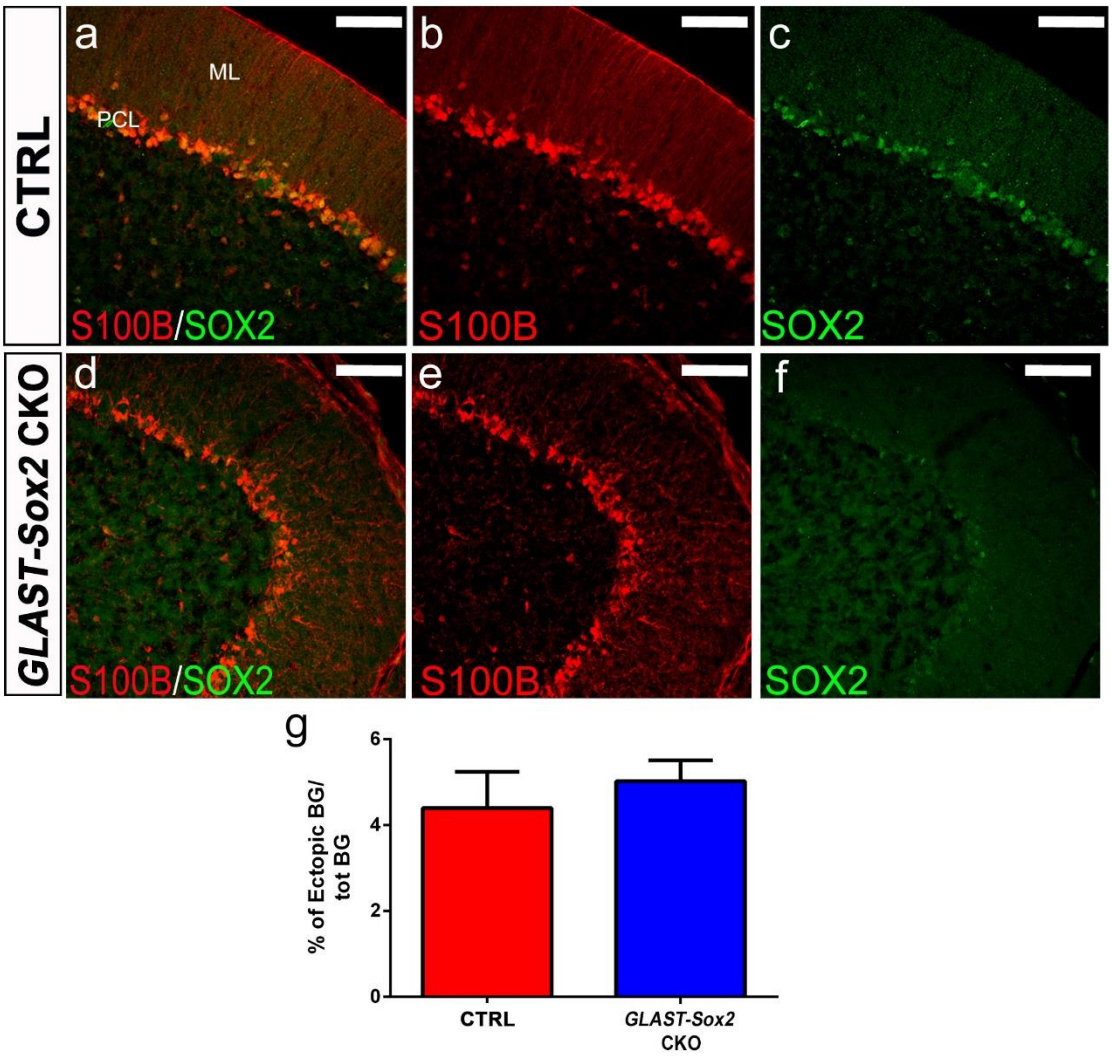

Figure 3.16. *Sox2* is not required to maintain BG features at adult stages. (**a-f**), In both controls (CTRL; **a-c**) and GLAST^{CreERT2};Sox2^{flfl} mutant mice induced with Tx at 6 months of life (GLAST-Sox2 CKO; **d-f**), most of S100β-expressing BG are correctly aligned to the PCL, independently from their SOX2 expression. (**g**), the fraction of ectopic BG found in the ML is similar between controls and mutants (Student T test, P=0.5562; GLAST-Sox2 CKO, n = 3, CTRL, n = 3). n = number of animals. ML, molecular layer; PCL, Purkinje cell layer. Scale bars: a-f, 50 µm.

Chapter 4: Discussion

In this study, we unveil novel mechanisms underlying the generation of astroglial diversity in the cerebellum. The simple cytoarchitecture of this territory with well-characterized and easily recognizable astroglial types allowed to overcome the current limitations in the study of the astrocyte ontogenesis due to poorly characterized cell diversity in other brain areas. Here for the first time, by means of in vivo clonal analyses, we provide evidence of clonal relationships among the major cerebellar astrocyte subtypes, demonstrating the existence, as early as E12, of gliogenic RG that give rise to both heterogeneous and homogeneous lineages including all, two or just one astroglial phenotype. Namely, we show that cerebellar astrogliogenesis follows a well-defined spatiotemporal pattern, exhibiting a time-dependent spatial allocation and a progressive cell-fate restriction, paralleled by a decrease of progenitor amplification and suggestive of the segregation of cortical and WM astrocyte lineages. Of note, clones including distinct astroglial phenotypes display a recurrent, stereotyped, modularity in their composition, revealing that astrogliogenesis is governed by unprecedented developmental rules at the clone level. Moreover, we show that while astrocyte spatial allocation is already established at birth, both clone heterogeneity and size emerge during postnatal development, in parallel with maximal tissue outgrowth. Indeed, astrogliogenesis continues after birth, when intermediate progenitors amplify and terminally differentiate in a time- and layer-specific manner. Interestingly, progenitors in the PCL niche maintain an unanticipated capability to generate distinct astrocyte subtypes. Finally, in order to define the rules governing astrogliogenesis, we attempted a first in silico modelling of these data. This simulation rejects the possibility that cerebellar astroglial diversity originates from a completely homogeneous population of multipotent progenitors that stochastically generate different lineages. Rather, it supports the existence of RG subsets with predetermined cell fates. Finally, in search for molecules involved in cerebellar astrocyte development and maturation, here we point to Sox2 as a cell autonomous regulator of BG monolayer formation.

4.1 Spatiotemporal pattern of embryonic cerebellar astrogliogenesis

While the spatial and temporal specification of distinct neuronal phenotypes and of oligodendrocytes has been extensively addressed, this topic has been poorly explored for astroglia (Molofsky and Deneen, 2015; Goetz et al., 2016). This study contributes to fill this

gap by exploiting the cerebellum as a model of investigation. In the mature cerebellum, E12- and E14-derived mature clones were distributed along the M-L and A-P axes according to a precise pattern already established at birth and clearly linked to the organization of the cerebellar territory. First, clones were always found in only one half of the cerebellum, similar to other in utero electroporation (IUE) studies (Kita et al., 2013). This was likely due to positional constraints of the electrodes that targeted only one side of the cerebellar primordium, as confirmed by inspections 24h post IUE, and is in line with the view of the two sides of the cerebellar anlage as discrete and independent developmental modules (Sillitoe and Joyner, 2007; Louvi, 2003). Second, in both adult and P0 cerebella, clones originating from E12-tagged RG were found predominantly in the cerebellar hemispheres through all the folia, whereas E14-derived RG gave rise to clones confined to the anterior and posterior lobules of the vermis (Fig. 4.1). The observation of this consistent pattern in all examined samples and the confirmation of a rather diffuse M-L and A-P targeting of the VZ early after IUE, excluded that a simple technical bias could explain such distribution. These results are consistent with a model where E12 astrogliogenic RG preferentially populate the hemispheres, while distinct RG, still rare at E12, become preponderant at later stages likely by cell amplification, and populate the vermis. Thus, distinct, consecutive, waves of RG amplification and detachment appear to happen, in agreement with former interpretations (Yuasa et al., 1996). In line with this view, a small subset of E12-derived clones was found in the vermis, and displayed a limited M-L dispersion closely resembling that of E14-derived clones (as shown in Fig. 3.2d), thereby suggesting that they resulted from the occasional targeting of those RG that, still rare at E12, become preponderant at E14 and thereafter populate the medial cerebellum. In regard to the A-P axis, only E14-targeted RG showed a specific pattern, mostly confined to anterior and posterior lobules, and were rarely found in the central folia VI and VII. These lobules are then likely to be populated by a third wave of astrogliogenesis. This developmental scheme along the two axes reminds of the well-described organization of cerebellar neurons born on different days and of their maturation processes. Indeed, as hinted by early birthdating analyses in rats (Altman and Bayer, 1997) and subsequently confirmed by more recent genetic fate mapping analyses, PCs production starts with neurons that will eventually settle in the hemispheres and paravermis (Sudarov et al., 2011). Yet, while PCs in the vermis disperse along the A-P axis first to central, then to posterior and finally to anterior lobes (Altman

and Bayer, 1997; Sudarov et al., 2011), astrocyte allocation shows an opposite pattern (delayed in central folia). Nevertheless, such a distribution resembles the pattern of maturation of both PCs (Sudarov and Joyner, 2007) and, more broadly, of lobules (Altman, 1969; Leguè et al., 2016).

4.2 Heterogeneity of astroglial lineages

RG are broadly considered as a heterogeneous population in terms of markers expression and regional fate specification (Pinto and Gotz, 2007). Here, we report the existence of RG endowed with the potential to generate distinct astroglial lineages, thus providing a further level of RG heterogeneity. Indeed, at both examined time points, RG showed the capability of generating all astroglial phenotypes as part of both HomCs and HetCs. However, as development proceeds, the multipotency of RG appeared to decline, as triple HetCs containing BG, GLA and WMA became less frequent, concomitantly with an expansion of WMA HomCs (Fig. 4a). These findings also highlight region-specific differences within the cerebellum, where distinct environmental cues in the vermis and hemisphere may influence the final composition of clones. However, it also conforms to the notion of time-dependent reduction in the differentiation potential of neurogenic RG (Shen et al., 2006; Guo et al., 2013). The above described behavior of RG could be explained by the stochastic fate choices of a homogeneous population of multipotent progenitors that, over time, undergo changes in their competence. Such a model has been proposed for the temporal changes in RG fate potency along neuronal lineages, and from the switch from neurons vs glia production in different CNS regions (Kohwi and Doe, 2013; Carletti and Rossi 2008; Shen et al., 2006; Guo et al., 2013). Alternatively, as also proposed for neuronal lineages (Franco et al., 2012; Ciceri et al., 2013; Gao et al., 2014), clone heterogeneity may originate from discrete subsets of progenitors predetermined toward specific fates, whose relative proportions change with time. These two options are currently highly debated in the field of brain development.

Despite the time-dependent tendency to increase of HomCs, HetCs constituted a relevant proportion at both examined time points. This strikingly differs from what the same Star Track-based clonal analysis performed at E14 revealed in the neocortex (Garcia-Marques and Lopez-Mascaraque, 2012). There, not only parenchymal and WM clones appeared fully

segregated, as opposed to the high frequency of our triple clones, but also clones within the cortex essentially displayed a homogeneous composition. Despite the poor morphological heterogeneity of neocortical parenchymal astrocytes may have partly masked their actual level of heterogeneity, these discrepancies may be due to area-specific differences in RG competence. Otherwise, forebrain RG may have been targeted too late to appreciate their multipotency and might produce HetCs at earlier time points. One remarkable feature of Hom lineages was the inclusion of single cell clones, in confirmation of the view that astrocytes derive directly from RG. This has been so far postulated for BG generation through RG translocation (Altman and Bayer, 1997; Yuasa et al., 1996; Yamada and Watanabe, 2002). However, our data indicate that direct transformation may occur for all astrocyte subtypes, being especially prominent for WM cells.

As a further level of potential lineage heterogeneity, we cannot exclude that some astroglial cerebellar lineages may contain neuronal derivatives that are masked in our analysis due to the employment of a promoter that drives the expression of fluorescence tags exclusively in astroglial cells. Interestingly, lineage and clonal studies showed that progenitors in the postnatal PWM divide asymmetrically and give rise to both ML interneurons and WMA astrocytes (Silbereis et al., 2009; Fleming et al., 2013; Parmigiani et., 2015). Hence, WMA HomCs may likely include sibling interneurons. However, since postnatal PWM and cortical lineages may share a common ancestor, also triple HetCs might include interneuron derivatives. Moreover, a pioneer clonal analysis in the chick at developmental stages earlier than those of this study has formerly shown the existence of a major proportion of clones composed of PCs and astrocytes (Lin and Cepko, 1999), thus suggesting potential broader clonal relationships between astroglial and neuronal cerebellar lineages.

4.3 Multiple-level regulation of clone features

In our data, time appears to directly affect the size and degree of M-L dispersion of clones, both of which decrease as development proceeds and according to the level of clones' heterogeneity: the biggest and most M-L dispersed clones are those generated earlier. Yet, clones generated at distinct developmental times also displayed a distinct settlement in

the hemispheres or vermis.

Notably, at P0, E12 and E14-derived clones were still very similar in terms of composition, size and degree of dispersion, whereas they already differed in their allocation to distinct cerebellar territories. This reveals that several key features distinguishing E12 and E14 clones only emerge postnatally. During this phase, pioneer astroglial precursors settle in the nascent cerebellar parenchyma and keep dividing in situ, as demonstrated to occur in the forebrain (Ge et al., 2012). Distinct factors may be involved in the regulation of this postnatal amplification. Early E12 progenitors producing the biggest families may be intrinsically endowed with a higher proliferative capability, which declines in a time-dependent manner in later generated families, as shown for neurogenic progenitors (Gao et al., 2014). On the other side, region-specific environmental factors may influence clone proliferation. In this respect, tissue expansion does not appear as the major regulator of clone size, as the vermis, where clones are small, has a volume double of that of individual hemispheres. Alternatively, small vermian clones may just reflect a higher number of RG available to support the full territorial occupation of the vermis.

If the degree of clones' dispersion along the M-L axis varied according to both time and space, their A-P spread remained quite constant. Indeed, most of both E12- and E14-generated clones were commonly found in a single lobule or in two adjacent folia. This is likely because the bulk of clone amplification occurs during the first postnatal week, when the cerebellar foliation pattern is defined and each lobule acts as an independent unit; as a result, each progeny rarely crosses the already established fissures, as previously described to occur for granule cells (Leguè, 2015). The only exception to this rule was played by E12 triple clones, that showed a much higher degree of A-P dispersion in the hemispheres. Pioneering progenitors of these clones may still be particularly numerous in the PMW around birth and sustain, by an intense proliferation, a broader distribution of daughter cells. However, delayed fissure formation in the hemispheres as compared to the vermis may also contribute to these findings.

Despite the general differences observed between E12 and E14-derived populations, a closer, clone-wise, inspection highlighted the presence of a strikingly recurrent modularity in HetC composition, to which the majority of astrocytes contribute according to our clonal data. These findings reveal unprecedented fixed developmental rules governing astrogliogenesis at the clone level. Indeed, similar clone subtypes derived from either E12

or E14 progenitors showed an analogous stoichiometry, with very few WMA and similar, higher, amounts of both BG and GLA in triple clones, and BG outnumbering GLA in double clones (Fig. 4a). Overall, these evidences suggest that, on the one side, the fate competence of the original progenitor (i.e. its capability to generate double vs triple clones) defines, independently of its E12 or E14 origin, the fixed relative amounts of cortical and, when present, of WM astrocytes, whereas, on the other side, the final cell numbers are affected by a time-dependent regulation as discussed above. Most remarkably, this general architecture was reflected also within each HetC. Indeed, most of the big and highly M-L distributed HetCs were formed by clusters of sister cells, rather than being randomly dispersed in the cerebellar volume. While WMA appeared to be less prone to form aggregates, the vast majority of the clusters consisted of groups of BGs and GLAs, that, in turn, mostly displayed a remakable uniform composition of BG outnumbering GLA observed at the clone level (Fig. 4a). These clusters may therefore represent the major unitary modules upon which HetCs clones are built.

Importantly, as proposed by a previous clonal study in the cerebral cortex, (García-Marqués and López-Mascaraque, 2012), the lineage origin might unveil a new level of astrocyte diversity likely associated with specific regional functions. Indeed, each clusters of sister cells found in our HetCs may act as a functional unit, specifically interacting with the same surrounding neurons and participating in the shaping and maintenance of the same microcircuit. Similarly, neighboring astrocytes in both the mouse hippocampus and cerebral cortex were shown to exhibit synchronous calcium fluctuations (Sasaki et al., 2011), although their clonal relationship still remains to be demonstrated. Further investigations are needed to elucidate whether a similar synchronization also occurs within our clusters of clonally related astrocytes and whether, in general, these cells are functionally correlated. Moreover, as a further level of functional correlation among clonally related cells, the time-dependent allocation of clones predominantly in the hemispheres or vermis, as well as their frequent lobule-restricted distribution also suggests that the astrocyte lineage identity contributes to the definition of the functional specialization of the diverse cerebellar zones, which serve topographically arranged functions (Sillitoe and Hawkes, 2013).

4.4 The contribution of postnatal progenitors in the PCL to cerebellar astrogliogenesis

Astroglial progenitors dividing in the PCL are generally considered to differentiate as BG after an amplification phase that parallels the tangential expansion of the cerebellar surface. Here we demonstrate that PCLp give rise to clones containing not only BG but also GLA, thereby showing that they are not fully committed to the BG fate and strongly suggesting that these progenitors are the most likely source of double HetCs and BG+GLA clusters. Of note, this finding is in agreement with the lack of GLA in En1;Ptpn11CKO cerebella, where bona fide BG progenitors fail to develop and BG is absent (Li et al., 2014). Interestingly, in these cortical clones the GLA:BG ratio revealed a slight predominance of BG and displayed an intermediate value to that of triple and double clones. Indeed, the cortical clones found in Confetti mice represent the "cortical collaterals" of the embryonically-traced Star Track clones and some of them are likely to have sister cells in the WM, therefore resulting in a cell stoichiometry with values in the middle between those of RG-derived double and triple clones.

In search for possible variations in cleavage plane orientation that may determine the fate of PCLp daughter cells, we saw that these progenitors rather always retained a horizontal division plane, from embryonic development (when the GL is still absent) to postnatal stages. Therefore, we conclude that no changes in cleavage plane orientation are involved in the generation of GLA from PCLp. Importantly, this evidence reveals an unprecedented similarity in cleavage plane orientation between PCLp and the outer RG (oRG) lacking the apical process, previously described to divide horizontally and to which PCLp morphologically resemble as for their basal process (Wang et al., 2011; Betizeau et al. 2013; LaMonica et al., 2013; Gertz et al., 2014).

Thus, here we unveil a novel gliogenic potential of progenitors sitting in the PCL, which appear as a source of both kinds of cortical astroglial subtypes. This discovery adds to the very recent report of the capability of these same cells of proliferating, migrating to the EGL and producing GCs after a major depletion of the perinatal EGL (Wojcinski et al., 2017), therefore pointing to a further neurogenic potential for PCLp, as indeed suggested by their close similarity with oRG described above. Taken together, these evidences point to progenitors in the postnatal PCL as a peculiar population, acting as a fundamental source for cortical clones and endowed with particular stem cell properties. Moreover, it is

intriguing to think that, before reaching the PCL and after their detachment from the VZ, a fraction of these progenitors could generate also WMA and therefore could be a source also of our triple clones (Fig. 4.1).

4.5 Layer-specific dynamics affect postnatal astrogliogenesis and set up HetC stoichiometry

The stereotyped architecture of HetCs in terms of cell composition, together with evidence that this architecture emerges after birth, prompted the analysis of postnatal proliferation and differentiation of the population of astroglial progenitors sitting in distinct cell layers, where they are supposed to mostly differentiate in the corresponding phenotypes. We found that both the rhythm of amplification and the final exit from the cell cycle vary among cerebellar layers, as revealed by proliferation and birthdating analyses performed in the vermis. Namely, WM astrocytes exited early from the cell cycle while proliferation in cortical layers was maintained for a longer time, especially in the PCL. These data well fit with the stoichiometry of triple and double vermian clones, that is therefore likely to be built upon these distinct rhythms of proliferation and differentiation. Of note, the conserved stoichiometry observed in both E12-derived families in the hemispheres and E14-tagged vermian clones make us confident that progenitors settled in the distinct layers follow the very same relative dynamics in both the cerebellar territories. We are anyway looking into this. On the other side, we can expect differences between the vermis and the hemispheres in the absolute amounts of proliferating cells in each layer at distinct time points, which can be in turn ascribed to the different amplification potentials of E12 and E14 lineages discussed above.

How are layer-specific dynamics regulated? Once the progenitors are specified toward a defined phenotype, their proliferation and differentiation may be controlled by an internal clock. Accordingly, a previous study in our laboratory revealed that PCL and PWM astrocytes rely on different types of cyclins D during their cell cycle transition (Parmigiani et al., 2015). Therefore, distinct molecular machineries could sustain different proliferative rhythms. Local cell-cell interactions could also contribute to distinct behaviors. Indeed, the PWM, GL and PCL are extremely different in terms of cell populations and can therefore provide a different array of signals. Consistently, co-culture studies independently showed that cerebellar neurons determine the morphology, antigenic profile and proliferation of

astrocytes (Hatten, 1985; Nagata et al., 1986). More recently, it has been pointed out the importance in vivo of PCs, not only in regulating BG specification (Eiraku et al., 2005), but also in influencing the acquisition of specific molecular traits (Farmer et al, 2016). The latter control is exerted through the release of Shh acting on BG, which is particularly enriched in Shh signaling components (Farmer et al., 2016). However, available data on the role of Shh in regulating the proliferation of BG progenitors are conflicting (Dahmane and Ruiz-i-Altaba, 1999; Wojcinski et al., 2017). Conversely, PC-derived Shh promotes the expansion of CD15-expressing astrocytes in the distant PWM (Fleming et al., 2013). Thus, the same factor might influence at various extent and with different outcomes astrocyte progenitors in different layers due to either different intrinsic cell sensibilities or to layer-dependent variations in this morphogen concentration, or both.

Other neuronal components (immature and mature granule neurons and interneurons) may also control the amplification and differentiation of neighboring astrocyte progenitors through unknown layer-specific soluble factors or cell-to-cell contact. It is interesting to note that GL and PCL astroglial progenitors display different behaviors despite the tight lineage relation unveiled by this study. Indeed, a role for environmental factors in the regulation of the properties of clonally-related mature astroglia was also proposed to explain the heterogenous response of some sibling astrocytes to cortical injury (Martín-López et al., 2013). Similarly, clonally-related PCL and GL astroglial progenitors might adopt distinct phenotypes and behaviors under the influence of extrinsic signals.

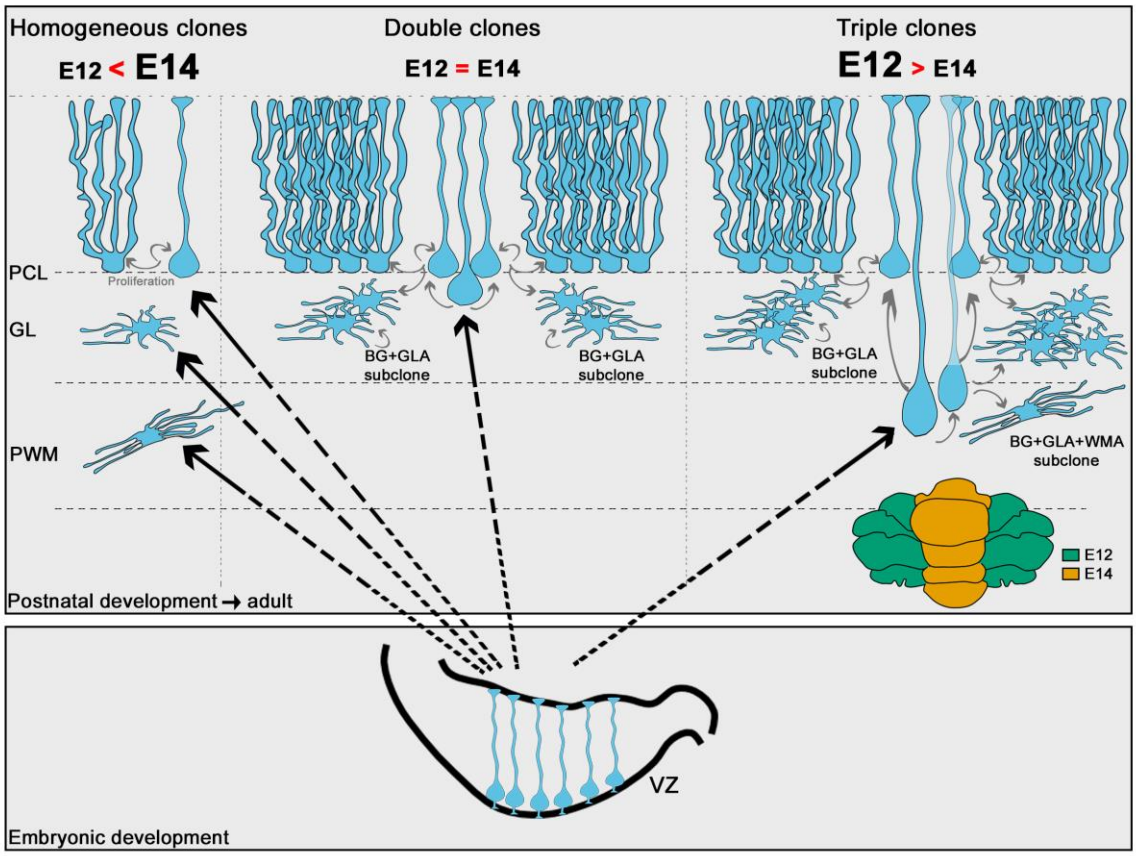

Figure 4.1. Schematic model for emergence of cerebellar astroglial lineages. Cerebellar astrogliogenesis occurs from RG that either generate HomCs for each major astrocyte phenotype - more frequent among vermian E14-P30 clones -, or HetCs. HetCs including double and triple clones are proposed to originate from intermediate basal progenitors derived from RG. Double clones are similarly produced by either E12 or E14 RG and appear composed on average of two subclones with the same modularity. In these subclones BG dominates over GLA, likely as the result of the amplification of ventricular progenitors translocated into the PCL. Triple clones, more frequent among E12-P30 lineages, include the three major astrocyte phenotypes and appear composed by three subclones belonging to distinct typologies, depending on the presence of WMA. Subclones can be formed by BG+GLA phenotypes, in which case they show modularity, and by BG+GLA+WMA phenotypes, in which case there is no apparent modularity, but a very diverse cell type composition.

4.6 Rules governing astrogliogenic RG fate decisions

As mentioned above, the unfolding of lineages during development may derive from stochastic fate choices within a homogeneous population of multipotent RG or, on the contrary, from distinct ventricular progenitors deterministically endowed with specific fates. Mathematical models have already been applied to address this ontogenic crossroad in studies on neurogenesis in distinct brain regions, implementing empirical data and

defining the rules governing cell fate decisions (Gomes et al., 2011; He et al., 2012; Gao et al., 2014). In a first attempt to solve this dilemma for astroglial lineages, here we similarly exploit a simple mathematical model that, starting from defined rules, assumes all RG as equivalent, uncommitted, precursors. Interestingly, this model suggests that the single multipotent progenitor hypothesis does not stand to explain our clonal outcomes. Indeed, although both the clone size distribution and the overall proportions of astrocyte subtypes were in good agreement with those of the empirically observed clones, this model failed to recapitulate the proportions of clone subtypes, producing generally too many heterogeneous clones containing WMA (i.e. triple, BG+WMA and GLA+WMA clones) at the expense of double clones and BG or GLA HomCs. It is important to note that this model was built as generation-dependent, with probabilities of producing the distinct astrocyte types depending on the generation in which they appear, as set according to birthdating data. Therefore, in the simulated lineages many WMA appeared, as expected, in the very first divisions, but they contributed mostly to HetCs rather than to WMA HomCs. This evidence suggests that, if solely multipotent progenitors existed in the cerebellar VZ, we would expect much more WMA-containing HetCs in our empirical clones, where, instead, WMA are mostly found in HomCs, therefore pointing to the existence of at least WMA fate-restricted progenitors. This possibility well fits with the progressive segregation of WMA and cortical lineages indicated in this study. Moreover, it is tempting to speculate that the WMA-related discrepancy specifically reflects the bipotent lineages that originate not only WMA but also interneurons (Silbereis et al., 2009; Fleming et al., 2013; Parmigiani et., 2015), and would be endowed with generation properties distinct from those of exclusively gliogenic families. Nevertheless, this issue is still far from being resolved. Moreover, one can argue that the observed differences between simulated and empirical lineages are also due to deterministic components acting during postnatal development, such as the above demonstrated bipotency of progenitors located in the PCL and/or layer-specific environmental stimuli influencing progenitors' fate choice as previously described for interneuron precursors (Leto et al., 2009). Indeed, the impossibility to implement the simple model here applied with space-dependent information, such as the distinct layer-specific proliferative dynamics described in this work, conceivably contributed to unprecise ratios of astrocyte subtypes within the triple clones simulated in our model, where the proliferation parameters were kept constant. To implement this information, a more

detailed knowledge on the length of the progenitors' cell cycle at subsequent developmental times together with the inspection of migratory behaviors in the cerebellar territory is needed. We plan to obtain these data in the future to test how the outcome of in silico simulation would vary upon incorporation of new datasets. Furthermore, deterministic mathematical models need to be employed to investigate and possibly confirm the suggested existence of one or more kinds of fate-restricted ventricular precursors.

4.7 Role of Sox2 in BG development

To understand astroglial development, a crucial issue is the identification of molecular players involved in the morphological and/or functional maturation of specific astrocyte subtypes. Here we addressed the role of Sox2, transcription factor previously shown to be required for the development and maintenance of RG in both the embryo and adult neurogenic niches (Pevny and Nicolis, 2010; Gómez-López et al., 2011). Sox2 conditional deletion either in the whole cerebellar territory starting from early embryonic stages or in postnatal astroglial cells resulted in a peculiar alteration of the typical radial morphology of BG leading to the acquisition of a multipolar-like shape, and in the improper formation of the BG layer along PC somata, with cells ectopically located in the ML. Neither the shape nor the density of the other astrocyte subtypes in both cerebellar WM and cortex were affected. On the other side, the abrogation of Sox2 in mature astrocytes at adult stages did not translate in similar phenotypic changes. These results show that Sox2 is a key intrinsic regulator of the correct development and maintenance of the BG phenotype during the first weeks of postnatal development. Indeed, in the absence of Sox2, BG progenitors appear to develop correctly and reach the PCL; nevertheless, a fraction of them fail to maintain their features during terminal differentiation at subsequent developmental stages and acquire an abnormal phenotype. On the contrary, when BG have completed their maturation, Sox2 is dispensable for the preservation of their correct morphology and layering. Interestingly, BG ectopia in the ML was not accompanied by a reduction in the density of BG correctly aligned to the PCL. This suggests that a proliferative response may happen to compensate for the lost cells. Moreover, the mutant phenotype appeared relatively mild in our study and did not seem to affect not only the production of other astroglial types but also, more broadly, RG functioning (not shown). This evidence suggests

that compensatory actions of other Sox family members take place. For instance, based on its well-established role in BG formation (Hoser et al., 2007) Sox4 could vicariate part of Sox2 functions.

BG morphogenesis requires a tight and timely regulated interaction with the surrounding cerebellar microenvironment. Signals and interactions with the basement membrane, PCs, and with the migratory and proliferative GCs are particularly crucial for the correct BG polarization, process outgrowth and positioning in the PCL. (see Buffo and Rossi, 2013 and Leto, Arancillo, Becker et al., 2015 for review). Notably, impairment of these regulatory mechanisms results in BG malpositioning and/or in the acquisition of a stellate morphology, which may thus represent a default differentiation pathway for cerebellar astroglial precursors.

Thus, the peculiar abnormal BG phenotype observed in our work may be indicative of incorrect interactions with these components of the cerebellar environment. In support of this hypothesis, a first and very preliminary analysis of RNAseq data of neurospheres derived from WT and Sox2-KO forebrain NSCs revealed a significant downregulation in KO cells of genes that may account for this process (Silvia Nicolis, Università Bicocca, Milano, personal communication). These genes, which show a 2- to 4-fold decrease in the mutant cells compared to controls, are APC2, DLL3 (a direct Sox2 target) and others coding for distinct integrin subunits. These targets are particularly interesting because other genes coding for proteins with structural and functional homologies have been demonstrated to govern BG morphogenesis and monolayer formation (Table 4.1). For instance, APC2 is an interactor of APC, with which it shares modulatory action on the WNT pathway. APC has been shown to promote BG fiber outgrowth and radial shape and regulate interactions with the basement membrane (Wang et al., 2011). Several integrins appear also downregulated in the absence of Sox2. Similar to integrin b1 e a6 (Frick et al., 2012; Marchetti et al., 2013), they could contribute to establish and maintain key positional signals needed for the proper positioning of BG. Moreover, among regulated genes, we also found DLL3, which is a Notch ligand and, similar to DLL1 (Hiraoka et al., 2013), could participate in the establishment of the Notch-dependent PCs juxtacrine signaling required for BG monolayer formation.

Importantly, the further investigation of long-range interactions between gene promoters and distal enhancers in the same NSC samples allowed to identify as Sox2 targets some

genes that, although not deregulated in mutant NSCs, have been previously involved either in BG morphogenesis (i.e. beta1 integrin, Erbb4, HUWE1, N-Myc, Notch1, RBPj, Jagged1) or in the early specification of BG progenitors (i.e. Sox4, Etv4, FGFR1, FGFR2 and FGFR3; see Table 4.2). These observations suggest that at least some of these pathways may be deregulated specifically in BG in the absence of Sox2.

Nevertheless, to clarify whether the expression of these or other genes is altered in the absence of Sox2 during BG development, the same kind of expression analyses need to be performed specifically in these cells. These analyses will allow to identify promising candidates to be subsequently studied by in situ hybridization and immunofluorescence in Sox2 mutant brains, and possibly for in vivo manipulation, in order to define the molecular mechanisms underlying the abnormal phenotype observed in the Sox2 mutant mice.

Deregulated gene	**Sox2 target**	**Change in Sox2 mutant NSCs**	**Reference gene with known implication in BG development**	**Implication in BG development of the reference gene**	**References**
APC2 (adenomatous polyposis coli protein 2)	NO	DOWN (about 2x, q 0.96)	**APC**	Maintenance of BG scaffold and radial morphology	Wang et al., 2011
DLL3 (Delta-like 3)	YES	DOWN (about 2x, q 0.95)	**DLL1 (Delta-like1)**	BG morphogenesis and monolayer formation	Hiraoka et al., 2013
Integrin beta-5	NO	DOWN (2x, q 0,98)	**Integrin beta-1** and **Integrin alpha-6**	Correct outgrowth of glial processes and monolayer formation	Frick et al., 2012
Integrin beta-7	NO	DOWN (4x, q 0,95)			
Integrin alpha-2	NO	DOWN (3x q 0,95)		Correct outgrowth of glial processes	Marchetti et al., 2013
Integrin alpha-7	NO	DOWN (2x 0,95)			

Table 4.1. Deregulated genes in Sox2 mutant NSCs and related reference genes with known implication in BG development. Q, false discovery rate corrected p value.

Gene	Known implication in BG development	Reference
Integrin beta-1	Correct outgrowth of glial processes and monolayer formation	Frick et al., 2012
Erbb4 (Erb-B2 Receptor Tyrosine Kinase 4)	Correct development of radial fibers	Rio et al., 1997; Perez-Garcia 2015
HUWE1 (HECT, UBA And WWE Domain Containing 1, E3 Ubiquitin Protein Ligase)	Outgrowth of glial processes and monolayer formation	D'Arca et al., 2010
N-Myc	Correct outgrowth of glial processes and monolayer formation	D'Arca et al., 2010
Notch1	Correct outgrowth of glial processes and attachment of endfeet to the pial surface	Kuang et al., 2012
RBPj (Recombining binding protein suppressor of hairless)	Correct outgrowth of glial processes and monolayer formation	Komine et al., 2007
Sox4	RG radial basal fiber formation, RG migration and transformation into BG.	Hoser et al., 2007
Etv4 **(Ets Variant Gene 4)**	BG induction from RG	Heng et al., 2017
FGFR1/2/3 **(Fibroblast growth factor receptor 1/2/3)**	BG induction from RG	Heng et al., 2017

Table 4.2 Sox2 target genes known to take part in BG differentiation

Conclusions

The experiments described in this PhD Thesis represent an unprecedented quantitative investigation on the ontogenesis of astroglial diversity. Indeed, by means of distinct *in vivo* approaches, astrogliogenesis was investigated in the cerebellum, where, as opposed to other brain regions, the major astrocyte subtypes have been fully characterized and can be easily distinguished from one another. The following conclusions can be drawn from this thesis:

Astrogliogenesis in the cerebellum occurs as early as E12 from RG capable of generating distinct kinds of homogeneous and heterogeneous clones, following a precise spatiotemporal pattern already established at birth and clearly linked to the organization of the cerebellar territory;

The cerebellar VZ is likely to be populated by distinct RG deterministically predestined to give rise to specific kinds of clones, rather than by a homogeneous population of multipotent RG that stochastically change their competence;

HetCs are the biggest and show a high level of cell clusterization. These families, at both the clone and cluster level, show a very recurrent and stereotyped modularity in their composition, thus revealing unprecedented rules governing astrogliogenesis;

Several key features of clones only emerge during postnatal development, when intermediate progenitors migrate to the secondary gliogenic niches and locally amplify, in parallel with the maximal growth of the cerebellar territory;

Progenitors located in the PCL with an immature BG phenotype (i.e. PCL progenitors) retain the capability of generating, during postnatal development, both type of cortical astrocytes (i.e. BG and GL astrocytes), but not fibrous astrocytes of the

WM. This reveals an unanticipated gliogenic capability of postnatal cerebellar progenitors.

Postnatally, astroglial progenitors amplify and differentiate in the distinct astrocyte subtypes according to layer-specific dynamics and to a precise time-schedule, that are likely to set up the stereotyped stoichiometry of HetCs.

Sox2 is a cell-autonomous regulator of the correct postnatal BG development and maintenance, but is dispensable when their maturation is fully accomplished.

Supplementary Material

Supplementary Table 1. $Sox2^{fl/fl}$/$Sox2^{fl/+}$ and Wnt1-Cre$Sox2^{fl/+}$ or $Glast^{CreERT2}Sox2^{fl/+}$ data pulled together as "control" animals.

Dataset	Time	Genotype	Mean ± SEM	N. of animals	Student T test
% of ectopic BG	P19	$Sox2^{fl/fl}$ or $Sox2^{fl/+}$	11.18 ± 1.2	2	n/a
		Wnt1-Cre$Sox2^{fl/+}$	6.22	1	
	8 months	$Sox2^{fl/fl}$ or $Sox2^{fl/+}$	5.179 ± 1.298	3	P=0.6445
		Wnt1-Cre$Sox2^{fl/+}$	6.081 ± 0.7485	2	
BG density in PCL (cells/mm^2)	P19	$Sox2^{fl/fl}$ or $Sox2^{fl/+}$	3832 ± 225.8	2	n/a
		Wnt1-Cre$Sox2^{fl/+}$	4085.58	1	
% of ectopic BG	P30	$Sox2^{fl/fl}$ or $Sox2^{fl/+}$	6.215 ± 0.4674	2	n/a
		$Glast^{CreERT2}Sox2^{fl/+}$	6.63	1	
	8 months	$Sox2^{fl/fl}$ or $Sox2^{fl/+}$	2.118 ± 0.6345	2	P=0.2992
		$Glast^{CreERT2}Sox2^{fl/+}$	4.207 ± 1.363	2	

Supplementary Table 2. List of Star Track clones and measured parameters

Animal n.	clone #	time of electroporation	time of analysis	clone type	clone subtype	M-L dispersion (µm)	clone size	n. of BG	n. of GLA	n. of WMA	n. of CNA	A-P dispersion
1	1	E12	P30	HetC	WMA+CNA	300	2			1	1	n.d.
1	2	E12	P30	HomC	WMA	50	1			1		n.d.
1	3	E12	P30	HomC	WMA	150	4			4		n.d.
1	4	E12	P30	HetC	GLA+WMA	400	4		2	2		n.d.
1	5	E12	P30	HomC	WMA	50	2			2		n.d.
1	6	E12	P30	HomC	WMA	50	1			1		n.d.
1	7	E12	P30	HetC	BG+GLA+WMA	150	8	1	6	1		n.d.
1	8	E12	P30	HetC	BG+WMA	650	3	1		2		n.d.
1	9	E12	P30	HomC	WMA	50	1			1		n.d.
1	10	E12	P30	HomC	WMA	50	1			1		n.d.
1	11	E12	P30	HetC	BG+GLA	1250	6	4	2			n.d.
1	12	E12	P30	HomC	WMA	50	1			1		n.d.
1	13	E12	P30	HomC	BG	50	2	2				n.d.
1	14	E12	P30	HetC	WMA+CNA	50	2			1	1	n.d.
1	15	E12	P30	HomC	WMA	50	2			2		n.d.
1	16	E12	P30	HomC	CNA	50	2				2	n.d.
1	17	E12	P30	HetC	WMA+CNA	200	3			1	2	n.d.
1	18	E12	P30	HomC	WMA	50	1			1		n.d.
1	19	E12	P30	HomC	WMA	50	2			2		n.d.
2	20	E12	P30	HetC	BG+GLA	1150	30	23	7			CrusI, Cp, VIb
2	21	E12	P30	HetC	BG+GLA+WMA	1600	40	16	14	10		Simplex, CrusI, CrusII, Pm, Cp, IX
2	22	E12	P30	HomC	CNA	50	1				1	Cerebellar Nuclei
2	23	E12	P30	HetC	BG+GLA	750	22	15	7			Pm
2	24	E12	P30	HetC	BG+GLA+WMA	950	17	8	6	3		Simplex, Cp
2	25	E12	P30	HetC	BG+GLA+WMA	350	12	7	1	4		Simplex, CrusII, Pm
2	26	E12	P30	HetC	BG+GLA+WMA	1350	14	6	5	3		Simplex, CrusII, Cp
2	27	E12	P30	HetC	GLA+WMA	300	5		3	2		CrusII, Cp

Supplementary Table 2. List of Star Track clones and measured parameters

Animal n.	clone #	time of electroporation	time of analysis	clone type	clone subtype	M-L dispersion (μm)	clone size	n. of BG	n. of GLA	n. of WMA	n. of CNA	A-P dispersion
2	28	E12	P30	HetC	BG+GLA	100	3	2	1			Pm
2	29	E12	P30	HomC	GLA	100	2		2			Cp
2	30	E12	P30	HetC	BG+GLA+WMA	1550	69	28	38	3		Cp, VIII/IX
2	31	E12	P30	HetC	BG+GLA+WMA	1150	33	11	15	7		Pm, Cp, VIII/IX
2	32	E12	P30	HomC	GLA	50	3		3			Cp
2	33	E12	P30	HomC	GLA	50	2		2			Pm
2	34	E12	P30	HetC	BG+GLA	150	7	3	4			Simplex
2	35	E12	P30	HomC	BG	50	2	2				Simplex
2	36	E12	P30	HetC	BG+GLA	900	11	8	3			CrusII
2	37	E12	P30	HetC	BG+GLA+WMA	1900	10	1	6	3		Simplex, Pm, Cp, VII
2	38	E12	P30	HomC	BG	50	1	1				CrusI
2	39	E12	P30	HomC	BG	50	1	1				Simplex
2	40	E12	P30	HetC	GLA+WMA	1200	11		5	6		CrusI, CrusII, Flocculus
2	41	E13	P31	HomC	WMA	50	1			1		Deep WM
2	42	E12	P30	HetC	BG+GLA	350	40	13	27			Pm, Cp, VIII
2	43	E12	P30	HomC	GLA	50	2		2			Cp
2	44	E12	P30	HomC	BG	50	2	2				Simplex
2	45	E12	P30	HomC	WMA	50	2			2		Cp
2	46	E12	P30	HetC	GLA+WMA	50	2		1	1		Pm
2	47	E12	P30	HetC	BG+GLA+WMA	1200	34	9	22	3		Simplex, CrusI, Pm, Cp
2	48	E12	P30	HomC	BG	200	6	6				Pm, Cp
2	49	E12	P30	HetC	BG+GLA+WMA+CNA	1850	31	6	21	2	2	CrusI, Pm, Cp, VIb, VIII/IX
2	50	E12	P30	HetC	BG+GLA+WMA+CNA	1650	44	23	10	10	1	CrusI, Flocculus
2	51	E12	P30	HomC	WMA	400	4			4		CrusI, Cp
2	52	E12	P30	HetC	BG+GLA+WMA	1000	40	20	16	4		CrusII, Pm, Cp
2	53	E12	P30	HomC	WMA	50	1			1		Deep WM
2	54	E12	P30	HetC	BG+GLA+WMA	100	14	7	6	1		Cp

Supplementary Table 2. List of Star Track clones and measured parameters

Animal n.	clone #	time of electroporation	time of analysis	clone type	clone subtype	M-L dispersion (μm)	clone size	n. of BG	n. of GLA	n. of WMA	n. of CNA	A-P dispersion
2	55	E12	P30	HetC	BG+GLA	500	9	2	7			Simplex
2	56	E12	P30	HetC	BG+GLA	50	4	2	2			Simplex
2	57	E12	P30	HomC	GLA	50	1		1			Flocculus
2	58	E12	P30	HetC	GLA+WMA	550	2		1	1		Simplex
2	59	E12	P30	HetC	BG+GLA	1550	43	37	6			Simplex
2	60	E12	P30	HomC	GLA	50	7		7			Simplex
2	61	E12	P30	HetC	BG+GLA	100	5	3	2			Simplex
2	62	E12	P30	HomC	GLA	50	2		2			Simplex
2	63	E12	P30	HetC	BG+GLA+WMA	1600	22	13	5	4		CrusI, Pm
2	64	E12	P30	HomC	GLA	50	1		1			CrusII
2	65	E12	P30	HomC	WMA	100	2			2		Pm, Cp
2	66	E12	P30	HetC	BG+GLA	1850	43	29	14			CrusI, CrusII, Pm, VII
2	67	E12	P30	HomC	BG	50	13	13				Cp
2	68	E12	P30	HetC	BG+WMA	200	3	2		1		CrusII, Pm
2	69	E12	P30	HomC	WMA	50	1			1		Cp
2	70	E12	P30	HetC	BG+GLA+WMA	950	14	4	5	5		Pm, Cp
2	71	E12	P30	HetC	BG+GLA+WMA	700	31	20	9	2		CrusI, Cp
2	72	E12	P30	HetC	BG+GLA+WMA	1250	60	20	30	10		CrusI, CrusII, Pm, Cp, VIb
2	73	E12	P30	HetC	BG+GLA+WMA	800	21	11	8	2		CrusI, Pm, Cp
2	74	E12	P30	HomC	WMA	50	1			1		Pm,
2	75	E12	P30	HetC	BG+GLA+WMA	700	50	38	10	2		Simplex, CrusI, CrusII
2	76	E12	P30	HetC	BG+GLA+WMA	900	18	11	4	3		CrusI, VIb
2	77	E12	P30	HomC	GLA	50	21		21			Cp
2	78	E12	P30	HomC	GLA	50	1		1			Flocculus
2	79	E12	P30	HomC	GLA	100	3		3			CrusI, Cp
2	80	E12	P30	HomC	WMA	150	2			2		CrusII, Pm
2	81	E12	P30	HomC	WMA	50	1			1		Simplex

Supplementary Table 2. List of Star Track clones and measured parameters

Animal n.	clone #	time of electroporation	time of analysis	clone type	clone subtype	M-L dispersion (μm)	clone size	n. of BG	n. of GLA	n. of WMA	n. of CNA	A-P dispersion
2	82	E12	P30	HetC	BG+GLA+WMA	300	18	11	6	1		Pm, Cp
2	83	E12	P30	HomC	GLA	100	2		2			CrusI
2	84	E12	P30	HomC	WMA	50	1			1		Cp
2	85	E12	P30	HomC	GLA	50	1		1			Flocculus
2	86	E12	P30	HomC	GLA	50	10		10			Simplex
2	87	E12	P30	HetC	BG+GLA	50	8	5	3			Simplex
2	88	E12	P30	HomC	BG	50	2	2				Cp
2	89	E12	P30	HomC	BG	50	1	1				Cp
2	90	E12	P30	HomC	WMA	50	2			2		Cp
2	91	E12	P30	HetC	BG+GLA+WMA	250	9	5	3	1		Pm, Cp
2	92	E12	P30	HetC	GLA+WMA	50	6		4	2		CrusI
2	93	E12	P30	HomC	WMA	50	1			1		Cp
2	94	E12	P30	HomC	GLA	50	1		1			Pm
2	95	E12	P30	HetC	BG+GLA+WMA	1000	8	1	6	1		CrusI, Flocculus
2	96	E12	P30	HetC	BG+GLA+WMA	1000	59	19	39	1		Cp, VIII/IX
2	97	E12	P30	HetC	BG+GLA	50	4	2	2			CrusII
2	98	E12	P30	HomC	GLA	50	1		1			Pm
2	99	E12	P30	HomC	WMA	50	3			3		Deep WM
2	100	E12	P30	HomC	WMA	50	1			1		CrusI
2	101	E12	P30	HomC	BG	50	1	1				Flocculus
2	102	E12	P30	HomC	GLA	50	1		1			Flocculus
2	103	E12	P30	HetC	GLA+WMA	400	6		3	3		Simplex
2	104	E12	P30	HomC	WMA	50	1			1		CrusI
2	105	E12	P30	HomC	WMA	50	1			1		Cp
2	106	E12	P30	HomC	GLA	50	1		1			Simplex
2	107	E12	P30	HetC	BG+GLA+WMA+CNA	1850	104	29	66	9		CrusI, CrusII, Flocculus
2	108	E12	P30	HetC	BG+GLA+WMA	1850	35	5	29	1		Simplex, CrusI, CrusII, Pm, Cp, Flocculus

Supplementary Table 2. List of Star Track clones and measured parameters

Animal n.	clone #	time of electroporation	time of analysis	clone type	clone subtype	M-L dispersion (μm)	clone size	n. of BG	n. of GLA	n. of WMA	n. of CNA	A-P dispersion
2	109	E12	P30	HetC	BG+GLA+WMA	1150	23	7	15	1		Simplex, CrusI, Cp, VIII/IX
2	110	E12	P30	HomC	GLA	50	2		2			CrusI
2	111	E12	P30	HetC	BG+GLA+WMA	1750	48	14	32	2		CrusI, CrusII, Pm, Cp, VIb, VIII/IX
2	112	E12	P30	HetC	BG+GLA+WMA	1900	131	83	42	6		Simplex, CrusI, Pm, Cp, Flocculus
2	113	E12	P30	HomC	GLA	50	1		1			CrusI
2	114	E12	P30	HetC	BG+WMA	50	2	1		1		Cp
2	115	E12	P30	HomC	GLA	50	2		2			Cp
2	116	E12	P30	HetC	BG+GLA	1150	58	42	16			CrusI, Pm, Cp
2	117	E12	P30	HetC	BG+GLA+WMA	350	6	1	4	1		Flocculus
2	118	E12	P30	HomC	GLA	450	8		8			Cp
2	119	E12	P30	HetC	BG+GLA	100	46	36	10			CrusII
2	120	E12	P30	HetC	BG+GLA+WMA	400	70	35	34	1		Flocculus
2	121	E12	P30	HomC	WMA	50	1			1		Cp
2	122	E12	P30	HomC	WMA	50	3			3		Cp
2	123	E12	P30	HomC	GLA	50	1		1			Cp
2	124	E12	P30	HomC	GLA	50	1		1			Pm
2	125	E12	P30	HetC	BG+GLA	1500	101	49	52			Cp, VIII
2	126	E12	P30	HomC	WMA	50	1			1		Cp
2	127	E12	P30	HetC	BG+GLA	50	6	4	2			Pm
2	128	E12	P30	HomC	BG	50	1	1				Pm
2	129	E12	P30	HetC	GLA+WMA	1100	11		7	4		Pm, Flocculus
2	130	E12	P30	HomC	WMA	250	2			2		Cp
2	131	E12	P30	HomC	WMA	200	2			2		CrusII, Cp
2	132	E12	P30	HomC	BG	50	1	1				Pm
2	133	E12	P30	HomC	WMA	50	1			1		Cp
2	134	E12	P30	HetC	BG+GLA+WMA	350	4	2	1	1		CrusII, Cp
2	135	E12	P30	HetC	BG+GLA	350	11	7	4			CrusI, VIb

Supplementary Table 2. List of Star Track clones and measured parameters

Animal n.	clone #	time of electroporation	time of analysis	clone type	clone subtype	M-L dispersion (μm)	clone size	n. of BG	n. of GLA	n. of WMA	n. of CNA	A-P dispersion
2	136	E12	P30	HetC	BG+GLA+WMA	1050	31	12	16	3		Pm, Cp, VIII/IX
2	137	E12	P30	HomC	GLA	50	2		2			Flocculus
2	138	E12	P30	HomC	GLA	50	1		1			Pm, CrusI
2	139	E12	P30	HetC	GLA+WMA	300	4		2	2		Cp
2	140	E12	P30	HomC	BG	50	1	1				CrusI
2	141	E12	P30	HetC	BG+GLA+WMA	1700	107	53	47	7		Simplex, Pm, Cp, Flocculus
2	142	E12	P30	HetC	BG+GLA	350	5	3	2			Cp, VIII
2	143	E12	P30	HetC	BG+GLA+WMA	550	20	5	13	2		CrusII, Cp, VIII/IX
2	144	E12	P30	HomC	GLA	550	2		2			CrusI
2	145	E12	P30	HomC	GLA	100	2		2			Cp
2	146	E12	P30	HomC	GLA	50	2		2			Flocculus
2	147	E12	P30	HomC	GLA	50	2		2			Cp
2	148	E12	P30	HomC	WMA	100	2			2		Pm, Cp
2	149	E12	P30	HomC	GLA	50	1		1			CrusI
2	150	E12	P30	HomC	GLA	50	1		1			Flocculus
2	151	E12	P30	HetC	BG+GLA+WMA	250	61	40	19	2		Pm, Cp
2	152	E12	P30	HetC	BG+GLA	150	12	7	5			Simplex, V/VIa
2	153	E12	P30	HetC	BG+GLA	150	8	6	2			CrusII
2	154	E12	P30	HetC	BG+GLA+WMA	900	10	4	5	1		CrusI, CrusII, Cp
2	155	E12	P30	HomC	GLA	50	1		1			Flocculus
2	156	E12	P30	HetC	BG+GLA	150	18	16	2			Cp
2	157	E12	P30	HetC	BG+GLA	600	3	1	2			CrusI, VIII
2	158	E12	P30	HomC	GLA	50	1		1			Flocculus
2	159	E12	P30	HetC	BG+GLA+WMA	500	23	12	9	2		Simplex
2	160	E12	P30	HomC	GLA	350	6		6			CrusII
2	161	E12	P30	HetC	BG+GLA+WMA	1450	67	38	23	6		Simplex
2	162	E12	P30	HomC	WMA	50	1			1		Cp, Deep WM

Supplementary Table 2. List of Star Track clones and measured parameters

Animal n.	clone #	time of electroporation	time of analysis	clone type	clone subtype	M-L dispersion (μm)	clone size	n. of BG	n. of GLA	n. of WMA	n. of CNA	A-P dispersion
2	163	E12	P30	HomC	GLA	50	1		1			Flocculus
2	164	E12	P30	HetC	BG+GLA	100	4	3	1			Cp
2	165	E12	P30	HetC	BG+GLA+WMA	1300	120	76	42	2		Simplex, CrusI, Pm, Cp
2	166	E12	P30	HomC	GLA	50	2		2			Simplex
2	167	E12	P30	HomC	GLA	50	1		1			Flocculus
2	168	E12	P30	HetC	BG+GLA+WMA	300	36	19	13	4		Cp
2	169	E12	P30	HomC	WMA	50	1			1		Cp
2	170	E12	P30	HetC	BG+GLA	50	5	2	3			CrusII
2	171	E12	P30	HomC	BG	50	2	2				Simplex
2	172	E12	P30	HomC	WMA	50	1			1		CrusII
2	173	E12	P30	HomC	BG	50	2	2				CrusI
2	174	E12	P30	HetC	BG+GLA	50	3	2	1			IX
3	175	E12	P30	HomC	WMA	50	1			1		II
3	176	E12	P30	HetC	WMA+CNA	350	8			5	3	VIII/IX, Cerebellar Nuclei
3	177	E12	P30	HomC	WMA	50	2			2		CrusII
3	178	E12	P30	HomC	WMA	50	1			1		III
3	179	E12	P30	HomC	GLA	50	1		1			VIII/IX
3	180	E12	P30	HetC	BG+GLA	150	5	1	4			Cp
3	181	E12	P30	HomC	WMA	50	1			1		VIII/IX
3	182	E12	P30	HomC	WMA	100	4			4		CrusII
3	183	E12	P30	HetC	BG+GLA	100	20	9	11			Pm
3	184	E12	P30	HomC	WMA	100	1			1		Deep WM
3	185	E12	P30	HomC	GLA	50	5		5			Pm
3	186	E12	P30	HomC	GLA	50	2		2			VIII/IX
3	187	E12	P30	HomC	CNA	50	1				1	Cerebellar Nuclei
3	188	E12	P30	HomC	CNA	50	5				5	Cerebellar Nuclei
3	189	E12	P30	HomC	WMA	150	7			7		CrusI, CrusII

Supplementary Table 2. List of Star Track clones and measured parameters

Animal n.	clone #	time of electroporation	time of analysis	clone type	clone subtype	M-L dispersion (μm)	clone size	n. of BG	n. of GLA	n. of WMA	n. of CNA	A-P dispersion
3	190	E12	P30	HomC	WMA	50	1			1		Cp
3	191	E12	P30	HomC	WMA	50	1			1		Deep WM
3	192	E12	P30	HetC	WMA+CNA	450	3			1	2	Cp, Cerebellar Nuclei
3	193	E12	P30	HomC	GLA	100	2		2			Cp, VIII/IX
3	194	E12	P30	HomC	BG	50	5	5				Simplex
3	195	E12	P30	HomC	WMA	50	2			2		CrusI
3	196	E12	P30	HomC	GLA	50	1		1			CrusII
3	197	E12	P30	HomC	BG	50	2	2				Pm
3	198	E12	P30	HomC	GLA	50	1		1			CrusII
3	199	E12	P30	HomC	WMA	50	1			1		IV/V
3	200	E12	P30	HetC	BG+GLA+WMA	350	19	10	5	4		Pm
3	201	E12	P30	HetC	BG+GLA+WMA	700	14	10	3	1		CrusII, Pm
3	202	E12	P30	HomC	BG	50	5	5				CrusII
3	203	E12	P30	HomC	BG	150	7	7				VIII/IX
3	204	E12	P30	HomC	BG	50	1	1				VIII/IX
3	205	E12	P30	HomC	WMA	50	1			1		IV/V
3	206	E12	P30	HetC	BG+GLA+WMA	100	4	1	2	1		III
3	207	E12	P30	HomC	WMA	50	1			1		IV/V
3	208	E12	P30	HomC	BG	50	3	3				VIII/IX
3	209	E12	P30	HomC	BG	50	5	5				VIII/IX
3	210	E12	P30	HetC	BG+GLA+WMA	400	44	24	15	5		CrusI, CrusII
3	211	E12	P30	HomC	WMA	50	2			2		Pm
3	212	E12	P30	HomC	WMA	50	1			1		2
3	213	E12	P30	HomC	WMA	50	1			1		Deep WM
3	214	E12	P30	HetC	BG+GLA+WMA	150	15	8	5	2		Flocculus, Deep WM
3	215	E12	P30	HetC	BG+GLA	1150	5	2	3			Pm, VIII/IX
3	216	E12	P30	HetC	BG+GLA	300	61	36	25			Simplex, Pm

Supplementary Table 2. List of Star Track clones and measured parameters

Animal n.	clone #	time of electroporation	time of analysis	clone type	clone subtype	M-L dispersion (μm)	clone size	n. of BG	n. of GLA	n. of WMA	n. of CNA	A-P dispersion
3	217	E12	P30	HomC	BG	50	2	2				Cp
3	218	E12	P30	HetC	BG+GLA+WMA+CNA	1450	91	32	12	29	18	CrusI, CrusII, Deep WM
3	219	E12	P30	HetC	BG+GLA	200	11	5	6			VIII/IX
3	220	E12	P30	HomC	WMA	100	5			5		Deep WM
3	221	E12	P30	HomC	CNA	50	2				2	Cerebellar Nuclei
3	222	E12	P30	HetC	BG+GLA+WMA	1050	54	36	16	2		Simplex, Pm, VIII
3	223	E12	P30	HetC	BG+GLA+WMA+CNA	2450	69	17	5	40	7	CrusI, CrusII, Pm, Deep WM, Cerebellar Nuclei
3	224	E12	P30	HomC	WMA	50	1			1		Deep WM
3	225	E12	P30	HetC	BG+GLA	250	5	1	4			VIII/IX
3	226	E12	P30	HetC	BG+GLA	50	5	4	1			Cp
3	227	E12	P30	HetC	BG+GLA	200	17	13	4			IV/V
3	228	E12	P30	HomC	WMA	50	1			1		CrusII
3	229	E12	P30	HetC	BG+GLA+WMA	1450	43	14	19	10		Cp, VIII, Deep WM
3	230	E12	P30	HomC	GLA	50	1		1			VIII/IX
3	231	E12	P30	HetC	BG+GLA	50	7	6	1			Cp
3	232	E12	P30	HetC	BG+GLA	700	20	16	4			Cp, VIII/IX
3	233	E12	P30	HomC	CNA	50	1				1	Cerebellar Nuclei
3	234	E12	P30	HomC	GLA	50	1		1			VIc/VII
3	235	E12	P30	HomC	BG	50	2	2				VII
3	236	E12	P30	HomC	WMA	50	1			1		Deep WM
3	237	E12	P30	HomC	WMA	100	3			3		Deep WM
3	238	E12	P30	HomC	WMA	50	2			2		Deep WM
3	239	E12	P30	HetC	BG+GLA	50	6	3	3			Cp
3	240	E12	P30	HomC	WMA	100	2			2		VIII/IX
3	241	E12	P30	HomC	WMA	50	1			1		Cp
3	242	E12	P30	HetC	BG+GLA+WMA	100	5	2	2	1		Cp
3	243	E12	P30	HomC	GLA	100	7		7			VIa

Supplementary Table 2. List of Star Track clones and measured parameters

Animal n.	clone #	time of electroporation	time of analysis	clone type	clone subtype	M-L dispersion (μm)	clone size	n. of BG	n. of GLA	n. of WMA	n. of CNA	A-P dispersion
3	244	E12	P30	HetC	BG+GLA+WMA+CNA	1400	47	4	13	29	1	CrusI, VIII/IX, Deep WM, Cerebellar Nuclei
3	245	E12	P30	HomC	WMA	50	1			1		VIII/IX
3	246	E12	P30	HomC	WMA	50	1			1		Pm
3	247	E12	P30	HetC	GLA+CNA	350	5		3		2	Pm, Cerebellar Nuclei
3	248	E12	P30	HetC	BG+GLA	50	2	1	1			VIII/IX
3	249	E12	P30	HetC	BG+GLA+WMA	800	134	77	50	7		Simplex, CrusI, CrusII, Cp, VIa, VII
3	250	E12	P30	HetC	WMA+CNA	300	4			3	1	Deep WM, Cerebellar Nuclei
3	251	E12	P30	HetC	BG+GLA	100	8	4	4			Cp
3	252	E12	P30	HomC	BG	50	2	2				Cp
3	253	E12	P30	HomC	GLA	50	1		1			Cp
3	254	E12	P30	HomC	BG	50	1	1				VIII/IX
3	255	E12	P30	HomC	WMA	150	2			2		Deep WM
3	256	E12	P30	HetC	WMA+CNA	400	4			3	1	Deep WM, Cerebellar Nuclei
3	257	E12	P30	HomC	CNA	50	2				2	Cerebellar Nuclei
3	258	E12	P30	HetC	BG+GLA	400	9	4	5			Cp, VIII/IX
3	259	E12	P30	HomC	WMA	50	1			1		CrusI
3	260	E12	P30	HomC	WMA	50	1			1		Cp
3	261	E12	P30	HomC	CNA	50	2				2	Cerebellar Nuclei
3	262	E12	P30	HetC	BG+GLA+WMA	800	69	46	21	2		Pm, Cp
3	263	E12	P30	HetC	BG+GLA	150	2	1	1			Pm,
3	264	E12	P30	HomC	GLA	50	1		1			VIII/IX
3	265	E12	P30	HomC	GLA	50	1		1			VIc, VII
3	266	E12	P30	HomC	CNA	50	1				1	Cerebellar Nuclei
3	267	E12	P30	HomC	CNA	50	1				1	Cerebellar Nuclei
3	268	E12	P30	HomC	BG	750	3	3				Pm, VIa
3	269	E12	P30	HomC	BG	50	1	1				CrusI
3	270	E12	P30	HetC	BG+GLA	100	9	8	1			xx

Supplementary Table 2. List of Star Track clones and measured parameters

Animal n.	clone #	time of electroporation	time of analysis	clone type	clone subtype	M-L dispersion (μm)	clone size	n. of BG	n. of GLA	n. of WMA	n. of CNA	A-P dispersion
3	271	E12	P30	HomC	BG	50	3	3				Cp
3	272	E12	P30	HomC	WMA	50	2			2		Deep WM
3	273	E12	P30	HomC	WMA	50	2			2		Deep WM
3	274	E12	P30	HetC	BG+GLA+WMA+CNA	950	37	13	12	8	4	CrusII, Cp, Cerebellar Nuclei
3	275	E12	P30	HetC	BG+GLA+WMA	1050	34	18	11	5		CrusI, Cp, VIII
3	276	E12	P30	HomC	GLA	50	1		1			VIII/IX
3	277	E12	P30	HetC	BG+GLA+WMA	1800	67	43	11	13		CrusI, Cp, VIII
3	278	E12	P30	HomC	WMA	50	1			1		VIII/IX
3	279	E12	P30	HomC	WMA	50	2			2		CrusI
3	280	E12	P30	HomC	WMA	50	1			1		Deep WM
3	281	E12	P30	HomC	WMA	150	4			4		VIII/IX
3	282	E12	P30	HomC	GLA	50	2		2			CrusI
3	283	E12	P30	HetC	BG+GLA	100	3	2	1			Cp
3	284	E12	P30	HomC	WMA	50	1			1		VIII/IX
1	1	E14	P30	HomC	GLA	50	1		1			IX
1	2	E14	P30	HetC	BG+GLA	50	10	3	7			X, IX
1	3	E14	P30	HetC	BG+GLA+WMA	100	7	4	2	1		IX, X
1	4	E14	P30	HomC	GLA	50	1		1			X
1	5	E14	P30	HomC	GLA	50	2		2			IX
1	6	E14	P30	HomC	WMA	50	1			1		X
1	7	E14	P30	HomC	GLA	100	5		5			IX, X
1	8	E14	P30	HomC	GLA	50	2		2			X
1	9	E14	P30	HomC	WMA	150	3			3		X, VIII
1	10	E14	P30	HomC	GLA	50	4		4			II, III
1	11	E14	P30	HomC	GLA	50	2		2			IX
1	12	E14	P30	HomC	GLA	50	1		1			IX
1	13	E14	P30	HomC	WMA	50	1			1		X

Supplementary Table 2. List of Star Track clones and measured parameters

Animal n.	clone #	time of electroporation	time of analysis	clone type	clone subtype	M-L dispersion (μm)	clone size	n. of BG	n. of GLA	n. of WMA	n. of CNA	A-P dispersion
1	14	E14	P30	HomC	WMA	50	2			2		Deep WM
1	15	E14	P30	HomC	GLA	50	1		1			X
1	16	E14	P30	HomC	WMA	50	2			2		IX
1	17	E14	P30	HomC	GLA	200	5		5			IX, X
1	18	E14	P30	HetC	GLA+WMA	50	12		10	2		II a VI
1	19	E14	P30	HetC	BG+GLA	50	3	2	1			IX
1	20	E14	P30	HomC	GLA	50	1		1			VIII
1	21	E14	P30	HomC	GLA	50	1		1			IX
1	22	E14	P30	HetC	BG+WMA	50	2	1		1		X
2	23	E14	P30	HomC	WMA	50	1			1		IX
2	24	E14	P30	HetC	BG+GLA	50	5	4	1			X
2	25	E14	P30	HetC	BG+GLA	50	6	n.d.	n.d.			X
2	26	E14	P30	HomC	GLA	50	3		3			X
2	27	E14	P30	HetC	GLA+WMA	50	3		n.d.	n.d.		X
2	28	E14	P30	HomC	WMA	50	1			1		X
2	29	E14	P30	HomC	GLA	50	1		1			X
2	30	E14	P30	HomC	GLA	50	4		4			X
3	31	E14	P30	HetC	BG+GLA+WMA	350	12	8	3	1		I/II, III
3	32	E14	P30	HetC	BG+GLA+WMA	400	25	7	12	6		I/II, IV/V
3	33	E14	P30	HetC	GLA+WMA	100	26		11	15		I/II
3	34	E14	P30	HetC	BG+GLA	450	16	10	6			IV/V, I/II
3	35	E14	P30	HomC	WMA	50	1			1		III
3	36	E14	P30	HetC	BG+GLA	50	6	5	1			III
3	37	E14	P30	HomC	BG	50	3	3				I/II
3	38	E14	P30	HetC	BG+GLA	450	74	31	43			I/II
3	39	E14	P30	HomC	WMA	50	1			1		IV/V
3	40	E14	P30	HomC	WMA	100	3			3		Deep WM

Supplementary Table 2. List of Star Track clones and measured parameters

Animal n.	clone #	time of electroporation	time of analysis	clone type	clone subtype	M-L dispersion (μm)	clone size	n. of BG	n. of GLA	n. of WMA	n. of CNA	A-P dispersion
3	41	E14	P30	HomC	WMA	100	2			2		Deep WM
3	42	E14	P30	HomC	WMA	50	3			3		Deep WM
3	43	E14	P30	HetC	BG+GLA	50	4	3	1			I/II
3	44	E14	P30	HetC	BG+GLA+WMA	350	91	12	60	19		I/II
3	45	E14	P30	HomC	WMA	50	1		1			III
3	46	E14	P30	HomC	WMA	50	1		1			III
3	47	E14	P30	HetC	BG+GLA	50	13	9	4			I/II
3	48	E14	P30	HetC	BG+GLA	450	16	9	7			IV/V, III
3	49	E14	P30	HomC	WMA	50	3			3		I/II Deep WM
3	50	E14	P30	HetC	BG+GLA	50	5	2	3			I/II
3	51	E14	P30	HomC	WMA	50	1			1		Deep WM
3	52	E14	P30	HomC	WMA	50	1			1		Deep WM
3	53	E14	P30	HetC	BG+GLA+WMA	200	16	8	7	1		I/II
3	54	E14	P30	HomC	WMA	50	1			1		Deep WM
3	55	E14	P30	HomC	BG	50	4	4				I/II
3	56	E14	P30	HetC	BG+GLA	50	13	7	6			I/II
3	57	E14	P30	HetC	BG+GLA	200	26	8	18			I/II
3	58	E14	P30	HomC	WMA	50	3			3		I/II Deep WM
3	59	E14	P30	HetC	BG+GLA	100	14	11	3			I/II
3	60	E14	P30	HetC	BG+GLA+WMA	350	40	11	25	4		I/II
3	61	E14	P30	HomC	WMA	50	1			1		Deep WM
4	62	E14	P30	HetC	BG+GLA+WMA	100	7	4	1	2		VI
4	63	E14	P30	HomC	WMA	50	1			1		Deep WM
4	64	E14	P30	HomC	WMA	50	1			1		Deep WM
4	65	E14	P30	HomC	WMA	100	4			4		VI
4	66	E14	P30	HomC	WMA	50	1			1		Deep WM
4	67	E14	P30	HomC	WMA	50	1			1		Deep WM

Supplementary Table 2. List of Star Track clones and measured parameters

Animal n.	clone #	time of electroporation	time of analysis	clone type	clone subtype	M-L dispersion (μm)	clone size	n. of BG	n. of GLA	n. of WMA	n. of CNA	A-P dispersion
4	68	E14	P30	HomC	WMA	50	1			1		Deep WM
4	69	E14	P30	HomC	CNA	50	1				1	Cerebellar Nuclei
4	70	E14	P30	HomC	WMA + CNA	900	2			1	1	Deep WM, Cerebellar Nuclei
4	71	E14	P30	HomC	WMA	50	2			2		Deep WM
4	72	E14	P30	HomC	WMA	50	4			4		Deep WM
4	73	E14	P30	HomC	WMA	50	2			2		Deep WM
4	74	E14	P30	HomC	WMA	50	1			1		Deep WM
4	75	E14	P30	HomC	WMA	50	1			1		Deep WM
4	76	E14	P30	HomC	GLA	50	1		1			X
4	77	E14	P30	HomC	WMA	100	2			2		Deep WM
4	78	E14	P30	HomC	WMA	50	2			2		Deep WM
4	79	E14	P30	HomC	BG	50	1	1				V
4	80	E14	P30	HomC	WMA	50	1			1		Deep WM
4	81	E14	P30	HomC	WMA	50	2			2		Deep WM
4	82	E14	P30	HomC	WMA	50	2			2		Deep WM
4	83	E14	P30	HomC	WMA	100	2			2		Deep WM
4	84	E14	P30	HomC	WMA	50	1			1		Deep WM
4	85	E14	P30	HomC	WMA	50	1			1		VI
4	86	E14	P30	HomC	WMA	100	4			4		Deep WM
4	87	E14	P30	HomC	WMA	50	1			1		Deep WM
4	88	E14	P30	HomC	CNA	250	3				3	Cerebellar Nuclei
4	89	E14	P30	HetC	BG+GLA+WMA	150	18	2	10	6		IV/V
4	90	E14	P30	HomC	WMA	50	1			1		Deep WM
4	91	E14	P30	HomC	CNA	50	1				1	Cerebellar Nuclei
4	92	E14	P30	HomC	WMA	50	2			2		Deep WM
4	93	E14	P30	HomC	WMA	50	1			1		Deep WM
4	94	E14	P30	HomC	WMA	50	3			3		Deep WM

Supplementary Table 2. List of Star Track clones and measured parameters

Animal n.	clone #	time of electroporation	time of analysis	clone type	clone subtype	M-L dispersion (µm)	clone size	n. of BG	n. of GLA	n. of WMA	n. of CNA	A-P dispersion
4	95	E14	P30	HomC	WMA	50	1			1		Deep WM
4	96	E14	P30	HomC	CNA	50	1				1	Cerebellar Nuclei
4	97	E14	P30	HetC	BG+WMA	600	2	1		1		Deep WM + VIII
4	98	E14	P30	HomC	WMA	50	1			1		Deep WM
4	99	E14	P30	HomC	WMA	50	1			1		Deep WM
4	100	E14	P30	HomC	WMA	400	4			4		Deep WM
4	101	E14	P30	HomC	WMA	50	1			1		Deep WM
4	102	E14	P30	HomC	WMA	50	2			2		Deep WM

Animal n.	clone n.	time of electroporation	time of analysis	clone type	clone subtype	M-L dispersion (µm)	clone size	n. of PCLp	n. of GLAp	n. of PWM	n. of VC	A-P dispersion
1	1	E12	P0	HomC	PCLp	400	4	4				middle-post
1	2	E12	P0	HomC	PCLp	50	8	8				middle
1	3	E12	P0	HomC	PCLp	50	3	3				ant-post
1	4	E12	P0	HomC	PCLp	200	9	9				middle-post
1	5	E12	P0	HomC	PCLp	50	6	6				ant
1	6	E12	P0	HomC	PCLp	50	2	2				ant
1	7	E12	P0	HomC	PCLp	50	2	2				ant
1	8	E12	P0	HomC	PWM	200	4			4		pwm
1	9	E12	P0	HomC	PCLp	100	8	8				middle
1	10	E12	P0	HomC	PCLp	50	3	3				ant
1	11	E12	P0	HomC	PCLp	50	4	4				ant

Supplementary Table 2. List of Star Track clones and measured parameters

Animal n.	clone n.	time of electroporation	time of analysis	clone type	clone subtype	M-L dispersion (μm)	clone size	n. of PCLp	n. of GLAp	n. of PWM	n. of VC	A-P dispersion
1	12	E12	P0	HomC	PCLp	50	2	2				ant
1	13	E12	P0	HomC	PWM	50	4			4		pwm
1	14	E12	P0	HomC	PWM	50	4			4		pwm
1	15	E12	P0	HomC	PCLp	50	3	3				ant
1	16	E12	P0	HetC	PCLp+GLAp	50	2	1	1			post
1	17	E12	P0	HomC	GLAp	50	1		1			post
1	18	E12	P0	HomC	PWM	50	1			1		pwm
1	19	E12	P0	HomC	PWM	50	1			1		pwm
1	20	E12	P0	HomC	PCLp	50	3	3				post
1	21	E12	P0	HomC	PCLp	50	1	1				post
1	22	E12	P0	HomC	PWM	50	1			1		pwm
1	23	E12	P0	HomC	PCLp	100	2	2				post
1	24	E12	P0	HomC	GLAp	50	1		1			post
1	25	E12	P0	HomC	PCLp	50	2	2				post
1	26	E12	P0	HomC	PCLp	50	3	3				post
1	27	E12	P0	HomC	PCLp	50	3	3				post
2	28	E12	P0	HomC	PWM	50	8			8		pwm
2	29	E12	P0	HomC	PWM	50	7			7		ant
2	30	E12	P0	HomC	VC	50	2				2	
2	31	E12	P0	HetC	PCLp+GLAp+PWM	300	8	5	1	2		post
2	32	E12	P0	HomC	PWM	50	2			2		pwm
2	33	E12	P0	HomC	VC	50	1				1	
2	34	E12	P0	HomC	PWM	50	1			1		pwm
2	35	E12	P0	HetC	GLAp+PWM	600	3		2	1		post
2	36	E12	P0	HomC	PWM	50	1			1		pwm
2	37	E12	P0	HetC	GLAp+PWM	50	5		3	2		post

Supplementary Table 2. List of Star Track clones and measured parameters

Animal n.	clone n.	time of electroporation	time of analysis	clone type	clone subtype	M-L dispersion (µm)	clone size	n. of PCLp	n. of GLAp	n. of PWM	n. of VC	A-P dispersion
2	38	E12	P0	HomC	PWM	50	5			5		pwm
2	39	E12	P0	HetC	PCLp+GLAp+PWM	50	17	5	4	8		middle
2	40	E12	P0	HomC	PWM	50	1			1		pwm
2	41	E12	P0	HomC	PWM	50	1			1		pwm
2	42	E12	P0	HomC	PWM	50	2			2		middle
2	43	E12	P0	HomC	PWM	50	7			7		pwm
2	44	E12	P0	HomC	PWM	50	2			2		pwm
2	45	E12	P0	HomC	PCLp	50	2	2				post
2	46	E12	P0	HomC	PCLp	50	4	4				post
2	47	E12	P0	HomC	PWM	200	14			14		middle
3	48	E12	P0	HetC	PCLp + PWM	50	11	1		10		post
3	49	E12	P0	HomC	PCLp	50	2	2				ant
3	50	E12	P0	HomC	PWM	50	6			6		pwm
3	51	E12	P0	HomC	PCLp	50	2	2				ant
3	52	E12	P0	HomC	PCLp	50	9	9				ant
3	53	E12	P0	HomC	PWM	50	2			2		pwm
3	54	E12	P0	HomC	PWM	50	6			6		pwm
3	55	E12	P0	HomC	PWM	50	2			2		pwm
3	56	E12	P0	HomC	PWM	50	3			3		pwm
3	57	E12	P0	HomC	PWM	50	1			1		pwm
3	58	E12	P0	HomC	PWM	50	3			3		pwm
3	59	E12	P0	HomC	PWM	50	1			1		pwm
3	60	E12	P0	HomC	PWM	50	3			3		pwm
3	61	E12	P0	HomC	PWM	50	1			1		pwm
3	62	E12	P0	HomC	PWM	50	2			2		pwm
3	63	E12	P0	HomC	PWM	50	1			1		pwm

Supplementary Table 2. List of Star Track clones and measured parameters

Animal n.	clone n.	time of electroporation	time of analysis	clone type	clone subtype	M-L dispersion (µm)	clone size	n. of PCLp	n. of GLAp	n. of PWM	n. of VC	A-P dispersion
1	1	E14	P0	HomC	PWM	50	3			3		pwm
1	2	E14	P0	HomC	PCLp	50	3	3				ant
1	3	E14	P0	HomC	PCLp	50	4	4				ant
1	4	E14	P0	HetC	PCLp+PWM	50	4	3		1		ant+pwm
1	5	E14	P0	HomC	PWM	50	2			2		pwm
1	6	E14	P0	HomC	PWM	50	3			3		pwm
1	7	E14	P0	HomC	PWM	50	6			6		pwm
1	8	E14	P0	HomC	PWM	50	1			1		pwm
1	9	E14	P0	HomC	PWM	50	3			3		pwm
1	10	E14	P0	HomC	PWM	50	3			3		pwm
1	11	E14	P0	HetC	PCLp+GLAp	50	2	1	1			ant
1	12	E14	P0	HomC	PWM	50	6			6		pwm
1	13	E14	P0	HomC	PCLp	50	5	5				ant
1	14	E14	P0	HomC	PCLp	50	1	1				ant
1	15	E14	P0	HomC	PCLp	50	1	1				ant
1	16	E14	P0	HomC	PWM	50	3			3		pwm
1	17	E14	P0	HomC	PWM	50	1			1		pwm
1	18	E14	P0	HomC	PWM	50	2			2		pwm
2	19	E14	P0	HomC	PWM	100	2			2		pwm
2	20	E14	P0	HomC	PCLp	50	3	3				ant
2	21	E14	P0	HomC	PWM	50	2			2		pwm
2	22	E14	P0	HomC	PWM	800	3			3		pwm
2	23	E14	P0	HomC	PWM	50	2			2		pwm
2	24	E14	P0	HetC	PCLp+GLAp	100	6	5	1			ant
2	25	E14	P0	HomC	VC	50	3				3	

Supplementary Table 2. List of Star Track clones and measured parameters

Animal n.	clone n.	time of electroporation	time of analysis	clone type	clone subtype	M-L dispersion (μm)	clone size	n. of PCLp	n. of GLAp	n. of PWM	n. of VC	A-P dispersion
2	26	E14	P0	HomC	PWM	50	1			1		pwm
2	27	E14	P0	HomC	PCLp	50	1	1				ant
2	28	E14	P0	HomC	PCLp	50	3	3				ant
2	29	E14	P0	HomC	PWM	50	2			2		pwm
2	30	E14	P0	HomC	PCLp	100	2	2				ant
2	31	E14	P0	HomC	PCLp	50	2	2				ant
2	32	E14	P0	HomC	PWM	50	1			1		pwm
2	33	E14	P0	HomC	PCLp	100	3	3				ant
2	34	E14	P0	HomC	PWM	50	1			1		pwm
2	35	E14	P0	HomC	GLAp	50	2		2			ant
2	36	E14	P0	HomC	PCLp	400	4	4				ant
2	37	E14	P0	HomC	PCLp	100	4	4				ant
2	38	E14	P0	HomC	PCLp	150	9	9				ant
2	39	E14	P0	HomC	PCLp	500	4	4				ant
2	40	E14	P0	HomC	PWM	50	3			3		pwm
2	41	E14	P0	HomC	PWM	100	5			5		pwm
2	42	E14	P0	HomC	VC	100	5				5	
2	43	E14	P0	HomC	GLAp	50	2		2			middle
2	44	E14	P0	HomC	PWM	50	7			7		pwm
2	45	E14	P0	HomC	PWM	150	4			4		pwm
2	46	E14	P0	HomC	PWM	50	2			2		pwm
2	47	E14	P0	HomC	PWM	50	2			2		pwm
2	48	E14	P0	HomC	GLAp	50	2		2			middle
2	49	E14	P0	HomC	PWM	100	3			3		pwm
2	50	E14	P0	HomC	PWM	50	1			1		pwm
2	51	E14	P0	HetC	GLAp+PWM	100	6	2		4		ant+pwm

Supplementary Table 2. List of Star Track clones and measured parameters

Animal n.	clone n.	time of electroporation	time of analysis	clone type	clone subtype	M-L dispersion (µm)	clone size	n. of PCLp	n. of GLAp	n. of PWM	n. of VC	A-P dispersion
2	52	E14	P0	HomC	PWM	100	4			4		pwm
2	53	E14	P0	HomC	PWM	250	5			5		pwm
2	54	E14	P0	HomC	PWM	50	4			4		pwm
2	55	E14	P0	HomC	PWM	50	1			1		pwm
2	56	E14	P0	HomC	PWM	50	2			2		pwm
2	57	E14	P0	HomC	PCLp	50	3	3				ant
2	58	E14	P0	HomC	PWM	50	3			3		pwm
2	59	E14	P0	HomC	VC	50	1				1	
2	60	E14	P0	HomC	PCLp	50	2	2				middle
3	61	E14	P0	HetC	GLAp+PWM	200	5		1	4		post+pwm
3	62	E14	P0	HomC	PWM	50	2			2		pwm
3	63	E14	P0	HomC	PWM	50	2			2		pwm
3	64	E14	P0	HomC	PWM	50	7			7		pwm
3	65	E14	P0	HomC	PWM	50	2			2		pwm
3	66	E14	P0	HomC	PCLp	200	2	2				ant+middle
3	67	E14	P0	HetC	PCLp+GLAp+PWM	500	12	3	3	6		ant+pwm
3	68	E14	P0	HomC	PWM	150	6			6		pwm
3	69	E14	P0	HomC	GLAp	50	3		3			ant
3	70	E14	P0	HetC	GLAp+PWM	250	7		2	5		middle+pwm
3	71	E14	P0	HomC	PWM	300	3			3		pwm
3	72	E14	P0	HomC	PCLp	50	2	2				post
3	73	E14	P0	HetC	PCLp+PWM	250	13	11		2		ant+pwm
3	74	E14	P0	HetC	PCLp+GLAp+PWM	450	9	4	3	2		middle+pwm
3	75	E14	P0	HomC	PWM	50	2			2		pwm
3	76	E14	P0	HomC	GLAp	50	3		3			anterior
3	77	E14	P0	HetC	GLAp+PWM	200	5		3	2		posterior+pwm

Supplementary Table 2. List of Star Track clones and measured parameters

Animal n.	clone n.	time of electroporation	time of analysis	clone type	clone subtype	M-L dispersion (µm)	clone size	n. of PCLp	n. of GLAp	n. of PWM	n. of VC	A-P dispersion
3	78	E14	P0	HomC	PCLp	50	1	1				anterior
3	79	E14	P0	HomC	PCLp	50	2	2				middle
3	80	E14	P0	HomC	PWM	50	2			2		pwm
3	81	E14	P0	HomC	PWM	50	1			1		pwm
3	82	E14	P0	HomC	PWM	50	2			2		pwm
3	83	E14	P0	HomC	GLAp	50	3		3			middle
3	84	E14	P0	HomC	PWM	650	3			3		pwm
3	85	E14	P0	HomC	PWM	50	9			9		pwm
3	86	E14	P0	HomC	PWM	100	10			10		pwm
3	87	E14	P0	HomC	PWM	200	5			5		pwm
3	88	E14	P0	HomC	PWM	50	2			2		pwm
3	89	E14	P0	HomC	GLAp	50	2		2			middle
3	90	E14	P0	HomC	PWM	50	1			1		pwm
3	91	E14	P0	HomC	PWM	150	3			3		pwm
3	92	E14	P0	HomC	PWM	50	4			4		pwm
3	93	E14	P0	HomC	GLAp	50	2		2			middle
3	94	E14	P0	HomC	PWM	50	1			1		pwm
3	95	E14	P0	HomC	GLAp	50	8		8			ant
3	96	E14	P0	HomC	PWM	50	1			1		pwm
3	97	E14	P0	HomC	PWM	50	1			1		pwm
3	98	E14	P0	HomC	PCLp	50	1	1				ant
3	99	E14	P0	HomC	PCLp	50	4	4				post
3	100	E14	P0	HetC	GLAp+PWM	100	5		3	2		ant+pwm
3	101	E14	P0	HomC	PWM	50	4			4		pwm
3	102	E14	P0	HomC	PWM	50	3			3		pwm
3	103	E14	P0	HomC	PWM	50	6			6		pwm

Supplementary Table 2. List of Star Track clones and measured parameters

Animal n.	clone n.	time of electroporation	time of analysis	clone type	clone subtype	M-L dispersion (μm)	clone size	n. of PCLp	n. of GLAp	n. of PWM	n. of VC	A-P dispersion
3	104	E14	P0	HomC	PWM	50	3			3		pwm
3	105	E14	P0	HomC	PWM	50	1			1		pwm
3	106	E14	P0	HomC	PWM	50	3			3		pwm
3	107	E14	P0	HomC	PWM	50	2			2		pwm
3	108	E14	P0	HomC	PWM	50	3			3		pwm
3	109	E14	P0	HomC	PCLp	50	1	1				middle
3	110	E14	P0	HomC	PCLp	50	1	1				middle
3	111	E14	P0	HomC	PWM	50	1			1		pwm
3	112	E14	P0	HomC	GLAp	50	2		2			ant
3	113	E14	P0	HomC	PWM	50	2			2		pwm
3	114	E14	P0	HomC	PWM	50	2			2		pwm
3	115	E14	P0	HomC	PWM	50	2			2		pwm
3	116	E14	P0	HomC	PWM	50	3			3		pwm
3	117	E14	P0	HomC	PWM	50	5			5		pwm
3	118	E14	P0	HomC	PCLp	50	1	1				middle
3	119	E14	P0	HomC	PCLp	50	3	3				ant
3	120	E14	P0	HomC	PCLp	50	2	2				ant
3	121	E14	P0	HomC	PWM	50	2			2		pwm
3	122	E14	P0	HomC	PWM	100	6			6		pwm
3	123	E14	P0	HomC	PCLp	50	3	3				ant
3	124	E14	P0	HomC	PWM	50	1			1		post

Clone type: HomC, Homogeneous clone; HetC, Heterogeneous clone.
Clone subtype: BG, Bergmann glia; GLA, granular layer astrocyte; WMA, white matter astrocyte; CNA, cerebellar nuclei astrocyte; PCLp, Purkinje cell layer progenitor; GLAp, granular layer astrocyte progenitor; PWM, prospective white matter; VC, ventricular cell.
A-P dispersion: Crus, cruciform; Pm, paramedian; Cp, copula pyramidis; ant, anterior cerebellum; post, posterior cerebellum; middle, middle cerebellum; pwm, prospective white matter.

Supplementary Table 3. List of Confetti clones and measured parameters.

Animal n.	clone n.	time of Tx injection	time of analysis	clone type	clone subtype	M-L dispersion (µm)	clone size	n. of BG	n. of GLA	A-P dispersion
#2 CFP	1	P6	P30	HetC	BG+GLA	60	2	1	1	IV-V
#2 CFP	2	P6	P30	HomC	BG+GLA	480	6	6		IV-V
#2 CFP	3	P6	P30	HetC	BG+GLA	120	6	5	1	IV-V
#2 CFP	4	P6	P30	HetC	BG+GLA	180	5	2	3	IV-V
#2 CFP	5	P6	P30	HetC	BG+GLA	60	8	5	3	IV-V
#2 CFP	6	P6	P30	HetC	BG+GLA	60	3	2	1	IV-V
#2 CFP	7	P6	P30	HetC	BG+GLA	60	2	1	1	IV-V
#2 CFP	8	P6	P30	HetC	BG+GLA	60	5	3	2	IV-V
#2 CFP	9	P6	P30	HetC	BG+GLA	60	5	2	3	IV-V
#2 CFP	10	P6	P30	HomC	BG	60	3	3		IV-V
#2 CFP	11	P6	P30	HetC	BG+GLA	60	7	5	2	IV-V
#2 CFP	12	P6	P30	HomC	BG	60	2	2		IV-V
#2 CFP	13	P6	P30	HomC	BG	60	2	2		IV-V
#2 CFP	14	P6	P30	HetC	BG+GLA	240	15	8	7	IV-V
#2 CFP	15	P6	P30	HetC	BG+GLA	180	5	4	1	IV-V
#2 CFP	16	P6	P30	HetC	BG+GLA	180	7	5	2	IV-V
#2 CFP	17	P6	P30	HetC	BG+GLA	120	4	1	3	IV-V
#2 CFP	18	P6	P30	HomC	BG	60	6	6		IV-V
#2 CFP	19	P6	P30	HetC	BG+GLA	60	5	2	3	IV-V
#2 CFP	20	P6	P30	HetC	BG+GLA	60	3	1	2	IV-V
#2 CFP	21	P6	P30	HomC	BG	60	2	2		IV-V
#2 CFP	22	P6	P30	HetC	BG+GLA	60	4	2	2	IV-V
#2 CFP	23	P6	P30	HomC	BG	300	5	5		IV-V
#2 CFP	24	P6	P30	HomC	BG	60	3	3		IV-V
#2 CFP	25	P6	P30	HetC	BG+GLA	180	8	5	3	IV-V
#2 CFP	26	P6	P30	HomC	BG	60	1	1		IV-V
#2 CFP	27	P6	P30	HomC	BG	60	1	1		IV-V

Supplementary Table 3. List of Confetti clones and measured parameters.

Animal n.	clone n.	time of Tx injection	time of analysis	clone type	clone subtype	M-L dispersion (µm)	clone size	n. of BG	n. of GLA	A-P dispersion
#2 CFP	28	P6	P30	HetC	BG+GLA	60	3	2	1	IV-V
#2 CFP	29	P6	P30	HomC	BG	120	3	3		IV-V
#2 CFP	30	P6	P30	HomC	BG	60	2	2		IV-V
#2 CFP	31	P6	P30	HomC	BG	60	3	3		IV-V
#2 CFP	32	P6	P30	HetC	BG+GLA	60	3	2	1	IV-V
#2 YFP	33	P6	P30	HetC	BG+GLA	60	2	1	1	IV-V
#2 YFP	34	P6	P30	HomC	GLA	60	1		1	IV-V
#2 YFP	35	P6	P30	HomC	BG	60	2	2		IV-V
#2 YFP	36	P6	P30	HetC	BG+GLA	60	3	1	2	IV-V
#2 YFP	37	P6	P30	HomC	BG	60	2	2		IV-V
#2 YFP	38	P6	P30	HomC	BG	60	3	3		IV-V
#2 YFP	39	P6	P30	HetC	BG+GLA	60	3	2	1	IV-V
#2 YFP	40	P6	P30	HomC	BG	60	2	2		IV-V
#2 YFP	41	P6	P30	HetC	BG+GLA	60	3	2	1	IV-V
#2 YFP	42	P6	P30	HetC	BG+GLA	60	6	3	3	IV-V
#2 YFP	43	P6	P30	HetC	BG+GLA	60	3	2	1	IV-V
#2 YFP	44	P6	P30	HomC	BG	60	1	1		IV-V
#2 YFP	45	P6	P30	HomC	BG	60	1	1		IV-V
#2 YFP	46	P6	P30	HomC	BG	60	5	5		IV-V
#2 YFP	47	P6	P30	HomC	GLA	60	1		1	IV-V
#2 YFP	48	P6	P30	HomC	BG	60	3	3		IV-V
#2 YFP	49	P6	P30	HomC	BG	360	8	8		IV-V
#2 YFP	50	P6	P30	HomC	BG	120	2	2		IV-V
#2 YFP	51	P6	P30	HetC	BG+GLA	60	3	2	1	IV-V
#2 YFP	52	P6	P30	HomC	BG	60	1	1		IV-V
#2 YFP	53	P6	P30	HomC	BG	60	1	1		IV-V
#2 YFP	54	P6	P30	HomC	BG	300	3	3		IV-V

Supplementary Table 3. List of Confetti clones and measured parameters.

Animal n.	clone n.	time of Tx injection	time of analysis	clone type	clone subtype	M-L dispersion (µm)	clone size	n. of BG	n. of GLA	A-P dispersion
#2 YFP	55	P6	P30	HetC	BG+GLA	60	5	2	3	IV-V
#2 YFP	56	P6	P30	HomC	BG	180	2	2		IV-V
#2 YFP	57	P6	P30	HomC	BG	120	5	5		IV-V
#2 YFP	58	P6	P30	HomC	BG	420	4	4		IV-V
#2 RFP	59	P6	P30	HetC	BG+GLA	60	3	2	1	IV-V
#2 RFP	60	P6	P30	HetC	BG+GLA	360	11	9	2	IV-V
#2 RFP	61	P6	P30	HetC	BG+GLA	60	3	2	1	IV-V
#2 RFP	62	P6	P30	HomC	GLA	60	1		1	IV-V
#2 RFP	63	P6	P30	HomC	BG	60	1	1		IV-V
#2 RFP	64	P6	P30	HetC	BG+GLA	60	2	1	1	IV-V
#2 RFP	65	P6	P30	HetC	BG+GLA	60	4	3	1	IV-V
#2 RFP	66	P6	P30	HomC	BG	60	2	2		IV-V
#2 RFP	67	P6	P30	HomC	BG	60	1	1		IV-V
#2 RFP	68	P6	P30	HetC	BG+GLA	60	2	1	1	IV-V
#2 RFP	69	P6	P30	HomC	BG	60	1	1		IV-V
#2 RFP	70	P6	P30	HetC	BG+GLA	60	3	1	2	IV-V
#2 RFP	71	P6	P30	HetC	BG+GLA	60	2	1	1	IV-V
#2 RFP	72	P6	P30	HetC	BG+GLA	60	2	1	1	IV-V
#2 RFP	73	P6	P30	HomC	BG	60	6	6		IV-V
#2 RFP	74	P6	P30	HetC	BG+GLA	120	7	4	3	IV-V
#2 RFP	75	P6	P30	HetC	BG+GLA	120	5	3	2	IV-V
#2 RFP	76	P6	P30	HomC	BG	60	2	2		IV-V
#2 RFP	77	P6	P30	HomC	BG	60	1	1		IV-V
#2 RFP	78	P6	P30	HetC	BG+GLA	60	2	1	1	IV-V
#2 RFP	79	P6	P30	HetC	BG+GLA	60	4	2	2	IV-V
#2 RFP	80	P6	P30	HetC	BG+GLA	60	8	5	3	IV-V
#2 RFP	81	P6	P30	HetC	BG+GLA	60	5	1	4	IV-V

Supplementary Table 3. List of Confetti clones and measured parameters.

Animal n.	clone n.	time of Tx injection	time of analysis	clone type	clone subtype	M-L dispersion (µm)	clone size	n. of BG	n. of GLA	A-P dispersion
#2 RFP	82	P6	P30	HomC	BG	60	2	2		IV-V
#2 RFP	83	P6	P30	HetC	BG+GLA	300	3	2	1	IV-V
#2 RFP	84	P6	P30	HetC	BG+GLA	360	7	2	5	IV-V
#2 RFP	85	P6	P30	HomC	BG	60	2	2		IV-V
#2 RFP	86	P6	P30	HetC	BG+GLA	60	4	2	2	IV-V
#2 RFP	87	P6	P30	HomC	BG	60	3	3		IV-V
#2 RFP	88	P6	P30	HetC	BG+GLA	60	2	1	1	IV-V
#2 RFP	89	P6	P30	HetC	BG+GLA	60	2	1	1	IV-V
#2 RFP	90	P6	P30	HomC	BG	180	12	12		IV-V
#2 RFP	91	P6	P30	HetC	BG+GLA	60	4	3	1	IV-V
#2 RFP	92	P6	P30	HomC	BG	60	1	1		IV-V
#2 RFP	93	P6	P30	HomC	BG	60	3	3		IV-V
#2 RFP	94	P6	P30	HetC	BG+GLA	120	3	2	1	IV-V
#2 RFP	95	P6	P30	HetC	BG+GLA	60	2	1	1	IV-V
#2 RFP	96	P6	P30	HetC	BG+GLA	60	3	2	1	IV-V
#2 RFP	97	P6	P30	HomC	BG	60	2	2		IV-V
#2 RFP	98	P6	P30	HomC	BG	120	3	3		IV-V
#2 RFP	99	P6	P30	HetC	BG+GLA	60	2	1	1	IV-V
#2 RFP	100	P6	P30	HetC	BG+GLA	60	3	2	1	IV-V
#2 RFP	101	P6	P30	HetC	BG+GLA	60	2	1	1	IV-V
#2 RFP	102	P6	P30	HetC	BG+GLA	60	4	1	3	IV-V
#2 RFP	103	P6	P30	HomC	BG	120	4	4		IV-V
#2 RFP	104	P6	P30	HetC	BG+GLA	60	5	2	3	IV-V
#2 RFP	105	P6	P30	HetC	BG+GLA	60	7	5	2	IV-V
#2 RFP	106	P6	P30	HetC	BG+GLA	120	5	2	3	IV-V
#2 RFP	107	P6	P30	HomC	BG	60	4	4		IV-V
#2 RFP	108	P6	P30	HomC	BG	60	1	1		IV-V

Supplementary Table 3. List of Confetti clones and measured parameters.

Animal n.	clone n.	time of Tx injection	time of analysis	clone type	clone subtype	M-L dispersion (µm)	clone size	n. of BG	n. of GLA	A-P dispersion
#2 RFP	109	P6	P30	HetC	BG+GLA	120	3	2	1	IV-V
#2 RFP	110	P6	P30	HetC	BG+GLA	60	5	4	1	IV-V
#3 CFP	111	P6	P30	HetC	BG+GLA	120	5	1	4	IV-V
#3 CFP	112	P6	P30	HetC	BG+GLA	120	4	1	3	IV-V
#3 CFP	113	P6	P30	HetC	BG+GLA	120	5	3	2	IV-V
#3 CFP	114	P6	P30	HomC	GLA	120	3		3	IV-V
#3 CFP	115	P6	P30	HetC	BG+GLA	60	5	2	3	IV-V
#3 CFP	116	P6	P30	HomC	BG	60	3	3		IV-V
#3 CFP	117	P6	P30	HetC	BG+GLA	120	5	2	3	IV-V
#3 CFP	118	P6	P30	HetC	BG+GLA	180	3	2	1	IV-V
#3 CFP	119	P6	P30	HomC	GLA	60	3		3	IV-V
#3 CFP	120	P6	P30	HomC	GLA	60	1		1	IV-V
#3 CFP	121	P6	P30	HomC	BG	60	2	2		IV-V
#3 CFP	122	P6	P30	HomC	BG	60	2	2		IV-V
#3 CFP	123	P6	P30	HomC	GLA	60	1		1	IV-V
#3 CFP	124	P6	P30	HomC	BG	60	1	1		IV-V
#3 CFP	125	P6	P30	HetC	BG+GLA	60	4	2	2	IV-V
#3 CFP	126	P6	P30	HetC	BG+GLA	60	3	1	2	IV-V
#3 CFP	127	P6	P30	HomC	BG	180	2	2		IV-V
#3 CFP	128	P6	P30	HetC	BG+GLA	60	6	3	3	IV-V
#3 CFP	129	P6	P30	HomC	BG	60	1	1		IV-V
#3 CFP	130	P6	P30	HomC	BG	60	2	2		IV-V
#3 CFP	131	P6	P30	HetC	BG+GLA	60	3	1	2	IV-V
#3 CFP	132	P6	P30	HetC	BG+GLA	60	6	5	1	IV-V
#3 CFP	133	P6	P30	HetC	BG+GLA	60	3	2	1	IV-V
#3 CFP	134	P6	P30	HomC	BG	60	2	2		IV-V
#3 CFP	135	P6	P30	HetC	BG+GLA	60	3	1	2	IV-V

Supplementary Table 3. List of Confetti clones and measured parameters.

Animal n.	clone n.	time of Tx injection	time of analysis	clone type	clone subtype	M-L dispersion (µm)	clone size	n. of BG	n. of GLA	A-P dispersion
#3 CFP	136	P6	P30	HetC	BG+GLA	60	2	1	1	IV-V
#3 CFP	137	P6	P30	HetC	BG+GLA	60	2	1	1	IV-V
#3 CFP	138	P6	P30	HetC	BG+GLA	60	2	1	1	IV-V
#3 CFP	139	P6	P30	HetC	BG+GLA	60	2	1	1	IV-V
#3 CFP	140	P6	P30	HetC	BG+GLA	60	3	2	1	IV-V
#3 CFP	141	P6	P30	HomC	BG	60	1	1		IV-V
#3 CFP	142	P6	P30	HetC	BG+GLA	120	6	5	1	IV-V
#3 CFP	143	P6	P30	HomC	BG	60	4	4		IV-V
#3 CFP	144	P6	P30	HetC	BG+GLA	60	3	1	2	IV-V
#3 CFP	145	P6	P30	HomC	BG	60	2	2		IV-V
#3 CFP	146	P6	P30	HetC	BG+GLA	60	3	1	2	IV-V
#3 CFP	147	P6	P30	HomC	GLA	60	2		2	IV-V
#3 CFP	148	P6	P30	HomC	BG	60	1	1		IV-V
#3 YFP	149	P6	P30	HetC	BG+GLA	60	3	2	1	IV-V
#3 YFP	150	P6	P30	HomC	BG	60	3	3		IV-V
#3 YFP	151	P6	P30	HomC	BG	60	2	2		IV-V
#3 YFP	152	P6	P30	HetC	BG+GLA	180	6	5	1	IV-V
#3 YFP	153	P6	P30	HetC	BG+GLA	60	3	2	1	IV-V
#3 YFP	154	P6	P30	HetC	BG+GLA	60	3	1	2	IV-V
#3 YFP	155	P6	P30	HetC	BG+GLA	60	2	1	1	IV-V
#3 YFP	156	P6	P30	HetC	BG+GLA	120	5	4	1	IV-V
#3 YFP	157	P6	P30	HomC	GLA	60	1		1	IV-V
#3 YFP	158	P6	P30	HomC	BG	60	1	1		IV-V
#3 YFP	159	P6	P30	HomC	GLA	60	2		2	IV-V
#3 YFP	160	P6	P30	HomC	BG	120	3	3		IV-V
#3 YFP	161	P6	P30	HomC	BG	60	1	1		IV-V
#3 YFP	162	P6	P30	HomC	BG	60	1	1		IV-V

Supplementary Table 3. List of Confetti clones and measured parameters.

Animal n.	clone n.	time of Tx injection	time of analysis	clone type	clone subtype	M-L dispersion (µm)	clone size	n. of BG	n. of GLA	A-P dispersion
#3 YFP	163	P6	P30	HomC	BG	60	1	1		IV-V
#3 YFP	164	P6	P30	HomC	BG	60	2	2		IV-V
#3 YFP	165	P6	P30	HomC	GLA	60	2		2	IV-V
#3 YFP	166	P6	P30	HetC	BG+GLA	60	2	1	1	IV-V
#3 YFP	167	P6	P30	HomC	BG	60	1	1		IV-V
#3 YFP	168	P6	P30	HomC	BG	120	3	3		IV-V
#3 YFP	169	P6	P30	HomC	BG	60	2	2		IV-V
#3 YFP	170	P6	P30	HetC	BG+GLA	60	3	2	1	IV-V
#3 YFP	171	P6	P30	HomC	GLA	60	1		1	IV-V
#3 YFP	172	P6	P30	HomC	BG	60	1	1		IV-V
#3 RFP	173	P6	P30	HomC	BG	60	2	2		IV-V
#3 RFP	174	P6	P30	HomC	BG	60	1	1		IV-V
#3 RFP	175	P6	P30	HomC	BG	60	2	2		IV-V
#3 RFP	176	P6	P30	HomC	GLA	60	1		1	IV-V
#3 RFP	177	P6	P30	HetC	BG+GLA	60	10	5	5	IV-V
#3 RFP	178	P6	P30	HetC	BG+GLA	60	2	1	1	IV-V
#3 RFP	179	P6	P30	HetC	BG+GLA	60	2	1	1	IV-V
#3 RFP	180	P6	P30	HomC	BG	60	3	3		IV-V
#3 RFP	181	P6	P30	HomC	BG	120	6	6		IV-V
#3 RFP	182	P6	P30	HetC	BG+GLA	60	2	1	1	IV-V
#3 RFP	183	P6	P30	HetC	BG+GLA	60	2	1	1	IV-V
#3 RFP	184	P6	P30	HetC	BG+GLA	60	2	1	1	IV-V
#3 RFP	185	P6	P30	HetC	BG+GLA	120	10	6	4	IV-V
#3 RFP	186	P6	P30	HomC	BG	60	1	1		IV-V
#3 RFP	187	P6	P30	HetC	BG+GLA	60	2	1	1	IV-V
#3 RFP	188	P6	P30	HetC	BG+GLA	60	2	1	1	IV-V
#3 RFP	189	P6	P30	HetC	BG+GLA	60	4	3	1	IV-V

Supplementary Table 3. List of Confetti clones and measured parameters.

Animal n.	clone n.	time of Tx injection	time of analysis	clone type	clone subtype	M-L dispersion (µm)	clone size	n. of BG	n. of GLA	A-P dispersion
#3 RFP	190	P6	P30	HetC	BG+GLA	60	3	1	2	IV-V
#3 RFP	191	P6	P30	HetC	BG+GLA	60	2	1	1	IV-V
#3 RFP	192	P6	P30	HomC	BG	120	4	4		IV-V
#3 RFP	193	P6	P30	HomC	GLA	60	1		1	IV-V
#3 RFP	194	P6	P30	HetC	BG+GLA	120	3	1	2	IV-V
#3 RFP	195	P6	P30	HomC	BG	60	4	4		IV-V
#3 RFP	196	P6	P30	HetC	BG+GLA	60	5	3	2	IV-V
#3 RFP	197	P6	P30	HetC	BG+GLA	60	3	2	1	IV-V
#3 RFP	198	P6	P30	HomC	GLA	60	2		2	IV-V
#3 RFP	199	P6	P30	HomC	BG	60	4	4		IV-V
#3 RFP	200	P6	P30	HomC	BG	60	1	1		IV-V
#3 RFP	201	P6	P30	HomC	BG	60	2	2		IV-V
#3 RFP	202	P6	P30	HomC	GLA	120	2		2	IV-V
#3 RFP	203	P6	P30	HomC	BG	60	1	1		IV-V
#3 RFP	204	P6	P30	HetC	BG+GLA	120	5	3	2	IV-V
#3 RFP	205	P6	P30	HomC	GLA	60	1		1	IV-V
#3 RFP	206	P6	P30	HetC	BG+GLA	120	3	1	2	IV-V
#3 RFP	207	P6	P30	HetC	BG+GLA	60	2	1	1	IV-V
#3 RFP	208	P6	P30	HetC	BG+GLA	60	5	2	3	IV-V
#3 RFP	209	P6	P30	HomC	BG	60	3	3		IV-V
#3 RFP	210	P6	P30	HomC	BG	60	2	2		IV-V
#3 RFP	211	P6	P30	HetC	BG+GLA	60	3	1	2	IV-V
#3 RFP	212	P6	P30	HetC	BG+GLA	60	4	1	3	IV-V
#3 RFP	213	P6	P30	HetC	BG+GLA	60	2	1	1	IV-V
#3 RFP	214	P6	P30	HetC	BG+GLA	60	3	1	2	IV-V
#3 RFP	215	P6	P30	HomC	GLA	60	1		1	IV-V
#3 RFP	216	P6	P30	HetC	BG+GLA	120	8	6	2	IV-V

Supplementary Table 3. List of Confetti clones and measured parameters.

Animal n.	clone n.	time of Tx injection	time of analysis	clone type	clone subtype	M-L dispersion (µm)	clone size	n. of BG	n. of GLA	A-P dispersion
#3 RFP	217	P6	P30	HetC	BG+GLA	60	2	1	1	IV-V
#3 RFP	218	P6	P30	HetC	BG+GLA	60	4	3	1	IV-V
#3 RFP	219	P6	P30	HomC	BG	60	1	1		IV-V
#3 RFP	220	P6	P30	HomC	BG	60	2	2		IV-V
#5 CFP	221	P6	P30	HetC	BG+GLA	60	4	2	2	IV-V
#5 CFP	222	P6	P30	HetC	BG+GLA	60	2	1	1	IV-V
#5 CFP	223	P6	P30	HetC	BG+GLA	60	2	1	1	IV-V
#5 CFP	224	P6	P30	HomC	BG	60	2	2		IV-V
#5 CFP	225	P6	P30	HomC	BG	60	1	1		IV-V
#5 CFP	226	P6	P30	HomC	BG	60	1	1		IV-V
#5 CFP	227	P6	P30	HomC	BG	60	3	3		IV-V
#5 CFP	228	P6	P30	HetC	BG+GLA	60	3	1	2	IV-V
#5 CFP	229	P6	P30	HetC	BG+GLA	60	3	2	1	IV-V
#5 CFP	230	P6	P30	HetC	BG+GLA	60	4	3	1	IV-V
#5 CFP	231	P6	P30	HomC	BG	60	1	1		IV-V
#5 CFP	232	P6	P30	HetC	BG+GLA	60	2	1	1	IV-V
#5 CFP	233	P6	P30	HetC	BG+GLA	60	2	1	1	IV-V
#5 CFP	234	P6	P30	HomC	BG	60	1	1		IV-V
#5 CFP	235	P6	P30	HetC	BG+GLA	60	8	3	5	IV-V
#5 CFP	236	P6	P30	HetC	BG+GLA	60	4	1	3	IV-V
#5 CFP	237	P6	P30	HomC	BG	60	5	5		IV-V
#5 CFP	238	P6	P30	HetC	BG+GLA	60	2	1	1	IV-V
#5 CFP	239	P6	P30	HomC	BG	60	1	1		IV-V
#5 CFP	240	P6	P30	HetC	BG+GLA	60	7	5	2	IV-V
#5 CFP	241	P6	P30	HetC	BG+GLA	60	4	3	1	IV-V
#5 CFP	242	P6	P30	HetC	BG+GLA	60	3	1	2	IV-V
#5 CFP	243	P6	P30	HetC	BG+GLA	60	3	2	1	IV-V

Supplementary Table 3. List of Confetti clones and measured parameters.

Animal n.	clone n.	time of Tx injection	time of analysis	clone type	clone subtype	M-L dispersion (µm)	clone size	n. of BG	n. of GLA	A-P dispersion
#5 CFP	244	P6	P30	HetC	BG+GLA	60	4	3	1	IV-V
#5 CFP	245	P6	P30	HetC	BG+GLA	60	2	1	1	IV-V
#5 CFP	246	P6	P30	HetC	BG+GLA	60	3	1	2	IV-V
#5 CFP	247	P6	P30	HomC	BG	60	2	2		IV-V
#5 CFP	248	P6	P30	HomC	BG	60	2	2		IV-V
#5 CFP	249	P6	P30	HomC	BG	60	2	2		IV-V
#5 CFP	250	P6	P30	HomC	BG	60	2	2		IV-V
#5 CFP	251	P6	P30	HetC	BG+GLA	60	4	3	1	IV-V
#5 YFP	252	P6	P30	HomC	BG	60	1	1		IV-V
#5 YFP	253	P6	P30	HomC	BG	60	2	2		IV-V
#5 YFP	254	P6	P30	HetC	BG+GLA	60	7	6	1	IV-V
#5 YFP	255	P6	P30	HomC	BG	180	5	5		IV-V
#5 YFP	256	P6	P30	HomC	BG	60	1	1		IV-V
#5 YFP	257	P6	P30	HetC	BG+GLA	120	5	4	1	IV-V
#5 YFP	258	P6	P30	HomC	BG	60	2	2		IV-V
#5 YFP	259	P6	P30	HetC	BG+GLA	60	3	2	1	IV-V
#5 YFP	260	P6	P30	HomC	BG	60	3	3		IV-V
#5 YFP	261	P6	P30	HomC	BG	60	3	3		IV-V
#5 YFP	262	P6	P30	HetC	BG+GLA	60	2	1	1	IV-V
#5 YFP	263	P6	P30	HetC	BG+GLA	60	4	3	1	IV-V
#5 YFP	264	P6	P30	HetC	BG+GLA	60	3	1	2	IV-V
#5 YFP	265	P6	P30	HetC	BG+GLA	60	4	2	2	IV-V
#5 YFP	266	P6	P30	HetC	BG+GLA	60	3	2	1	IV-V
#5 YFP	267	P6	P30	HetC	BG+GLA	60	2	1	1	IV-V
#5 YFP	268	P6	P30	HetC	BG+GLA	60	2	1	1	IV-V
#5 YFP	269	P6	P30	HomC	BG	120	2	2		IV-V
#5 YFP	270	P6	P30	HetC	BG+GLA	60	2	1	1	IV-V

Supplementary Table 3. List of Confetti clones and measured parameters.

Animal n.	clone n.	time of Tx injection	time of analysis	clone type	clone subtype	M-L dispersion (µm)	clone size	n. of BG	n. of GLA	A-P dispersion
#5 YFP	271	P6	P30	HetC	BG+GLA	60	2	1	1	IV-V
#5 YFP	272	P6	P30	HomC	BG	60	3	3		IV-V
#5 YFP	273	P6	P30	HetC	BG+GLA	60	2	1	1	IV-V
#5 YFP	274	P6	P30	HetC	BG+GLA	60	3	2	1	IV-V
#5 YFP	275	P6	P30	HomC	BG	60	4	4		IV-V
#5 YFP	276	P6	P30	HetC	BG+GLA	60	3	1	2	IV-V
#5 YFP	277	P6	P30	HomC	BG	60	2	2		IV-V
#5 YFP	278	P6	P30	HomC	BG	120	5	5		IV-V
#5 YFP	279	P6	P30	HetC	BG+GLA	60	2	1	1	IV-V
#5 YFP	280	P6	P30	HomC	BG	60	5	5		IV-V
#5 YFP	281	P6	P30	HetC	BG+GLA	60	2	1	1	IV-V
#5 RFP	282	P6	P30	HomC	BG	60	5	5		IV-V
#5 RFP	283	P6	P30	HomC	GLA	60	1		1	IV-V
#5 RFP	284	P6	P30	HomC	BG	60	3	3		IV-V
#5 RFP	285	P6	P30	HetC	BG+GLA	60	4	1	3	IV-V
#5 RFP	286	P6	P30	HomC	BG	60	4	4		IV-V
#5 RFP	287	P6	P30	HetC	BG+GLA	60	2	1	1	IV-V
#5 RFP	288	P6	P30	HomC	BG	120	8	8		IV-V
#5 RFP	289	P6	P30	HetC	BG+GLA	60	2	1	1	IV-V
#5 RFP	290	P6	P30	HomC	BG	60	1	1		IV-V
#5 RFP	291	P6	P30	HetC	BG+GLA	120	8	7	1	IV-V
#5 RFP	292	P6	P30	HetC	BG+GLA	60	4	2	2	IV-V
#5 RFP	293	P6	P30	HetC	BG+GLA	60	2	1	1	IV-V
#5 RFP	294	P6	P30	HetC	BG+GLA	60	4	3	1	IV-V
#5 RFP	295	P6	P30	HomC	BG	60	3	3		IV-V
#5 RFP	296	P6	P30	HomC	BG	60	2	2		IV-V
#5 RFP	297	P6	P30	HetC	BG+GLA	60	3	2	1	IV-V

Supplementary Table 3. List of Confetti clones and measured parameters.

Animal n.	clone n.	time of Tx injection	time of analysis	clone type	clone subtype	M-L dispersion (µm)	clone size	n. of BG	n. of GLA	A-P dispersion
#5 RFP	298	P6	P30	HomC	BG	60	1	1		IV-V
#5 RFP	299	P6	P30	HomC	GLA	60	1		1	IV-V
#5 RFP	300	P6	P30	HetC	BG+GLA	60	4	3	1	IV-V
#5 RFP	301	P6	P30	HetC	BG+GLA	60	3	2	1	IV-V
#5 RFP	302	P6	P30	HomC	BG	60	3	3		IV-V
#5 RFP	303	P6	P30	HetC	BG+GLA	60	6	4	2	IV-V
#5 RFP	304	P6	P30	HomC	BG	60	2	2		IV-V
#5 RFP	305	P6	P30	HetC	BG+GLA	120	4	3	1	IV-V
#5 RFP	306	P6	P30	HetC	BG+GLA	60	2	1	1	IV-V
#5 RFP	307	P6	P30	HomC	BG	60	4	4		IV-V
#5 RFP	308	P6	P30	HomC	BG	60	2	2		IV-V
#5 RFP	309	P6	P30	HetC	BG+GLA	60	4	2	2	IV-V
#5 RFP	310	P6	P30	HetC	BG+GLA	60	4	3	1	IV-V
#5 RFP	311	P6	P30	HetC	BG+GLA	60	4	2	2	IV-V
#5 RFP	312	P6	P30	HetC	BG+GLA	60	2	1	1	IV-V
#5 RFP	313	P6	P30	HetC	BG+GLA	180	13	9	4	IV-V
#5 RFP	314	P6	P30	HetC	BG+GLA	60	2	1	1	IV-V
#5 RFP	315	P6	P30	HetC	BG+GLA	60	2	1	1	IV-V
#5 RFP	316	P6	P30	HetC	BG+GLA	60	3	1	2	IV-V
#5 RFP	317	P6	P30	HomC	BG	120	3	3		IV-V
#5 RFP	318	P6	P30	HetC	BG+GLA	60	5	2	3	IV-V
#5 RFP	319	P6	P30	HetC	BG+GLA	60	3	1	2	IV-V
#5 RFP	320	P6	P30	HetC	BG+GLA	60	10	5	5	IV-V
#5 RFP	321	P6	P30	HetC	BG+GLA	60	3	2	1	IV-V
#5 RFP	322	P6	P30	HetC	BG+GLA	60	5	2	3	IV-V
#5 RFP	323	P6	P30	HomC	BG	60	3	3		IV-V
#5 RFP	324	P6	P30	HetC	BG+GLA	60	6	5	1	IV-V

Supplementary Table 3. List of Confetti clones and measured parameters.

Animal n.	clone n.	time of Tx injection	time of analysis	clone type	clone subtype	M-L dispersion (µm)	clone size	n. of BG	n. of GLA	A-P dispersion
#5 RFP	325	P6	P30	HomC	BG	60	3	3		IV-V
#5 RFP	326	P6	P30	HetC	BG+GLA	60	3	2	1	IV-V
#5 RFP	327	P6	P30	HomC	BG	60	2	2		IV-V
#5 RFP	328	P6	P30	HetC	BG+GLA	60	2	1	1	IV-V
#5 RFP	329	P6	P30	HomC	GLA	60	3		3	IV-V

Clone type: Homc, Homogeneous clone; HetC, Heterogeneous clone.
Clone subtype: BG, Bergmann glia; GLA, granular layer astrocyte.
Tx: Tamoxifen.

Supplementary Table 4. Statistical analyses and associated significant P values

Fig.	Dataset	Analysis*	Global effects	Pairwise comparisons (where applicable)	Number of animals analysed
Fig. 3.2	**Frequency of A-P dispersion E12-P30 vs E14-P30**	**Chi-square test**	P<0.0001		E12-P30: 3; E14-P30: 4
Fig. 3.3	**Clone type frequency E12-P30 vs E14–P30**	**Fisher's exact test**	P=0.0089		E12-P30: 3; E14-P30: 4
	Clone frequency **E12-P30 vs E14-P30** **HomC subtype**	**Fisher's exact test**	E12 WMA vs E14 WMA, P<0.0001 E12 BG vs E14 BG, P=0.0211		
	Clone frequency **E12-P30 vs E14-P30** **HetC subtype**	**Fisher's exact test**	E12 triple vs E14 triple, P=0.0227		
Fig. 3.4	**Size** **E12-P30 vs E14-P30**	**GEE-Poisson**	Time, P=0.002 Type, P<0.0001	P=0.005	E12-P30: 3; E14-P30: 4
	Size **E12-P30, E14-P30** **HomC** **Subtype**	**GEE-Poisson**	Subtype, P<0.0001	E12 WMA vs E12 GLA, P<0.0001 E12 WMA vs E12 BG, P<0.0001 E14 WMA vs E14 GLA, P=0.003 E12 WMA vs E14 BG, P<0.0001 E12 BG vs E14 WMA, P<0.0001 E12 BG vs E14 GLA P=0.017	E12-P30: 3; E14-P30: 4
	Size **E12-P30, E14-P30** **HetC** **Subtype**	**GEE-Poisson**	Subtype, P<0.0001	E12 triple vs E12 double, P<0.0001 E12 triple vs E14 double, P<0.0001	E12-P30: 3; E14-P30: 4
	Frequency of single cell clones E12-P30 **HomC**	**Fisher's exact test**	E12 WMA vs E12 BG, P=0.0265		E12-P30: 3; E14-P30: 4

Supplementary Table 4. Statistical analyses and associated significant P values

Fig.	Dataset	Analysis*	Global effects	Pairwise comparisons (where applicable)	Number of animals analysed
Fig. 3.5	**Phenotype contribution to clones** **E12-P30, E14-P30**	**GEE-Linear**	Cell type, P=0.01	Triple E12 WM vs GLA,BG, P<0.001	E12-P30: 3; E14-P30: 4
	Clone stoichiometry E12-P30, E14-P30	**GEE-Linear**	Time, P<0.001 Subtype ratio, P=0.019 Time x Type,P=0.031	E12 Triple BG:GLA vs E12, E14 Double BG:GLA, P<0.001 E14 Triple BG:GLA vs E14 Double BG:GLA, P<0.001, vs E12 Double P=0.005	E12-P30: 3; E14-P30: 4
Fig. 3.6	**Dispersion** **E12-P30, E14-P30**	**GEE-Linear**	Time, Type, Time x type, P<0.0001	E12 vs E14, P<0.0001 E12 HomC vs E12 HetC, P<0.0001 E14 HomC vs E14 HetC, P=0.016 E12 HomC vs E14 HomC, P=0.031 E12 HetC vs E14 HetC, P<0.0001 E12 HomC vs E14 HetC, P=0.017 E14 HomC vs E12 HetC, P<0.0001	E12-P30: 3; E14-P30: 4
	Dispersion **E12-P30, E14-P30** **HomC** **Subtype**	**GEE-Linear**	Time, P<0.001 Subtype, P<0.034 Time x subtype, P=0.05	E12 WMA vs E12 GLA P<0.0001 E12 WMA vs E14 BG P=0.007 E12 GLA vs E14 GLA P=0.006 E14 WMA vs E14 GLA P<0.0001 E14 WMA vs E12 GLA P= 0.005 E12 BG vs GLA E14 P<0.0001	E12-P30: 3; E14-P30: 4
	Dispersion **E12-P30, E14-P30** **HetC** **subtype**	**GEE-Linear**	Time, Subtype, Time x subtype, P<0.0001	E12 triple vs E12 double P<0.0001 E12 triple vs E14 triple P<0.0001 E12 triple vs E14 double P<0.0001 E14 triple vs E14 double, P=0.010	E12-P30: 3; E14-P30: 4

Supplementary Table 4. Statistical analyses and associated significant P values

Fig.	Dataset	Analysis*	Global effects	Pairwise comparisons (where applicable)	Number of animals analysed
Fig. 3.6	**Correlation clone size-dispersion E12-P30, E14-P30**	**Pearson**	E12, E14 P<0.001		E12-P30: 3; E14-P30: 4
	Frequency of A-P dispersion E12-P30, E14-P30	**Binomial test**	E12 Hom, E14 Hom, P<0.0001 E12 double, P=0.0034 E12 triple, P=0.0195		E12-P30: 3; E14-P30: 4
Fig. 3.7	**E12, double, triple, triple no WMA vs random distributions**	**Kolmogorov-Smirnov test for 2 independent samples**	Double clones: z=0.800, p<0.001 Triple clones: z=0.3625, p<0.001 Triple clones, no WMA: z=0.3375, p<0.001		E12-P30: 2
Fig. 3.8	**Clone type frequency P0 vs P30**	**Chi-squared test**	E12 P0 vs E12 P30, P=0.0126 E14 P0 vs E14 P30, P=0.0003 E12 HetC P0 vs E12 HetC P30, P<0.0001 E14 HetC P0 vs E14 HetC P30, P=0.0003 E12 PWM HomC P0 vs WM HomC P30, P=0.0007 E14 PWM HomC P0vs WM HomC P30, P=0.2866 E12 Cortical HomC P0 vs Cortical HomC P30, P=0.0963 E14 Cortical HomC P0 vs Cortical HomC P30, P=0.0324 E12 PCL HomC P0 vs BG HomC P30, P<0.0001 E14 PCL HomC P0 vs BG HomC P30, P<0.0001 E12 GLAp HomC P0 vs GLAp HomC P30, P<0.0017 E14 GLAp HomC P0 vs GLAp HomC P30, P<0.0938		E12-P0: 3; E14-P0: 3; E12-P30: 3; E14-P30: 4

Supplementary Table 4. Statistical analyses and associated significant P values

Fig.	Dataset	Analysis*	Global effects	Pairwise comparisons (where applicable)	Number of animals analysed
Fig. 3.8	**Size** **E12-P0, E14-P0**	**GEE-Poisson**	Time, Type, P<0.0001	E12 vs E14, P<0.0001 E12 Hom vs E12 Het, P<0.001 E14 Hom vs E14 Het, P<0.0001 E12 Hom vs E14Hom, P=0.027 E12 Hom vs E14Het P<0.0001 E14 Hom vs E12 Het P<0.0001	E12-P0: 3; E14-P0: 3; E12-P30: 3; E14-P30: 4
	Dispersion **E12-P0, E14-P0**	**GEE-Linear**	Type, P<0.0001	E14 HomC vs E14 HetC P=0.009 E12 HomC vs E14 HetC P=0.001 E14 HomC vs E12 CetC P=0.019	
Fig. 3.9	**Clone type Confetti**	**Chi Test**	P=0.0003	BG+GLA P1 vs P6 P<0.0001 BG P1 vs P6 P<0.0001 GLA P1 vs P6 P=0.5630	P1: 2; P6: 3
	Clone size Confetti **P1-P30, P6-P30**	**GEE-Poisson**	Time, P<0.0001 Type, P=0.003 Time x Type, P<0.0001	P1 BG+GLA vs P1, P6 BG, GLA P<0.0001 P6 BG+GLA, BG vs P6, P1 GLA P<0.0001	
	Clone stoichiometry, **P1-P30, P6-P30, vs E12-P30, E14-P30**	**GEE-Poisson**	Subtype ratio, P<0.001	P1, P6 BG:GLA vs E12, E14 double BG:GLA, P<0.001	
	Proportions of cleavage planes, p-vimentin	**GEE-Linear**	Proportions of distinct cleavage planes, P<0.0001	Proportion of Horizontal divisions vs Vertical, vs Oblique P<0.0001	E17.5, P1, P4: 3; P7: 4
	Cleavage plane type frequency	**Chi-square test**	P=0.7236		

Supplementary Table 4. Statistical analyses and associated significant P values

Fig.	Dataset	Analysis*	Global effects	Pairwise comparisons (where applicable)	Number of animals analysed
Fig. 3.10	**Active proliferation**	**GEE-Linear**	Time, P<0.0001 Layer, P<0.0001 Time x Layer, P<0.0001	P1, P<0.0001 in all contrasts P4, PWM vs PCL, P<0.0001 GL vs PCL, P< 0.0001 P7, PWM vs PCL, P=0.05 GL vs PCL, P=0.012 PWM, P1 vs P7, P<0.0001 P4 vs P7, P<0.0001 GL, P<0.0001 in all contrasts PCL, P<0.0001 in all contrasts	P1, P4: 3; P7: 6
Fig. 3.11	**Birthdating**	**GEE-Linear**	BrdUHigh Time, P<0.0001 Phenotype, P=0.06 Time x Phenotype, P<0.0001	BrdUHigh WM, E15 vs P1, P=0.032, P1 vs P7, P<0.0001, P1 vs P15, P<0.0001 GL, E15 vs P1, P=0.025, E15 vs P7, P=0.12, E15 vs P15; P1 vs P15, P<0.0001; P7 vs P15, P<0.001 PCL, E15 vs P7, P<0.0001, P1 vs P7, P<0.0001, P1 vs P15, P=0.05; P7 vs P15, P<0.0001 P1, WM vs GL P=0.034, WM vs BG, P<0.0001 P7, WM vs GL, P=0.003, WM vs BG, P=0.001 GL vs BG, P=0.003	3 per time point
	Proportions of BrdUHigh	**GEE-Linear**	Time, P<0.0001 Layer, P<0.0001 Time x layer, P<0.0001	P1-P4, PWM vs GL, P=0.013, PWM vs PCL, P=0.021 GL vs PCL, P=0.014 P4-P7, PWM vs GL, P=0.011 PWM vs PCL, P<0.0001 GL vs PCL, P< 0.0001 P1-P7, PWM vs PCL, P<0.0001 GL vs PCL, P< 0.001 PWM, P1-P4 vs other time points, P<0.0001,	

Supplementary Table 4. Statistical analyses and associated significant P values

Fig.	Dataset	Analysis*	Global effects	Pairwise comparisons (where applicable)	Number of animals analysed
Fig. 3.11	**Proportions of BrdUHigh**	**GEE-Linear**		GL, P1-P4 vs other time points, P<0.001, P4-P7 vs P1-P7, P=0.05 BG, P1-P4 vs other time points, P<0.0001	3 per time point
	Proportions of BrdULow and High	**GEE-Linear**	Proportion of BrdULow vs BrdUHigh, P<0.0001 Time, Proportion x time, P<0.0001	WMA, BrdULow vs BrdUHigh E15 P<0.0001, P1, P<0.0001 GLA, BrdULow vs BrdUHigh E15, P=0.001 P1, P7 P<0.0001 BG, BrdULow vs BrdUHigh E15, P=0.002 P1, P7, P<0.0001	
Fig. 3.12	Proportions of clone subtypes P30 simulated vs observed clones	**Chi-square test**	P < 2.2e-16		E12-P30: 3
	Proportions of clone types P0 (Generation 6) observed E12-P0 clones vs simulated generation 6	**Chi-square test**	P = 2.402e-15		E12-P0: 3
	Proportions of clone subtypes P0 (Generation 6) observed E12-P0 clones vs simulated generation 6	**Chi-square test**	P = 6.114e-12		E12-P0: 3
Fig. 3.14	**Proportions of ectopic BG** **P19** **controls + vs Wnt1CreSox2fl/fl mutants**	**Student t test**	P = 0,011		controls: 3; Wnt1CreSox2fl/fl mutants: 2
	Proportions of ectopic BG **8 months** **controls + vs Wnt1CreSox2fl/fl mutants**	**Student t test**	P = 0,0012		controls: 5; Wnt1CreSox2fl/fl mutants: 3

Supplementary Table 4. Statistical analyses and associated significant P values

Fig.	Dataset	Analysis*	Global effects	Pairwise comparisons (where applicable)	Number of animals analysed
Fig. 3.15	**Proportions of ectopic BG** **P30** **controls + vs GlastCreERT2Sox2flfl mutants**	**Student t test**	P = 0,0011		controls: 3; GlastCreERT2Sox2flfl mutants: 3
	Proportions of ectopic BG **8 months** **controls + vs GlastCreERT2Sox2flfl mutants**	**Student t test**	P = 0,013		controls: 4; GlastCreERT2Sox2flfl mutants: 4

Subtypes, HomCs: WMA, GLA, BG; HetC: triple (BG+GLA+WMA), double (G+GLA). *Only main effects and contrasts leading to P≤0.05 are reported

References

Aberg, F. & Kozlova, E. N. Metastasis-associated mts1 (S100A4) protein in the developing and adult central nervous system. J. Comp. Neurol. 424, 269–282 (2000).

Adamaszek, M. et al. Consensus Paper: Cerebellum and Emotion. The Cerebellum 16, 552–576 (2017).

Adams, K. a, Maida, J. M., Golden, J. a & Riddle, R. D. The transcription factor Lmx1b maintains Wnt1 expression within the isthmic organizer. Development 127, 1857–67 (2000).

Ahlfeld, J. et al. Neurogenesis from Sox2 expressing cells in the adult cerebellar cortex. Sci. Rep. 7, 6137 (2017).

Alcock, J. & Sottile, V. Dynamic distribution and stem cell characteristics of Sox1-expressing cells in the cerebellar cortex. Cell Res. 19, 1324–33 (2009).

Alder, J., Lee, K. J., Jessell, T. M. & Hatten, M. E. Generation of cerebellar granule neurons in vivo by transplantation of BMP-treated neural progenitor cells. Nat. Neurosci. 2, 535–40 (1999).

Altman, J. Autoradiographic and histological studies of postnatal neurogenesis. IV. Cell proliferation and migration in the anterior forebrain, with special reference to persisting neurogenesis in the olfactory bulb. J. Comp. Neurol. 137, 433–457 (1969).

Altman, J., B. S. A. Development of the Cerebellar System in Relation to its Evolution, Structure and Functions. (1997).

Alvarado-Mallart, R. M. The chick/quail transplantation model: Discovery of the isthmic organizer center. Brain Res. Rev. 49, 109–113 (2005).

Anderson, M. A. et al. Astrocyte scar formation aids central nervous system axon regeneration. Nature 532, 195–200 (2016).

Anderson, M. A., Ao, Y. & Sofroniew, M. V. Heterogeneity of reactive astrocytes. Neuroscience letters 0, 23–29 (2014).

Andriezen, W. L. The Neuroglia Elements in the Human Brain. British Medical Journal 2, 227–230 (1893).

Ango, F. et al. Bergmann Glia and the Recognition Molecule CHL1 Organize GABAergic Axons and Direct Innervation of Purkinje Cell Dendrites. PLOS Biol. 6, 1–18 (2008).

Anthony, T. E. & Heintz, N. Genetic lineage tracing defines distinct neurogenic and gliogenic stages of ventral telencephalic radial glial development. Neural Dev. 3, 30 (2008).

Anthony, T. E. & Heintz, N. The folate metabolic enzyme ALDH1L1 is restricted to the midline of the early CNS, suggesting a role in human neural tube defects. J. Comp. Neurol. 500, 368–383 (2007).

Anthony, T. E. et al. Radial glia serve as neuronal progenitors in all regions of the central nervous system. Neuron 41, 881–90 (2004).

Arkell, R. & Beddington, R. S. BMP-7 influences pattern and growth of the developing hindbrain of mouse embryos. Development 124, 1–12 (1997).

Bachoo, R. M. et al. Molecular diversity of astrocytes with implications for neurological disorders. Proc. Natl. Acad. Sci. U. S. A. 101, 8384–8389 (2004).

Bandeira, F., Lent, R. & Herculano-Houzel, S. Changing numbers of neuronal and non-neuronal cells underlie postnatal brain growth in the rat. Proc. Natl. Acad. Sci. U. S. A. 106, 14108–14113 (2009).

Bardehle, S. et al. Live imaging of astrocyte responses to acute injury reveals selective juxtavascular proliferation. Nat Neurosci 16, 580–586 (2013).

Barnabe-Heider, F. et al. Evidence that embryonic neurons regulate the onset of cortical gliogenesis via cardiotrophin-1. Neuron 48, 253–265 (2005).

Bayraktar, O., Rowitch ,D., Astrocyte heterogeneity across layers of the cerebral cortex [abstract]. In: Proceedings of the XIII European Meeting on Glial Cells in Ealth and Disease; 2017 July 8-11; Glia 65. Abstract n. 822.

Belvindrah, R. et al. Integrin-linked kinase regulates Bergmann glial differentiation during cerebellar development. Mol. Cell. Neurosci. 33, 109–125 (2006).

Ben-Arie, N. et al. Math1 is essential for genesis of cerebellar granule neurons. Nature 390, 169–172 (1997).

Bergles, D. E., Dzubay, J. A. & Jahr, C. E. Glutamate transporter currents in Bergmann glial cells follow the time course of extrasynaptic glutamate. Proceedings of the National Academy of Sciences of the United States of America 94, 14821–14825 (1997).

Betizeau, M. et al. Precursor diversity and complexity of lineage relationships in the outer subventricular zone of the primate. Neuron 80, 442–57 (2013).

Bignami, A. & Dahl, D. Astrocyte-specific protein and radial glia in the cerebral cortex of newborn rat. Nature 252, 55–56 (1974).

Boda, E., Nato, G. & Buffo, A. Emerging pharmacological approaches to promote neurogenesis from endogenous glial cells. Biochem. Pharmacol. 141, 23–41 (2017).

Brancaccio M, Pivetta C, Granzotto M, Filippis C, Mallamaci A. 2010. Emx2 and Foxg1 inhibit gliogenesis and promote neuronogenesis. Stem Cells 28, 1206–1218.

Broccoli, V., Boncinelli, E. & Wurst, W. The caudal limit of Otx2 expression positions the isthmic organizer. Nature 401, 164–168 (1999).

Buffo, A. & Rossi, F. Origin, lineage and function of cerebellar glia. Prog. Neurobiol. 109, 42–63 (2013).

Buffo, A. et al. Origin and progeny of reactive gliosis: A source of multipotent cells in the injured brain. Proc. Natl. Acad. Sci. 105, 3581–3586 (2008).

Cahoy, J. D. et al. A Transcriptome Database for Astrocytes, Neurons, and Oligodendrocytes: A New Resource for Understanding Brain Development and Function. J. Neurosci. 28, 264 LP-278 (2008).

Cai, N., Kurachi, M., Shibasaki, K., Okano-Uchida, T. & Ishizaki, Y. CD44-positive cells are candidates for astrocyte precursor cells in developing mouse cerebellum. Cerebellum 11, 181–93 (2012).

Cajal, R. y. (1926.) Beitrag zur Kenntnis der Neuroglia des Groß- und Kleinhirns bei der progressiven Paralyse mit einigen technischen Bemerkungen zur Silber-imprägnation des pathologischen Nervengewebes. Z Neur Psych, 100, 738-793.

Calzolari, F. et al. Fast clonal expansion and limited neural stem cell self-renewal in the adult subependymal zone. Nat. Neurosci. 18, 490–2 (2015).

Campbell, K. Dorsal-ventral patterning in the mammalian telencephalon. Curr. Opin. Neurobiol. 13, 50–56 (2003).

Carletti, B. & Rossi, F. Neurogenesis in the Cerebellum. Neurosci. 14, 91–100 (2007).

Cayouette, M., Barres, B. a & Raff, M. Importance of intrinsic mechanisms in cell fate decisions in the developing rat retina. Neuron 40, 897–904 (2003).

Chaboub, L. S. et al. Temporal Profiling of Astrocyte Precursors Reveals Parallel Roles for Asef during Development and after Injury. J Neurosci 36, 11904–11917 (2016).

Chédotal, A. Should I stay or should I go? Becoming a granule cell. Trends Neurosci. 33, 163–172 (2010).

Chen, Z., Li, X. & Desplan, C. Deterministic or Stochastic Choices in Retinal Neuron Specification. Neuron 75, 739–742 (2012).

Christopherson, K. S. et al. Thrombospondins are astrocyte-secreted proteins that promote CNS synaptogenesis. Cell 120, 421–433 (2005).

Ciceri, G. et al. Lineage-specific laminar organization of cortical GABAergic interneurons. Nat. Neurosci. 16, 1199–1210 (2013).

Clark, B. A. & Barbour, B. Currents evoked in Bergmann glial cells by parallel fibre stimulation in rat cerebellar slices. The Journal of Physiology 502, 335–350 (1997).

Clayton, E., Doup, D. P., Klein, A. M., Winton, D. J., Simons, B. D., and Jones, P. H. (2007). A single type of progenitor cell maintains normal

Corrales, J. D., Blaess, S., Mahoney, E. M. & Joyner, A. L. The level of sonic hedgehog signaling regulates the complexity of cerebellar foliation. Development 133, 1811–21 (2006).

Corrales, J. D., Rocco, G. L., Blaess, S., Guo, Q. & Joyner, A. L. Spatial pattern of sonic hedgehog signaling through Gli genes during cerebellum development. Development 131, 5581–90 (2004).

Costa, M. R., Bucholz, O., Schroeder, T. & Gotz, M. Late origin of glia-restricted progenitors in the developing mouse cerebral cortex. Cereb. Cortex 19 Suppl 1, i135-43 (2009).

Crossley, P. H., Minowada, G., MacArthur, C. A. & Martin, G. R. Roles for FGF8 in the induction, initiation, and maintenance of chick limb development. Cell 84, 127–136 (1996).

D'Arca, D. et al. Huwe1 ubiquitin ligase is essential to synchronize neuronal and glial differentiation in the developing cerebellum. Proc. Natl. Acad. Sci. U. S. A. 107, 5875–5880 (2010).

Dahmane, N. & Ruiz i Altaba, a. Sonic hedgehog regulates the growth and patterning of the cerebellum. Development 126, 3089–3100 (1999).

Danielian, P. S., Muccino, D., Rowitch, D. H., Michael, S. K. & McMahon, A. P. Modification of gene activity in mouse embryos in utero by a tamoxifen-inducible form of Cre recombinase. Curr. Biol. 8, 1323-S2 (1998).

Dastjerdi, F. V, Consalez, G. G. & Hawkes, R. Pattern formation during development of the embryonic cerebellum. Front. Neuroanat. 6, 10 (2012).

De Luca, A. et al. Distinct modes of neuritic growth in Purkinje neurons at different developmental stages: Axonal morphogenesis and cellular regulatory mechanisms. PLoS One 4, (2009).

De Luca, A. et al. Exogenous Shh modulates the pool of GABAergic interneurons during cerebellar development. Cerebellum (2014).

Deneen, B. et al. The transcription factor NFIA controls the onset of gliogenesis in the developing spinal cord. Neuron 52, 953–968 (2006).

Denis-Donini, S., Glowinski, J. & Prochiantz, A. Glial heterogeneity may define the three-dimensional shape of mouse mesencephalic dopaminergic neurones. Nature 307, 641–643 (1984).

Eiraku, M. et al. DNER acts as a neuron-specific Notch ligand during Bergmann glial development. Nat. Neurosci. 8, 873–880 (2005).

Emsley, J. G. and Macklis, J. D. Astroglial heterogeneity closely reflects the neuronal-defined anatomy of the adult murine CNS. Neuron glia biology 2, 175–186 (2006).

Englund, C. Unipolar Brush Cells of the Cerebellum Are Produced in the Rhombic Lip and Migrate through Developing White Matter. J. Neurosci. 26, 9184–9195 (2006).

Espinosa de los Monteros, A., Zhang, M. & De Vellis, J. O2A progenitor cells transplanted into the neonatal rat brain develop into oligodendrocytes but not astrocytes. Proc. Natl. Acad. Sci. U. S. A. 90, 50–54 (1993).

Espinosa, J. & Luo, L. Timing Neurogenesis and Differentiation: Insights from Quantitative Clonal Analyses of Cerebellar Granule Cells J. Neurosciences 28, 2301–2312 (2008).

Estivill-Castro, V. Why So Many Clustering Algorithms: A Position Paper. SIGKDD Explor. Newsl. 4, 65–75 (2002).

Falcone, C., Filippis, C., Granzotto, M. & Mallamaci, A. Emx2 expression levels in NSCs modulate astrogenesis rates by regulating EgfR and Fgf9. Glia 63, 412–22 (2015).

Fañanas, J. R. Y. (1916). Contribucion al estudo de la neuroglia del cerebelo. Trab Lab Invest biol (Madrid), 14, 163-179.

Farmer, W. T. et al. Neurons diversify astrocytes in the adult brain through sonic hedgehog signaling. Science 351, 849–54 (2016).

Faulkner, J. R. et al. Reactive astrocytes protect tissue and preserve function after spinal cord injury. J. Neurosci. 24, 2143–2155 (2004).

Favaro, R. et al. Hippocampal development and neural stem cell maintenance require Sox2-dependent regulation of Shh. Nat. Neurosci. 12, 1248–1256 (2009).

Favor, J. et al. The mouse Pax2(1Neu) mutation is identical to a human PAX2 mutation in a family with renal-coloboma syndrome and results in developmental defects of the brain, ear, eye, and kidney. Proc. Natl. Acad. Sci. U. S. A. 93, 13870–5 (1996).

Fiala, J. C. Reconstruct: A free editor for serial section microscopy. J. Microsc. 218, 52–61 (2005).

Figueres-Oñate, M., García-Marqués, J. & López-Mascaraque, L. UbC-StarTrack, a clonal method to target the entire progeny of individual progenitors. Sci. Rep. 6, 33896 (2016).

Fink, A. J. Development of the Deep Cerebellar Nuclei: Transcription Factors and Cell Migration from the Rhombic Lip. J. Neurosci. 26, 3066–3076 (2006).

Fleming, J. T. et al. The Purkinje Neuron Acts as a Central Regulator of Spatially and Functionally Distinct Cerebellar Precursors. Dev. Cell 27, 278–292 (2013).

Florio, M. et al. Neurogenin 2 regulates progenitor cell-cycle progression and Purkinje cell dendritogenesis in cerebellar development. Development 139, 2308–20 (2012).

Franco, S. J. et al. Fate-restricted neural progenitors in the mammalian cerebral cortex. Science 337, 746–749 (2012).

Franzdottir, S. R. et al. Switch in FGF signalling initiates glial differentiation in the Drosophila eye. Nature 460, 758–761 (2009).

Freeman, M. R. & Rowitch, D. H. Evolving concepts of gliogenesis: a look way back and ahead to the next 25 years. Neuron 80, 613–23 (2013).

Frick, A. et al. Proper cerebellar development requires expression of beta1-integrin in Bergmann glia, but not in granule neurons. Glia 60, 820–832 (2012).

Fuentealba, L. C. et al. Embryonic Origin of Postnatal Neural Stem Cells. Cell 161, 1644–1655 (2015).

Furuta, Y., Piston, D. W. & Hogan, B. L. Bone morphogenetic proteins (BMPs) as regulators of dorsal forebrain development. Development 124, 2203–2212 (1997).

Gaiano, N., Nye, J. S. & Fishell, G. Radial glial identity is promoted by Notch1 signaling in the murine forebrain. Neuron 26, 395–404 (2000).

Gao, P. et al. Deterministic progenitor behavior and unitary production of neurons in the neocortex. Cell 159, 775–788 (2014).

Gao, W. Q. & Hatten, M. E. Immortalizing oncogenes subvert the establishment of granule cell identity in developing cerebellum. Development 120, 1059–1070 (1994).

García-Marín, V., García-López, P. & Freire, M. Cajal's contributions to glia research. Trends Neurosci. 30, 479–487 (2007).

García-Marqués, J. & López-Mascaraque, L. Clonal identity determines astrocyte cortical heterogeneity. Cereb. Cortex 23, 1463–72 (2012).

Garcia-Marques, J. & Lopez-Mascaraque, L. Clonal Mapping of Astrocytes in the Olfactory Bulb and Rostral Migratory Stream. Cereb. Cortex 27, 2195–2209 (2017).

Ge, W.-P., Miyawaki, A., Gage, F. H., Jan, Y. N. & Jan, L. Y. Local generation of glia is a major astrocyte source in postnatal cortex. Nature 484, 376–80 (2012).

Gertz, C. C., Lui, J. H., LaMonica, B. E., Wang, X. & Kriegstein, A. R. Diverse behaviors of outer radial glia in developing ferret and human cortex. J. Neurosci. 34, 2559–70 (2014).

Gilbert, S. Developmental Biology. 6th edition. (2000).

Gillespie, D. T. (1976). A general method for numerically simulating the stochastic time evolution of coupled chemical reactions. Journal of Computational Physics, 22(4):403-434.

Gilyarov, A. V. Nestin in central nervous system cells. Neurosci. Behav. Physiol. 38, 165–169 (2008).

Globus, J. H. (1927). The Cajal and Hortega Glia staining methods. A new step in the preparation of formaldehyd-fixed material. Arch Neurol Psych, 8, 263-271.

Goetz, M., Ohlig, S., Sirko, S., Mattugini, N., The role of astrocyte heterogeneity – from stem cells to scar formation [abstract]. In: Proceedings of the XIII European Meeting on Glial Cells in Ealth and Disease; 2017 July 8-11; Glia 65. Abstract n. 83.

Golden, J. A., Fields-Berry, S. C. & Cepko, C. L. Construction and characterization of a highly complex retroviral library for lineage analysis. Proc. Natl. Acad. Sci. U. S. A. 92, 5704–8 (1995).

Gomes, F. L. A. F. et al. Reconstruction of rat retinal progenitor cell lineages in vitro reveals a surprising degree of stochasticity in cell fate decisions. Development 138, 227–235 (2011).

Gotz, M., Nakafuku, M. & Petrik, D. Neurogenesis in the Developing and Adult Brain-Similarities and Key Differences. Cold Spring Harb. Perspect. Biol. 8, (2016).

Graus-Porta, D. et al. Beta1-class integrins regulate the development of laminae and folia in the cerebral and cerebellar cortex. Neuron 31, 367–379 (2001).

Grimaldi, P., Parras, C., Guillemot, F., Rossi, F. & Wassef, M. Origins and control of the differentiation of inhibitory interneurons and glia in the cerebellum. Dev. Biol. 328, 422–33 (2009).

Grosche, J. et al. Microdomains for neuron-glia interaction: parallel fiber signaling to Bergmann glial cells. Nat. Neurosci. 2, 139–143 (1999).

Groves, A. K. et al. Repair of demyelinated lesions by transplantation of purified O-2A progenitor cells. Nature 362, 453–455 (1993).

Guijarro, P. et al. Netrin1 exerts a chemorepulsive effect on migrating cerebellar interneurons in a Dcc-independent way. Mol. Cell. Neurosci. 33, 389–400 (2006).

Guo, C. et al. Fezf2 expression identifies a multipotent progenitor for neocortical projection neurons, astrocytes, and oligodendrocytes. Neuron 80, 1167–1174 (2013).

Hadjieconomou, D. et al. Flybow: genetic multicolor cell labeling for neural circuit analysis in Drosophila melanogaster. Nat. Methods 8, 260–266 (2011).

Haim, L. Ben & Rowitch, D. Functional diversity of astrocytes in neural circuit regulation. Nat. Rev. Neurosci. 18, 31–41 (2016).

Hallonet, M. & Alvarado-Mallart, R. The chick/quail chimeric system: a model for early cerebellar development. Perspect Dev Neurobiol 5, 17–31 (1997).

Hallonet, M. E. R. & Douarin, N. M. Tracing Neuroepithelial Cells of the Mesencephalic and Metencephalic Alar Plates During Cerebellar Ontogeny in Quail - chick Chimaeras. Eur. J. Neurosci. 5, 1145–1155 (1993).

Hallonet, M. E., Teillet, M. a & Le Douarin, N. M. A new approach to the development of the cerebellum provided by the quail-chick marker system. Development 108, 19–31 (1990).

Hansen, D. V, Lui, J. H., Parker, P. R. L. & Kriegstein, A. R. Neurogenic radial glia in the outer subventricular zone of human neocortex. Nature 464, 554–561 (2010).

Hashimoto, R. et al. Origins of oligodendrocytes in the cerebellum, whose development is controlled by the transcription factor, Sox9. Mech. Dev. 140, 25–40 (2016).

Hatten, M. E. Central nervous system neuronal migration. Annu. Rev. Neurosci. 22, 511–539 (1999).

Hatten, M. E. Neuronal regulation of astroglial morphology and proliferation in vitro. J. Cell Biol. 100, 384–396 (1985).

He, J. et al. How Variable Clones Build an Invariant Retina. Neuron 75, 786–798 (2012).

Heng, X., Guo, Q., Leung, A. W. & Li, J. Y. H. Analogous mechanism regulating formation of neocortical basal radial glia and cerebellar Bergmann glia. 1–30 (2017). doi:10.7554/eLife.23253

Hertz, L., Chen, Y. & Song, D. Astrocyte Cultures Mimicking Brain Astrocytes in Gene Expression, Signaling, Metabolism and K+ Uptake and Showing Astrocytic Gene Expression Overlooked by Immunohistochemistry and In Situ Hybridization. Neurochem. Res. 42, 254–271 (2017).

Hewett, J. a. Determinants of regional and local diversity within the astroglial lineage of the normal central nervous system. J. Neurochem. 110, 1717–36 (2009).

Hidalgo-Sánchez, M., Simeone, a & Alvarado-Mallart, R. M. Fgf8 and Gbx2 induction concomitant with Otx2 repression is correlated with midbrain-hindbrain fate of caudal prosencephalon. Development 126, 3191–3203 (1999).

Hiraoka, Y. et al. Delta-like 1 regulates Bergmann glial monolayer formation during cerebellar development. Mol. Brain 6, 25 (2013).

His, W. Die Entwickelung des menschlichen Rautenhirns vom Ende des ersten bis zum Beginn des dritten Monats. (S. Hirzel, 1891).

Hoch, R. V, Rubenstein, J. L. R. & Pleasure, S. Genes and signaling events that establish regional patterning of the mammalian forebrain. Semin. Cell Dev. Biol. 20, 378–386 (2009).

Hochstim, C., Deneen, B., Lukaszewicz, A., Zhou, Q. & Anderson, D. J. Identification of positionally distinct astrocyte subtypes whose identities are specified by a homeodomain code. Cell 133, 510–522 (2008).

Hoogland, T. M. & Kuhn, B. Recent developments in the understanding of astrocyte function in the cerebellum in vivo. Cerebellum 9, 264–271 (2010).

Hoogland, T. M. et al. Radially expanding transglial calcium waves in the intact cerebellum. Proc. Natl. Acad. Sci. 106, 3496–3501 (2009).

Hori, K. & Hoshino, M. GABAergic neuron specification in the spinal cord, the cerebellum, and the cochlear nucleus. Neural Plast. 2012, (2012).

Hoser, M. et al. Prolonged glial expression of Sox4 in the CNS leads to architectural cerebellar defects and ataxia. J. Neurosci. 27, 5495–505 (2007).

Hoshino, M. et al. Ptf1a, a bHLH transcriptional gene, defines GABAergic neuronal fates in

Huang, W. et al. Novel NG2-CreERT2 knock-in mice demonstrate heterogeneous differentiation potential of NG2 glia during development. Glia 62, 896–913 (2014).

Iino, M. et al. Glia-Synapse Interaction Through Ca²⁺-Permeable AMPA Receptors in Bergmann Glia. Science (80-.). 292, 926 LP-929 (2001).

Jacobs, J. J., Kieboom, K., Marino, S., DePinho, R. A. & van Lohuizen, M. The oncogene and Polycomb-group gene bmi-1 regulates cell proliferation and senescence through the ink4a locus. Nature 397, 164–168 (1999).

John Lin, C.-C. et al. Identification of diverse astrocyte populations and their malignant analogs. Nat. Neurosci. 20, (2017).

Joyner, A. L., Liu, A. & Millet, S. Otx2, Gbx2 and Fgf8 interact to position and maintain a mid-hindbrain organizer. Curr. Opin. Cell Biol. 12, 736–741 (2000).

Kamei Y, Inagaki N, Nishizawa M, Tsutsumi O, Taketani Y, I. M. Visualization of mitotic radial glial lineage cells in the developing rat brain by Cdc2 kinase-phosphorylated vimentin. Glia 23, 191–199 (1998).

Kerjan, G. et al. The transmembrane semaphorin Sema6A controls cerebellar granule cell migration. Nat. Neurosci. 8, 1516–1524 (2005).

Kettenmann, H. & Verkhratsky, A. Neuroglia: the 150 years after. Trends Neurosci. 31, 653–659 (2008).

Kimelberg, H. K. Functions of mature mammalian astrocytes: a current view. Neuroscientist 16, 79–106 (2010).

Kita, Y., Kawakami, K., Takahashi, Y. & Murakami, F. Development of cerebellar neurons and glias revealed by in utero electroporation: Golgi-like labeling of cerebellar neurons and glias. PLoS One 8, e70091 (2013).

Klein, C., Butt, S. J. B., Machold, R. P., Johnson, J. E. & Fishell, G. Cerebellum- and forebrain-derived stem cells possess intrinsic regionalcharacter. Development 132, 4497–4508 (2005).

Knoepfler, P. S., Cheng, P. F. & Eisenman, R. N. N- myc is essential during neurogenesis for the rapid expansion of progenitor cell populations and the inhibition of neuronal differentiation. Genes Dev. 2699–2712 (2002). doi:10.1101/gad.1021202.mediate

Kohwi, M. & Doe, C. Q. Temporal fate specification and neural progenitor competence during development. Nat. Rev. Neurosci. 14, 823–838 (2013).

Kolliker, A. Handbuch der Gewebelehre des Menschen. Journal of Anatomy and Physiology 31, 162 (1896).

Komine, O. et al. The monolayer formation of Bergmann glial cells is regulated by Notch/RBP-J signaling. Dev. Biol. 311, 238–250 (2007).

Komuro, H. & Rakic, P. Distinct modes of neuronal migration in different domains of developing cerebellar cortex. J. Neurosci. 18, 1478–1490 (1998).

Komuro, H. & Rakic, P. Dynamics of granule cell migration: a confocal microscopic study in acute cerebellar slice preparations. J. Neurosci. 15, 1110–1120 (1995).

Komuro, H., Yacubova, E., Yacubova, E. & Rakic, P. Mode and tempo of tangential cell migration in the cerebellar external granular layer. J. Neurosci. 21, 527–40 (2001).

Koulakoff, A., Ezan, P. & Giaume, C. Neurons control the expression of connexin 30 and connexin 43 in mouse cortical astrocytes. Glia 56, 1299–1311 (2008).

Kriegstein, A. & Alvarez-buylla, A. The Glial Nature of Embryonic and Adult Neural Stem Cells. Annu. Rev. Neurosci. 149–184 (2011). doi:10.1146/annurev.neuro.051508.135600.The

LaMonica, B. E., Lui, J. H., Hansen, D. V. & Kriegstein, A. R. Mitotic spindle orientation predicts outer radial glial cell generation in human neocortex. Nat. … 9, 1665 (2013).

Lavialle, M. et al. Structural plasticity of perisynaptic astrocyte processes involves ezrin and metabotropic glutamate receptors. Proc. Natl. Acad. Sci. U. S. A. 108, 12915–12919 (2011).

Lee, A. et al. Isolation of neural stem cells from the postnatal cerebellum. Nat. Neurosci. 8, 723–729 (2005).

Legué, E. & Joyner, A. L. Genetic fate mapping using site-specific recombinases. Methods Enzymol. 477, 153–181 (2010).

Legué, E. et al. Differential timing of granule cell production during cerebellum development underlies generation of the foliation pattern. Neural Dev. 11, 17 (2016).

Legué, E., Riedel, E. & Joyner, A. L. Clonal analysis reveals granule cell behaviors and compartmentalization that determine the folded morphology of the cerebellum. Development 142, 1661–71 (2015).

Lehre, K. P., Levy, L. M., Ottersen, O. P., Storm-Mathisen, J. & Danbolt, N. C. Differential expression of two glial glutamate transporters in the rat brain: quantitative and immunocytochemical observations. J. Neurosci. 15, 1835–1853 (1995).

Lein, E. S. et al. Genome-wide atlas of gene expression in the adult mouse brain. Nature 445, 168–176 (2007).

Leto, K. et al. Consensus Paper: Cerebellar Development. Cerebellum (2015). doi:10.1007/s12311-015-0724-2

Leto, K. et al. Laminar Fate and Phenotype Specification of Cerebellar GABAergic Interneurons. J. Neurosci. 29, 7079–7091 (2009).

Leto, K., Bartolini, A. & Rossi, F. Development of cerebellar GABAergic interneurons: origin and shaping of the 'minibrain' local connections. Cerebellum 7, 523–9 (2008).

Leto, K., Carletti, B., Williams, I. M., Magrassi, L. & Rossi, F. Different types of cerebellar GABAergic interneurons originate from a common pool of multipotent progenitor cells. J. Neurosci. 26, 11682–94 (2006).

Levitt, P. & Rakic, P. Immunoperoxidase localization of glial fibrillary acidic protein in radial glial cells and astrocytes of the developing rhesus monkey brain. J. Comp. Neurol. 193, 815–840 (1980).

Li, K., Leung, A. W., Guo, Q., Yang, W. & Li, J. Y. H. Shp2-dependent ERK signaling is essential for induction of Bergmann glia and foliation of the cerebellum. J. Neurosci. 34, 922–31 (2014).

Li, X. et al. MEK Is a Key Regulator of Gliogenesis in the Developing Brain. Neuron 75, 1035–1050 (2012).

Lin, J. C. & Cepko, C. L. Biphasic dispersion of clones containing Purkinje cells and glia in the developing chick cerebellum. Dev. Biol. 211, 177–97 (1999).

Lin, Y. et al. Neuron-derived FGF9 is essential for scaffold formation of Bergmann radial fibers and migration of granule neurons in the cerebellum. Dev. Biol. 329, 44–54 (2009).

Lippman Bell, J. J., Lordkipanidze, T., Cobb, N. & Dunaevsky, A. Bergmann glial ensheathment of dendritic spines regulates synapse number without affecting spine motility. Neuron Glia Biol. 6, 193–200 (2010).

Livesey, F. J. & Cepko, C. L. Vertebrate neural cell-fate determination: lessons from the retina. Nat. Rev. Neurosci. 2, 109–118 (2001).

Livet, J. et al. Transgenic strategies for combinatorial expression of fluorescent proteins in the nervous system. Nature 450, 56–62 (2007).

Louvi, A. & Artavanis-Tsakonas, S. Notch signalling in vertebrate neural development. Nat. Rev. Neurosci. 7, 93–102 (2006).

Louvi, A., Alexandre, P., Métin, C., Wurst, W. & Wassef, M. The isthmic neuroepithelium is essential for cerebellar midline fusion. Development 130, 5319–5330 (2003).

Lovatt, D. et al. The transcriptome and metabolic gene signature of protoplasmic astrocytes in the adult murine cortex. J. Neurosci. 27, 12255–12266 (2007).

Lundell, T. G., Zhou, Q. & Doughty, M. L. Neurogenin1 expression in cell lineages of the cerebellar cortex in embryonic and postnatal mice. Dev. Dyn. 238, 3310–3325 (2009).

Lutolf, S., Radtke, F., Aguet, M., Suter, U. & Taylor, V. Notch1 is required for neuronal and glial differentiation in the cerebellum. Development 129, 373–385 (2002).

Ma, S., Kwon, H. J. & Huang, Z. Ric-8a, a guanine nucleotide exchange factor for heterotrimeric G proteins, regulates bergmann glia-basement membrane adhesion during cerebellar foliation. J. Neurosci. 32, 14979–93 (2012).

Ma, S., Kwon, H. J. & Huang, Z. Ric-8a, a guanine nucleotide exchange factor for heterotrimeric G proteins, regulates bergmann glia-basement membrane adhesion during cerebellar foliation. J. Neurosci. 32, 14979–14993 (2012).

Machold, R. & Fishell, G. Math1 is expressed in temporally discrete pools of cerebellar rhombic-lip neural progenitors. Neuron 48, 17–24 (2005).

Machold, R. P., Kittell, D. J. & Fishell, G. J. Antagonism between Notch and bone morphogenetic protein receptor signaling regulates neurogenesis in the cerebellar rhombic lip. Neural Dev. 2, 5 (2007).

Macnab, L. T. & Pow, D. V. Expression of the exon 9-skipping form of EAAT2 in astrocytes of rats. Neuroscience 150, 705–711 (2007).

Magavi, S., Friedmann, D., Banks, G., Stolfi, A. & Lois, C. Coincident generation of pyramidal neurons and protoplasmic astrocytes in neocortical columns. J. Neurosci. 32, 4762–4772 (2012).

Magnusson, J. P. et al. A latent neurogenic program in astrocytes regulated by Notch signaling in the mouse. Science 346, 237–241 (2014).

Mallamaci A, Iannone R, Briata P, Pintonello L, Mercurio S, Boncinelli E,Corte G. 1998. EMX2 protein in the developing mouse brain and olfactory area. Mech Dev 77,165–172.

Mallamaci, A. & Stoykova, A. Gene networks controlling early cerebral cortex arealization. Eur. J. Neurosci. 23, 847–856 (2006).

Mallamaci, A. Developmental control of cortico-cerebral astrogenesis. Int. J. Dev. Biol. 57, 689–706 (2013).

Mallamaci, A. et al. The lack of Emx2 causes impairment of Reelin signaling and defects of neuronal migration in the developing cerebral cortex. J. Neurosci. 20, 1109–1118 (2000).

Maragakis, N. J. & Rothstein, J. D. Mechanisms of Disease: astrocytes in neurodegenerative disease. Nat. Clin. Pract. Neurol. 2, 679–689 (2006).

Marin, F. & Puelles, L. Patterning of the embryonic avian midbrain after experimental inversions: a polarizing activity from the isthmus. Dev. Biol. 163, 19–37 (1994).

Martinez, S. & Alvarado-Mallart, R.-M. Rostral Cerebellum Originates from the Caudal Portion of the So-Called 'Mesencephalic' Vesicle: A Study Using Chick/Quail Chimeras. Eur. J. Neurosci. 1, 549–560 (1989).

Martinez, S., Crossley, P. H., Cobos, I., Rubenstein, J. L. & Martin, G. R. FGF8 induces formation of an ectopic isthmic organizer and isthmocerebellar development via a repressive effect on Otx2 expression. Development 126, 1189–1200 (1999).

Martinez, S., Wassef, M. & Alvarado-Mallart, R.-M. Induction of a mesencephalic phenotype in the 2-day-old chick prosencephalon is preceded by the early expression of the homeobox gene en. Neuron 6, 971–981 (1991).

Martín-López, E., García-Marques, J., Núñez-Llaves, R. & López-Mascaraque, L. Clonal astrocytic response to cortical injury. PLoS One 8, e74039 (2013).

Mathiesen, C., Brazhe, A., Thomsen, K. & Lauritzen, M. Spontaneous calcium waves in Bergman glia increase with age and hypoxia and may reduce tissue oxygen. J. Cereb. Blood Flow Metab. 33, 161–169 (2013).

Matsunaga, E., Katahira, T. & Nakamura, H. Role of Lmx1b and Wnt1 in mesencephalon and metencephalon development. Development 129, 5269–77 (2002).

Matthias, K. et al. Segregated expression of AMPA-type glutamate receptors and glutamate transporters defines distinct astrocyte populations in the mouse hippocampus. J. Neurosci. 23, 1750–1758 (2003).

Matyash, V. & Kettenmann, H. Heterogeneity in astrocyte morphology and physiology. Brain Res. Rev. 63, 2–10 (2010).

McMahon, A. P. & Bradley, A. The Wnt-1 (int-1) proto-oncogene is required for development of a large region of the mouse brain. Cell 62, 1073–1085 (1990).

Mecklenburg, N. et al. Growth and differentiation factor 10 (Gdf10) is involved in Bergmann glial cell development under Shh regulation. Glia 62, 1713–23 (2014).

Mehler, M. F., Mabie, P. C., Zhu, G., Gokhan, S. & Kessler, J. A. Developmental changes in progenitor cell responsiveness to bone morphogenetic proteins differentially modulate progressive CNS lineage fate. Dev. Neurosci. 22, 74–85 (2000).

Meyers, E. N., Lewandoski, M. & Martin, G. R. An Fgf8 mutant allelic series generated by Cre- and Flp-mediated recombination. Nat. Genet. 18, 136–41 (1998).

Miale, I. L. & Sidman, R. L. An autoradiographic analysis of histogenesis in the mouse cerebellum. Exp. Neurol. 4, (1961).

Millet, S. et al. A role for Gbx2 in repression of Otx2 and positioning the mid/hindbrain organizer. Nature 401, 161–164 (1999).

Milosevic, A., Noctor, S. C., Martinez-Cerdeno, V., Kriegstein, A. R. & Goldman, J. E. Progenitors from the postnatal forebrain subventricular zone differentiate into cerebellar-like interneurons and cerebellar-specific astrocytes upon transplantation. Mol. Cell. Neurosci. 39, 324–334 (2008).

Miyata, T. et al. Asymmetric production of surface-dividing and non-surface-dividing cortical progenitor cells. Development 131, 3133–3145 (2004).

Molne, M. et al. Early cortical precursors do not undergo LIF-mediated astrocytic differentiation. J. Neurosci. Res. 59, 301–311 (2000).

Molofsky, A. V et al. Astrocyte-encoded positional cues maintain sensorimotor circuit integrity. Nature 509, 189–94 (2014).

Molofsky, A. V et al. Astrocytes and disease : a neurodevelopmental perspective. 891–907 (2012). doi:10.1101/gad.188326.112.tal

Molofsky, A. V et al. Expression Profiling of Aldh1l1-Precursors in the Developing Spinal Cord Reveals Glial Lineage-Specific Genes and Direct Sox9-Nfe2l1 Interactions. Glia 61, 1518–1532 (2013).

Molofsky, A. V. & Deneen, B. Astrocyte development: A Guide for the Perplexed. Glia 63, 1320–1329 (2015).

Moore, S. A. et al. Deletion of brain dystroglycan recapitulates aspects of congenital muscular dystrophy. Nature 418, 422–425 (2002).

Morales, D. & Hatten, M. E. Molecular markers of neuronal progenitors in the embryonic cerebellar anlage. J. Neurosci. 26, 12226–12236 (2006).

MORI, T., TANAKA, K., BUFFO, A., WURST, W. & KUHN, RALF AND GOTZ1, M. Inducible Gene Deletion in Astroglia and Radial Glia—A Valuable Tool for Functional and Lineage Analysis. Glia 21–34 (2006).

Muhr, J., Jessell, T. M. & Edlund, T. Assignment of early caudal identity to neural plate cells by a signal from caudal paraxial mesoderm. Neuron 19, 487–502 (1997).

Muller Smith, K., Williamson, T. L., Schwartz, M. L. & Vaccarino, F. M. Impaired motor coordination and disrupted cerebellar architecture in Fgfr1 and Fgfr2 double knockout mice. Brain Res. 1460, 12–24 (2012).

Muroyama, Y., Fujiwara, Y., Orkin, S. H. & Rowitch, D. H. Specification of astrocytes by bHLH protein SCL in a restricted region of the neural tube. Nature 438, 360–363 (2005).

Muzio L, DiBenedetto B, Stoykova A, Boncinelli E, Gruss P, Mallamaci A. 2002. Conversion of cerebral cortex into basal ganglia in Emx2(2/2) Pax6(-Sey/Sey) double-mutant mice. Nat Neurosci 5,737–745.

Muzio L, Soria JM, Pannese M, Piccolo S, Mallamaci A. 2005. A mutually stimulating loop involving Emx2 and canonical wnt signalling specifically promotes expansion of occipital cortex and hippocampus. Cereb Cortex 15, 2021–2028.

Muzio, L. & Mallamaci, A. Emx1, emx2 and pax6 in specification, regionalization and arealization of the cerebral cortex. Cereb. Cortex 13, 641–647 (2003).

Nagata, I., Keilhauer, G. & Schachner, M. Neuronal influence on antigenic marker profile, cell shape and proliferation of cultured astrocytes obtained by microdissection of distinct layers from the early postnatal mouse cerebellum. Brain Res. 389, 217–232 (1986).

Nagy, J. ., Patel, D., Ochalski, P. A. . & Stelmack, G. . Connexin30 in rodent, cat and human brain: selective expression in gray matter astrocytes, co-localization with connexin43 at gap junctions and late developmental appearance. Neuroscience 88, 447–468 (1999).

Naka-Kaneda, H. et al. The miR-17/106–p38 axis is a key regulator of the neurogenic-to-gliogenic transition in developing neural stem/progenitor cells. Proc. Natl. Acad. Sci. 111, 1604–1609 (2014).

Namihira, M. et al. Committed neuronal precursors confer astrocytic potential on residual neural precursor cells. Dev. Cell 16, 245–255 (2009).

Nato, G. et al. Striatal astrocytes produce neuroblasts in an excitotoxic model of Huntington's disease. Development 142, 840–845 (2015).

Noctor, S. C. et al. Cortical neurons arise in symmetric and asymmetric division zones and migrate through specific phases. Nat Neurosci 7, 136–144 (2004).

Noctor, S. C. et al. Dividing Precursor Cells of the Embryonic Cortical Ventricular Zone Have Morphological and Molecular Characteristics of Radial Glia. J. Neurosci. 22, 3161–3173 (2002).

Noctor, S. C., Flint, A. C., Weissman, T. A., Dammerman, R. S. & Kriegstein, A. R. Neurons derived from radial glial cells establish radial units in neocortex. Nature 409, 714–720 (2001).

Noctor, S. C., Martinez-Cerdeno, V. & Kriegstein, A. R. Distinct behaviors of neural stem and progenitor cells underlie cortical neurogenesis. J. Comp. Neurol. 508, 28–44 (2008).

Oberheim, N. A. et al. Uniquely hominid features of adult human astrocytes. J. Neurosci. 29, 3276–3287 (2009).

Oberheim, N. A., Wang, X., Goldman, S. & Nedergaard, M. Astrocytic complexity distinguishes the human brain. Trends Neurosci. 29, 547–53 (2006).

Okano-Uchida, T., Himi, T., Komiya, Y. & Ishizaki, Y. Cerebellar granule cell precursors can differentiate into astroglial cells. Proc. Natl. Acad. Sci. U. S. A. 101, 1211–1216 (2004).

Olsen, M. L., Campbell, S. L. & Sontheimer, H. Differential Distribution of Kir4.1 in Spinal Cord Astrocytes Suggests Regional Differences in K(+) Homeostasis. Journal of neurophysiology 98, 786–793 (2007).

Omez-I, S. G. et al. Sox2 and Pax6 Maintain the Proliferative and Developmental Potential of Gliogenic Neural Stem Cells In Vitro. 1599, 1588–1599 (2011).

Owada, Y., Yoshimoto, T. & Kondo, H. Spatio-temporally differential expression of genes for three members of fatty acid binding proteins in developing and mature rat brains. J. Chem. Neuroanat. 12, 113–122 (1996).

Papadopoulos, M. C. & Verkman, A. S. Aquaporin water channels in the nervous system. Nat. Rev. Neurosci. 14, 265–277 (2013).

Parmigiani, E. et al. Heterogeneity and Bipotency of Astroglial-Like Cerebellar Progenitors along the Interneuron and Glial Lineages. J. Neurosci. 35, 7388–402 (2015).

Pascual, M. et al. Cerebellar GABAergic progenitors adopt an external granule cell-like phenotype in the absence of Ptf1a transcription factor expression. Proc Natl Acad Sci U S A 104, 5193–5198 (2007).

Pekny, M. & Pekna, M. Astrocyte reactivity and reactive astrogliosis: costs and benefits. Physiol. Rev. 94, 1077–1098 (2014).

Petit, A., Pierret, P., Vallée, A. & Doucet, G. Astrocytes from Cerebral Cortex or Striatum Attract Adult Host Serotoninergic Axons into Intrastriatal Ventral Mesencephalic Co-Grafts. J. Neurosci. 21, 7182 LP-7193 (2001).

Pevny, L. H. & Nicolis, S. K. The International Journal of Biochemistry Sox2 roles in neural stem cells. 42, 421–424 (2010).

Pierce, E. T. Histogenesis of the deep cerebellar nuclei in the mouse: an autoradiographic study. Brain Res. 95, 503–518 (1975).

Pinto, L. & Gotz, M. Radial glial cell heterogeneity--the source of diverse progeny in the CNS. Prog. Neurobiol. 83, 2–23 (2007).

Pixley, S. K. & de Vellis, J. Transition between immature radial glia and mature astrocytes studied with a monoclonal antibody to vimentin. Brain Res. 317, 201–209 (1984).

Porter, J. T. & McCarthy, K. D. Astrocytic neurotransmitter receptors in situ and in vivo. Prog. Neurobiol. 51, 439–455 (1997).

Pringle, N. P. et al. Fgfr3 expression by astrocytes and their precursors: evidence that astrocytes and oligodendrocytes originate in distinct neuroepithelial domains. Development 130, 93–102 (2003).

Qiu, Z., Cang, Y. & Goff, S. P. Abl family tyrosine kinases are essential for basement membrane integrity and cortical lamination in the cerebellum. J. Neurosci. 30, 14430–14439 (2010).

Qu, Q. & Smith, F. I. Neuronal migration defects in cerebellum of the Largemyd mouse are associated with disruptions in Bergmann glia organization and delayed migration of granule neurons. Cerebellum 4, 261–270 (2005).

Redies, C., Neudert, F. & Lin, J. Cadherins in cerebellar development: translation of embryonic patterning into mature functional compartmentalization. Cerebellum 10, 393–408 (2011).

Reeber, S. L., Arancillo, M. & Sillitoe, R. V. Bergmann Glia are Patterned into Topographic Molecular Zones in the Developing and Adult Mouse Cerebellum. Cerebellum (2014). doi:10.1007/s12311-014-0571-6

Reichenbach, A. & Wolburg, H. in Astrocytes in (Patho)Physiology of the Nervous System (eds. Haydon, P. G. & Parpura, V.) 251–286 (Springer US, 2009). doi:10.1007/978-0-387-79492-1_10

Reichenbach, A. et al. Distribution of Bergmann glial somata and processes: implications for function. J. Hirnforsch. 36, 509–517 (1995).

Renault-Mihara, F. et al. Spinal cord injury: emerging beneficial role of reactive astrocytes' migration. Int. J. Biochem. Cell Biol. 40, 1649–1653 (2008).

Rio, C., Rieff, H. I., Qi, P., Khurana, T. S. & Corfas, G. Neuregulin and erbB receptors play a critical role in neuronal migration. Neuron 19, 39–50 (1997).

Rolando, C. et al. Extracerebellar progenitors grafted to the neurogenic milieu of the postnatal rat cerebellum adapt to the host environment but fail to acquire cerebellar identities. Eur. J. Neurosci. 31, 1340–1351 (2010).

Rompani, S. B. & Cepko, C. L. A Common Progenitor for Retinal Astrocytes and Oligodendrocytes. The Journal of neuroscience : the official journal of the Society for Neuroscience 30, 4970–4980 (2010).

Rowitch, D. H. & Kriegstein, A. R. Developmental genetics of vertebrate glial-cell specification. Nature 468, 214–22 (2010).

Rowitch, D. H. Glial specification in the vertebrate neural tube. Nat. Rev. Neurosci. 5, 409–419 (2004).

Saab, A. S. et al. Bergmann glial AMPA receptors are required for fine motor coordination. Science 337, 749–753 (2012).

Sandmann, W. (2008). Discrete-time stochastic modeling and simulation of biochemical networks. Computational Biology and Chemistry, 32(4):292-297.

Sasaki, T., Kuga, N., Namiki, S., Matsuki, N. & Ikegaya, Y. Locally synchronized astrocytes. Cereb. Cortex 21, 1889–1900 (2011).

Sato, T., Araki, I. & Nakamura, H. Inductive signal and tissue responsiveness defining the tectum and the cerebellum. Development 128, 2461–2469 (2001).

Satz, J. S. et al. Brain and eye malformations resembling Walker-Warburg syndrome are recapitulated in mice by dystroglycan deletion in the epiblast. J. Neurosci. 28, 10567–10575 (2008).

Schilling, K. Lineage, development and morphogenesis of cerebellar interneurons. Prog. Brain Res. 124, 51–68 (2000).

Schmid, R. S. et al. Neuregulin 1-erbB2 signaling is required for the establishment of radial glia and their transformation into astrocytes in cerebral cortex. Proc. Natl. Acad. Sci. U. S. A. 100, 4251–4256 (2003).

Schwartz, J. P. & Taniwaki, T. Heterogeneity of expression of neuropeptide genes by astrocytes: functional implications. Perspect. Dev. Neurobiol. 2, 251–257 (1994).

Sekerková, G., Ilijic, E. & Mugnaini, E. Time of origin of unipolar brush cells in the rat cerebellum as observed by prenatal bromodeoxyuridine labeling. Neuroscience 127, 845–858 (2004).

Seto, Y. et al. Temporal identity transition from Purkinje cell progenitors to GABAergic interneuron progenitors in the cerebellum. Nat. Commun. 5, 3337 (2014).

Seuntjens, E. et al. Sip1 regulates sequential fate decisions by feedback signaling from postmitotic neurons to progenitors. Nat. Neurosci. 12, 1373–1380 (2009).

Shaw, G., Osborn, M. & Weber, K. An immunofluorescence microscopical study of the neurofilament triplet proteins, vimentin and glial fibrillary acidic protein within the adult rat brain. Eur. J. Cell Biol. 26, 68–82 (1981).

Shen, Q. et al. The timing of cortical neurogenesis is encoded within lineages of individual progenitor cells. Nat. Neurosci. 9, 743–751 (2006).

Sherwood, C. C. et al. Evolution of increased glia-neuron ratios in the human frontal cortex. Proc. Natl. Acad. Sci. U. S. A. 103, 13606–13611 (2006).

Shibuki, K. et al. Deficient cerebellar long-term depression, impaired eyeblink conditioning, and normal motor coordination in GFAP mutant mice. Neuron 16, 587–599 (1996).

Shiga, T., Ichikawa, M. & Hirata, Y. A Golgi study of Bergmann glial cells in developing rat cerebellum. Anat. Embryol. (Berl). 167, 191–201 (1983).

Shimazaki, T. & Okano, H. Heterochronic microRNAs in temporal speci fi cation of neural stem cells : application toward rejuvenation. Nat. Publ. Gr. (2016). doi:10.1038/npjamd.2015.14

Shitamukai, A., Konno, D. & Matsuzaki, F. Oblique radial glial divisions in the developing mouse neocortex induce self-renewing progenitors outside the germinal zone that resemble primate outer subventricular zone progenitors. J. Neurosci. 31, 3683–95 (2011).

Shiwaku, H. et al. Suppression of the novel ER protein Maxer by mutant ataxin-1 in Bergman glia contributes to non-cell-autonomous toxicity. EMBO J. 29, 2446–2460 (2010).

Sievers, J., Pehlemann, F. W., Gude, S., Hartmann, D. & Berry, M. The development of the radial glial scaffold of the cerebellar cortex from GFAP-positive cells in the external granular layer. J. Neurocytol. 23, 97–115 (1994).

Silbereis, J., Cheng, E., Ganat, Y. M., R., M. L. & and Vaccarino, F. M. Precursors with GFAP promoter activity transiently generate GABA interneurons in the postnatal cerebellum. Stem Cells 27, 1152–1163 (2009).

Sillitoe, R. & Joyner, A. Morphology, molecular codes, and circuitry produce the three-dimensional complexity of the cerebellum. Annu. Rev. Cell Dev. Biol. 23, 549–577 (2007).

Sillitoe, R. V & Hawkes, R. in Handbook of the Cerebellum and Cerebellar Disorders (eds. Manto, M., Schmahmann, J. D., Rossi, F., Gruol, D. L. & Koibuchi, N.) 43–59 (Springer Netherlands, 2013). doi:10.1007/978-94-007-1333-8_3

Simat, M., Ambrosetti, L., Lardi-Studler, B. & Fritschy, J.-M. GABAergic synaptogenesis marks the onset of differentiation of basket and stellate cells in mouse cerebellum. Eur. J. Neurosci. 26, 2239–2256 (2007).

Simeone, A., Acampora, D., Mallamaci, A. Stornaiuolo, A., D'Apice, M.R., Nigro, V. and Boncinelli, E. (1993). A vertebrate gene related to orthodenticle contains a homeodomain of the bicoide class and demarcates anterior neuroectoderm in gastrulation mouse embryo. EMBO J. 12, 2735-2747.

Sloan, S. A. & Barres, B. A. Mechanisms of astrocyte development and their contributions to neurodevelopmental disorders. Curr. Opin. Neurobiol. 27, 75–81 (2014).

Smart, I. & Leblond, C. P. Evidence for division and transformations of neuroglia cells in the mouse brain, as derived from radioautography after injection of thymidine-H3. J. Comp. Neurol. 116, 349–367 (1961).

Snippert, H. J. et al. Intestinal crypt homeostasis results from neutral competition between symmetrically dividing Lgr5 stem cells. Cell 143, 134–44 (2010).

Solecki, D. J. Sticky situations: recent advances in control of cell adhesion during neuronal migration. Current opinion in neurobiology 22, 791–798 (2012).

Solecki, D. J., Liu, X., Tomoda, T., Fang, Y. & Hatten, M. E. Activated Notch2 signaling inhibits differentiation of cerebellar granule neuron precursors by maintaining proliferation. Neuron 31, 557–568 (2001).

Soriano, P. Generalized lacZ expression with the ROSA26 Cre reporter strain. Nature genetics 21, 70–71 (1999).

Sotelo, C. Cellular and genetic regulation of the development of the cerebellar system. Prog. Neurobiol. 72, 295–339 (2004).

Sottile, V., Li, M. & Scotting, P. J. Stem cell marker expression in the Bergmann glia population of the adult mouse brain. Brain Res. 1099, 8–17 (2006).

Srinivas, S. et al. Cre reporter strains produced by targeted insertion of EYFP and ECFP into the ROSA26 locus. BMC Developmental Biology 1, 4 (2001).

Stein, C. S., Martins, I. & Davidson, B. L. The lymphocytic choriomeningitis virus envelope glycoprotein targets lentiviral gene transfer vector to neural progenitors in the murine brain. Mol. Ther. 11, 382–389 (2005).

Stoodley, C. J. & Schmahmann, J. D. in Essentials of Cerebellum and Cerebellar Disorders: A Primer For Graduate Students (eds. Gruol, D. L. et al.) 373–381 (Springer International Publishing, 2016). doi:10.1007/978-3-319-24551-5_51

Stump, G. et al. Notch1 and its ligands Delta-like and Jagged are expressed and active in distinct cell populations in the postnatal mouse brain. Mech. Dev. 114, 153–159 (2002).

Sudarov, A. & Joyner, A. L. Cerebellum morphogenesis: the foliation pattern is orchestrated by multi-cellular anchoring centers. Neural Dev. 2, 26 (2007).

Sudarov, A. et al. Ascl1 genetics reveals insights into cerebellum local circuit assembly. J. Neurosci. 31, 11055–69 (2011).

Sun, W. et al. SOX9 is an astrocyte-specific nuclear marker in the adult brain outside the neurogenic regions. J. Neurosci. 37, 3199–16 (2017).

Suzuki-Hirano, A., Harada, H., Sato, T. & Nakamura, H. Activation of Ras-ERK pathway by Fgf8 and its downregulation by Sprouty2 for the isthmus organizing activity. Dev. Biol. 337, 284–293 (2010).

Swarz, J. R. & Del Cerro, M. Lack of evidence for glial cells originating from the external granular layer in mouse cerebellum. J. Neurocytol. 6, 241–250 (1977).

Takizawa, T. et al. DNA Methylation Is a Critical Cell-Intrinsic Determinant of Astrocyte Differentiation in the Fetal Brain. Dev. Cell 1, 749–758 (2001).

Tang, X., Taniguchi, K. & Kofuji, P. Heterogeneity of Kir4.1 channel expression in glia revealed by mouse transgenesis. Glia 57, 1706–1715 (2009).

Tao, J. et al. Deletion of astroglial Dicer causes non-cell-autonomous neuronal dysfunction and degeneration. J. Neurosci. 31, 8306–19 (2011).

Temple, S. & Raff, M. C. Differentiation of a bipotential glial progenitor cell in a single cell microculture. Nature 313, 223–225 (1985).

Thomas, K. R. & Capecchi, M. R. Targeted disruption of the murine int-1 proto-oncogene resulting in severe abnormalities in midbrain and cerebellar development. Nature 346, 847–850 (1990).

Tien, A.-C. et al. Regulated temporal-spatial astrocyte precursor cell proliferation involves BRAF signalling in mammalian spinal cord. Development 139, 2477 LP-2487 (2012).

Tsai, H.-H. et al. Regional astrocyte allocation regulates CNS synaptogenesis and repair. Science 337, 358–62 (2012).

Tsuyama, J. et al. MicroRNA-153 Regulates the Acquisition of Gliogenic Competence by Neural Stem Cells. Stem cell reports 5, 365–377 (2015).

Turner, D. L. & Cepko, C. L. A common progenitor for neurons and glia persists in rat retina late in development. Nature 328, 131–136 (1987).

Turner, D. L., Snyder, E. Y. & Cepko, C. L. Lineage-independent determination of cell type in the embryonic mouse retina. Neuron 4, 833–845 (1990).

Ugbode, C. I., Hirst, W. D. & Rattray, M. Astrocytes Grown in Alvetex((R)) Three Dimensional Scaffolds Retain a Non-reactive Phenotype. Neurochem. Res. 41, 1857–1867 (2016).

Ulloa, F. & Briscoe, J. Morphogens and the Control of Cell Proliferation and Patterning in the Spinal Cord. Cell Cycle 6, 2640–2649 (2007).

Unni, D. K. et al. Multiple Slits regulate the development of midline glial populations and the corpus callosum. Dev. Biol. 365, 36–49 (2012).

Verkhratsky, A. & Butt, A. in Glial Physiology and Pathophysiology 73–104 (John Wiley & Sons, Ltd, 2013). doi:10.1002/9781118402061.ch3

Viti, J., Feathers, A., Phillips, J. & Lillien, L. Epidermal growth factor receptors control competence to interpret leukemia inhibitory factor as an astrocyte inducer in developing cortex. J. Neurosci. 23, 3385–3393 (2003).

Voskuhl, R. R. et al. Reactive astrocytes form scar-like perivascular barriers to leukocytes during adaptive immune inflammation of the CNS. J. Neurosci. 29, 11511–11522 (2009).

Wallace, V. A. Purkinje-cell-derived Sonic hedgehog regulates granule neuron precursor cell proliferation in the developing mouse cerebellum. Curr. Biol. 9, 445–448 (1999).

Wang, F., Xu, Q., Wang, W., Takano, T. & Nedergaard, M. Bergmann glia modulate cerebellar Purkinje cell bistability via Ca2+-dependent K+ uptake. Proc. Natl. Acad. Sci. U. S. A. 109, 7911–7916 (2012).

Wang, J. et al. Anatomy and spatial organization of Müller glia in mouse retina. J. Comp. Neurol. 525, 1759–1777 (2017).

Wang, V. Y. & Zoghbi, H. Y. Genetic regulation of cerebellar development. Nat. Rev. Neurosci. 2, 484–491 (2001).

Wang, V. Y., Rose, M. F. & Zoghbi, H. Y. Math1 expression redefines the rhombic lip derivatives and reveals novel lineages within the brainstem and cerebellum. Neuron 48, 31–43 (2005).

Wang, X., Imura, T., Sofroniew, M. V & Fushiki, S. Loss of adenomatous polyposis coli in Bergmann glia disrupts their unique architecture and leads to cell nonautonomous

Watase, K. et al. Motor discoordination and increased susceptibility to cerebellar injury in GLAST mutant mice. Eur. J. Neurosci. 10, 976–988 (1998).

Weber, K. et al. RGB marking facilitates multicolor clonal cell tracking. Nat. Med. 17, 504–509 (2011).

Wechsler-Reya, R. J. & Scott, M. P. Control of neuronal precursor proliferation in the cerebellum by sonic hedgehog. Neuron 22, 103–114 (1999).

Weller, M., Krautler, N., Mantei, N., Suter, U. & Taylor, V. Jagged1 ablation results in cerebellar granule cell migration defects and depletion of Bergmann glia. Dev. Neurosci. 28, 70–80 (2006).

Wetherington, J., Serrano, G. & Dingledine, R. Astrocytes in the Epileptic Brain. Neuron 58, 168–178 (2008).

Wilhelmsson, U. et al. Redefining the concept of reactive astrocytes as cells that remain within their unique domains upon reaction to injury. Proc. Natl. Acad. Sci. U. S. A. 103, 17513–17518 (2006).

Wojcinski, A. et al. Cerebellar granule cell replenishment postinjury by adaptive reprogramming of Nestin + progenitors. (2017). doi:10.1038/nn.4621

Wurst, W. & Bally-Cuif, L. Neural plate patterning: upstream and downstream of the isthmic organizer. Nat Rev Neurosci 2, 99–108 (2001).

Wurst, W., Auerbach, a B. & Joyner, a L. Multiple developmental defects in Engrailed-1 mutant mice: an early mid-hindbrain deletion and patterning defects in forelimbs and sternum. Development 120, 2065–2075 (1994).

Xu, J., Liu, Z. & Ornitz, D. M. Temporal and spatial gradients of Fgf8 and Fgf17 regulate proliferation and differentiation of midline cerebellar structures. 1843, 1833–1843 (2000).

Y. Gotoh, D. Lanjakornsiripan, S. Furutachi, B.-J. Pior, Y. Kishi, Y. Hirabayashi, M. Nagao, Regulation of astrocyte production in the developing mouse neocortex [abstract]. In: Proceedings of the XIII European Meeting on Glial Cells in Ealth and Disease; 2017 July 8-11; Glia 65. Abstract n. 893.

Yamada, K. & Watanabe, M. Cytodifferentiation of Bergmann glia and its relationship with Purkinje cells. Anat. Sci. Int. 77, 94–108 (2002).

Yamada, K. et al. Dynamic Transformation of Bergmann Glial Fibers Proceeds in Correlation With Dendritic Outgrowth and Synapse Formation of Cerebellar Purkinje Cells. 120, 106–120 (2000).

Yamada, M. et al. Specification of Spatial Identities of Cerebellar Neuron Progenitors by Ptf1a and Atoh1 for Proper Production of GABAergic and Glutamatergic Neurons. J. Neurosci. 34, 4786–4800 (2014).

Yamanaka, K. et al. Astrocytes as determinants of disease progression in inherited amyotrophic lateral sclerosis. Nat. Neurosci. 11, 251–253 (2008).

Yang, Y. et al. Molecular comparison of GLT1+ and ALDH1L1+ astrocytes in vivo in astroglial reporter mice. Glia 59, 200–207 (2011).

Yang, Y. et al. Presynaptic regulation of astroglial excitatory neurotransmitter transporter GLT1. Neuron 61, 880–894 (2009).

Yang, Y., Higashimori, H. & Morel, L. Developmental maturation of astrocytes and pathogenesis of neurodevelopmental disorders. Journal of Neurodevelopmental Disorders 5, 22 (2013).

Yuasa, S. Bergmann glial development in the mouse cerebellum as revealed by tenascin expression. Anat. Embryol. (Berl). 194, 223–34 (1996).

Yuasa, S., Kawamura, K., Ono, K., Yamakuni, T. & Takahashi, Y. Development and migration of Purkinje cells in the mouse cerebellar primordium. Anat. Embryol. (Berl). 184, 195–212 (1991).

Yue, Q. et al. PTEN deletion in Bergmann glia leads to premature differentiation and affects laminar organization. Development 132, 3281–3291 (2005).

Zerlin, M., Milosevic, A. & Goldman, J. E. Glial progenitors of the neonatal subventricular zone differentiate asynchronously, leading to spatial dispersion of glial clones and to the persistence of immature glia in the adult mammalian CNS. Dev. Biol. 270, 200–213 (2004).

Zhang, L. & Goldman, J. E. Generation of cerebellar interneurons from dividing progenitors in white matter. Neuron 16, 47–54 (1996).

Zhang, X. M., Lin, E. & Yang, X. J. Sonic hedgehog-mediated ventralization disrupts formation of the midbrain-hindbrain junction in the chick embryo. Dev. Neurosci. 22, 207–216 (2000).

Zhang, X., Santuccione, A., Leung, C. & Marino, S. Differentiation of postnatal cerebellar glial progenitors is controlled by Bmi1 through BMP pathway inhibition. Glia 59, 1118–31 (2011).

Zhang, Y. & Barres, B. A. Astrocyte heterogeneity: An underappreciated topic in neurobiology. Curr. Opin. Neurobiol. 20, 588–594 (2010).

Zhang, Y. et al. Purification and Characterization of Progenitor and Mature Human Astrocytes Reveals Transcriptional and Functional Differences with Mouse. Neuron 89, 37–53 (2016).

Zhu, X. et al. Age-dependent fate and lineage restriction of single NG2 cells. Development (Cambridge, England) 138, 745–753 (2011).

Zhu, X., Hill, R. A. & Nishiyama, A. NG2 cells generate oligodendrocytes and gray matter astrocytes in the spinal cord. Neuron Glia Biol. 4, 19–26 (2008).

Zhuo, L., Sun, B., Zhang, C. & Fine, A. Live Astrocytes Visualized by Green Fluorescent Protein in Transgenic Mice. 42, 36–42 (1997).

Zong, H., Espinosa, J. S., Su, H. H., Muzumdar, M. D. & Luo, L. Mosaic analysis with double markers in mice. Cell 121, 479–492 (2005).

Zordan, P., Croci, L., Hawkes, R. & Consalez, G. G. Comparative analysis of proneural gene expression in the embryonic cerebellum. Dev. Dyn. 237, 1726–1735 (2008).

Acknowledgments

Come amo spesso ripetere, questi quattro anni di dottorato mi hanno “cambiata”. In senso positivo ovviamente. Mi guardo allo specchio e mi vedo cresciuta, professionalmente ma soprattutto personalmente, rafforzata e con quel pizzico di sicurezza in più che non guasta mai. Sono stati quattro anni ricchi di esperienze, positive e negative, che sarò felice di portarmi dietro come bagaglio per affrontare ciò che verrà. Se sono riuscita a completare questo percorso lo devo a molte persone che ho incontrato lungo questo cammino ed a tante altre che da sempre mi accompagnano, sopportano e supportano in ogni (o quasi…) mia scelta.

Il primo e più speciale ringraziamento va a Ferdinando, una grande persona che rimpiangerò sempre di non aver conosciuto, e apprezzato, abbastanza. È grazie a lui se ho potuto intraprendere questo meraviglioso cammino e riscoprire il desiderio, ormai un pochino accantonato, di fare ricerca, ritrovando una passione ed un entusiasmo inaspettati. Ora, alla fine di questo percorso, mi domando che cosa penserebbe lui dei frutti di questo progetto, a cui lui teneva così tanto, e spero, nel mio piccolo, di non aver deluso le sue aspettative.

Il secondo ringraziamento va ad Annalisa, che riesce a stupirmi giorno per giorno con la sua preparazione, passione ed assoluta dedizione per il suo lavoro. Mi ritengo molto fortunata ad essere stata affidata a lei in questo percorso e vorrei ringraziarla per avermi letteralmente accompagnata in ogni momento, con la sua costante presenza e disponibilità. Mi auguro, un giorno, di poter ereditare almeno un pizzico del suo spirito critico e della sua capacità di entrare nei dati fino a sviscerarli e ribaltarli completamente, trovando sempre nuovi spunti da cui ripartire.

Un altro ringraziamento speciale va ad Elena, di cui c’è anche un po’ in questa tesi. Collega e amica, fin dal primo giorno in laboratorio mi ha seguita passo a passo e, nonostante la distanza, continua ad essere tutt’ora un punto di riferimento indispensabile. Molto di ciò che è presentato in questa tesi lo devo ai suoi preziosi insegnamenti e consigli.

Ringrazio, poi, tutte le persone che ho avuto il piacere di conoscere al NICO. Alle mie colleghe di laboratorio (Elena compresa) va un ringraziamento particolare per avermi sopportata e supportata nei momenti di rabbia e disperazione per i disastri combinati dagli

studenti, per esperimenti che tardavano a venire (dannata BrdU!) e per tutti quei momenti di sconforto che, si sa, nella vita di un dottorando non mancano mai: Roberta, vicina di banco e compagna di momenti di pazzia, alla quale sento con piacere di avvicinarmi sempre di più, Giulia, che con la sua risata contagiosa ed i suoi soprannomi improbabili riesce a farti sorridere anche nei momenti di disperazione totale, Enrica, che con la sua passione e preparazione rappresenta un altro importante punto di riferimento, Martina, la piccola del gruppo alla quale auguro di poter affrontare un percorso di dottorato stimolante e formativo quanto il mio, ed Elisa, ultima ma non per importanza, compagna di risate e di favolosi test comportamentali la cui assenza in laboratorio continua a farsi sentire. Ringrazio, infine, le mie compagne di viaggio e di dottorato Marilena e Sara, con le quali ho condiviso e spero di condividere ancora bellissime esperienze.

Un “gracias” va anche a Laura e Marieta, che durante la mia esperienza Madrileña mi hanno accolta in laboratorio facendomi sentire una di loro (anche se di imparare un po’ di spagnolo proprio non c’è stato verso) e mi hanno salutata con un regalo speciale, che tengo ancora sulla mia scrivania e che mi suscita sempre un po’ di malinconia. Mi auguro che la nostra collaborazione, che si è rivelata così fruttuosa per il mio progetto di dottorato, porti a meravigliosi risultati anche in futuro.

Un altro importante ringraziamento va al favoloso budget del 10%, che ogni anno mi ha consentito di partecipare a congressi e corsi formativi in giro per il mondo, ampliando la mia rete di conoscenze e visitando posti magnifici: Fraueninsel, Bilbao, San Diego, Göteborg, Cagliari, Edimburgo, Madrid.

Un grazie speciale va ad Alessio, che soprattutto nell’ultimo anno mi è stato accanto nei momenti più difficili, quelli in cui l’ansia e l’agitazione prendono il sopravvento e da solo non ce la puoi fare. Grazie per supportarmi nella mia scelta di andare avanti in questo cammino così in salita, grazie per condividere sempre con me le tue giornate (anche se, lo sai, dico sempre sì ma capisco un buon 25% del discorso), grazie per volermi il bene che mi vuoi.

Il più grande ringraziamento va a mamma e papà. Da loro ho imparato a vivere e comportarmi sempre umilmente, esigendo ogni volta il massimo senza peccare di presunzione e mettendomi sempre in discussione. La loro costante presenza è un punto fermo della mia vita ed il loro supporto in ciò che faccio un punto di partenza

imprescindibile.

Infine, vorrei ringraziare la mia nonnina, ultima solo per i suoi 94 anni di età, che ha sempre un pensiero per la sua unica nipote e che mi chiede sempre se “domani vado a fare i’ sperimenti”, ma chissà poi per lei che cosa mai significherà.